DoE/JPL 954372 — 78/

CHEMICAL VAPOR DEPOSITION GROWTH

FINAL REPORT

Covering Period December 29, 1975, to August 31, 1977

By

R. P. Ruth, H. M. Manasevit, A. G. Campbell,
R. E. Johnson, J. L. Kenty, L. A. Moudy,
G. L. Shaw, W. I. Simpson, and J. J. Yang

Publication Date: October 1978

Contract No. 954372

The JPL Low-cost Silicon Solar Array Project is sponsored by the U.S. Department of Energy and forms part of the Solar Photovoltaic Conversion Program to initiate a major effort toward the development of low-cost solar arrays. This work was performed for the Jet Propulsion Laboratory, California Institute of Technology, by agreement between NASA and DoE.

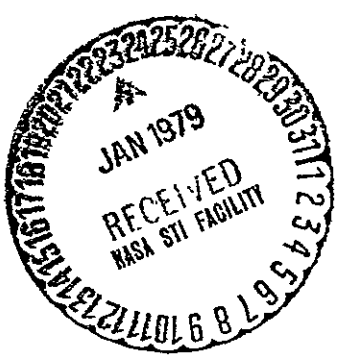

Rockwell International

C76-320/501

DoE/JPL 954372 – 78/6
Distribution Category UC-63

CHEMICAL VAPOR DEPOSITION GROWTH

FINAL REPORT

Covering Period December 29, 1975, to August 31, 1977

By

R. P. Ruth, H. M. Manasevit, A. G. Campbell,
R. E. Johnson, J. L. Kenty, L. A. Moudy,
G. L. Shaw, W. I. Simpson, and J. J. Yang

Publication Date: October 1978

Contract No. 954372

ROCKWELL INTERNATIONAL
Electronics Research Center
Electronic Devices Division
Anaheim, CA 92803

The JPL Low-cost Silicon Solar Array Project is sponsored by the U.S. Department of Energy and forms part of the Solar Photovoltaic Conversion Program to initiate a major effort toward the development of low-cost solar arrays. This work was performed for the Jet Propulsion Laboratory, California Institute of Technology, by agreement between NASA and DoE.

ABSTRACT

The technical objective of this contract was to investigate and develop chemical vapor deposition (CVD) techniques for the growth of large areas of Si sheet on inexpensive substrate materials, with resulting sheet properties suitable for fabricating solar cells that would meet the technical goals of the Low Cost Silicon Solar Array (LSSA) Project. The results of 20 months of experimental work are summarized.

The program involved six main technical tasks: (1) modification and test of an existing vertical-chamber CVD reactor system; (2) identification and/or development of suitable inexpensive substrate materials; (3) experimental investigation of CVD process parameters using various candidate substrate materials; (4) preparation of Si sheet samples for various special studies, including solar cell fabrication; (5) evaluation of the properties of the Si sheet material produced by the CVD process; and (6) fabrication and evaluation of experimental solar cell structures by OCLI, using impurity diffusion and other standard and near-standard processing techniques, supplemented late in the program by the in situ CVD growth of $n^+/p/p^+$ sheet structures subsequently processed into experimental cells. The principal CVD process used was silane (SiH_4) pyrolysis, although a few experiments were done with the dichlorosilane ($SiH_2C\ell_2$) process for Si deposition.

Several glasses (e.g., Corning Code 1715 and Owens-Illinois GS211 and GS213) were found that are compatible with CVD Si growth in an inert (viz., He) atmosphere in the 800-900°C range, although a maximum in the Si deposition rate from SiH_4 pyrolysis in He at ~850°C sets an upper limit on film growth rates. The polycrystalline Si films on glasses showed strong preferred orientation parallel to {100} and — to a smaller degree — {110} planes, depending upon deposition temperature, film thickness, and the glass involved as substrate. Evidence was found of unidentified donor impurities entering the films, presumably from the glass substrates, to affect the electrical properties obtained and possibly set an upper limit on the available hole concentrations achievable in p-type B-doped polycrystalline films on these glasses.

Low-purity (<99 percent) alumina and similar ceramics were found not suitable as substrates for growth of CVD Si of uniform quality. High-purity (≥99.5 percent) aluminas, however — such as Coors Vistal, MRC Superstrate, and certain aluminas manufactured by the 3M Co. — permitted growth of polycrystalline CVD Si layers of controllable quality, highly preferred orientations, and grain sizes that scaled directly with the grain size in the substrate. Refired aluminas that had acquired large individual grains (200μm or more across) produced locally epitaxial Si grains of corresponding dimensions on those substrate grains that were favorably oriented crystallographically. The aluminas, however, are too costly to be considered for meeting the LSSA Project goals and thus were used primarily for study of polycrystalline film growth mechanisms and related investigations. For example, the electrical properties of p-type (B-doped) polycrystalline Si films grown by SiH_4 pyrolysis in H_2 at ~1025°C on polycrystalline aluminas were analyzed in some detail. The relationship between added dopant concentration and measured available hole concentration was established in the range 10^{14}-10^{19} cm^{-3}, and the results have been interpreted in terms of existing models of electrical conduction in polycrystalline Si.

Attempts were made to produce polycrystalline Si films of enhanced grain size on glass substrates by means of a two-step CVD process in which an initial continuous layer (~1μm thick) was deposited by normal SiH_4 pyrolysis (in He at ~850°C) and a second layer was formed by pyrolysis of a SiH_4-$HC\ell$ mixture, but no improvement was observed. However, some evidence was found of a change in the size and distribution of islands in partial-coverage layers of CVD Si grown by SiH_4 pyrolysis at ~850°C in He on substrates of several glasses and single-crystal sapphire when the deposit was annealed in situ, without concurrent deposition, at the growth temperature.

Generally poor photovoltaic performance was exhibited by solar cells fabricated in CVD Si sheet grown by SiH_4 pyrolysis directly onto substrates of aluminas, glasses, or even single-crystal sapphire. V_{oc} values up to ~80 percent of those of single-crystal Si control cells were obtained, but J_{sc} values only 40 to 70 percent of those of a control cell were obtained under simulated AM0 illumination. Depressed long-wavelength response and other performance factors indicated low minority-carrier (electron) diffusion lengths were characteristics of the n/p cell structures made in this Si sheet material by the SiH_4 process and were probably primarily responsible for the poor observed properties. However, epitaxial p-type (B-doped) CVD Si sheet grown on single-crystal Si substrates by $SiH_2C\ell_2$ pyrolysis in H_2 at ~1075°C provided relatively good photovoltaic performance (simulated AM0 illumination) in solar cell structures produced by P diffusion to form the p-n junctions. V_{oc} values of ~560mV, J_{sc} values of ~22 mA/cm^2, curve fill factors of ~0.7, and power efficiencies of 6-7 percent were found in these cells.

The presence of a p^+ layer below and adjoining a p-type (B-doped) CVD Si polycrystalline or epitaxial layer (on alumina or sapphire, respectively) enhanced the photovoltaic response of solar cell structures formed by P diffusion into the p layer. A comparison of the photovoltaic response of P-diffused and P-doped in-situ-grown $n^+/p/p^+$ solar cell structures ~20μm thick on polycrystalline fine-grained and large-grained alumina substrates and on single-crystal sapphire substrates showed that the deposited junctions were superior in the fine-grained Si sheet, the two were about equal in the large-grained Si sheet (with a slight preference for the deposited junctions), and the diffused junctions were superior in the epitaxial structures, for given doping concentrations in the p layer. In all cases the epitaxial cells were much better than the polycrystalline cells, mainly because of current collection (carrier diffusion length) effects and junction leakage current effects, and the large-grained polycrystalline cells were better than the fine-grained cells. A comparison of diffused-junction and deposited-junction $n^+/p/p^+$ structures in three different p-layer thickness ranges (~20, ~45, ~70μm total thickness) on the same three classes of substrate showed a direct increase in photovoltaic response with p-layer thickness for the epitaxial cells but less distinct differences for the polycrystalline cells.

The evaluation of various possible substrate materials, the CVD parameter investigations, and the experimental solar cell fabrication and characterization are described in considerable detail. Specific conclusions of the work are discussed, and recommendations for continued investigations in certain areas are given.

1. INTRODUCTION

This contract began 29 December 1975. The experimental performance period extended through 31 August 1977. This is the Final Report for the contract program.

The purpose of the contract has been to explore the chemical vapor deposition (CVD) method for the growth of Si sheet on inexpensive substrate materials for solar cell applications. The work has been carried out at the Rockwell Electronics Research Center in Anaheim, and also involved some experimental solar cell fabrication and evaluation by the Photoelectronics Group of Optical Coating Laboratory, Inc. (OCLI), in City of Industry, California.

The formal objective of the contract has been to develop CVD techniques for producing large areas of Si sheet on inexpensive substrate materials, with sheet properties suitable for fabricating solar cells meeting the technical goals of the Low-cost Silicon Solar Array (LSSA) Project. The techniques to be developed were to be directed toward (1) minimum-cost processing, (2) production of sheet having properties adequate to result in cells with terrestrial array efficiency of 10 percent or more, and (3) eventual scale-up to large-quantity production.

The CVD method as applied to Si sheet growth in this program involves pyrolysis or reduction of a suitable Si compound at elevated temperature and (approximately) atmospheric pressure in a flow-through (open-tube) system. A carrier gas is used to transport the reactants to the deposition chamber, in which the substrate is mounted on a SiC-coated carbon pedestal heated by rf from outside the chamber. The properties of the Si sheet are determined primarily by deposition temperature, reactant concentrations, the nature of the carrier gas, the Si source compound used, growth rate, doping impurities (added by introduction of appropriate compounds into the carrier gas stream), and the properties of the substrate.

The specific technical goals initially established for this contract include the following:

Si sheet area (per sample)	30 cm^2
Si sheet deposition rate	5μm per min
Si sheet thickness	20 to 100μm
Si sheet crystal structure	100μm average grain size
Intragrain dislocation density	$<10^4$ per cm^2

The principal technical problem areas involved in pursuit of these goals have been (1) establishing preferred CVD process parameters (temperature, reactant concentrations, carrier gas composition, doping impurities, growth rate) for optimized intragrain properties for the Si sheet grown on various substrate materials; (2) identifying suitable substrate materials that can survive the environment of the CVD process and be potentially inexpensive and available in large areas, yet be as favorable as possible to Si grain

growth; and (3) achieving adequate grain size in the Si sheet to provide satisfactory solar cell properties.

In evaluating the prospects for achieving the 1986 technical and cost goals of the LSSA Project at the start of this contract work, it appeared that many characteristics of the CVD method indicated considerable promise for its successful application:

(1) It produces only that amount of Si that is actually required for the photovoltaic effect, without the requirement of additional Si for purely structural reasons

(2) It is a relatively low-temperature process and thus is energy-conservative, not requiring melting of Si at any stage

(3) It does not require refined/purified polycrystalline Si starting material, using instead a high-purity compound of Si that can be a product of one of the early steps in the preparation of polycrystalline semiconductor-grade or perhaps solar-grade Si

(4) It is inherently a large-area process, capable of potential scale-up to areas that are practical for large array fabrication in the LSSA Project

(5) Impurity doping for junction formation can be carried out during CVD growth of the Si sheet

(6) Thicknesses are closely controllable by reactant flow-rate adjustments

(7) It has the capability for eventual development of a continuous fabrication process in which the Si material, the junction or barrier, and the required contacts are all fabricated in a single integrated series of operations in one apparatus.

Si sheet growth by CVD on typical inexpensive substrates was expected to be polycrystalline, because such substrates are either amorphous or microcrystalline and thus provide little or no ordering influence on the growth mechanism. However, the prospects of closely approaching the project goal of 10 percent terrestrial array efficiency after sufficient development were considered good, and the chances of obtaining a major cost reduction per unit area of active cell surface appeared very strong. It thus appeared that a cost-per-watt figure within the project goals would be achievable with this process.

These performance goals had not yet been achieved at the conclusion of the experimental work of this contract program, as described in this report. As a result, it has been concluded by the LSSA Project that the method of direct CVD growth of Si on low-cost substrates is not likely to develop sufficiently - or with sufficient timeliness - to qualify it as a first-line candidate for achieving the longer-term (1986) goals of the LSSA Project, much less the recently established short-term (1980-1981) goals. The CVD

method as defined and investigated under this contract is therefore not being further pursued as part of the LSSA Project activities.

However, the fundamental attributes of the CVD technique for large-area semiconductor thin-film device fabrication remain, and the prospects of achieving acceptable overall performance and advantageous economic parameters with polycrystalline Si thin-film solar cell arrays produced by CVD methods have not been put to rest by the results of this contract program. Many technical difficulties have been identified, with some having been solved and others remaining unsolved. In particular, the limitations associated with the lack of available low-cost substrate materials having properties adequate to permit growth of large-grain polycrystalline Si layers have been emphasized.

Much has been learned about the properties of polycrystalline Si grown by the CVD process (particularly by SiH_4 pyrolysis) and about the fabrication of solar cell structures in such material. Numerous experiments and procedures, identified either prior to or during the program, that should be undertaken in order to provide a more complete evaluation of direct CVD growth of Si on low-cost substrates as a potential method for achieving the long-term goals of the National Photovoltaic Conversion Program were not investigated or completed during this work because of limitations of contract scope or of time and funding. Some of these items are addressed in the section on Conclusions and Recommendations, and should be the basis for additional work with the CVD technique for low-cost solar cell applications outside of the context and schedule of the LSSA Project.

The contract program has consisted of six main technical tasks:

(1) Modification and test of an existing CVD reactor system

(2) Identification and/or development of suitable inexpensive substrate materials

(3) Experimental investigation of Si CVD process parameters using various candidate substrate materials

(4) Preparation of Si sheet samples for various special studies, including solar cell fabrication

(5) Evaluation of the properties of the Si sheet material produced by the CVD process

(6) Fabrication and evaluation of experimental solar cell structures, using standard and near-standard processing techniques.

It is important to note that the fabrication of solar cell structures had been restricted - during most of the contract program - to the use of conventional thermal diffusion of impurities, as a result of negotiation of the contract Statement of Work with JPL and its specific interpretation by LSSA Project personnel and the JPL Technical Manager. However, during the

final few months of the program a modification in the Statement of Work permitted the fabrication of experimental solar cell structures in CVD Si sheet material by the sequential growth of appropriately doped layers to produce p/p^+ and $n^+/p/p^+$ structures on insulating substrate materials, with subsequent cell fabrication and evaluation by OCLI. This expanded activity was included within the framework of the above main technical tasks.

This Final Report is divided into two main sections - Section 2, Technical Discussion, and Section 3, Conclusions and Recommendations. Whereas the quarterly progress reports have treated the six principal tasks separately, for management and progress monitoring purposes, the technical discussion in Section 2 of this report is organized along slightly different lines to facilitate a more orderly presentation of the results of the entire 20 months of work. Task identification is still preserved in some parts of the discussion, but only if it contributes to the clarity and continuity of the presentation of the subject matter.

2. TECHNICAL DISCUSSION

This section contains a summary of the experimental investigations carried out during the 20 months of this contract, with more details given for the work of the final five months of the program in the absence of a quarterly progress report covering any portion of that period.

There are four main technical areas covered in this discussion, as follows: Section 2.1, Modification and Test of Existing CVD Reactor System (Task 1); Section 2.2, Identification and Development of Suitable Substrate Materials (Task 2); Section 2.3, Experimental Investigation of Si CVD Process Parameters and Properties of Films Grown on Selected Substrates (Tasks 3 and 5); Section 2.4, Preparation and Evaluation of Solar Cell Structures in CVD Si Sheet Material (Tasks 4 and 6).

2.1 MODIFICATION AND TEST OF EXISTING CVD REACTOR SYSTEM (TASK 1)

The apparatus used for the chemical vapor deposition of Si films has been highly developed in recent years. The typical experimental system used at Rockwell consists of six main components: (1) deposition chamber (reactor), with provision for supporting the heated substrates on which Si is deposited; (2) reactant gas manifold and distribution line system, with appropriate metering, valving, and controls; (3) reservoirs or tanks of the required reactant and carrier gases, with associated purifiers and/or filters; (4) vacuum system for evacuating selected portions of the reactor and gas manifold, as needed; (5) provision for burning, reprocessing, or otherwise discharging the exhaust gases existing from the reactor system; and (6) power supply for heating the substrates in the reactor chamber - usually an rf generator with an external coil which couples to a susceptor, which also serves as the substrate support.

Throughout the first quarter of this program an existing laboratory-type CVD reactor system with a vertical deposition chamber was used. This system is similar to that used extensively at Rockwell in previous studies of semiconductor epitaxial growth by CVD (Ref 1).

However, to improve the control of the Si CVD process for this program a number of modifications were made on this reactor system. These changes were intended to provide a more versatile system that would offer greater reproducibility and reliability than previously available.

The modifications were originally scheduled for completion by the end of the first quarter, but because of vendor delays in delivery of some of the key components they were completed early in the second quarter. The contractually required Design and Performance Review of the modified system was conducted for JPL personnel on 15 April 1976. A Standard Operation Procedure for the modified reactor system was also completed and delivered to JPL personnel at the time of this design review. Revisions in this standard procedure were made later in the program, and a final revised procedure was submitted to JPL just prior to the end of the experimental performance period.

A schematic diagram of the reactor system incorporating the modifications is given in Figure 2-1. The modifications included the following main items:

1. Thirteen Tylan Model FC-260 Mass Flow Controllers. All gas lines involved directly in the CVD process are controlled by this means. The only lines not so controlled are the carrier gas bypass and reactant "dump-out" line leading to the burn-box at the top of the reactor-system hood enclosure, and a separate H_2 line to admit that gas to the chamber for pre-deposition "etching" when carrier gases other than H_2 are used. The controller locations are as follows (see Figure 2-1):

   2 in parallel main gas flow lines, one leading into the reactor chamber and the other provided for mixing reactants in desired proportions and at constant total flow rate prior to introduction into the chamber

   3 in Si source compound supply lines (SiH_4, $SiH_2C\ell_2$, and a bubbler for $SiHC\ell_3$ or $SiC\ell_4$)

   1 in bubbler-source carrier gas line

   1 in $HC\ell$ line

   2 in dopant lines (n- and p-type impurity source compounds)

   2 in gas lines for dilution of doping compounds

   2 in diluted dopant lines (n and p type).

2. One Tylan Model GPT-104 Automatic Sequence Timer associated with the controllers. The timer is capable of providing automatically-timed control of flow intervals in 10 different lines (i.e., 10 signal channels), with up to four different events (such as on and off) per channel programmable in each cycle of the sequencer.

3. Four Tylan Model RO-14 Control and Readout Units. These are included in the centralized control panel to handle the outputs of the 13 mass flow controllers. Each readout unit has a maximum capacity of four input channels.

4. Two Model 5150A Hewlett-Packard Thermal Printers. Each of these is capable of sequential printing of 20 channels of digital information per cycle of the printer (printing time ~1/3 sec per line, data input acceptance interval adjustable down to one second). These can be used to provide permanent records of experimental parameters when desired. Each printer includes a timer, so that all data are related to printed digital time recordings.

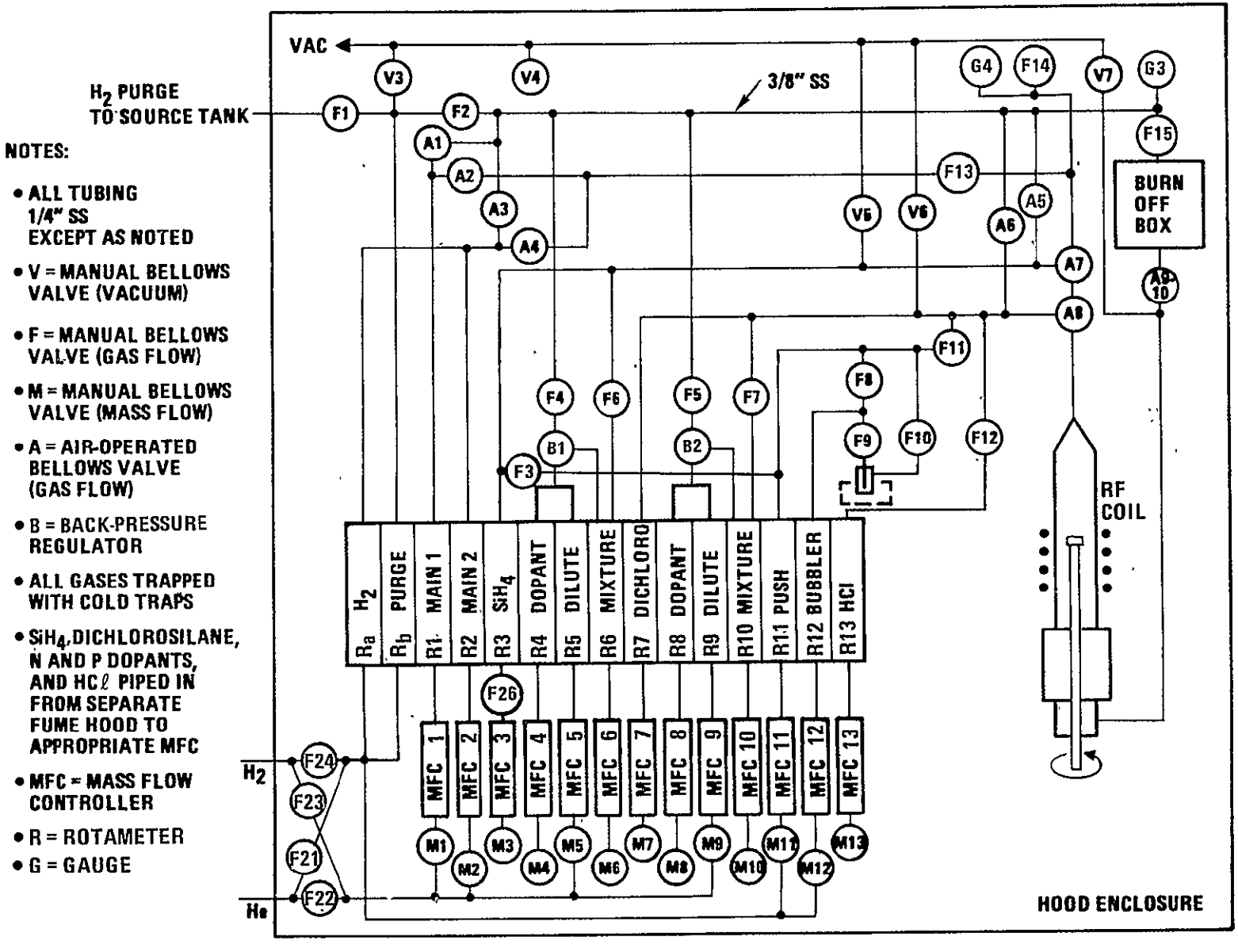

Figure 2-1. Schematic Diagram of Modified Si CVD Reactor System

5. Ten Nupro Model 4BK air-operated valves. These are triggered by switch-activated solenoids, and are installed on the reactor system to improve control over film thickness, growth of partial layers, and impurity concentration and distribution. Two of these valves are Nupro Model SS-4BK-S2 zero-dead-space valves, to further reduce the amount of uncontrolled and/or unwanted reactant flow in the system.

6. One Alcatel Model ZM2012C Vacuum Pump. This pump serves both as the forepump for the trapped mercury-vapor diffusion pump and as the roughing pump for the reactor system. This type of pump has improved pumping speed over conventional oil-immersed mechanical vane pumps, provides essentially zero backstreaming of hydrocarbon vapors because of its "dry" construction, and is relatively quiet in operation.

In addition to the reactor system itself, which is enclosed in a separate high-flow-rate fume hood, an external control center is housed in a separate floormounted cabinet at the side of the hood. This cabinet accommodates the sequencer timer, the four readout units, two recorder-printers, and the master valve-control panel.

The entire CVD reactor system is shown in the photograph in Figure 2-2; the external control cabinet can be seen at the left, the bank of mass flow controllers in the lower center, and the vertical reactor chamber at the right. A close-up view of the mass flow controllers is shown in Figure 2-3. The conventional rotameters can be seen above the mass flow controllers; these were left in the system to provide convenient visual indication of gas flow and a continuing check on the functioning of the controllers. Later developments indicated this to have been a fortunate decision.

Several other minor changes were made during the second quarter in achieving full operational capability of the reactor system. For example, a four-way ball valve was found to allow He from the input gas line to leak into the input H_2 line. In its place, separate stainless steel lines for each gas and connecting manual bellows-sealed valves were installed. In addition, a manual bellows-sealed valve was added between the SiH_4 mass flow controller and the glass rotameter to help minimize contamination of the SiH_4 mass flow controller by possible entry of water vapor or air through any minute leaks in the system.

Following completion of the reactor modifications and during the later course of the program problems relating to the mass flow controllers (MFC) appeared, e.g., faulty temperature sensors, faulty insulating cement, and development of obstructions in the MFC in the SiH_4 line. Existence of these problems was indicated by the conventional rotameters that had been left in the lines in series with the controllers. When no correlations could be made between MFC flow-rate readings and rotameter values during the sixth quarter of the program, the rotameters for $HC\ell$ and SiH_4 were calibrated in-house using a volumeter (manufactured by George K. Porter, Hatfield, PA).

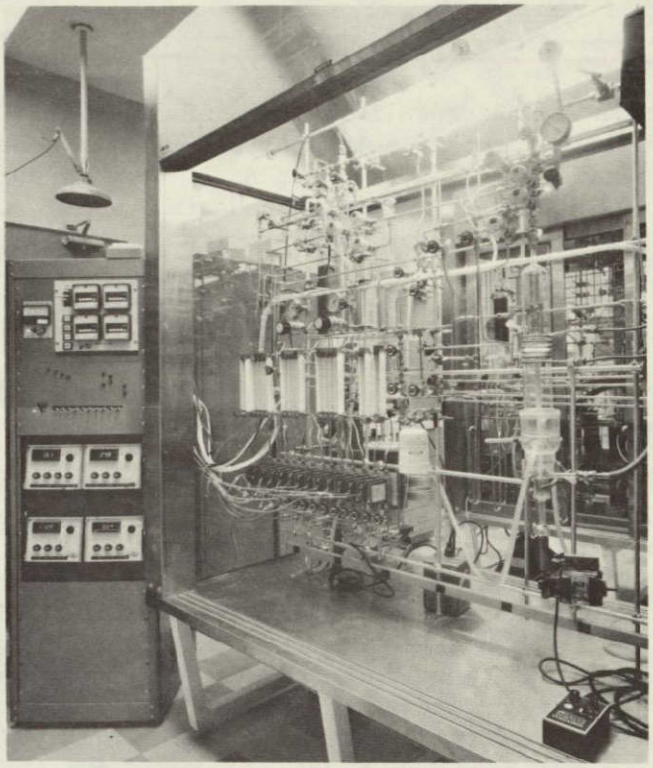

Figure 2-2. Overall View of Modified Si CVD Reactor System, Showing Control Center in Separate Cabinet, Bank of Mass Flow Controllers in Lower Center, and Vertical Reactor Chamber at Right

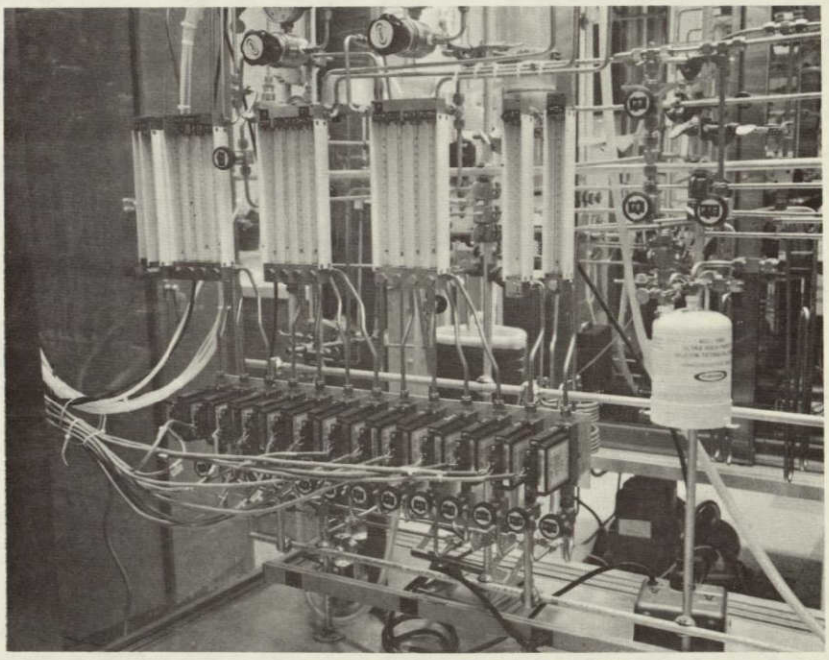

Figure 2-3. Close-up View of Bank of 13 Mass Flow Controllers

The results obtained in these calibrations indicated that the rotameter flow-rate charts supplied by Brooks Instrument Division of Emerson Electric Company are in error for SiH_4 by as much as 30 percent for the flow-rate range used in these studies. However, the data for HCℓ supplied by Brooks correlate better with the Rockwell calibration measurements than do those supplied by Matheson Gas Products. For example, for a 5cm pyrex float position for HCℓ a flow rate of 85 ccpm was measured. The Brooks chart reading for this float position is 70 ccpm, but the Matheson data indicate 170 ccpm. With this type of discrepancy in vendors' data it is not surprising that results of certain types of experiment are not reproducible from laboratory to laboratory.

Unfortunately, difficulties continued with the MFC unit in the SiH_4 line. Prior to the above calibrations this MFC had been temporarily removed from the SiH_4 line and a micrometer metering valve was installed just ahead of the rotameter, to provide means for SiH_4 flow rate adjustment pending calibration of the rotameter and cleaning and recalibration of the MFC. When the buildup of deposits in the MFC continued to occur with disturbing frequency after the SiH_4 rotameter calibration had been made, the decision was finally made in the sixth quarter of the program to bypass the MFC permanently. This arrangement was employed for the remainder of the program.

During the final three months of the program a flat baffle in the form of a disk was installed in the reactor chamber at a point about 1½ in below the inlet aperture at the top of the chamber. By increasing the total H_2 carrier gas flow rate from 1.5 to 2.5 ℓpm, films of satisfactory quality with thickness variations of ~±5 percent were obtained across the 2 in diam pedestal. (See discussion in Section 2.3.) This final modification in the reactor system was made for the purpose of improving the uniformity of film growth across the entire sample pedestal surface, and was used without further change to the conclusion of the experimental performance period.

Next, it must be available in relatively large areas - if not now, then at least by 1986. In addition, the properties of the substrate material must be compatible with those of Si. Its linear thermal expansion coefficient (TEC) behavior should duplicate that of Si as closely as possible, from at least the Si sheet deposition temperature down to room temperature.

The importance of the TEC of the substrate material relative to that of Si in the range between room temperature and the Si deposition temperature is emphasized by the data given in Figure 2-4. This shows the TEC as a function of temperature for several glasses and other possible substrate materials, as well as for some other familiar materials for comparison, throughout the range from below room temperature up to Si CVD temperatures. These data provided guidance in the selection of candidate materials for experimental evaluation in the early stages of the program.

The Si film must also be chemically stable with respect to the substrate surface, so that there will not be a transition layer at the interface that might cause separation of film and substrate or other adverse effects. The substrate must also be stable relative to the carrier gas and the products of Si formation - notably, H_2 when SiH_4 is the source of Si, and HCℓ if the Si-containing halides are used to produce the Si.

Only a few classes of materials now readily available could be considered as candidate substrate materials, based on cost, availability, and reported properties. These include the amorphous glasses, glass-ceramics, and various polycrystalline ceramics. Various metals in bulk thin-sheet form were eliminated as candidate materials at the beginning because of cost or reactivity with Si in the CVD environment or both. Graphite was excluded from consideration at the direction of LSSA Project personnel because of extensive investigations of its use for polycrystalline thin-film Si solar cell growth in other contract programs (Ref 2).

Many glasses are available in large sheet form, and others are potentially susceptible to fabrication into large sheets. It is believed that flat substrates could be produced of most glasses by techniques well-known in the glass industry if sufficient need were demonstrated. Some glass-ceramics are also produced in large sheets (the order of square meters), and many low-cost polycrystalline ceramic materials are now available in areas up to about 300 cm^2.

A combination of two of the above classes, namely, a glass film produced on a polycrystalline ceramic, i.e., a glazed ceramic, was also considered as a potential substrate for Si sheet growth. The typical glaze formed on ceramic offers a surface finish better than that which can be achieved on the ceramic itself (in an as-fired condition) without polishing. The glaze tends to fill in the pores of the surface and can be used with a relatively inexpensive non-smooth substrate of purity lower than that which might otherwise be required. Although the commercial availability of glazed ceramics is quite limited, and glazes with low softening temperatures appear to be the rule, some glazes were obtained from interested suppliers, as indicated below.

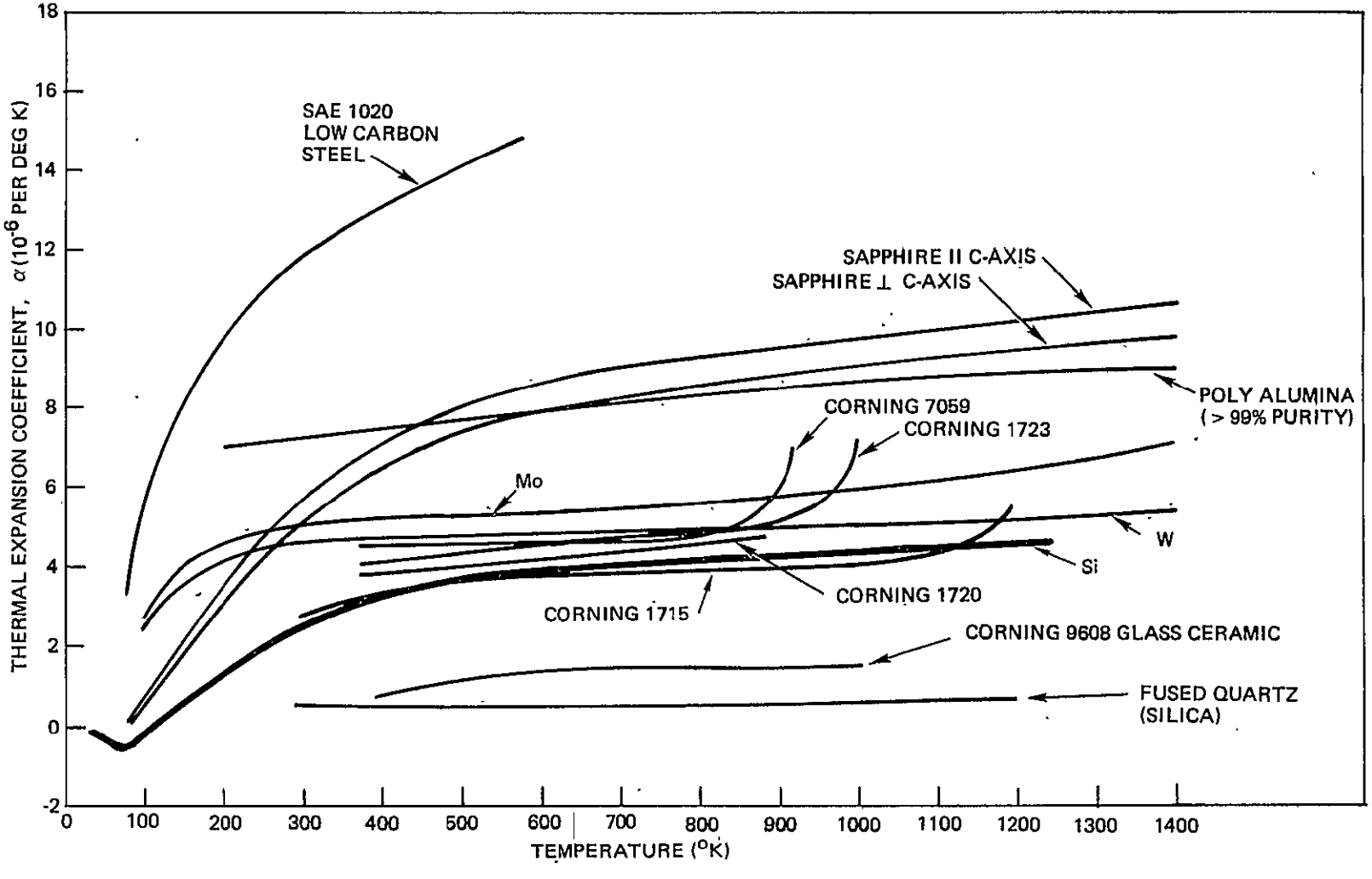

Figure 2-4. Linear Thermal Expansion Coefficients as a Function of Temperature for Si and Various Other Materials

In considering the use of an amorphous glass as a substrate, it is necessary to evaluate the effect of temperature on certain glass properties, notably the TEC and the viscosity. Specific viscosity values are associated with some of the important physical characteristics of glasses: strain point, ~$3x10^{14}$ poises; annealing point, ~10^{13} poises; softening point, ~$10^{7.6}$ poises; and working point, ~10^{4} poises. From room temperature to just below the strain point, which is generally regarded as the upper limit for use of an annealed glass, TEC values for glasses tend to remain nearly constant, increasing only slightly with temperature. However, with further increase in temperature into the annealing range the viscosity decreases and a large and rapid increase in TEC occurs. Although this might appear to eliminate the glass from consideration as a substrate for Si sheet growth, there have been instances of successful Si layer growth on such surfaces (Ref 3). However, because previous studies of polycrystalline Si growth on SiO_2 have indicated that higher temperatures lead to larger grain sizes (Ref 4), initial experiments with glass substrates in this program involved those with relatively high softening points.

Only two readily available commercial glasses have strain points above the lowest temperatures at which Si growth is considered technically possible by CVD techniques; these are the aluminosilicates Corning Code 1720 and Code 1723. However, since Si growth by CVD on other glasses could be possible at temperatures between the annealing point of the glass and its softening point, i.e., above ~600°C (the lowest temperature consistent with growth of Si from SiH_4), and since it is not known with certainty what condition of viscosity of a glass surface is best for the formation of Si films of solar-cell quality, glasses have remained in strong contention as candidate substrate materials throughout the program.

Glass-ceramics are materials which have been converted from their original glassy state to polycrystalline ceramics by controlled nucleation and devitrification. Through variations in composition and heat treatment, glass-ceramics offer a wide range of grain sizes, crystalline orientations, and thermal expansion coefficients - from high positive values to negative values, including some that are zero over a limited temperature range. Glass-ceramics with TEC's similar to that of Si were sought for evaluation as substrates for solar cell structures, but relatively little success in obtaining such materials with those properties was realized.

The third class of substrate material of major initial interest is the polycrystalline ceramic, which is available in many compositions and purities. Based on TEC values only, likely materials for study include zircon ($ZrO_2 \cdot SiO_2$), with TEC ~$4.9x10^{-6}$ per deg C (25-900°C); cordierite ($2MgO \cdot 2Al_2O_3 \cdot 5SiO_2$), with TEC ~$3.7x10^{-6}$ per deg C (25-900°C); a number of aluminas, with TEC's $7.7-8.0x10^{-6}$ per deg C (25-900°C), and mullite ($3Al_2O_3 \cdot 2SiO_2$), with TEC ~$4.8x10^{-6}$ per deg C (40-800°C). In today's market, demand has resulted in "supersmooth" as-fired surfaces only on the aluminas. Further efforts for producing better surfaces (without polishing) on the other ceramics are necessary; such work is in progress in the laboratories of some manufacturers of ceramics.

Once a substrate material was identified as a candidate for experimental use in this work its surface and internal structural properties were characterized by various analytical methods, and it was then used for exploratory Si CVD

growth in both H_2 and He atmospheres at temperatures consistent with its known properties. A relatively thick ($\geq$20μm) Si film was usually grown on the candidate material, in the presence of a small wafer of sapphire which served effectively as a monitor of the particular deposition parameters used as well as an indicator of the stability of the candidate material in the CVD environment.

2.2.2 Contacts with Potential Suppliers of Substrate Materials

Early in the first quarter and again in the third quarter of the program various potential suppliers of low-cost substrate materials were contacted personally, on two extended trips. Some contacts were also made by telephone and/or by mail early in (and in some cases prior to) the contract program.

Table 2-1 lists the vendors (with locations) that were contacted during the program and those that supplied materials for possible experimental use. In each case the vendor's specialty is indicated, as are the types of substrate materials that were supplied.

The response of most of the glass and ceramic manufacturers contacted for assistance in solving the substrate problem was excellent. Both commercially-available and specially-prepared materials have been supplied in various quantities for evaluation. Several of the manufacturers indicated a strong interest in attempting to prepare and supply samples of non-standard glasses, glass-ceramics, ceramics, and glazes for exploratory use without charge. Others indicated the effort could not continue throughout the contract period without some specific external financial support, from the contract or otherwise. Four of the suppliers of substrate materials - Corning, 3M, Kyocera, and MRC - visited Rockwell early in the program to discuss details of the substrate requirements. A visit was also made by Rosenthal USA, Ltd., late in the program.

2.2.3 Candidate Substrate Materials Obtained for Evaluation

All of the candidate substrate materials received from the suppliers given in Table 2-1 are listed in Tables 2-2 through 2-4. Table 2-2 lists the glasses and glass-ceramics, Table 2-3 the aluminas, and Table 2-4 the other ceramics. In each table the materials are grouped by vendor and are identified by the vendor's type numbers or trade names and by the nominal purity of the material as specified by the vendor. Available data on TEC's are given, as is information about the surface finish - the latter in some cases supplied by the vendor and in some cases measured by Rockwell. Thicknesses of the various individual groups of substrates obtained are also included.

2.2.4 Properties of Substrate Materials

A wide range of surface topography is represented by the three main types of substrate materials used in the contract work--namely, glasses, glass-ceramics, and polycrystalline aluminas and similar fired ceramics. The surface of a CVD film deposited on a substrate usually has a topography directly related to that of the substrate, especially if the latter is heavily textured. In

Table 2-1. Manufacturers and Suppliers of Substrate Materials for Use in CVD Si Growth Experiments

VENDOR (LOCATION)	PERTINENT SPECIALTY	SUBSTRATE SAMPLES SUPPLIED
Corning Glass Works[1,2,4] (Corning, NY)	Glasses, glass-ceramics	Corning Codes 0211; 0317; 1723; 7059; 191CCA SnO_2-coated 0317; 1715 glasses Corning Codes 9606; 9608; 9609 glass-ceramics
Owens-Illinois, Inc.[1,2] (Toledo, OH)	Glasses	GS-186; GS-210; GS-211; GS-213, EE-2, EE-5, GS-238
3M Co. (Laurens, SC)[1,4] (St. Paul, MN)[2]	Ceramics	Cordierite; zircon; glazed alumina; aluminas of various purities, firing histories, process types; mullite; steatite
Coors Porcelain Co.[1] (Golden, CO)	Ceramics	ADS96F; ADS995; Vistal (as-fired and refired)
Materials Research Corp.[1,4] (Orangeburg, NY)	Ceramics	Superstrate (96 and 99.6 percent); Au-coated superstrate
Kyocera[4] (San Diego, CA)	Ceramics	Forsterite; alumina; zircon; glazed alumina
Pemco Glidden-Durkee[1] (Baltimore, MD)	Enamels, frits	Two different glazes on cordierite and alumina
Morganite, Inc.[3] (Dunn, NC)	Ceramics	Recrystallized alumina; Hilox 961 (96 percent)
Chi-Vit Corp.[2] (Cicero, IL)	Enamels, glazes	Glazed Kovar-type alloy (aluminosilicate glass)
Magneco Electronics[2] (Addison, IL)	Ceramics	Alumina (96 percent)
Saxonburg Ceramics[2] (Saxonburg, PA)	Ceramics	Alumina (97.5 percent) steatite, cordierite
Plessey-Ceramics Div.[2] (Frenchtown, NJ)	Ceramics	Ceramistik; black No. 7231; tape alumina
Ferro Corp.[2] (Independence, OH)	Frits, glazes, specialty ceramics	High-density cordierite; glazed aluminas
Schott Optical Glass, Inc.[2] (Duryea, PA)	Glasses (IR, solar, optical), glass-ceramics	Glass-ceramic
Atomics Intl.[3] (Canoga Pk, CA)	Glazes	Glazed alumina
Honeywell Ceramic Center[3] (Golden Valley, MN)	Ceramics	Mullite
Associated Ceramics and Technology[3] (Sarver, PA)	Ceramics	Steatite; extruded and pressed alumina
Metsch Refractories[3] (Chester, WV)	Ceramics	Mullite; porcelain
General Electric Glass Products and Lamp Div.[2] (Cleveland, OH)	Lucalox (alumina); quartz	Quartz ribbon
Rosenthal USA Lmt.[4] (New York, NY)	Ceramics	Aluminas (96 and 99.5 percent)
Ceradyne[3] (Santa Ana, CA)	Specialty ceramics	
Comco Inc.[3] (Sun Valley, CA)	Aluminas	Aluminas (99.5 and 96 percent)

[1] Contact on first trip
[2] Contact on second trip
[3] Phone contact only
[4] Visited Rockwell

Table 2-2. Candidate Glass or Glass-based Materials Received from Various Suppliers

SUBSTRATE IDENTIFICATION	MATERIAL/TYPE	THERMAL EXPANSION COEFF (TEMP RANGE) (10^{-6} PER DEG C)	THICKNESS (mm)	STRAIN POINT (°C)	ANNEAL POINT (°C)	SOFTENING POINT (°C)
Corning 0211	Lime Borosilicate	7.4 (0–300°C)	0.25	508	550	720
0317	Alumina Soda Lime	8.7 (0–300°C)	1.52	574	622	871
1723	Aluminosilicate	5.4 (25–670°C)	0.76, 1.27	665	710	908
7059	Barium Alumino-borosilicate	4.6 (0–300°C)	0.81	587	635	842
1715	Calcium Aluminosilicate	~3.5 (0–300°C)	–	834	866	1060
Owens-Illinois GS-186	Proprietary High-temperature Glass	4.7 (0–300°C)	0.76, 1.02	–	–	982
GS-210	Proprietary High-temperature Glass	3.8 (0–300°C)	1.02	–	–	869
GS-211	Proprietary High-temperature Glass	3.6 (0–300°C)	1.02	–	–	1075
GS-213	Proprietary High-temperature Glass	2.6 (0–300°C)	1.07	–	–	1135
GS-238	Proprietary High-temperature Glass	3.7 (0–300°C)	0.75	(743)	790	1040
EE-2	Calcium Magnesium Aluminosilicate	4.2 (0–300°C)	0.75	(728)	775	970
EE-5	Calcium Magnesium Barium Aluminosilicate	3.1 (0–300°C)	0.75	(768)	815	1065
Atomics International (Rockwell)	Proprietary Glass (on ASM 805 Alumina)	–	0.063-0.076	–	–	830
Chi-Vit Corp.	Aluminosilicate glass (on Ni steel)	~4.5	0.15, 0.30	–	–	–
Pemco-Glidden-Durkee	Li aluminosilicate glaze (on cordierite)	~3	0.008-0.010	–	–	–
	Boron aluminosilicate glaze (on 94% alumina)	~5.5	0.005-0.006	–	–	–
3M 743 Glaze on ASM614	Lead borosilicate (on 96% alumina)	6.5 (40-540°C)	0.71 total	–	–	–
Kyocera GS-3	Glaze (on A473 alumina)	~7.6	0.008/0.63	–	–	–
Ferro Corp RX3638-1	Pb-free, alkali-containing low fire glaze on alumina	7.1 (25–400°C)	–	–	–	–
RX3638-2	Pb-free, alkali-free high fire glaze on alumina	7.7 (25-400°C)	–	–	–	–
Corning GC9606	Magnesium aluminosilicate glass-ceramic	5.7	6.4 (as cut)	–	–	–
GC9608	Lithium aluminosilicate glass-ceramic	~2.0 (0-300°C)	4.5	–	–	–
GC9609	Sodium aluminosilicate glass-ceramic	9.8	–	–	–	–
Schott Glass GC8559	Glass-ceramic	~2 (20-1000°C)	5.0	–	–	–

Table 2-3. Candidate Alumina Materials Received from Various Suppliers

SUBSTRATE IDENTIFICATION		NOMINAL PURITY (%)	METHOD OF PREPARATION	THERMAL EXPANSION COEFF (TEMP RANGE) (10^{-6} PER DEG C)	AVERAGE SURFACE GRAIN SIZE (μm)** [AV SURFACE ROUGHNESS (μm)]*	THICKNESS (mm)
Coors	ADS 96F	96	Dry press	8.1 (25–1000°C)	–	0.63
	ADS 995	99.5	Tape	7.7 (25–1000°C)	1–10 (av 1.1) [~0.35]	0.69
	Refired Large-grain $A\ell_2O_3$	99.3 (before firing)	Tape	~7.3 (25–800°C)	–	0.56
	Vistal 1	99.9 (before firing)	Dry press	8.3 (25–1200°C)	20 (1st firing)†	0.97
	2				36 (2nd firing)†	
	3				80–100 (3rd firing)†	
	4				28 (4th firing)†	
	5				–	
MRC Superstrate	(a)	99.6	Tape	7.3 (25–800°C)	~1.5 [~0.15]	0.63
	(b)	96	Tape		1–4 [0.5–1.0]	
3M	ASM 614[a]	96	Tape	7.9 (25–900°C)	[1.2–1.5]	0.63, 0.89
			Dry press	–	[2.5–3.5]	0.79, 1.09
	ASM 805[a]	99.9	Tape	7.7 (25–900°C)	<1.0 [0.1–0.2]***	0.63
	ASM 805 Refired 1 time	99.9	Tape	7.7 (25–900°C)	10–60 [<0.3]	0.63
	ASM 805 Refired 2 times				[<0.3]	0.63
	ASM 805 Refired 3 times				5–40 [<0.3]	
	ASM 838[a]	99.5	Tape	7.7 (25–900°C)	[0.4–0.6]	0.13, 0.71
	ASM 772[a]	99.5	Tape	7.7 (25–900°C)	[0.5–1.2]	0.25, 1.02
	ASM 777	94	Tape	8.7 (25–900°C)	[1.6–2.0]	0.48
Saxonburg S 697		97.5	Dry press	7.8 (25–900°C)	[1–5]	1.27
Morganite Recrystallized		99.8	Dry press	8.4 (20–1000°C)	–	3.12
	Hilox 961	96	Dry press	8.2 (20–1000°C)	–	1.02, 2.04
Plessey	7231	92	Dry press	7.2 (25–700°C)	–	0.61
	Ceramislik	99.7	Tape	~7.7	3–15 [<0.5]	0.25
Kyocera	A473	96	Tape	~7.6 (40–800°C)	–	0.63
Magneco Electronics		96	Rolled tape	~7.8 (25–900°C)	2–15 [0.5–4.5]	0.63
Comco, Inc.		96	Tape	–	[0.5–2.5]	0.63
		99.5	Tape	–	4–12 [0.5–3]	0.58
Rosenthal USA Limited		96.0	Tape	8.3 (20–1000°C)	–	0.75
		99.5	Tape	8.5 (20–1000°C)	–	0.75
Associated Ceramics		96	Extruded	–	2–5 [0.5–8]	1.2–3.1
				–	[1–6]	2.5

*Average peak-to-valley dimension
**Dimensions of surface features measured in SEM photographs
***Smooth side $\leq 0.1\ \mu$m; rough side ~0.25 μm (average surface roughness)
†See text for discussion
[a]Also provided in various refired conditions

Table 2-4. Miscellaneous Candidate Substrate Materials Received from Various Suppliers

SUBSTRATE IDENTIFICATION		METHOD OF PREPARATION	THERMAL EXPANSION COEFF (TEMP RANGE) (10^{-6} PER DEG C)	AVERAGE SURFACE GRAIN SIZE (μm) [AV SURF ROUGHNESS (μm)]*	THICKNESS (mm)
Honeywell	Mullite ($3\,Al_2O_3 \cdot 2\,SiO_2$)	Rolled Sheet	~5.0	–	1.65–1.78
Kyocera	Z360 Zircon ($ZrO_2 \cdot SiO_2$)	–	~4.7 (40–800°C)	–	1.02
Kyocera	F1330 Forsterite ($2\,MgO \cdot SiO_2$)	–	10.5 (40–400°C)	–	1.32
3M Co.	ASM475 Zircon ($ZrO_2 \cdot SiO_2$)	Dry Press	4.9 (25–900°C)	[4.0–5.0]	0.56
3M Co.	ASM701 Cordierite ($2\,MgO \cdot 2\,Al_2O_3 \cdot 5\,SiO_2$)	Dry Press	3.7 (25–900°C)	[6.5–15]	1.02
3M Co.	ASM665 ($MgO \cdot SiO_2$)	–	8.0 (25–900°C)	–	
Ferro	FB 266M Cordierite	Dry Press	1.8–2.0 (25–1000°C)	–	Cylinder
Union Carbide	Oriented Pyrolytic Graphite	Pyrolytic	2.8 (c) (300–1100°K)	–	0.97, 1.52
Associated Ceramics	Steatite	Pressed	–	[2–6]	2.1
Metsch Refractories	Mullite	Pressed	–	–	1.4–1.8
	Porcelain	Pressed	–	–	1.4–1.8
Saxonburg	Cordierite	Pressed	–	–	1.3

*Average peak-to-valley dimension

addition, if epitaxial growth occurs in the film the characteristics of its surface will also be influenced by crystallographic features resulting from the nature of the growth. In any case, it is important to know the nature and magnitude of the surface irregularities on a substrate. Optical microscopy and photomicrographs, scanning electron microscope (SEM) examination, and surface profilometry are among the methods that were used to characterize these surfaces throughout the contract.

The properties of several different polycrystalline aluminas are listed in Table 2-5. These are the substrate materials used most extensively and characterized most thoroughly during the contract. Included in the table are five different Vistal aluminas, which will be described further below.

SEM examination of the surfaces of the first three aluminas in the table confirmed an earlier observation that the ASM805 substrates exhibited a difference in surface smoothness on opposite sides visible to the unaided eye upon careful examination. The SEM photographs in Figure 2-5 demonstrate the difference quite clearly, with the rough side shown in Figure 2-5a and the smooth side in Figure 2-5b.

All three alumina substrates are microscopically rough, with three-dimensional surface features up to ~3μm in height. Figures 2-6a and 2-6b show the MRC Superstrate and the ADS995 (Coors) surfaces, respectively, at approximately the same magnification and the same viewing angle (45 deg) as the photographs of Figure 2-5. The surface morphology is seen to be similar for the four surfaces, but the surface grain size is not. The average size of the surface grains for the three aluminas, as determined from direct measurements on SEM photographs, is given in Table 2-5.

Surface profilometry, employing a Sloan Dektak, was used to examine and record the surface finish on the fired polycrystalline alumina materials of interest, including those in Table 2-5. This procedure was found useful for the rapid screening of substrate surfaces to provide both a qualitative overall view of the surface finish and a quantitative measure of localized surface features.

The average surface roughness of each of the aluminas in Table 2-5, as measured with the Dektak and expressed as an average vertical peak-to-valley difference, is also included in the table. A large number of other as-fired polycrystalline ceramic substrates (mostly aluminas) obtained from the 3M Company were also characterized by surface profilometry in the second quarter of the program; the results of those measurements are included in the properties that were given in Tables 2-3 and 2-4.

X-ray diffraction analysis of representative samples of three of the polycrystalline aluminas of interest produced some interesting results. Comparison of the principal low-index diffraction line intensities obtained with Cu K-alpha radiation (at 50 KV and 20 mA) for these samples (all of which consist of corundum, or polycrystalline α-alumina, which is trigonal with lattice parameters of $a_o = 4.758\text{Å}$ and $c_o = 12.91\text{Å}$) with those for a standard randomly oriented polycrystalline sample indicated some preferred orientation is present.

Table 2-5. Properties of Several As-fired Polycrystalline Alumina Ceramic Substrate Materials

	ASM 805 (3M) (SMOOTH)	ASM 805 (3M) (ROUGH)	SUPERSTRATE (MRC)	ADS 995 (COORS)	ASM 805 (REFIRED) (3M) (SMOOTH)	ASM 805 (REFIRED) (3M) (ROUGH)	VISTAL (REFIRED) (COORS) 1	2	3	4	5
Al_2O_3 Purity (%)	99.9		99.6	99.5	99.9		99.9	99.9	99.9	99.9	99.9
Surface Crystal Size (μm) – manufacturer's specification	>1.0		~1.5	1–10 (2 av.)	–	–	–	–	–	–	–
Surface Finish as Fired (Microin.*) – manufacturer's specification	1.0–2.0		4–5 max.	8–10	–	–	–	–	–	–	–
Apparent Surface Grain Size (μm) – Meas. in SEM	0.4	0.5	0.8–1.0	1.1	12.5	–	20	36	80–100	28	–
Average Surface Roughness as Vertical Peak-to-valley Dimension (μm) – Meas. with Dektak	≤0.1	~0.25	~0.15	~0.35	≤0.1	~0.26	2.5	3.0	3.5	3.5	–
Camber† (in. per in.) – manufacturer's specification	0.003–0.004		0.003 (max.)	0.002–0.003	–		–	–	–	–	–

*Center-line average

†Measure of surface curvature of wafer, expressed as amount by which minimum separation of parallel plates through which wafer can pass under its own weight exceeds the nominal thickness per unit length.

(a)

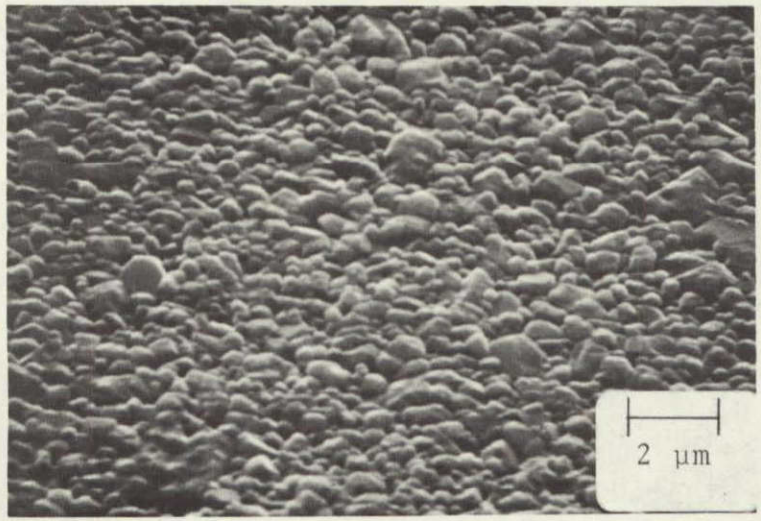

(b)

Figure 2-5. Surface Morphology of ASM805 Fired Alumina Substrate (3M Co.). (a) Rough Side, (b) Smooth Side

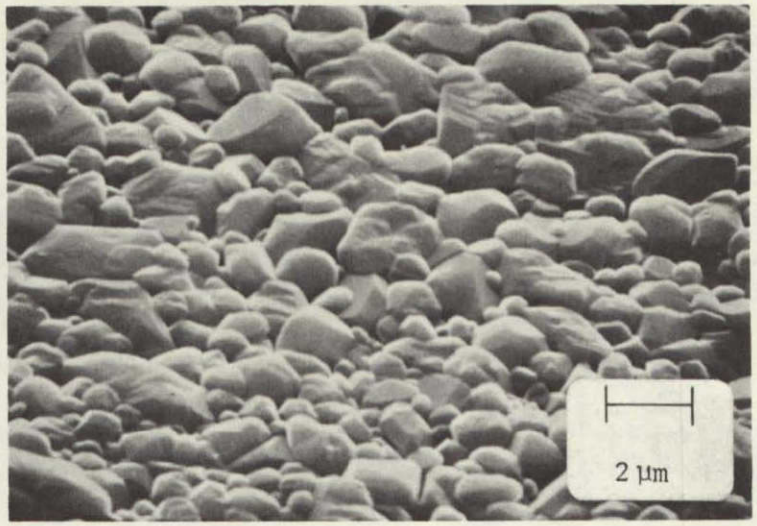

(a)

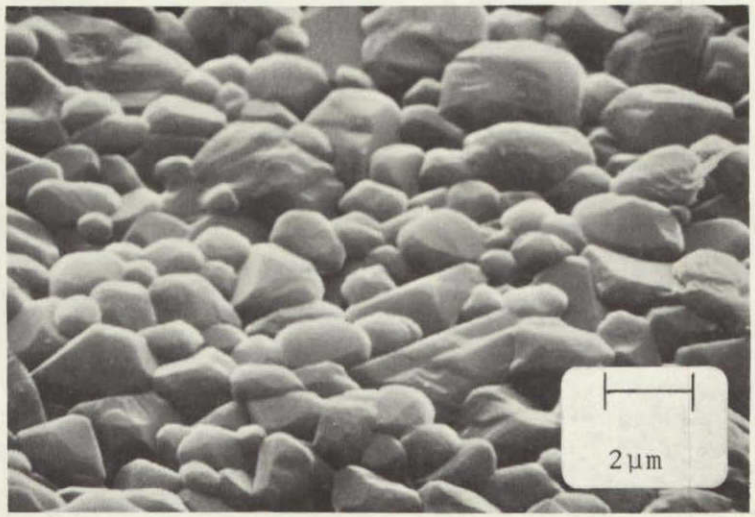

(b)

Figure 2-6. Surface Morphology of Fired Alumina Substrates. (a) MRC Superstrate, (b) ADS995 (Coors)

Specifically, the ADS995 shows the strongest preferred orientation of the three, with a tendency for {10$\bar{1}$4} and {11$\bar{2}$6} planes to align parallel to the surface. The ASM805 also exhibits both {10$\bar{1}$4} and {11$\bar{2}$6} preferential orientation. The Superstrate appears to be the most randomly oriented of the three, although it also has some tendency for {11$\bar{2}$6} planes to be parallel to the surface. In addition, x-ray line-broadening methods were applied to determination of average grain size in some of the substrate materials, but most of the samples examined by this means had grain sizes sufficiently large that no line broadening was observed.

Several substrate materials were prepared by the 3M Company for this program by refiring two of its standard highest-purity aluminas (ASM838 and ASM805) a number of times. The substrates were refired both as isolated single wafers (plates) and in stacked configurations. Optical examination of the stacked substrates showed an "imprint" of some substrates on others, and it was concluded that such stacking during refiring probably would not lead to substrates with uniform grain sizes or other properties, since only the substrate on top of the stack appeared to be similar to the substrates that were fired singly. Therefore, SEM examination was undertaken only on those substrates that were singly fired.

The SEM photographs are shown in Figures 2-7 and 2-8. A comparison of Figure 2-5 with Figure 2-7 indicates that a single refiring causes a major increase in the grain size of ASM805 alumina on both sides of the substrate. ASM838 (Figure 2-8) appears to require several additional refiring cycles before grain sizes similar to those found in refired ASM805 are produced.

Vistal alumina, five different examples of which are listed in Table 2-5, is a large-grained high-purity alumina (99.9 percent) manufactured by Coors Porcelain Company. Each of the five groups of Vistal substrates has a different firing history; these substrates were fired beyond the normal alumina processing by one, two, three, four, and five consecutive firings at $>1800^{o}C$ for six hours each. As a result, five different average grain sizes are achieved.

The SEM photographs in Figure 2-9, which show representative areas of samples of each of the first four Vistal groups in the as-fired condition, illustrate the wide range of grain sizes present in each group; grains from 5μm to over 200μm across can be seen. (The apparent debris on the surface--especially prominent in Figure 2-9c--is caused by incomplete cleaning of the substrate prior to examination in the SEM.) Based on the observed surfaces of these substrate wafers as seen in the SEM it appeared that Vistal 3 had larger grains than did Vistal 4. Counts made on representative samples indicated that the average surface grain sizes listed in Table 2-5 are indeed typical of the as-fired materials. It was later learned that the segregation of smaller crystal grains to the surfaces of this type of ceramic during extended firing is a normal occurrence. Thus, a more accurate observation of true grain size is made after removal of a surface layer, by polishing or other means. This was later done for the Vistals, as they were among the substrates that were polished to improve their surfaces for CVD Si growth. This is discussed further in later sections.

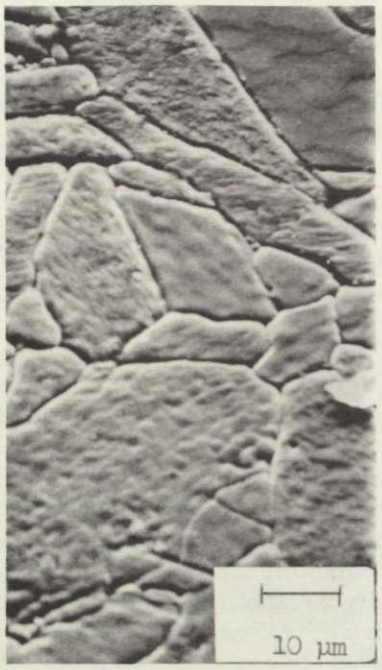

(a)

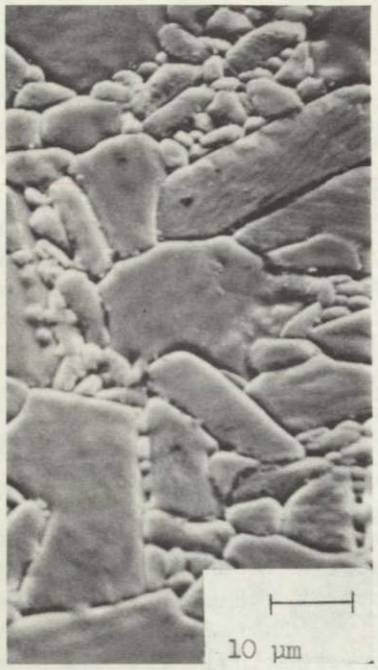

(c)

(b)

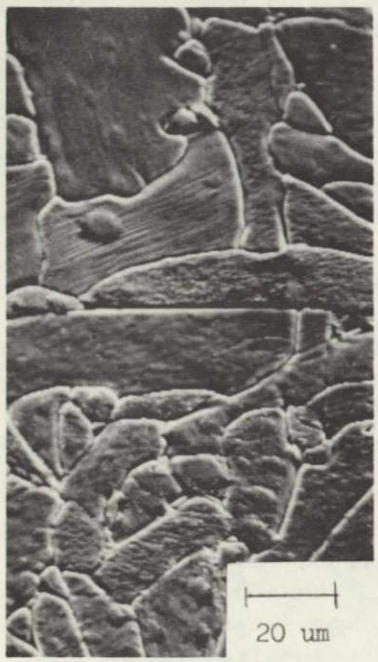

(d)

Figure 2-7. Photographs of Refired ASM805 (3M).
(a) Side a, Refired Singly 1 Time; (b) Side b, Refired Singly 1 Time;
(c) Side a, Refired Singly 3 Times; (d) Side b, Refired Singly 3 Times.

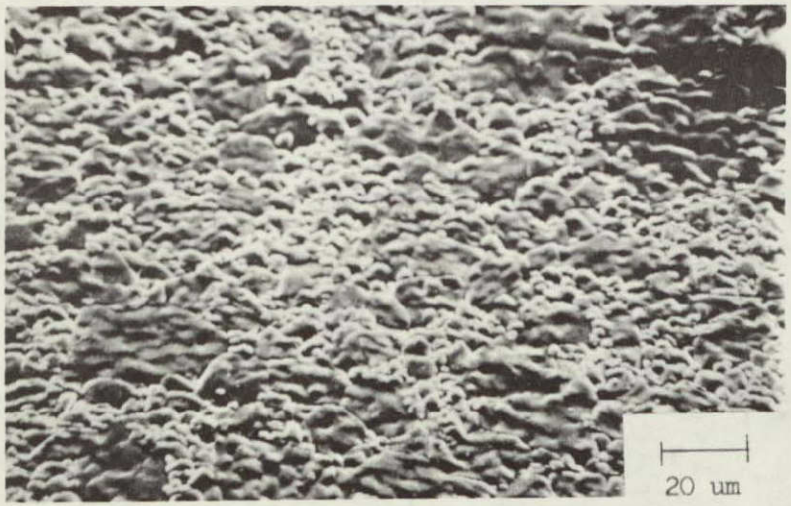

(a)

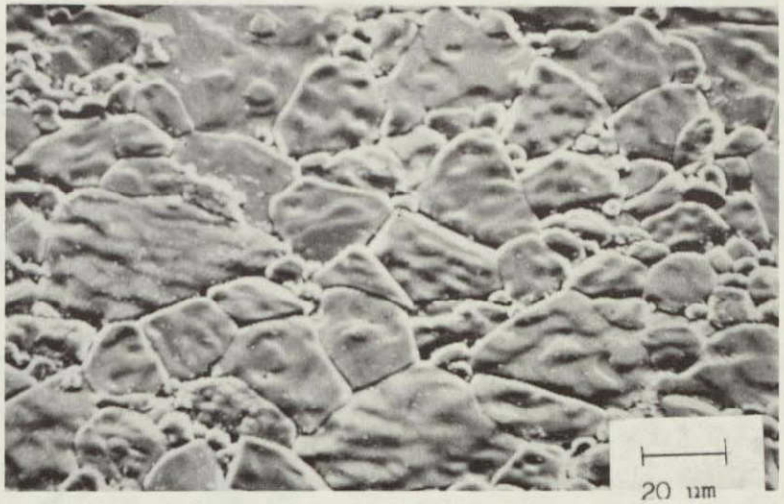

(c)

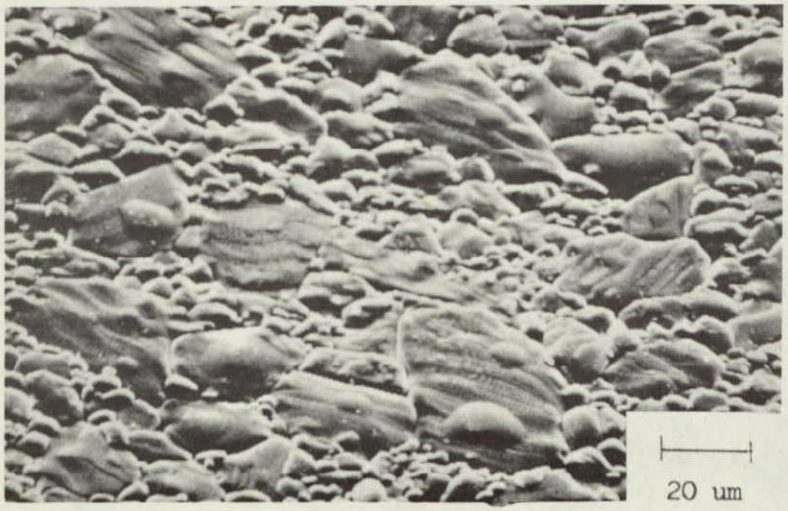

(b)

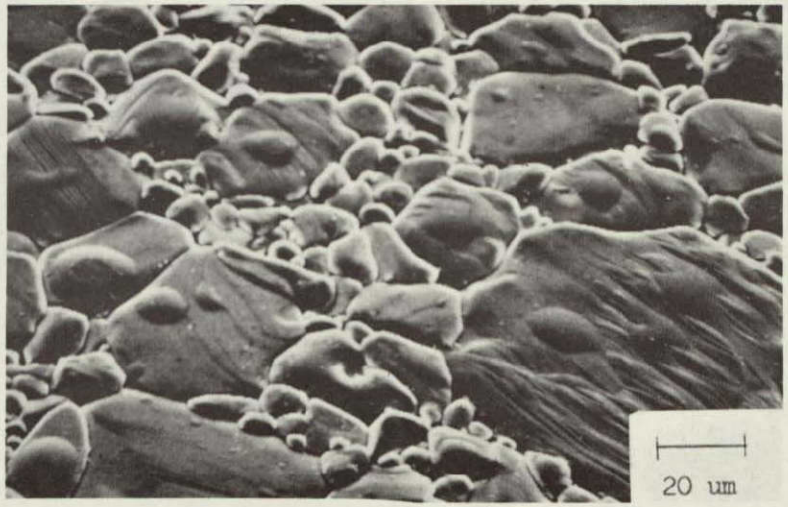

(d)

Figure 2-8. SEM Photographs of Refired ASM838 (3M).
(a) Side a, Refired Singly, 1 Time; (b) Side b, Refired Singly 1 Time;
(c) Side a, Refired Singly 5 Times; (d) Side b, Refired Singly 5 Times.

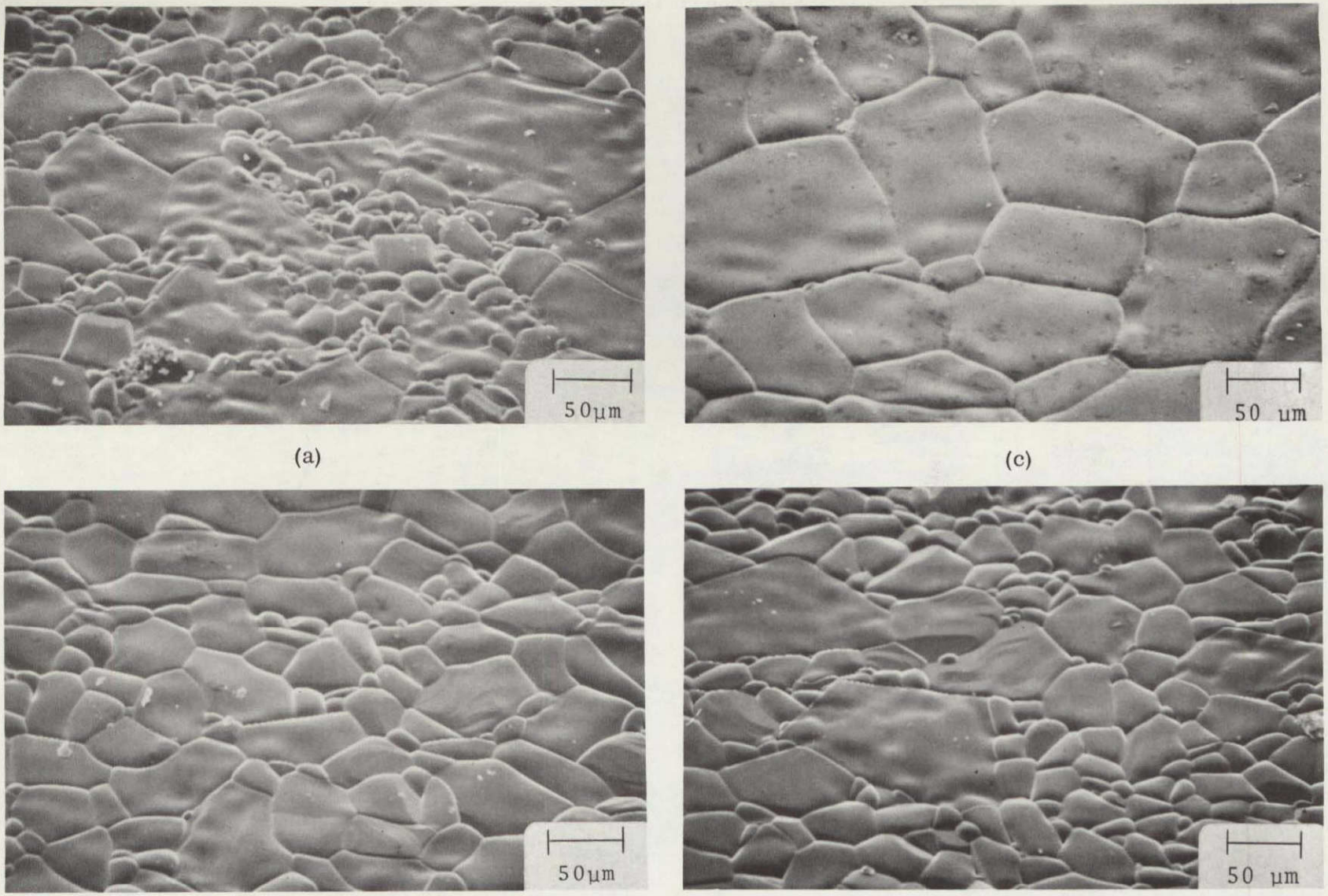

Figure 2-9. SEM Photographs of Vistal Alumina Substrates in As-fired Condition. (a) Vistal 1 (one firing at >1800°C for 6 hr); (b) Vistal 2 (two consecutive firings); (c) Vistal 3 (three consecutive firings); (d) Vistal 4 (four consecutive firings). (All photographs taken at 45 deg viewing angle with sample surface.)

All of the as-fired Vistal substrates exhibited a three-dimensional surface with gently rounded grains projecting less than ~10μm in a vertical direction, as shown in Figure 2-10 for a Vistal 4 (four consecutive firings) substrate. Figure 2-10a is with the sample oriented for the standard viewing angle of 45 deg, while Figure 2-10b shows the same sample (at approximately the same magnification) viewed at a low angle of 25 deg with the sample surface, showing more clearly the height of the individual projecting crystals.

Characterization of other substrate surfaces by SEM examination was carried out at various times during the contract. Analyses of surfaces of two aluminas from the 3M Company produced the photographs shown in Figures 2-11 and 2-12, the former of as-manufactured ASM772 (99.5 percent purity) and the latter of ASM838 (also 99.5 percent purity). In each case the upper view is normal to the substrate surface and the bottom at a 30 deg viewing angle with the surface. Larger and more uniformly-sized grains seem to be present in as-fired ASM772 (Figure 2-11) than in the as-fired ASM838 (Figure 2-12a). The refiring of ASM838 appears to have led to larger grains at the substrate surface, with some size differences apparent on the two sides of the substrate (Figures 2-12c and d, e and f).

Comparisons were also made of the uniformity of the individual grains of alumina (α-Al_2O_3) at the surface of some of the 96 percent (lower cost) aluminas. From Figures 2-13 and 2-14 it can be seen that the grains in as-fired samples of these aluminas vary considerably in size and are relatively large compared with the grains in as-fired ASM772 and ASM838 (Figures 2-11 and 2-12). The material from Kyocera appears to possess larger grains and possibly a higher degree of crystallinity than the others, although the differences in magnification in the figure can be misleading. The mullite (ASM832) also displays a very rough surface consisting of particles of many sizes.

One of the glass-ceramics obtained for use in the program - Corning Code 9606 - was received with its surface polished by the manufacturer, since this material as manufactured has a typical surface too rough for direct use in film growth experiments. Examination of the surface of this material in the SEM revealed at high magnification (1200X) the presence of elongated inclusions or particles on/in the surface, as shown in Figure 2-15. This was noted subsequent to growth of Si films on the glass-ceramic, the growth habits of which are mentioned in later sections. Discussions held with Corning personnel indicated the particles may have been material embedded in the surface during the polishing process and/or merely a residual contamination. Improved surfaces were subsequently obtained when alumina powder was used in place of CeO_2 powder for polishing the glass-ceramic.

The surfaces of the glazed ceramics are usually undulating and sometimes contain pits probably generated at the time of glass solidification. These surfaces were not physically abraded prior to film growth studies.

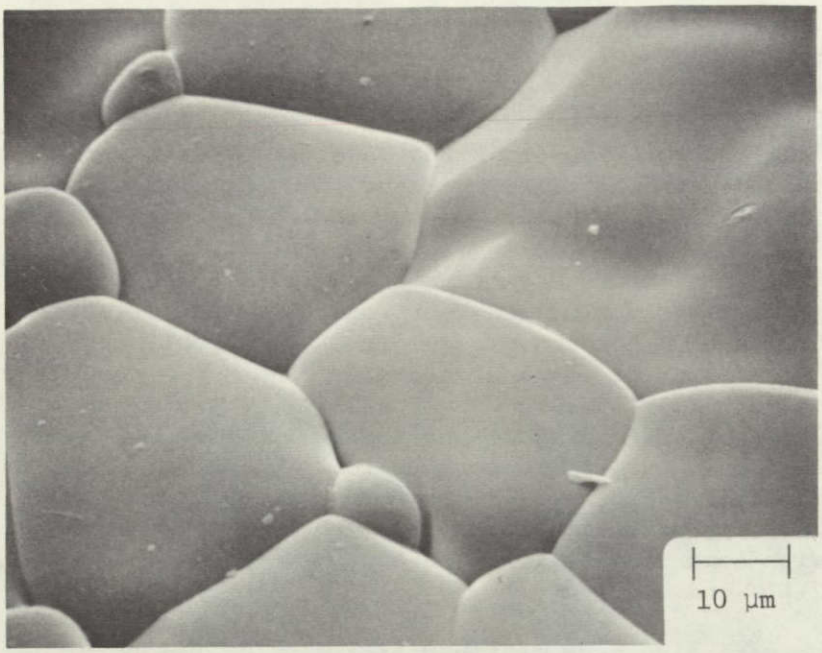

(a)

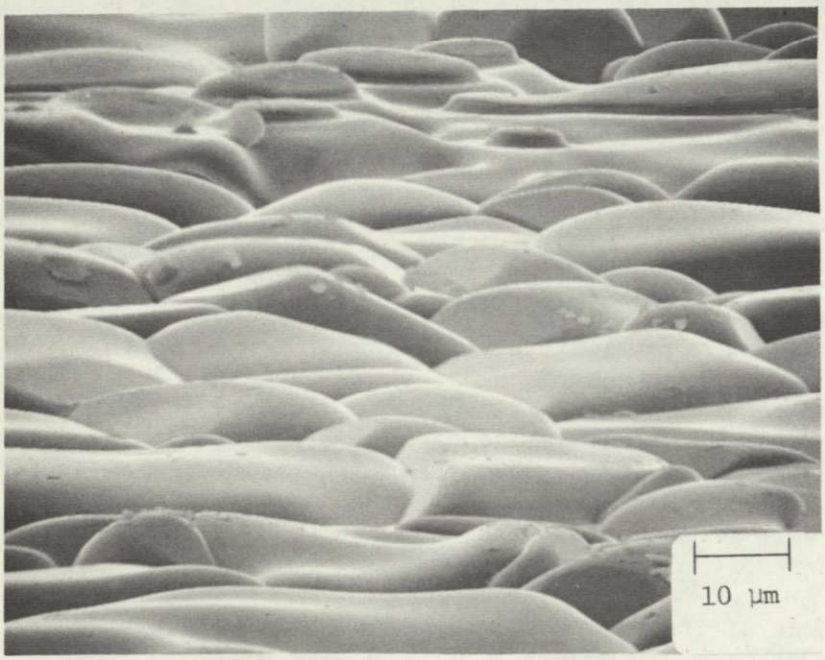

(b)

Figure 2-10. SEM Photographs of Vistal 4 (four consecutive firings) Alumina Substrate Surface in As-fired Condition. (a) Viewing Angle 45 deg; (b) Viewing Angle 25 deg with Sample Surface.

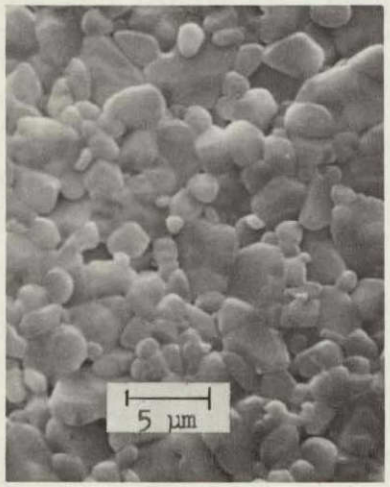

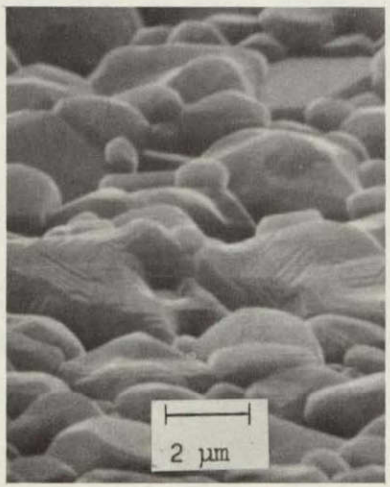

Figure 2-11. SEM Photographs of Surface of As-manufactured ASM772 Alumina (3M Co.). a) Viewed Normal to Surface, b) Viewed at 30 deg with Surface.

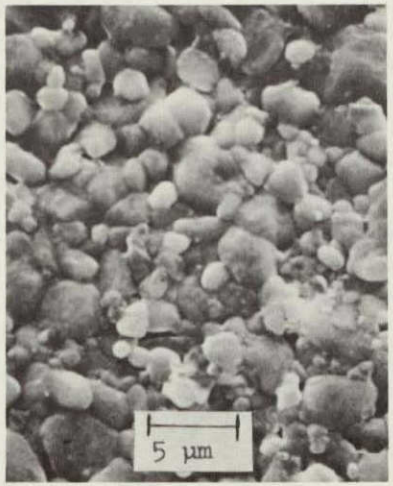

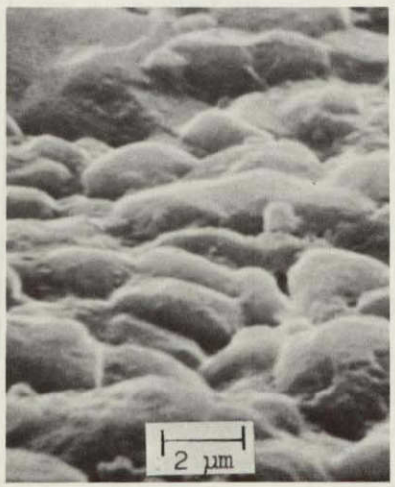

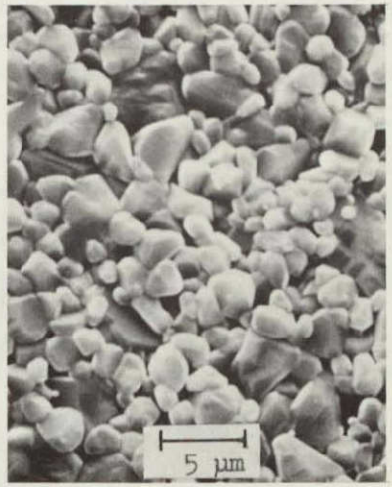

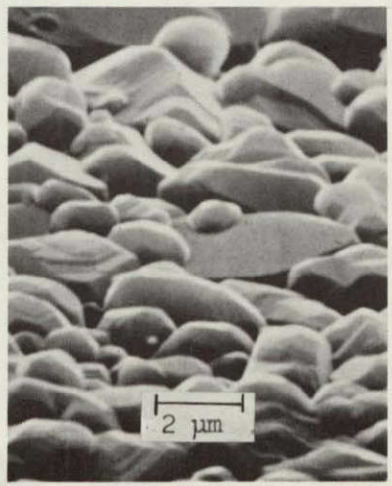

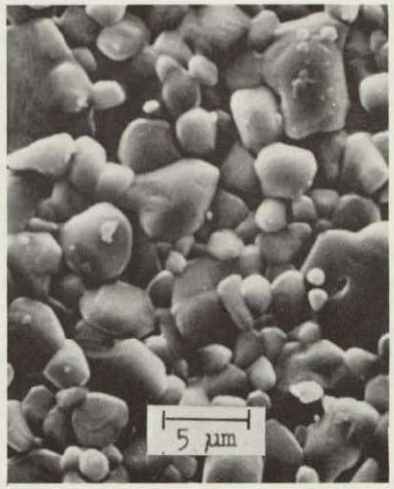

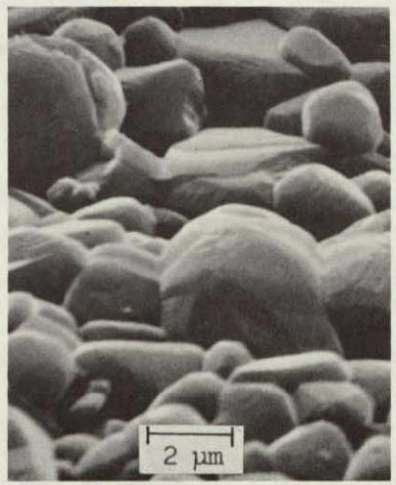

Figure 2-12. SEM Photographs of Surfaces of ASM838 Alumina (3M Co.) in As-manufactured and Refired Conditions. a) As-manufactured, Viewed Normal to Surface; b) As-manufactured, Viewed at 30 deg with Surface; c) Refired, Viewed Normal to Surface of First Side; d) Refired, Viewed at 30 deg with Surface of First Side; e) Refired, Viewed Normal to Surface of Second Side; f) Refired, Viewed at 30 deg with Surface of Second Side.

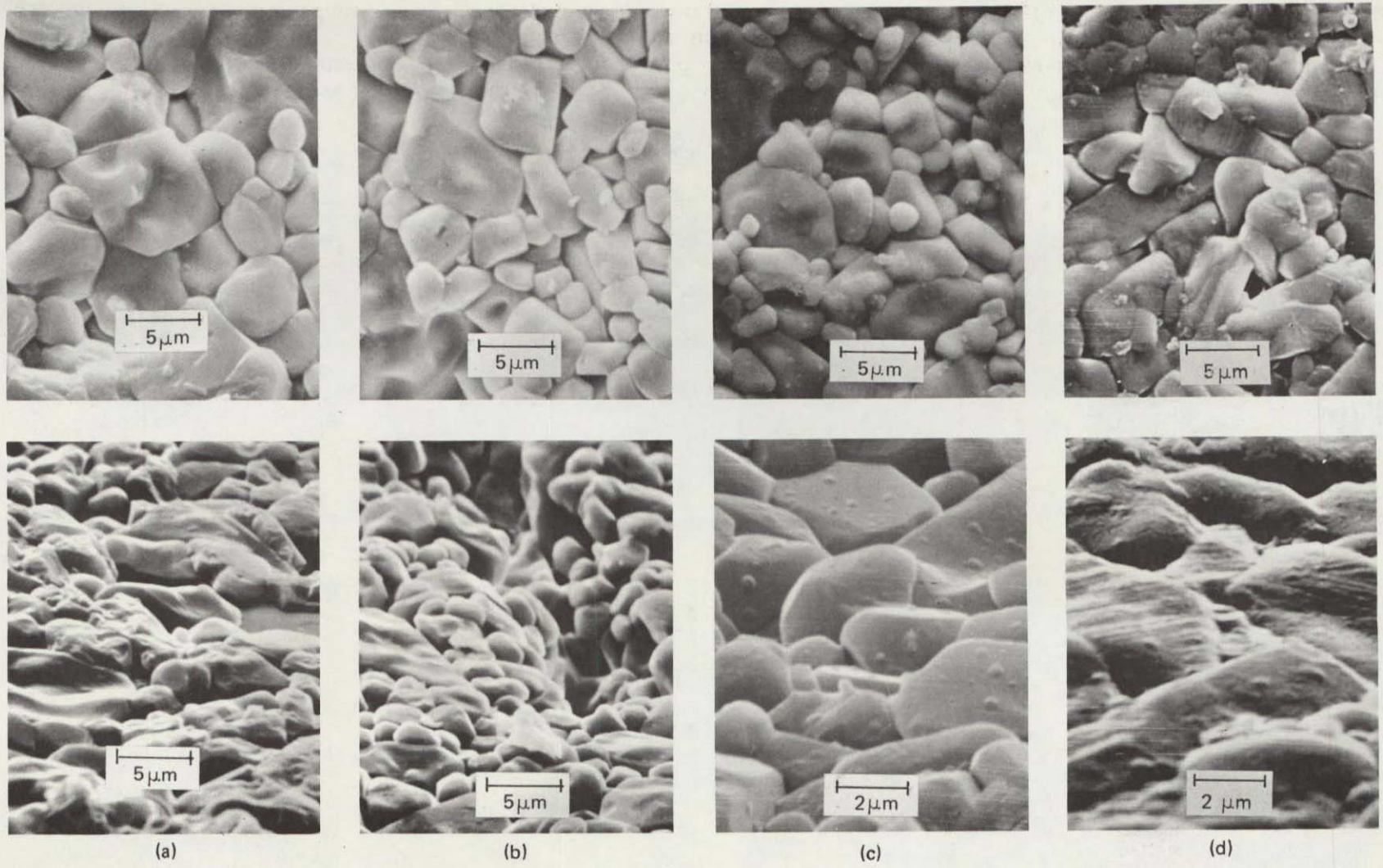

Figure 2-13. SEM Photographs of Commercial Grades of Ceramic Substrates. (a) ASM614 Alumina (3M): Top View at Normal Incidence, Bottom View at 30 deg to Surface; (b) S697 Alumina (Saxonburg): Top View at Normal Incidence, Bottom View at 30 deg to Surface; (c) A476 Alumina (Kyocera - 96%): Top View at Normal Incidence, Bottom View at 30 deg to Surface; (d) ASM832 Mullite (3M): Top View at Normal Incidence, Bottom View at 30 deg to Surface.

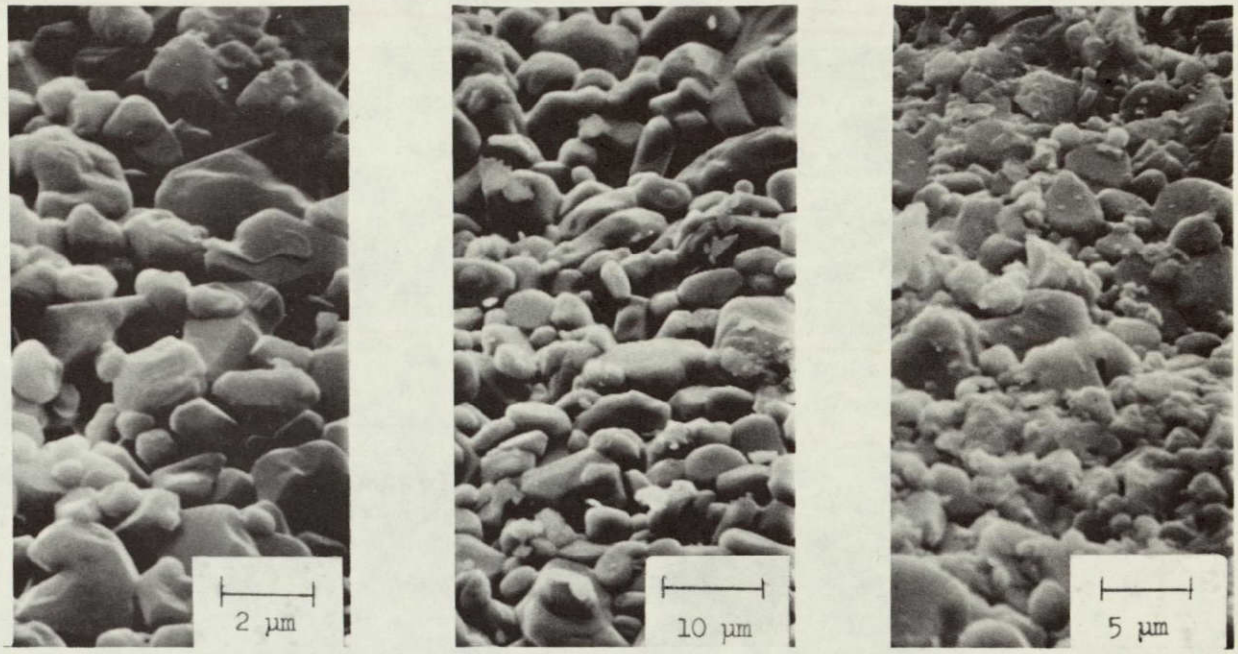

(a) (b) (c)

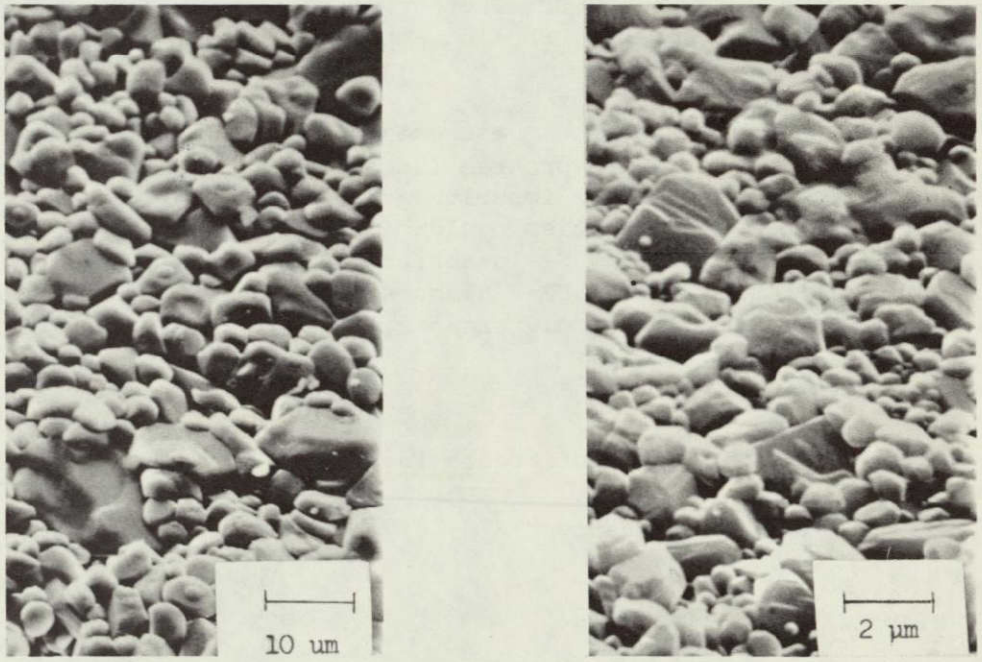

(d) (e)

Figure 2-14. SEM Photographs of Commercial Grades of 96 Percent Alumina. (a) MRC960; (b) Magneco; (c) Associated Ceramics and Technology (Extruded Alumina); (d) Comco 995; (e) Ceramislik (Plessey)

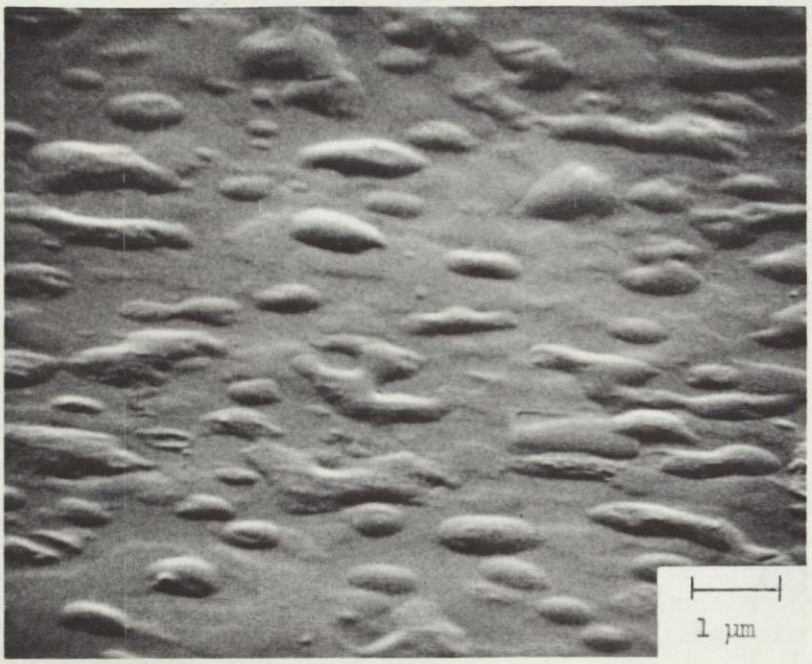

Figure 2-15. SEM Photograph of Surface of Corning Code 9606 Glass-ceramic, Showing Apparent Inclusions on/in Surface.

Since spreading resistance measurements on CVD Si films grown on several of the glasses used in this program (see Section 2.3.9) suggested the presence of an electrically-active impurity at the Si-glass interface, it was decided to determine what impurities could be found by spectrochemical analysis of several of the glasses. Semiquantitative analysis of Corning Code 1715, Owens-Illinois GS213 and EE-2 glasses, and Corning Code 9606 glass-ceramic showed major composition differences, as indicated in Table 2-6.

Table 2-6. Major Constituents in Several Glass Substrate Materials

Glass Designation*	Major Elements Present**
A	Si, Ca, Aℓ
C	Si, Ca, Aℓ, Ti, Pb, Zr
D	Si, Ca, Aℓ, Mg
E	Si, Aℓ, Mg, Ti

*Vendors requested that specific compositions of certain glasses supplied for experimental evaluation not be revealed publicly, so glasses are identified by letter code only.

**As oxides in concentrations exceeding 1 percent.

As many as 17 different elements (as oxides) were listed in the analyses for these four glasses; some elements major in one glass were not even detected in others. In addition to the major elements listed in the table chemical impurities such as Sr, As, Fe, B, Mn, Ga, W, Cu, Ag, Sr and Ni were detected. In some glasses Sr, As, B, and Fe are present (as oxides) in concentrations as high as 0.3 percent. Because Si formation from SiH_4 depends on pyrolysis to form the element, contamination from the substrate is probably minimized compared with that obtained in a halide Si deposition process in which etching may occur; there may be little or no relation between such impurities in the substrate and impurities that may be found in the film. Studies are needed to establish such correlations for various glass substrates used in Si CVD growth experiments; it was not possible to include such investigations in this contract program.

2.2.5 Substrate Surface Preparation

The condition of the substrate surface strongly affects the properties of the film grown on that surface. In many cases the properties obtained in as-manufactured substrates, even though not optimum, are sufficient for the intended application. For substrates to be low in cost, a minimum of surface preparation is preferred. For glasses, a nascent as-produced surface can be flat, uniform, and clean. For aluminas, the as-fired surfaces have been (in most cases) grossly rough compared with those on the glasses, yet Si films grown on some of the as-fired aluminas have had surface characteristics similar to those obtained on polished aluminas, as is discussed later.

However, many of the glasses evaluated in this program were not "run-of-the-mill" glasses, but were specially processed into substrates with polished surfaces. These surfaces were then handled and contaminated, by fingerprints, oils, less-than-electronic-grade water, embedded polishing agents, and other impurities, and therefore had to be cleaned before use. The manufacturers of the glasses suggested that acids and bases not be used in cleaning processes; what might be good for cleaning one glass of a given composition is not necessarily good for cleaning another. This dilemma led early in the program to the use of only organic solvents as cleaning agents in the surface preparation of the glasses used for Si CVD experiments. Also, in the absence of an extensive investigation of possible organic solvents, the reagents used were trichloroethane, acetone, and Freon, in that order.

Experimentation showed that most of the glass substrates appeared to be contaminating the Si films grown on the companion sapphire substrates, as is discussed further in later sections. It is not known if this apparent contamination was the result of dirty surfaces, decomposition of the substrates, or some reaction of the substrates with the Si deposit - especially in regions where the Si film was relatively thin.

Any non-organic chemicals used in cleaning a glass substrate surface may also change it by leaving a residual film or etching the surface; this might even provide a surface that enhances nucleation and larger grain growth. Consequently, part of the standard procedure used for cleaning sapphire substrates

was then tested on the glasses being used for Si growth. The cleaning procedure as applied to the glasses involved first the "standard" organic cleaning followed by hot H_2O_2:H_2SO_4, hot $HC\ell$:H_2O_2:$6H_2O$, and H_2O rinses. SEM photographs of the glass surfaces indicated no observable differences between the acid-treated surfaces and those only organically cleaned. Thin films of Si grown simultaneously on glass surfaces cleaned both ways also showed no detectable differences in adherence or other gross properties. Therefore, as a precautionary measure, the acid-cleaning method was used routinely thereafter for glasses that were shown to be stable to the method.

In order to obtain an indication of the probable condition of the glass surfaces just prior to Si deposition, several glasses were exposed to flowing He carrier gas for 15 min at deposition temperatures (~850-900°C). Four glasses from Owens-Illinois and one from Corning were used. SEM examination of the surfaces of the glass samples after this exposure and of the surfaces of other parts of the same original wafers that had not been subjected to the He treatment indicated little, if any, change in the surfaces of GS211, GS213, GS186, and Corning Code 1715 glasses.

The surface of Owens-Illinois GS210 may have been improved by the annealing; the lapped back surface of the GS210 sample (which was in direct contact with the SiC-covered carbon pedestal) actually became much smoother during this annealing period. SEM photographs of the GS210 surfaces with and without the anneal are shown in Figure 2-16. These results are consistent with the fact that GS210 has the lowest softening point (869°C) of the glasses evaluated. (Unfortunately, Owens-Illinois did not provide strain and annealing temperature data for the glasses it supplied for use in this program.)

The SEM examinations also showed that the poorest polished surfaces were those found in certain areas of the Corning Code 1715 samples, as shown in Figure 2-17. Holes, scratches, and grooved areas were sufficiently prevalent to affect light scattering from the surface when viewed with the naked eye. The Corning glass-ceramic Code 9606 also possessed defective surfaces, as indicated earlier (Figure 2-15).

The polycrystalline aluminas were also given a sapphire surface cleaning treatment before use. These lower-purity materials may be reactive to the cleaning procedure used for sapphire, and the reagents used may not have been completely removed at times from the crevices and other defects on the ceramic surfaces. In any case, the aluminas tested were found on occasion to move about on the pedestal surface during the pre-deposition heating period, to impart a yellow-orange color to the burning H_2 exhaust flame, and to contaminate neighboring sapphire substrates.

Because of the rough surfaces on the as-fired aluminas and on some of the other ceramic materials (Tables 2-3 and 2-4) obtained from various manufacturers, several groups of substrates from among those listed were selected for mechanical polishing. The purpose of this polishing procedure was twofold. First, polishing generates smooth surfaces on the substrates and thus results in smoother film surfaces, and yet retains benefits to the Si sheet nucleation

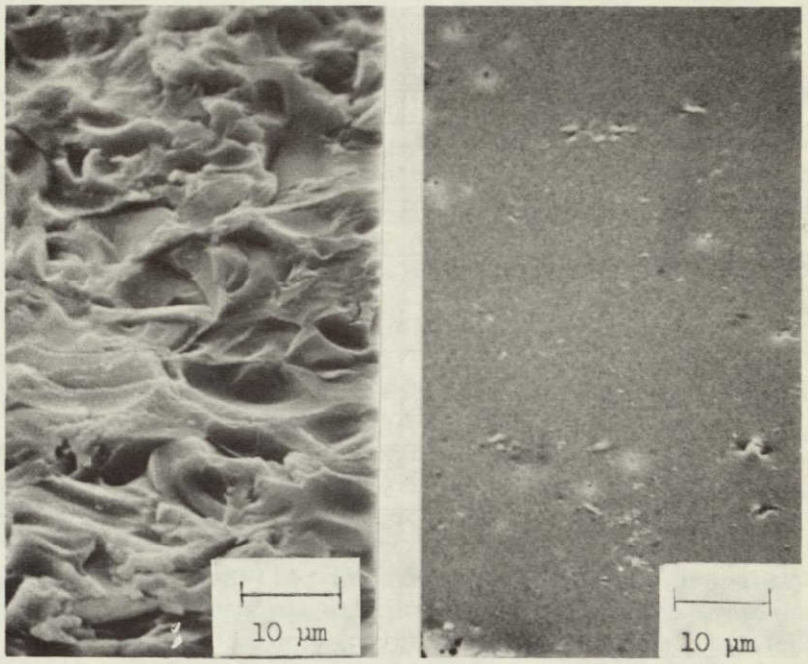

Figure 2-16. SEM Photographs of Back of Owens-Illinois GS210 Glass Wafer, a) As Supplied by Manufacturer and b) after Anneal in He at 850-900°C (in contact with sample pedestal).

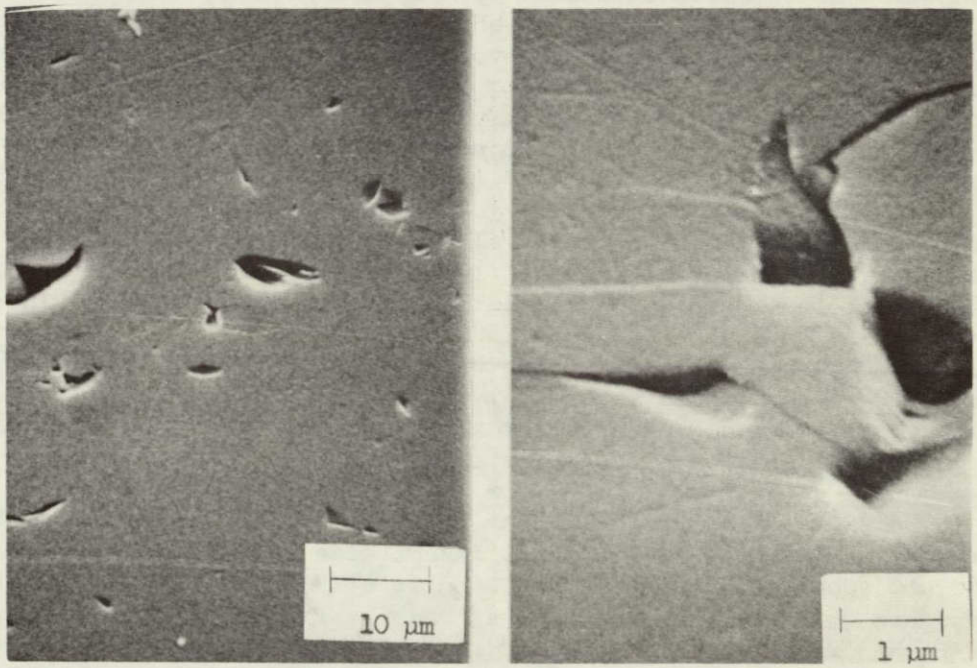

Figure 2-17. SEM Photographs of Surface of Corning Code 1715 Glass, as Polished by Corning, at Two Magnifications.

and growth process that accrue from the presence of the substrate crystal grains that intersect the mechanically generated surface.

Second, simultaneous Si CVD growth experiments on polished and as-fired polycrystalline substrates were considered important in the early part of the program. The actual growth facets of an as-fired polycrystalline substrate are not--on the average--in the same crystallographic orientations as those that are delineated in x-ray analyses for preferred orientation in the substrate materials. This is because the crystal planes so identified are referenced to the nominal surface plane of the substrate wafer as it is mounted for x-ray analysis; that is, the planes identified as preferred orientations in the substrate are parallel to the nominal wafer surface, but the growth facets are nearly all at appreciable angles to this plane. Thus, to establish correlations between substrate preferred orientations and the observed Si film habit it is necessary to grow Si on a polished surface coinciding with the nominal substrate surface.

Results of Si sheet growth experiments on polished substrates also helped to determine a reasonable balance between the increased cost of preparing substrates using this additional processing step and the expected improvement in the surface characteristics (and perhaps internal structure) of the resulting polycrystalline Si films.

Only in the case of the highest purity aluminas ($\geq$99.5 percent) was surface pitting not observed at low optical magnification. Even in those materials, however, it was observed upon examination in the SEM. Small voids (pits) were typically found in MRC Superstrate aluminas and in the highest-purity aluminas from other manufacturers - such as ASM772 and ASM838 from 3M Company and ADS995 from Coors Porcelain, as shown in Figure 2-18. The lower the purity, the greater the size of the voids and the coarser the structure, generally. In Figure 2-19 Saxonburg S697 (97 percent) appears to be slightly more compact than ASM614 (96 percent, dry press) from 3M, and the latter has smaller crystals than ASM614ASB (96 percent, tape process), both as-manufactured and refired.

Substrate wafers of the high-purity aluminas ASM805, MRC Superstrate, and Vistal, as well as other aluminas of lower purity, plus zircon, mullite, and cordierite were polished for use in Si film growth experiments. In most instances the wafers were lapped with Microgrit (12μm alumina abrasive compound) and the polishing was done with Syton (Monsanto). A few of the substrates were not lapped first--only polished with Syton--but the removal rate was very low. In general, approximately a 1-mil thickness of material was removed in the Syton polishing step.

From Figure 2-20, it can be seen that polished zircon (ASM475 from 3M) consists of grains of a number of different sizes (1-20μm across) in a binder that is not specifically identified. Mullite (Figure 2-20b and c) shows a more uniform grain size and structure than the zircon, but the grains again appear to be dispersed in a "sea" of some material that appears non-crystalline. Polished cordierite (ASM701 from 3M) shows very little grain structure, with some irregular pits in the surface (Figure 2-20d). It is not known how these pits are generated.

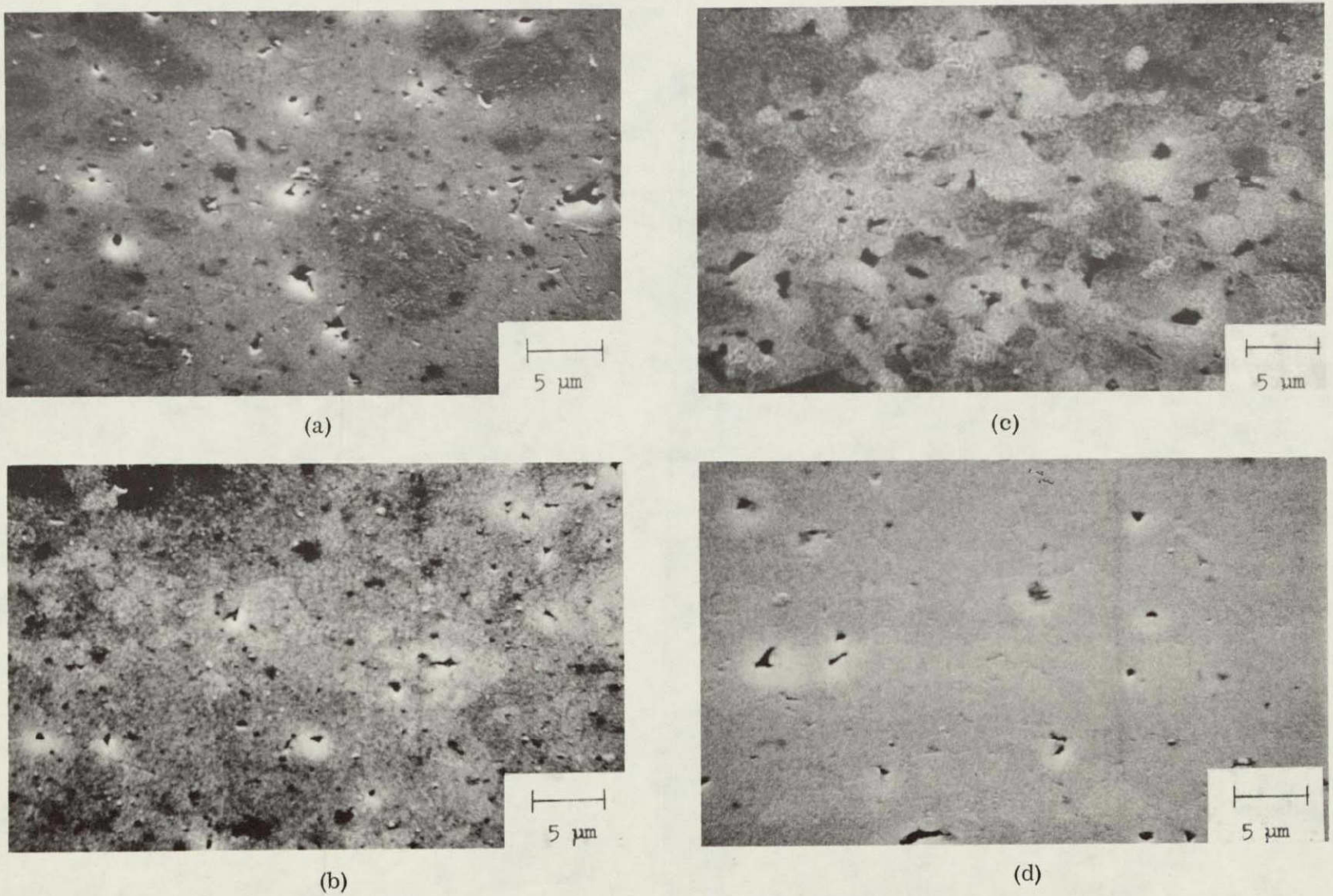

Figure 2-18. SEM Photographs of Polished Commercial Grades of 99+ Percent Alumina. (a) ASM838, as-fired (3M); (b) ASM838 Refired (3M); (c) ADS772, as-fired (3M); (d) ADS995, as-fired (Coors).

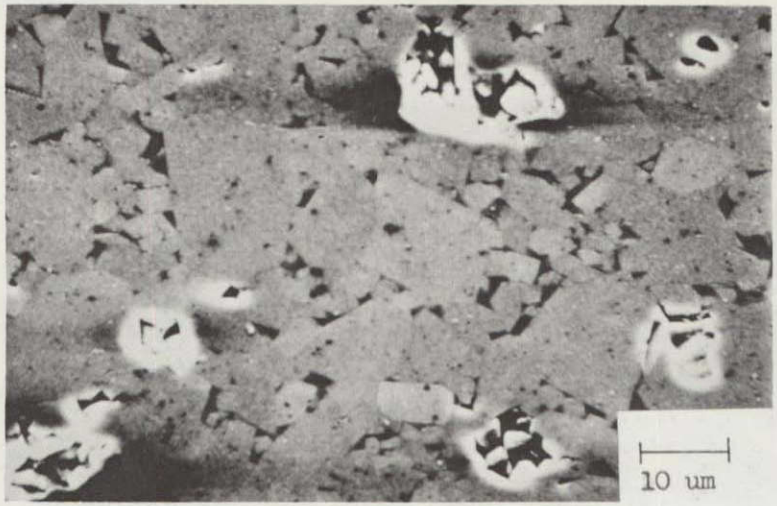

(a)

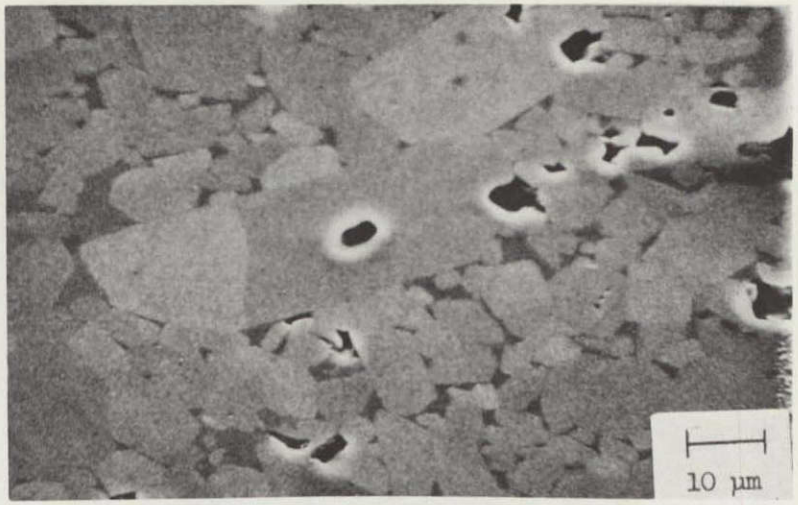

(c)

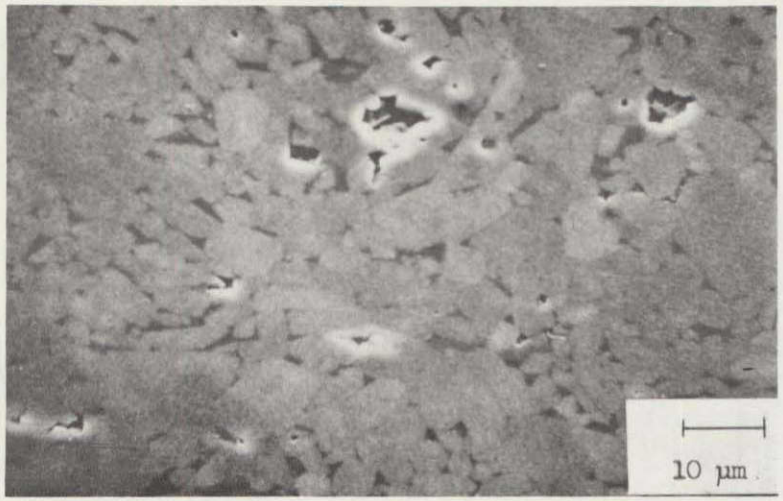

(b)

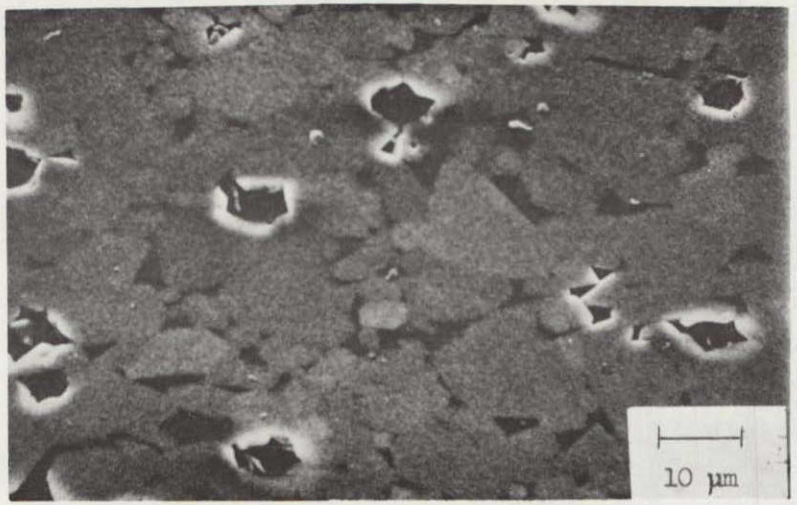

(d)

Figure 2-19. SEM Photographs of Polished Commercial Grades of 96-97 Percent Alumina. (a) S697 (Saxonburg); (b) ASM614, Dry Press (3M); (c) ASM614ASB (3M); (d) ASM614ASB, Refired (3M).

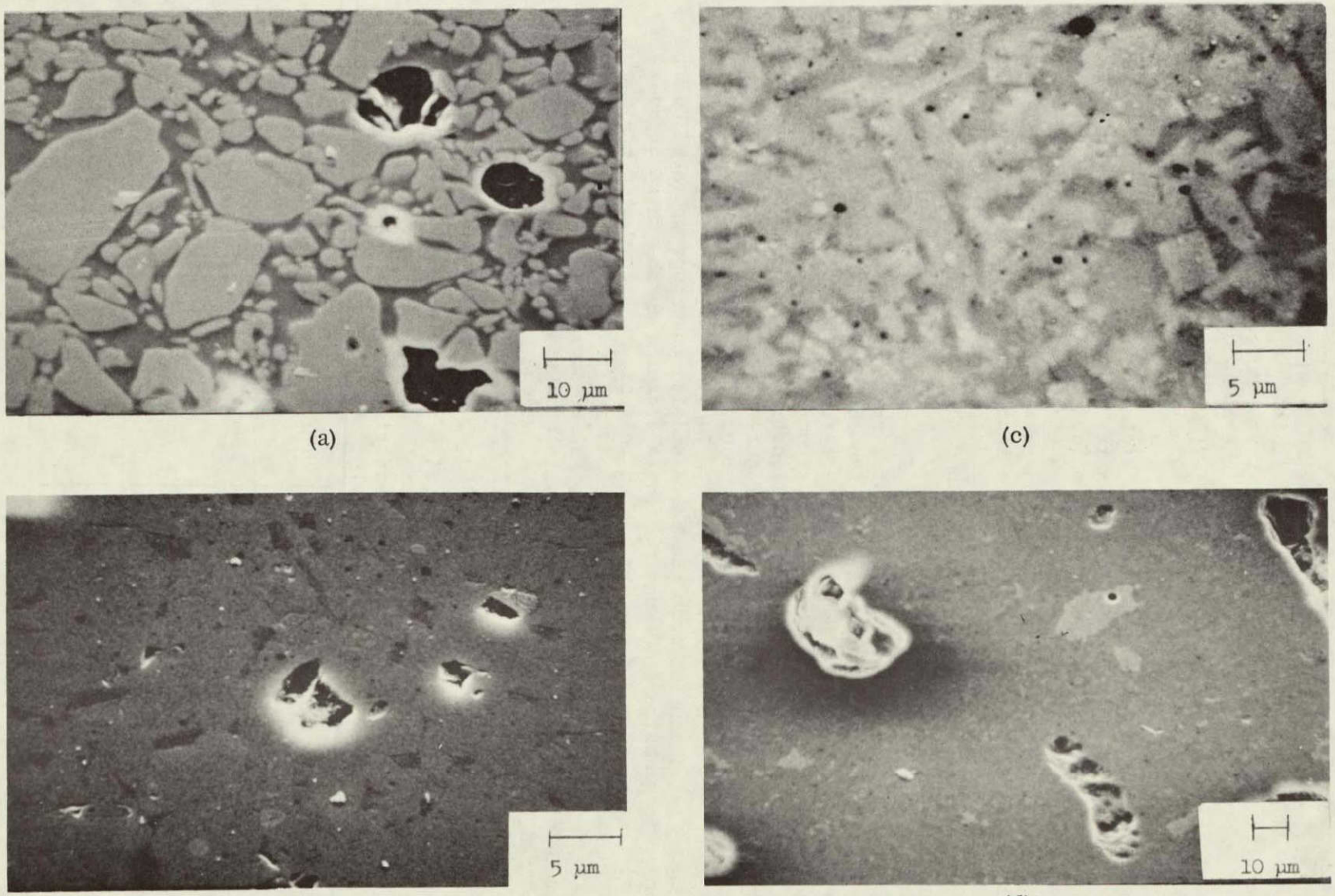

Figure 2-20. SEM Photographs of Polished Zircon, Mullite and Cordierite.
(a) ASM475 Zircon (3M); (b) ASM832 Mullite (3M); (c) Mullite (Honeywell); (d) ASM701 Cordierite (3M).

One batch of Vistal substrates, including several samples of each of the four shorter firing histories, was lapped for 10 hr with a slurry of 5μm SiC particles to produce a flat fine-lapped finish. Prominent irregular crevices intersecting the lapped surfaces on the four samples clearly delineated the range of grain sizes that resulted from the consecutive firings, even without any chemical etching. Surface photomicrographs of each of the four lapped surfaces are shown in Figure 2-21.

A comparison of profilometer traces for Vistal substrates in the as-fired, lapped, and polished conditions is shown in Figure 2-22 for material with one and two firings and in Figure 2-23 for material with three and four firings. In each case the horizontal scale is such that one major chart division corresponds to a distance of 0.2mm along the sample surface. These figures show the expected improvement in surface smoothness resulting from lapping and polishing, but also clearly show the deep crevices between neighboring crystal grains in the lapped condition and the shallow but finite steps between grains in the polished condition.

The surfaces of polished Vistal substrates from each of the four groups Vistal 1 through Vistal 4 are shown in the optical photomicrographs of Figure 2-24, made with the Nomarski interference-contrast objective on the microscope. These photographs show in strong relief the individual crystal grains in each of the four groups and illustrate clearly a progression in grain size from Vistal 1 to Vistal 4 (Figures 2-24a to 2-24d). The polished Vistal 4 substrate shows the largest average grain size and more uniform distribution of large grains. During the lapping stage, however, it was noted that Vistal samples from the third and fourth groups appeared to have similar grain sizes, and in some regions the grains in the third group appeared larger, as noted earlier. When polishing was completed the photomicrographs of the surfaces of the polished substrates (Figure 2-24) clearly delineated the apparent grain boundaries at the surface, and at this stage the sample of the fourth group appeared to have significantly larger individual grains than that of the third group. The average apparent grain size observed in the surfaces of the four Vistals in the polished condition, measured by SEM examination, is given in Table 2-7.

Table 2-7. Average Apparent Grain Size of Several Polished Polycrystalline Alumina Substrate Materials as Measured on Sample Surfaces by SEM Examination.

Substrate Material	Ave Grain Size at Surface of Polished Material (μm)
Vistal 1 (Coors)	35
Vistal 2 (Coors)	74
Vistal 3 (Coors)	70
Vistal 4 (Coors)	>120
Superstrate (MRC)	~1.5

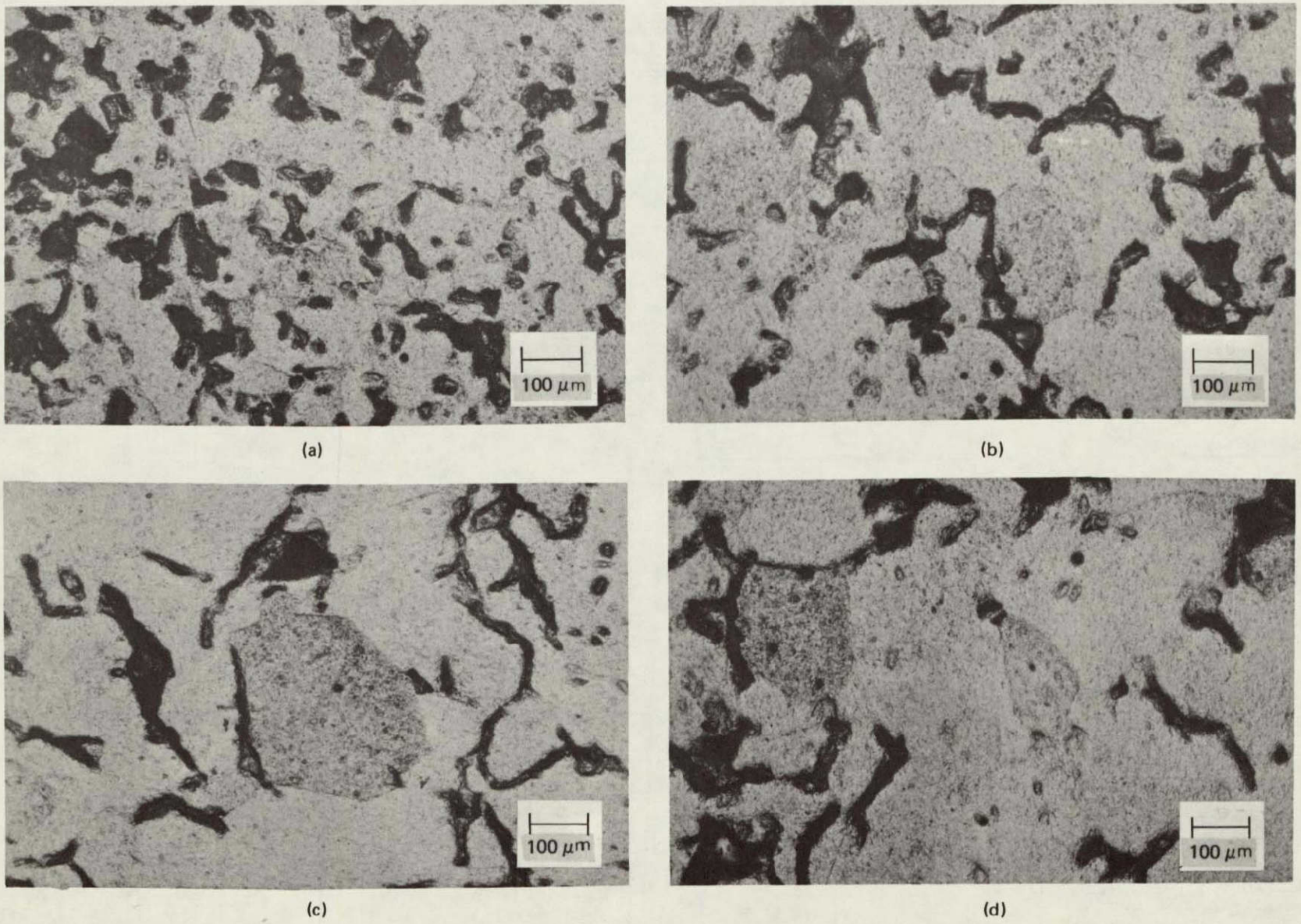

Figure 2-21. Surfaces of Four Vistal (Coors) Polycrystalline Alumina Substrates after Successive Firings Above 1800°C for 6 Hr.
(a) One, (b) Two, (c) Three, (d) Four Firings

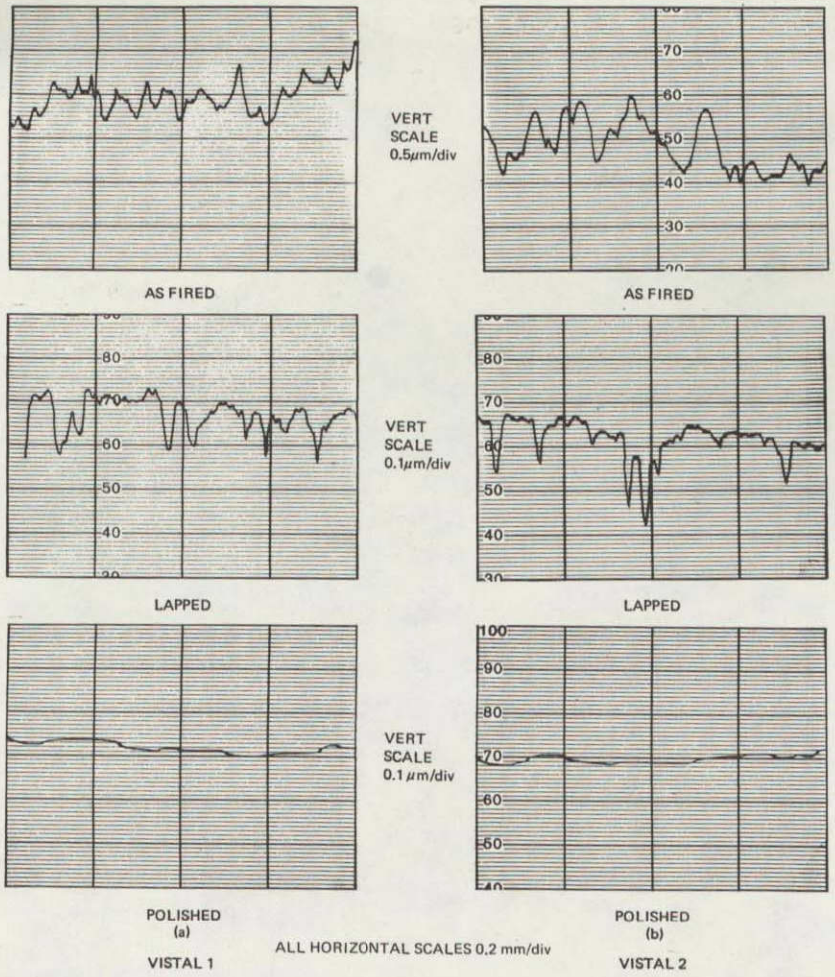

Figure 2-22. Dektak Profilometer Traces of Surfaces of Vistal Polycrystalline Alumina Substrates at Three Stages of Preparation. (a) Vistal 1 (one firing at >1800°C for 6 hr); (b) Vistal 2 (two consecutive firings).

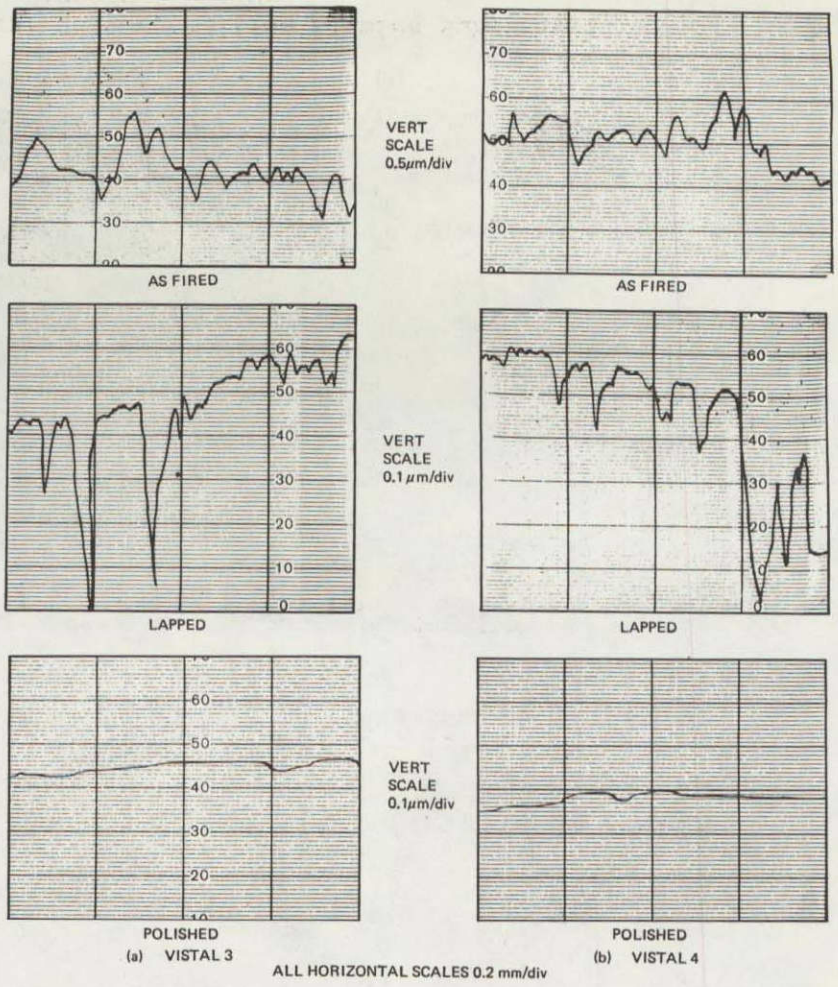

Figure 2-23. Dektak Profilometer Traces of Surfaces of Vistal Polycrystalline Alumina Substrates at Three Stages of Preparation. (a) Vistal 3 (three consecutive firings at >1800°C for 6 hr); (b) Vistal 4 (four consecutive firings).

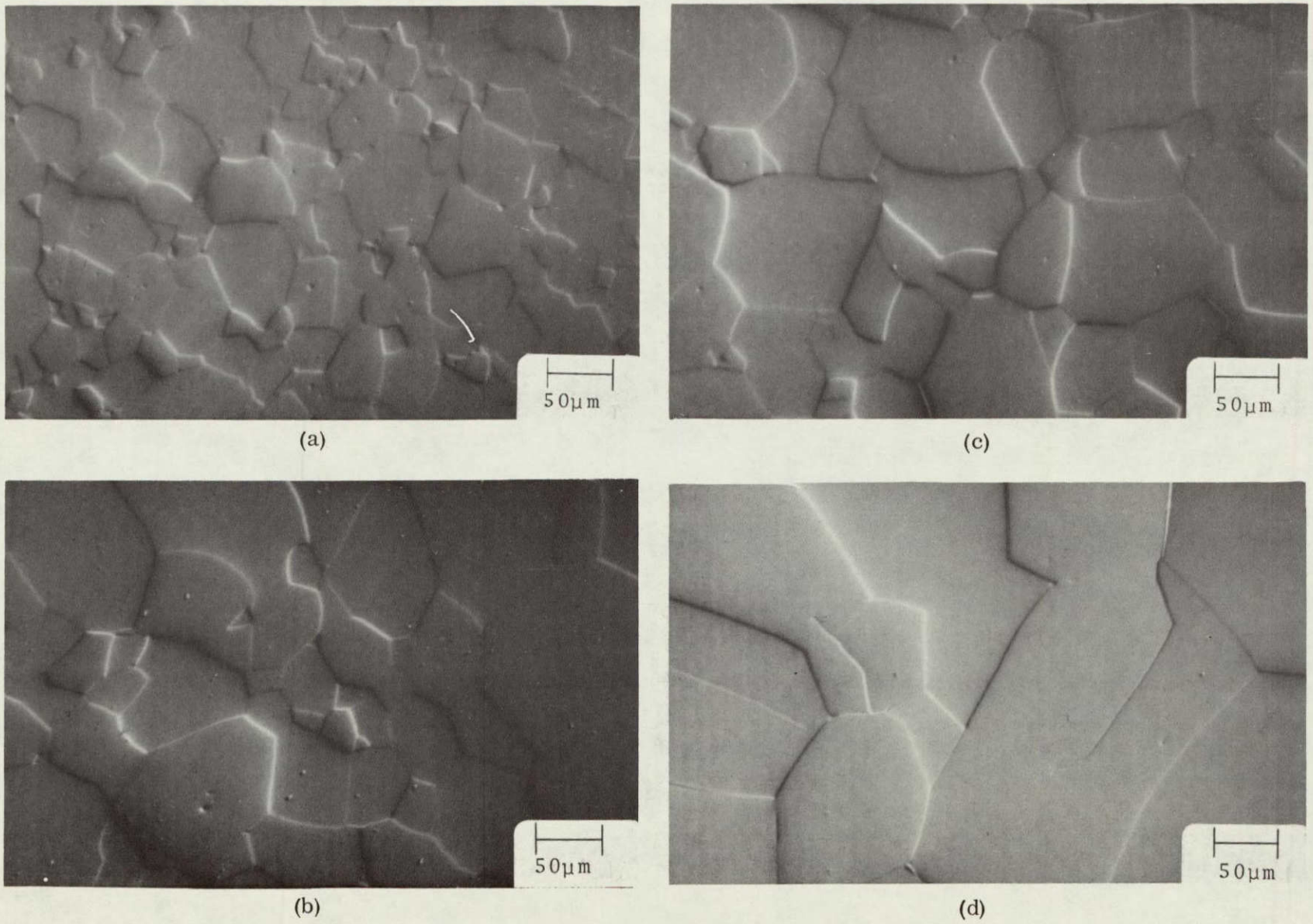

Figure 2-24. Nomarski Interference-contrast Photomicrographs of Surfaces of Polished Vistal Alumina Substrates of Four Different Firing Histories. (a) Vistal 1 (one firing at >1800°C for 6 hr); (b) Vistal 2 (two consecutive firings); (c) Vistal 3 (three consecutive firings); (d) Vistal 4 (four consecutive firings). (All photographs at normal incidence.)

(a)

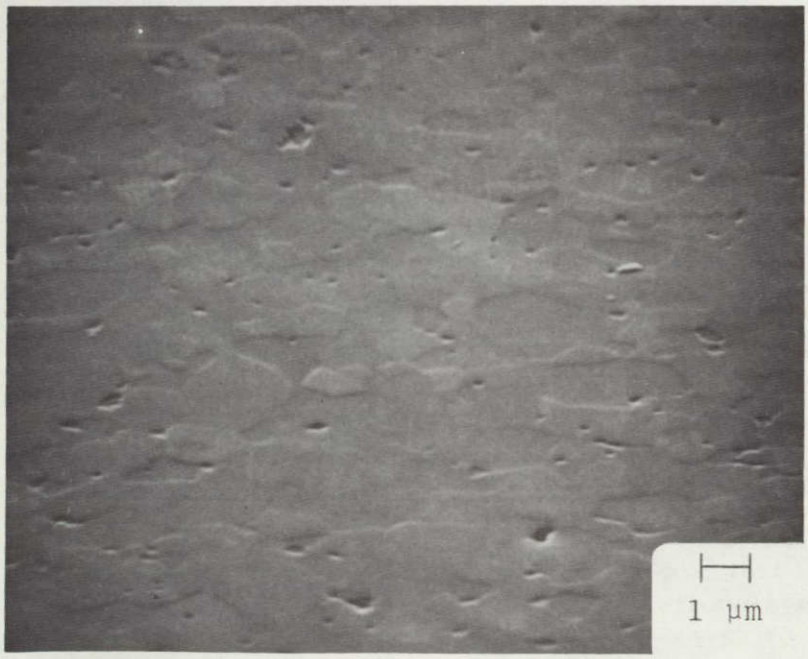

(b)

Figure 2-25. SEM Photographs of Surface of MRC Superstrate Polycrystallin Alumina Substrate, Viewed at 30 deg Angle with Sample Surface. (a) As-fir (b) Polished.

The surface of MRC Superstrate, an alumina of 99.6 percent purity, is shown in both the as-fired and the polished condition in Figure 2-25. Both surfaces are quite different from the corresponding surfaces on any of the Vistal aluminas. First, the apparent average grain size is considerably smaller than that of Vistal 1 (the smallest-grained of the Vistal series), averaging about 1μm. Second, the Superstrate exhibits numerous grain boundary voids that show up especially in the polished surface (Figure 2-25b). Apart from the grain size itself, the presence of such voids makes it difficult to achieve adequate cleaning (and drying) of these substrates prior to use in deposition experiments. The average value for grain size in this polished material also is given in Table 2-7.

2.2.6 Substrate Costs and Related Considerations

The probable cost of a candidate substrate material produced and used in large quantities in the 1986 time frame is an important factor in determining the ultimate feasibility of that material as the support for the CVD Si sheet used in terrestrial solar arrays. It has been difficult to obtain meaningful cost estimates in the present-day market for some of the candidate materials since they were specially produced in limited experimental quantities, and often in non-standard configuration for testing in this program. However, several suppliers provided cost figures for some of the polycrystalline aluminas of interest.

A partial compilation of these data for selected candidate aluminas is given in Table 2-8. These recent costs are based on quotations from the identified vendors. In most cases there is cost information for various quantities of the particular unit-size substrate, although the costs are given on a per-unit-area basis. It should be emphasized that these are not projected future costs but merely today's costs for various quantities of the materials listed. For comparison purposes, costs for two different sizes of Corning Code 7059 barium-aluminoborosilicate glass are included, in each case for a single range of quantities.

The table does not include such substrate materials as mullite, zircon, cordierite, or the special glasses from Corning and Owens-Illinois that were evaluated in this program. It has been difficult to obtain prices for volume purchases for mullite, zircon, and certain cordierites in the substrate configuration; further, these materials do not now appear to be readily available in the purity, density, and homogeneity required in a practical substrate for semiconductor CVD growth. However, these materials are believed to be potentially lower in cost than the aluminas. In addition, based on TEC values alone, they would be preferred to the aluminas for Si growth. For this reason they were characterized as to their chemical stability in the CVD growth environment even though they are deficient in quality in their currently available forms.

Table 2-8. Representative Costs of Selected Polycrystalline Alumina Substrate Materials*

SUBSTRATE IDENTIFICATION		PURITY (PERCENT)	SUBSTRATE UNIT SIZE† (IN INCHES)	APPROXIMATE COST IN $/IN^2 FOR QUANTITIES INDICATED				
				1000	10,000	50,000	100,000	250,000
Coors	ADS596F	96	2x2	0.0875	0.053	–1	0.044	–
	ADS995	99.5	3-3/4x4-1/2	0.11	0.095	–	0.080	–
	Vistal (commercial)	~99.9	1/2x1/2	0.72	–	0.58	0.50	–
Magneco		96	2x2	0.062	0.052	–	0.040	0.039
			3x3	0.044	0.035	0.027	0.027	0.026
3M	ASM614	96	2x2	0.078	0.065	0.057	0.054	0.051
			3-3/4x4-1/2	0.040	0.080	0.065	0.059	0.055
	ASM772	99.5	2x2	0.117	0.098	0.085	0.080	0.076
			3-3/4x4-1/2	0.134	0.120	0.097	0.088	0.084
	ASM838	99.5	2x2	–	0.105	–	–	–
			3-3/4x4-1/2	0.143	0.127	0.104	0.094	0.089
	ASM805	99.9	2x2	0.625	0.526	0.453	0.428	0.408
			2x3	0.50	–	–	–	–
MRC	HiRel Superstrate	99.6	2x2	0.71	0.60	–	–	–
			3-3/4x4-1/2	0.52	0.48	–	–	–
			4x4	0.68	0.64	–	–	–
	Hybrid Superstrate	99.6	2x2	0.31	0.26	–	–	–
			3-3/4x4-1/2	0.22	0.18	–	–	–
			4x4	0.30	0.28	–	–	–
	Commercial	99.6	2x2	0.095	0.09	–	–	–
			3-3/4x4-1/2	0.10	0.09	–	–	–
			4x4	0.12	0.11	–	–	–
Kyocera	A476	96	2x2	–	0.046	–	–	–
Saxonburg	S697**	97	1x2	0.18	0.054	–	0.047	0.045
			2x2	0.09	0.058	–	0.050	0.048

*As of October 1976

†Thickness in all cases is 0.025 in. except where indicated otherwise

**$250 setup charge if 6-week lead time is given

Table 2-8 (Cont)

SUBSTRATE IDENTIFICATION		PURITY (PERCENT)	SUBSTRATE UNIT SIZE† (IN INCHES)	APPROXIMATE COST IN $/IN.^{2} FOR QUANTITIES INDICATED				
				1000	10,000	50,000	100,000	250,000
GE	Lucalox	99.9	1 dia x 1/16 thick (disk)	3.95 ea.				
		99.9	1 wide x 1-8 lg. x 1/8 thick (rectangular bar)	8.35/in. (< 3 in.); 10.45/in. (> 3 in.)				
INSACO	Polished Vistal	99.9	1-3/8dia x 0.030 thick	11.20 ea (up to 5 pieces)				
Corning	Code 7059	Barium-aluminoborosilicate glass	12x14 (0.032 thick)	0.037 – 0.053/in.^{2} (up to 10,000 pieces				
			4x4 (0.032 thick)	0.14 – 0.16/in.^{2} (up to 50,000 pieces)				

Similarly, the costs associated with the most promising glasses have also been difficult to determine. The glasses with high strain points were either prepared specially for this program or were reprocessed from a commercial form, such as a tube or rod, into a flat substrate by non-automated techniques. Corning personnel have indicated that any glass (or glass-ceramic) found suitable for large-area solar array use can probably be produced in large volumes at costs that would meet the 1986 LSSA Project goals (Ref 5).

Corning Code 7059 glass, although found not to be useful in this program, has been included in Table 2-8 because it represents a high-quality glass that has been mass-produced and thus provides a cost comparison. Based on the sizes and quantities shown, Corning 7059 and the 96 percent aluminas are in about the same price range. Whereas the aluminas permit film growth at high temperatures, the glasses offer potentially uniform and flat surfaces for film growth and device processing. Also, the glasses can be expected to be produced in much larger sheets than can the ceramics, at least in terms of the technology now practiced for producing these materials in standard forms.

2.3 EXPERIMENTAL INVESTIGATION OF Si CVD PROCESS PARAMETERS AND PROPERTIES OF FILMS GROWN ON SELECTED SUBSTRATES (TASKS 3 AND 5)

Si deposition experiments performed in the period prior to the contract start date had indicated that some substrates received from various glass and ceramic manufacturers were reactive in a H_2 atmosphere at the high growth temperatures used. Major contamination was in evidence in films grown on companion pieces of single-crystal sapphire used as control wafers in those experiments. The use of an inert carrier gas such as He was thus regarded as necessary for studying Si growth phenomena on substrate materials reactive to H_2.

During the first quarter a variety of CVD experiments was carried out to establish baseline performance data for the reactor system, including temperature distributions on the sample pedestal, effects of carrier gas flow rate on temperature, effects of carrier gas flow rate on film thickness uniformity in H_2 and in He, and Si film growth rates by SiH_4 pyrolysis as a function of temperature for H_2 and for He.

2.3.1 Effect of Carrier Gas Flow Rate on Pedestal Temperature

The horizontal pedestal used in the CVD reactor system is heated by coupling of the rf field of an external coil (see Figure 2-1). The resulting temperature of the surface of this SiC-covered carbon susceptor (pedestal) is non-uniform, the areas near the periphery being hotter than the central region. The differential is greater at high temperatures (e.g., 1025°C) than at the lower end of the region of interest for this work (~600°C), and the average temperature of the pedestal for a given amount of rf power input is affected by the total gas flow rate used.

Experiments were carried out early in the first quarter to establish the magnitude of this effect, for both H_2 and He carrier gases. The temperature of the pedestal was measured by means of an infrared radiation thermometer mounted near the chamber, in the arrangement shown schematically in Figure 2-26. Use of the radiation thermometer in position A permits measuring the temperature at any location on the pedestal surface. Corrections for the emittance of the pedestal surface and for losses associated with viewing the hot surface through the fused quartz wall of the reactor chamber were determined experimentally. Normally, during a Si CVD experiment, the pedestal temperature was monitored by viewing the vertical cylindrical surface of the rotating pedestal through one of the spaces between turns of the rf coil (position B in Figure 2-26). The corresponding temperature of the top surface of the pedestal could be related to this value by a correction known from previous experimental determinations of corresponding temperatures at both locations.

To measure the effect of gas flow rate on pedestal surface temperatures the temperatures were observed for three different positions on the pedestal and at three different carrier gas flow rates in three different temperature regions, without any Si compound in the chamber and thus no deposition. In each temperature region the rf power input to the pedestal was not changed

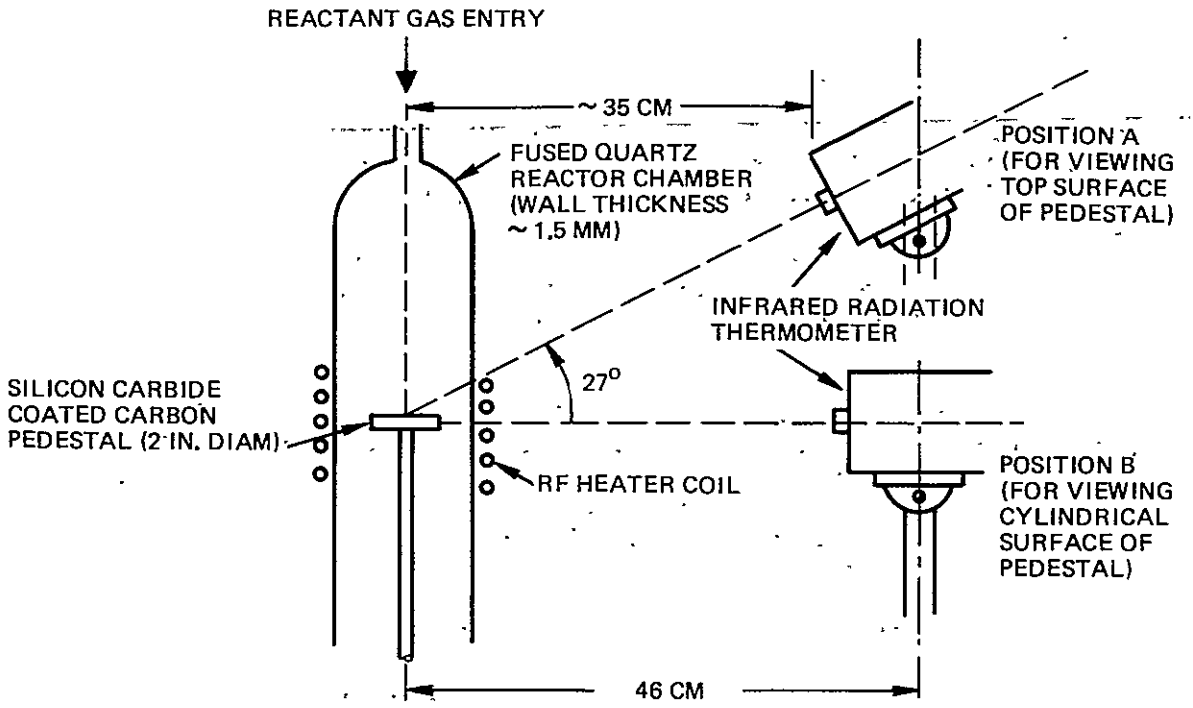

Figure 2-26. Schematic Diagram of Apparatus Arrangement for Measuring Pedestal Temperature with Infrared Radiation Thermometer ($2.0 \leq \lambda \leq 2.6 \mu m$).

during the observations at the three flow rates; therefore, the differences in temperature at a given location on the pedestal were caused solely by the changes in gas flow rate.

Results of these measurements in terms of observed temperatures are given in Table 2-9 and Figure 2-27 for both H_2 and He carrier gases, for the 5-cm-diameter pedestal used in the vertical reactor chamber. Inspection of the data for either gas (Table 2-9) for any one of the three locations on the pedestal shows the expected effect of reduced temperature (i.e., increased cooling of the pedestal) as the total gas flow rate increases. Generally, the magnitude of this cooling effect was found similar for the two gases at a given location on the pedestal.

For a given gas flow rate an indication of the temperature profile obtained on the pedestal surface can be seen from an inspection of the three temperatures T_s, T_t, and T_c in the low-, mid-, and high-temperature regions. This temperature distribution is a consequence of the combined effects of the non-uniform heating of the pedestal/susceptor by the rf field and the several processes of heat transfer away from the pedestal, including heat conduction by the carrier gas moving past the pedestal surfaces.

Table 2-9. Observed Temperature at Three Locations on SiC-coated Carbon Pedestal (5 cm dia) for H_2 and He Carrier Gases

Carrier Gas Flow Rate (ℓpm)	H_2 Carrier Gas Observed Pedestal Temperatures (°C)					He Carrier Gas Observed Pedestal Temperatures (°C)				
	T_s*	T_t**	T_c†	(T_s-T_c)	(T_t-T_c)	T_s*	T_t**	T_c†	(T_s-T_c)	(T_t-T_c)
4	590	586	580	10	6	590	590	583	7	7
	920	911	893	27	18	874	877	857	17	20
	1030	1019	987	43	32	1053	1042	1008	45	34
6	566††	573	568	-2	5	571	571	563	8	8
	911	899	879	33	20	872	870	850	22	20
	1024	1012	980	44	32	1026	1039	1002	24	37
8	548	549	542	6	7	555	551	544	11	7
	857††	874	854	3	20	854	862	835	19	27
	1012	1002	965	47	37	1018	1028	985	33	43

*Measured on vertical cylindrical surface or "side" of pedestal

**Measured on top pedestal surface at distance d= $\frac{3}{4}$ r from center, where r is radius

†Measured at center of top surface of pedestal

††These readings of doubtful validity

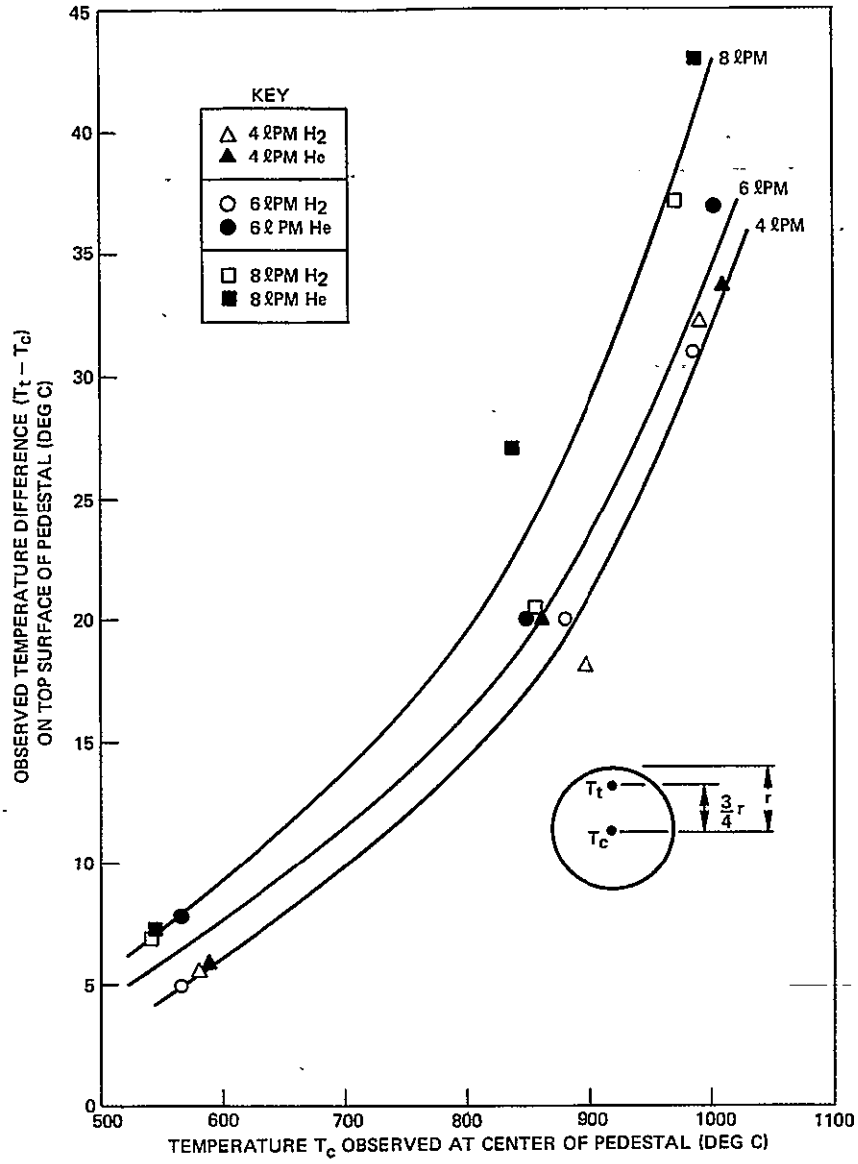

Figure 2-27. Observed Temperature Difference (T_t-T_c) on Top of rf-heated Pedestal for H_2 and He Carrier Gases at Three Different Flow Rates

The temperature difference between the center of the pedestal surface and points approximately three-fourths of the distance from the center to the edge of the top surface is given by the quantity (T_t-T_c) in Table 2-9. This difference is shown in Figure 2-27 as a function of the observed temperature T_c at the center of the pedestal surface, for the three gas flow rates used and for both gases. The results clearly show that the radial temperature gradient on the pedestal surface depends strongly on the magnitude of the pedestal temperature but is nearly independent of the carrier gas and only moderately dependent on the gas flow rate.

The difference between the temperature at the center of the pedestal surface--where most substrates were placed for Si CVD experiments--and that observed on the cylindrical side of the pedestal (with the infrared thermometer in position B in Figure 2-26) followed a similar dependence on pedestal temperature, as can be verified by inspection of the values for (T_s-T_c) in Table 2-9. The difference was such that the temperature in the center of the pedestal surface was 8-10 deg C below that of the cylindrical side surface in the low temperature region, 20-25 deg C below it in the mid-range, and 35 to 45 deg C below in the high-temperature region. Except where specifically noted, deposition temperatures given in this report are those observed on the side cylindrical surface of the pedestal.

2.3.2 Effect of Carrier Gas Flow Rate on Film Thickness Uniformity

Experiments were also undertaken early in the program to determine preferred total flow rates of H_2 and He carrier gases which would lead to acceptable Si film thickness (i.e., growth rate) uniformity across the 5-cm diameter SiC-covered carbon pedestal, over a temperature range of 600-1025°C. Total gas flows of 4, 6, and 8 ℓpm were used with pedestal temperatures of about 600, 850, and 1025°C, with SiH_4 flows of 10 ccpm for H_2 and 25 and/or 50 ccpm for He. The results are summarized in Figure 2-28.

For H_2 carrier gas the thickness or growth-rate uniformity was better than ±10 percent across the pedestal for most conditions tested. A flow rate of 4 ℓpm was selected as the preferred rate for subsequent CVD experiments using H_2 as the carrier early in the program.

For He carrier gas the thickness uniformity appeared to be best for 6 ℓpm at ~850 and ~1025°C, and slightly better for 8 ℓpm at ~600°C. However, a considerable variation in growth rate between center and edge was found across the 38-mm-diameter single-crystal sapphire substrates used for the experiments, especially at the temperature extremes of 600 and 1025°C. A He flow rate of 6 ℓpm was selected for use in the first three quarters of the program in growth studies employing the original reactor chamber design, with substrates placed at or near the center of the pedestal whenever possible.

Early in the fourth quarter a change was made in the carrier gas flow rate used in the film growth studies. Si films grown in He carrier gas at flow rates of 4-8 ℓpm had generally not had sufficiently uniform thickness. By changing the total He carrier gas flow rate to 1.5 ℓpm the film thickness uniformity was improved considerably. For example, growth on a single-crystal sapphire wafer at 850°C then produced a film 34μm thick which varied by only three percent in thickness across about 80 percent of its 2 in diameter and about 10 percent in thickness for the other 20 percent.

At 1.5 ℓpm He flow rate, however, the formation of deposits on the reactor wall is increased considerably, and a turbulent brown "smoke" is evident in the reactor during film growth. The role of the products of this smoke during growth of polycrystalline films is not known, but its presence did not seem to impede epitaxy on sapphire and spinel single-crystal substrates during work

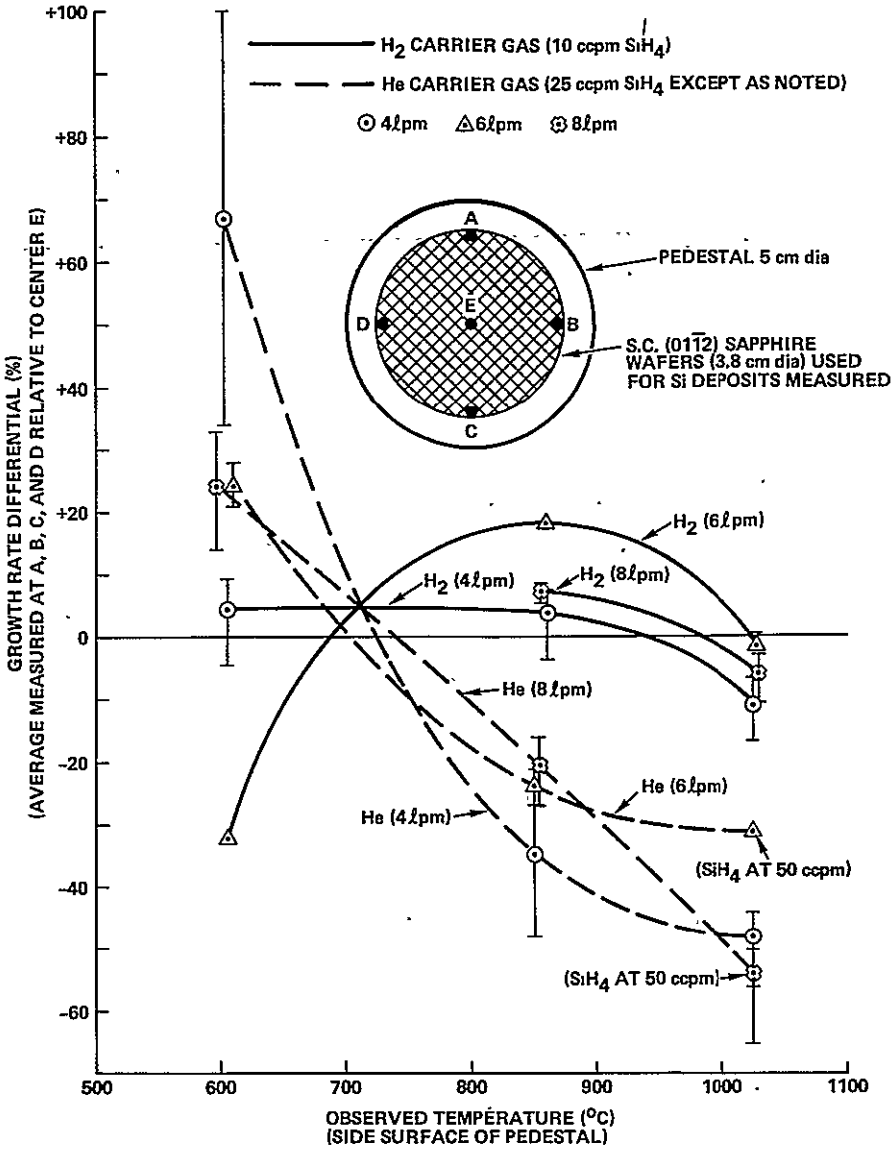

Figure 2-28. Si Film Thickness Uniformity Obtained with H_2 and He Carrier Gases for Various Flow Rates and Deposition Temperatures

performed previously at Rockwell on another program (Ref 6). Carrier gas flow rates of 1.5 ℓpm for both H_2 and He were thus used for most of the remainder of the program.

Finally, late in the program a baffle was introduced into the reactor chamber, as already described (Section 2.1), and at that time the typical carrier gas flow rate was increased to 2.5 ℓpm for H_2 and 3.5 ℓpm for He.

2.3.3 Effect of Deposition Temperature on Si Film Growth Rate

Using 4 ℓpm for H_2 and 6 ℓpm for He, baseline growth rate determinations were made, with (01$\bar{1}$2)-oriented single-crystal sapphire as the substrate and a

constant flow rate of SiH_4 (25 ccpm). For these experiments, a 1000-g tank of SiH_4 (from 3H Corporation) was used. This SiH_4 was reportedly H_2-free (less than 10 ppm); this is important in order to minimize reaction with substrates reactive with H_2. The only H_2 present when a He or inert atmosphere is used, therefore, is that generated by SiH_4 decomposition.

The results of these experiments are summarized for H_2 and for He as the carrier gas in plots of growth rate vs reciprocal absolute temperature in Figure 2-29. The temperatures used in plotting the data in these curves are corrected temperatures, representing the temperatures of the pedestal surface in regions adjoining the substrates on which Si deposition occurred. Consequently, a determination of activation energies associated with the process of Si layer growth by SiH_4 pyrolysis in H_2 and in He carrier gas atmospheres can be made.

It is clear that different mechanisms are operative in the deposition of Si by SiH_4 pyrolysis in the presence of H_2 and of He. In H_2, a rapid increase in growth rate with increasing temperature occurs for temperatures below about 900°C; above that, the rate still increases with temperature but much less rapidly. The activation energies characterizing the two regions are 1.8 and 0.14eV, respectively. These results are similar to those reported by other investigators (Refs 7,8), who report a surface-controlled reaction for Si growth from SiH_4 below 900°C and a mass-transfer-controlled reaction in the temperature range 900-1050°C.

In He, the Si growth rate increase was also found to be rapid at low temperatures (activation energy 1.8eV), but at about 850°C the growth rate passes through a maximum and then decreases for further increases in the deposition temperature up to at least 1050°C, the highest temperature used for these experiments. This maximum in the growth rate at ~850°C may be controlled by appreciable decomposition of SiH_4 caused by radiation a finite distance away from the hot pedestal, with the formation of silicon hydride polymers $(SiH_2)_x$ which do not efficiently reach the hot pedestal for pyrolysis to form Si. Si formation from $(SiH_2)_x$ is, however, catalyzed by the presence of H_2 (Ref 9). It is significant that the activation energies observed in both cases in the range below ~850°C are the same.

The difference in growth rate in H_2 and He below 850°C may be due to differences in flow characteristics in the reactor; on the other hand, the somewhat lower growth rate in H_2 in this range may be caused by H_2 adsorption on the substrate surface, thereby hindering SiH_4 adsorption and pyrolysis to Si. Previous studies at Rockwell demonstrated an increase in Si growth rate at 1025°C when additions of H_2 were made to SiH_4-He mixtures (Ref 6).

The observed difference in Si deposition rate by SiH_4 pyrolysis at temperatures above 850-900°C in H_2 and in He tends to discourage the use of He at higher temperatures because of the increased time required to obtain a given Si film thickness. Further, the film thickness uniformity across the pedestal was found to be much better for Si deposited in H_2 than in He, particularly at higher temperatures. In addition, generally better looking Si films were achieved--on substrates other than glasses--by deposition in H_2 than in He. However, for Si deposition by CVD on various glasses there is little doubt that He (or other inert gas) is the required carrier gas, irrespective of the above disadvantages.

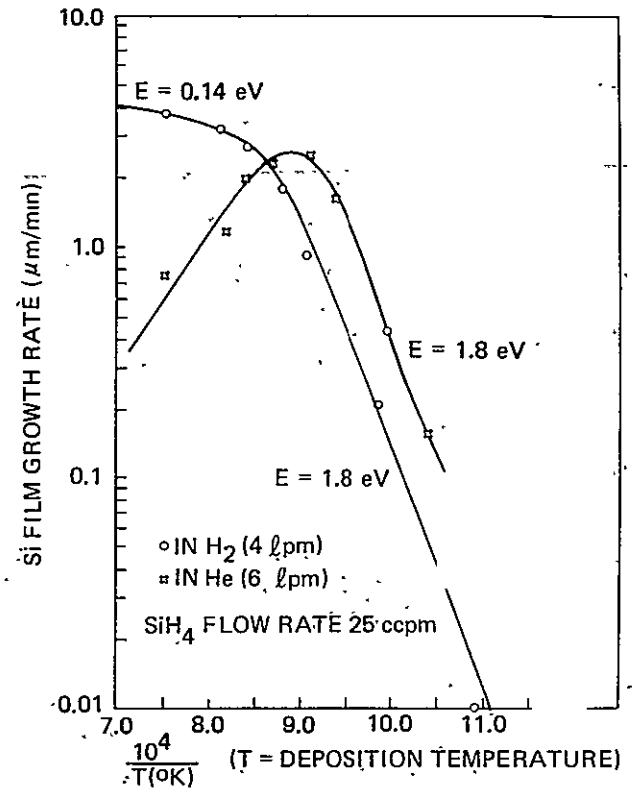

Figure 2-29. Si Film Deposition on $(01\bar{1}2)$ Sapphire Substrates as Function of Reciprocal Temperature for SiH_4 Pyrolysis in H_2 and in He (Temperatures used are corrected from observed values.)

2.3.4 Background Impurity Doping Level in Reactor System

Early in the first quarter the electrical properties of several undoped epitaxial Si films grown on single-crystal sapphire and Si substrates were measured by both the van der Pauw and the conventional Hall bridge methods (see Section 2.3.7) as a means of obtaining a measure of the background impurity doping level characteristic of the reactor system and the reactants in use at that time. The films were grown on single-crystal $(01\bar{1}2)$-oriented polished sapphire and on high-resistivity single-crystal Si substrates, the former at temperatures of 1025 and 1100°C and the latter at 1025°C, in H_2 and in He carrier gases.

The results of these measurements indicated that the undoped films were p type, with the carrier concentrations typically ~10^{15} cm^{-3}. This concentration level was believed to be high for such a system, but it was verified on several epitaxial samples measured during the first quarter.

After the reactor modifications were completed early in the second quarter additional measurements were made on undoped epitaxial Si films grown on sapphire substrates in H_2 and in He carrier gas, at ~1000 and ~1100°C. Two films grown in H_2 were deposited at nearly the same rate (3.3μm/min and 3.7μm/min), while the films grown in He were deposited at different rates (1.2μm/min and 0.72μm/min). The films grown in H_2 were more uniform in

thickness, consistent with earlier observations of film uniformity obtained with H_2 and with He carrier gases.

The apparent background impurity doping level of ~$4x10^{14}$ cm^{-3} indicated by these measurements (even though made on films grown on sapphire rather than on single-crystal Si substrates) was a more acceptable value than the ~10^{15} cm^{-3} obtained in the first quarter. It is not known if the lower value was associated with a real reduction in the unintentional acceptor doping level in the films relative to those measured earlier or if the difference was in some way attributable to a measuring apparatus problem that was found to exist early in the second quarter (and corrected at that time).

In any case, subsequent measurements on undoped epitaxial films (on sapphire) from time to time as the program progressed confirmed the range 1-$4x10^{14}$ cm^{-3} as the background imperfection (impurity and/or defect) level typical of the reactor system and reactant materials used in this program.

2.3.5 Preparation of P-type Boron-doped Si Films

Si layers grown by CVD can be readily doped during growth by introduction of an appropriate compound containing the doping impurity into the carrier gas stream along with the Si compound being used. In some ways the method is almost ideal for producing either n- or p-type Si sheet on a substrate, since the dopant gases are homogeneously mixed with the Si compound external to the reactor and prior to film deposition. Such n-type sources as AsH_3 and PH_3 and the p-type source B_2H_6 have been almost universally used for doping epitaxial Si films.

However, the crystallographic properties of polycrystalline films grown in different atmospheres and under different growth conditions can be expected to vary considerably with the dopant source and to affect the electrical properties of the films. For example, it has been reported that B atoms enhance the growth rate and the grain size of polycrystalline Si films, especially at higher concentrations (>10^{18} cm^{-3}), whereas As tends to have the reverse effect. This favors the use of p-type Si films for the thicker base region of a solar-cell structure, and the formation of the thin n-type front layer either by subsequent post-growth counterdoping (diffusion or ion implantation) with As or P or by sequential CVD growth of an As-doped or P-doped film.

Such observations were made by investigators using H_2 atmospheres. However, earlier studies at Rockwell showed that much larger amounts of dopant are needed to produce a given impurity concentration in SOS films (Ref 6) grown in a He atmosphere than in a H_2 atmosphere. Also, the efficiency of the doping process changes with growth temperature and the specific growth process used; preliminary data obtained in earlier research (Ref 6) indicated decreases in carrier concentration at high growth temperatures in SOS films for a constant growth rate and constant dopant flow rate, but no definite trend was apparent over the limited temperature range studied (1040-1080°C). At the lower temperatures used in this program it was not evident in advance what the doping trends would be.

It was also expected that higher concentrations of dopants would have to be added in the gas phase to achieve a given effective impurity concentration in the Si as the layer becomes more polycrystalline, especially if the defects in the layer act as sinks for the impurities. The results of electrical measurements on films doped for various nominal concentrations were expected to indicate any such effects. Early in the program a series of doping experiments was performed to establish the relationship that exists between added dopant concentration and measured active carrier concentration in films grown simultaneously on polycrystalline aluminas and on sapphire, especially at low B doping levels. Films 20-25μm thick were grown with B_2H_6 flow rates as low as 0.2 ccpm to as high as 500 ccpm. The results of these experiments are described in detail in Section 2.3.10.2.

It was also necessary to establish some reference data for the growth of B-doped films in a He atmosphere in order to produce p-type films on those glasses or other substrates unstable in H_2. Single-crystal sapphire substrates and a range of B_2H_6 dopant gas (46 ppm in He) flow rates from 5 to 500 ccpm were used for these experiments, at an observed pedestal temperature of ~850°C. The resulting film growth rates on the single-crystal sapphire substrates were in the range 0.41 to 0.76μm/min for SiH_4 flow rates of 10 ccpm and He carrier gas flow rates of 1.5 ℓpm; the average growth rate for these parameters was about 0.5μm/min.

The above sets of experiments led to the data shown in Figure 2-30, which shows the observed hole concentrations in B-doped epitaxial Si films on sapphire as a function of the diborane (46 ppm B_2H_6 in He) flow rate added to the carrier gas stream. These data provided the basis for the preparation of p-type Si sheet material throughout most of the remainder of the program.

2.3.6 Preparation of N-type Phosphorus-doped Si Films

During the last quarter of the program experiments were begun with PH_3 as a dopant gas to achieve heavy phosphorus (n-type) doping of a thin surface layer to produce deposited n/p structures for solar cell formation. The PH_3 source gas was also in a nominal concentration of 46 ppm in He, and $(01\bar{1}2)$-oriented sapphire was used as the reference substrate.

From the resulting experimental doping curve, shown in Figure 2-31, PH_3-in-He flow rates of approximately 100-200 ccpm in a H_2 carrier gas are seen to be sufficient to produce n-type Si films with carrier concentrations exceeding 10^{19} cm^{-3}. A different doping curve would be expected for film growth in an all-He atmosphere.

Although some shift in the data might be expected for films grown on Si substrates, in the desired doping range for n^+ films ($\geq 10^{19}$ cm^{-3}) the carrier concentration for films on Si would be expected to be essentially that measured for films on sapphire, i.e., the concentrations shown in the figure.

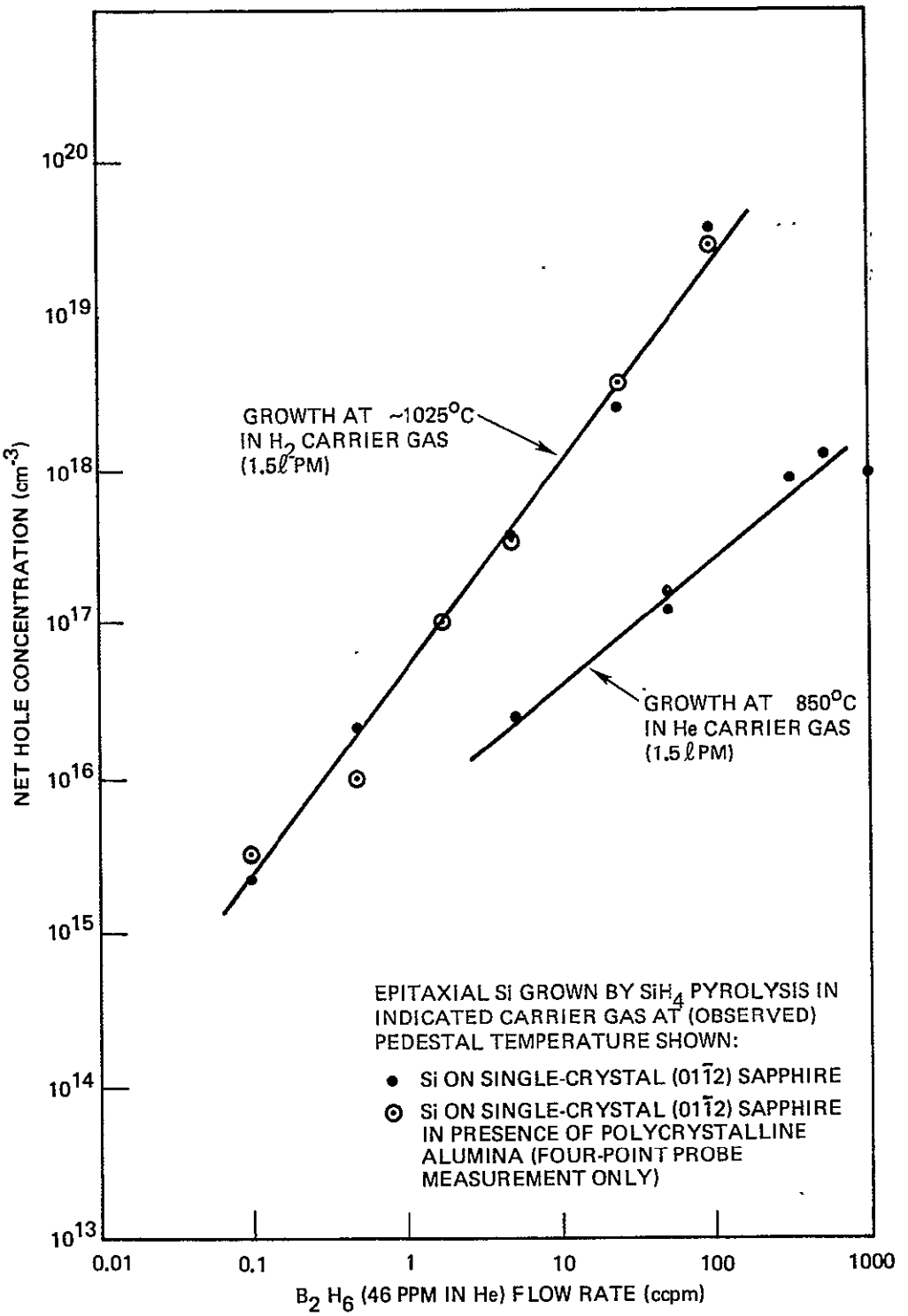

Figure 2-30. Measured Hole Concentrations in B-doped Epitaxial CVD Si Films as Function of Added B_2H_6-in-He (46 ppm) Flow Rate for Growth in H_2 Carrier Gas at ~1025°C and in He Carrier Gas at ~850°C.

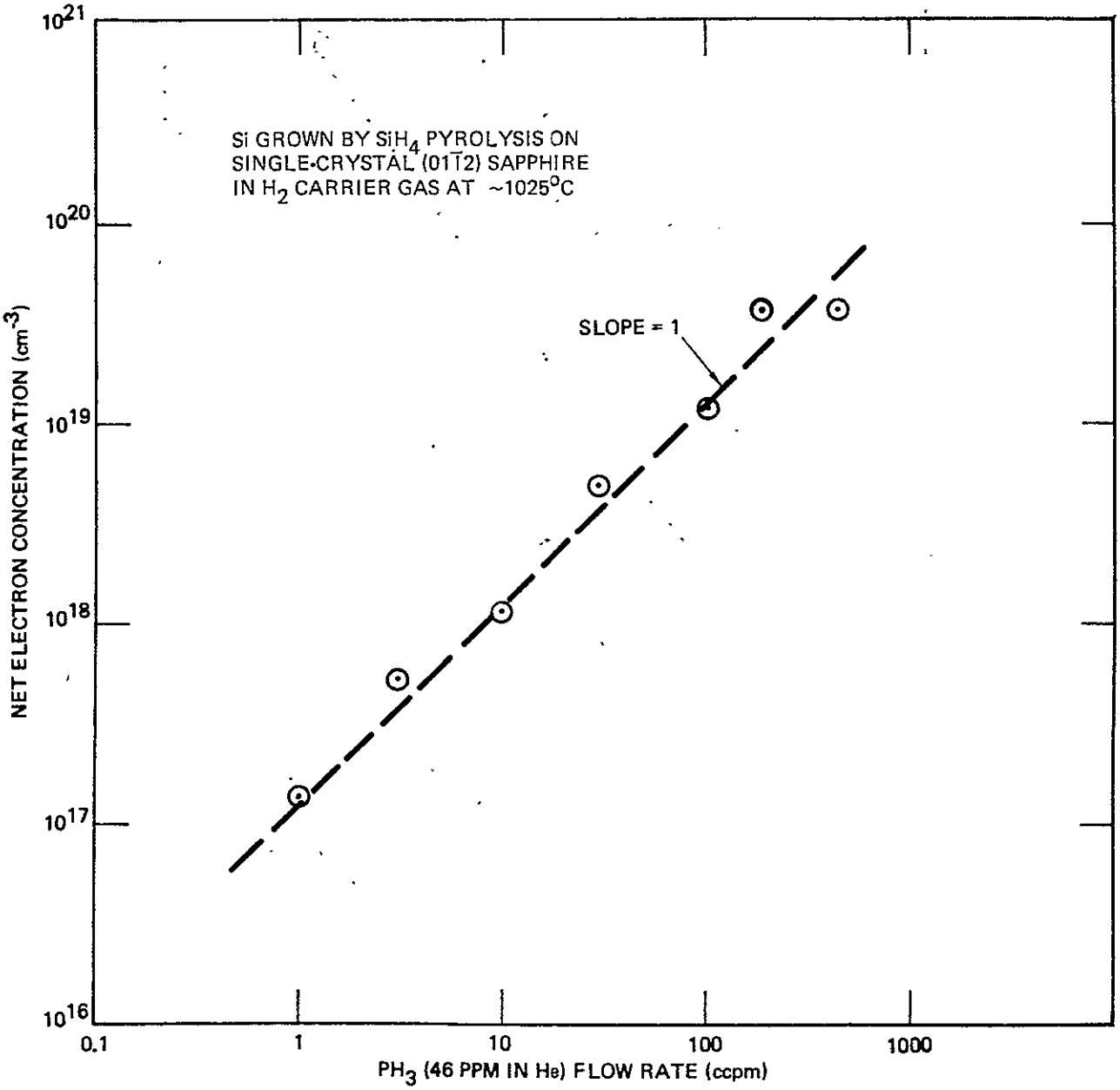

Figure 2-31. Measured Electron Concentrations in P-doped Epitaxial CVD Si Films as Function of Added PH_3-in-He (46 ppm) Flow Rate

2.3.7 Methods for Evaluation of CVD Si Sheet Material Properties

A variety of procedures were developed and/or applied to the characterization of Si sheet material produced by CVD on various substrates under investigation during this program. The surfaces of the films were characterized by x-ray diffraction, reflection electron diffraction, scanning electron microscopy, optical microscopy, and surface profilometric techniques. X-ray diffraction methods were used to obtain information on the amount of preferred orientation and the grain size in films deposited on polycrystalline alumina at several different temperatures. Methods of SEM analysis and classical metallography combined with etching procedures were used to provide some evidence of vertical or columnar growth in Si films on alumina.

When doped films were prepared, additional techniques were utilized for film evaluation, including (1) the spreading resistance method for obtaining profiles of electrical properties (and thus impurity and/or defect concentrations) in polycrystalline Si films, and (2) measurement of minority carrier lifetime in CVD Si films on various substrates, using the pulsed C-V method in MOS structures. A comparison of van der Pauw and Hall bridge methods for measurement of charge transport properties in CVD Si films was also undertaken, and a laser etching method of defining Hall bridge patterns in Si film samples was evaluated.

Several of these characterization procedures are outlined in the following sections.

2.3.7.1 Surface Profilometry

Surface roughness and details of other topographic features of both films and substrates were measured by surface profilometry using a Sloan Dektak. This instrument can also be used for film thickness measurement when an abrupt step from film to substrate is formed by removal of the Si film by masking and etching procedures.

Surface profilometry was used to examine and record the surface finish on a variety of the polycrystalline ceramic substrates of interest - both polished and as fired. It is a rapid and useful screening procedure to provide a view of the overall surface finish as well as a quantitative measure of localized surface features, such as pits, steps, etc. Similar information on the Si films deposited on various substrate surfaces was obtained by this means.

2.3.7.2 X-ray Diffraction Analyses

To apply the techniques of x-ray diffraction line broadening to the determination of average particle or grain size in a polycrystalline specimen, such as Si films prepared under conditions that do not produce epitaxial (single-crystal) growth, it is necessary to know the diffraction line width in the absence of any grain-size broadening effects. This line width is the combined result of the true diffraction line width - which is finite because of such factors as non-perfect crystals and non-monochromatic incident radiation -

and instrumental line broadening, associated with factors such as the width of the effective x-ray source and imperfectly collimated x-ray beams in the particular diffractometer used.

Grain sizes in excess of ~0.1μm generally do not produce any x-ray line broadening due to crystal size effects alone. Thus, the diffractometer trace obtained with a polycrystalline sample containing randomly oriented grains significantly larger than ~0.1μm should provide a measurable reference line width free of size broadening effects, i.e., with zero grain-sizing broadening. Such a zero-broadening Si sample was prepared by grinding single-crystal (Czochralski) wafers with an agate mortar and pestle. The resulting charge was then passed through a No. 140 sieve (105μm apertures), and this charge in turn was passed through a No. 325 sieve (44μm apertures). The powder remaining on the latter sieve consisted of single-crystal Si particles in the size range 44-105μm; although smaller particles would have permitted preparation of a more uniform sample for x-ray purposes, the sieved powder was adequate. Masking tape was then used as a "floor" in the sample aperture of a standard diffractometer sample holder, the tape was sprayed with Krylon, and layers of dispersed powder and Krylon were built up to form the reference sample. After drying, the sample was used to produce reference diffraction lines free of particle-size broadening.

The width of an x-ray diffraction line is usually measured as the breadth at half-maximum intensity and is expressed as an angular width, in terms of the Bragg angle. The measured breadth of a Si line exhibiting broadening due to particle-size effects is corrected for the observed zero-broadening breadth of the same Si diffraction line obtained with the reference powder sample, and the resulting value for the broadening is then used in the Scherrer formula to obtain an estimate of the particle (or grain) size.

This method was applied in the evaluation of grain size in a number of CVD Si films grown throughout the program. It was used in conjunction with reflection electron diffraction (RED) and with inspection of the Debye rings in back-reflection Laue patterns obtained for the same samples. The latter method - that of examining the "graininess" or continuity of Debye rings in back-reflection patterns - provides a relatively rapid screening procedure for estimating grain sizes in the range down to a few microns.

A Phillips Model 3181S Angle Mode Programmer System with teletypewriter output was used with the x-ray diffractometer system employed in these studies. This equipment permits rapid acquisition (with printout) of diffraction line profile data by automatic angle-stepping, counting, and repeat cycling. This facilitates examination of film samples where line broadening due to grain size is to be measured.

Another application of x-ray diffraction techniques is the determination of preferred orientation tendencies in polycrystalline materials. The degree of preferred orientation in some of the Si films prepared in these studies was evaluated by examination of the relative intensities of the principal low-index diffraction lines in the x-ray spectrum obtained with the diffractometer.

For example, in one of the first applications of the technique early in the program, a film grown on a single-crystal $(01\bar{1}2)$-oriented sapphire substrate in H_2 (flow rate 4 ℓpm) at ~1025°C at a growth rate of ~0.5μm/min to a thickness of ~10μm (but without the pre-deposition high-temperature etch) was evaluated. It and two similar films grown at lower temperatures (~600 and ~850°C) were examined for preferred orientation using Cu K-alpha radiation at 50KV and 20mA. Epitaxial growth was found, as expected, in the 1025°C sample, with the {100}Si planes parallel to the $(01\bar{1}2)$ plane of sapphire - i.e., the surface plane. (This is a previously observed and reported epitaxial relationship.)

With both the ASTM Index line intensities and the intensities from a standard Si specimen as the comparison basis, it was found that the 600°C film was randomly oriented polycrystalline Si with very small grain sizes. The 850°C film, on the other hand, exhibited a {110} preferred orientation parallel to the interface. This sample had an average grain size several times larger than the low-temperature film but still quite small.

This procedure was also applied to the evaluation of substrate materials having polycrystalline structure, such as the fired aluminas. The polycrystalline substrate materials of major interest - including the glass-ceramics in which firing has produced varying amounts of crystallization and preferential orientation - were systematically examined by this method prior to carrying out extensive CVD experiments.

2.3.7.3 RED and SEM Analyses

The transmission electron microscope (AEI Model EM6) can be operated in the reflection electron diffraction (RED) mode to produce a diffraction pattern of the sample surface, from which the degree of polycrystallinity or crystal perfection can be deduced. Electrons of 100 KeV energy are directed at the sample at a glancing angle (typically 1/2 to 1 deg), producing a diffraction pattern characteristic of the crystal perfection. Because of the glancing angle, the effective penetration depth which gives the diffraction pattern is only a few hundred angstroms.

Some of the CVD Si films were examined by this method, generally used in conjunction with SEM analyses. Because RED samples only the surface region of a film it is often useful to combine the technique with x-ray diffraction studies as well, since the latter methods sample greater thicknesses; the combined evaluation sometimes permits differentiation of surface and bulk structural characteristics in thin-film samples.

SEM analysis, occasionally combined with RED examination as indicated above, was used regularly to evaluate film surface topography, internal crystal structure (including grain size) of the Si films, and characteristics of the film-substrate interfacial region.

Other operational modes of the scanning electron microscope - including electron channeling pattern generation for characterizing crystal perfection

and orientation when grain sizes were sufficiently large, and the electron-beam-induced current (EBIC) mode for observing electrical characteristics such as minority carrier diffusion lengths when potential barriers are introduced - were also available for sample evaluation.

2.3.7.4 Electrical Measurements

Measurements of Si film resistivity, carrier concentration, and carrier mobility were made routinely on most of the film samples, utilizing either the van der Pauw method (Ref 10) or the more accurate and conventional Hall-effect bridge method. The former method is particularly convenient as it permits measurements on a film sample of arbitrary shape without extensive processing. However, for films on insulating substrates a bridge pattern etched in the film by photolithographic techniques is more desirable for Hall-effect and resistivity measurements. A major advantage is that a composite pattern of several Hall bridges arranged in various orientations can be etched in the layer; thus, data may be obtained on anisotropy effects and/or variations in film properties with position on the film.

The van der Pauw method for measuring the electrical properties of semiconductor films was examined in earlier studies at Rockwell (Ref 6) to determine the accuracy of the technique when applied to the evaluation of Si films on sapphire. Electrical data obtained by this method were compared with those found with the standard bridge-type samples subsequently etched into each of the films. In most cases the resistivity found by the two methods differed at most by less than six percent, with the bridge method always yielding the smaller value. The carrier concentrations had a wider range of variation, with the bridge value being an average of 12 percent smaller. The largest variation occurred in the Hall mobility; the bridge values were an average of 16 percent larger than those found by the van der Pauw technique. Comparisons of the two techniques were also made on Si films prepared in this program; observed differences are indicated in various sections later in the report.

Measurements of the Hall coefficient to obtain carrier mobilities in polycrystalline films require careful interpretation. The barrier model for charge transport in polycrystalline films, as developed by Kamins (Ref 11) and later by Rai-Choudhury and Hower (Ref 12), provides a framework for cautious application of the conventional measurements of Hall mobility. In a film in which the resistivity may be largely determined by the grain boundaries, the measured Hall effect will be mainly that associated with carrier transport in the lower resistivity regions, that is, in the interior of the crystal grains. Thus, the resistivity and Hall coefficient (i.e., carrier concentration) values that are combined to give carrier mobility may not represent the same portions of the film. As a result, the calculated Hall mobility will be a somewhat artificial parameter which, although useful as a figure of merit for the film as a whole and of special interest in its variation with the impurity doping concentration in the films, may not have its usual rigorous significance.

The resistivity of polycrystalline Si films has occasionally been measured by simple two-terminal voltage-current methods; the agreement between results obtained by such a procedure and those from van der Pauw measurements, for example, has usually been acceptable--in one reported instance less than six

percent difference (Ref 13). When large numbers of film samples are to be measured there is real advantage to this simpler technique, but four-terminal methods are generally to be preferred. For rapid evaluation of electrical properties of some of the Si films prepared in this program a conventional four-point probe was used to provide an indication of film resistivity. In most instances it was found that the four-point probe data agreed surprisingly closely with resistivity values obtained by the van der Pauw or the bridge methods.

The Hall bridge pattern used for most such measurements is shown in the photograph of Figure 2-32. The pattern shown is etched in single-crystal Si grown on a sapphire substrate; the sapphire was polished on one side only, accounting for the grainy background showing through from the backside of the wafer. The film in this case was 3.4μm thick. Several mask sizes were available with this particular pattern, but the one shown is approximately 0.3 cm on a side.

The formation of sharply defined Hall bridge patterns in thick (20-50μm) polycrystalline Si films presents several problems. Conventional photoresist and masking techniques are generally difficult, as the resist is degraded by the required long exposure to the etchant and the rough polycrystalline film surface reduces the effectiveness of the resist bond to the sample surface.

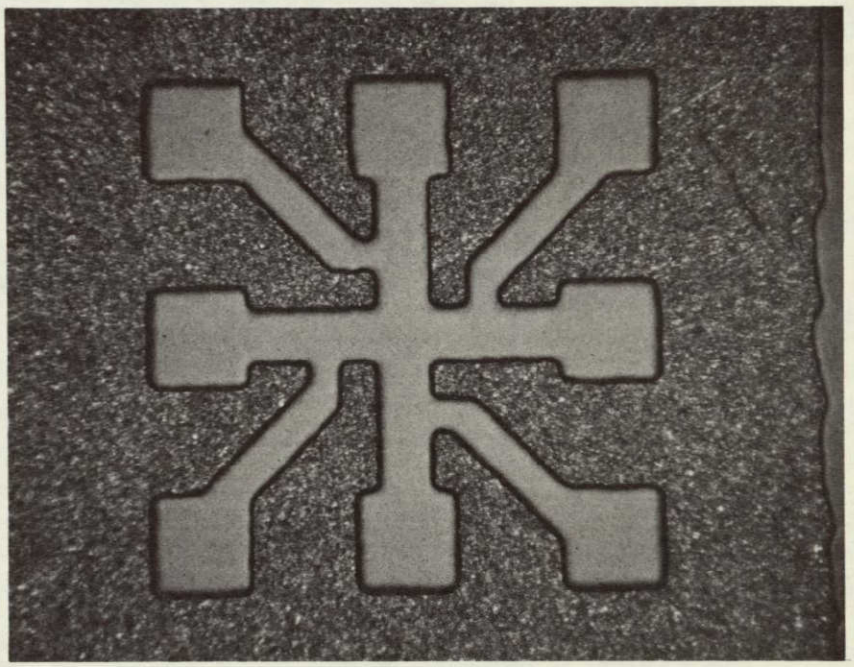

Figure 2-32. Hall-effect Bridge Pattern Photolithographically Etched in CVD Si Film on Single-crystal Sapphire Substrate. (Width of current path 310μm, length 910μm, pattern approximately 2.8mm square.)

Two possible solutions were investigated. One involved the use of the focused beam of 5-Kw YAG laser Q-switched at 1200 pps and computer-programmed to trace the outline of a bridge pattern in the film. The beam could be used either to melt a patterned groove in a protective mask, to be followed by chemical etching in the groove to isolate the bridge, or to melt/vaporize a groove in the Si film directly, in this same pattern. In the latter modification the pulsed laser beam "scribes" a channel in the film; the channel is then etched to remove any remaining Si at the bottom of the channel as well as the Si on the sidewalls of the channel that may have been damaged (or altered in its properties) by the local fusion produced by the laser beam.

The results obtained in one application of the technique are shown in Figure 2-33. In this instance a portion of a thick (~45μm) polycrystalline Si film grown on ASM805 polycrystalline alumina was laser-scribed to define the edges of a Hall bridge pattern, one corner of which is shown in the SEM photograph in Figure 2-33a. SEM examination of the film after laser-scribing the full thickness of the film showed that essentially no Si remained on the substrate at the bottom of the channel. Figure 2-33b shows a vertical view of the channel in the thick Si film, before etching. Evidence of the regularly-spaced laser-beam "strikes" can be seen in the alumina substrate surface along the channel bottom.

The second method involved a two-step varnish-and-photoresist application, in which the desired pattern is developed in the photoresist and then transferred to the varnish, which is then used to produce the patterned region in the Si. This method is satisfactory for etching layer thicknesses of at least 20μm, but the amount of control over lateral dimensions of the pattern is variable.

The pulsed MOS C-V (or C-V-t) method for measurement of minority-carrier lifetimes in Si, applied successfully to the determination of lifetimes in Si-on-sapphire epitaxial material (Refs 14, 15), was viewed as a possible method for determination of this parameter in the polycrystalline films prepared in this program. The C-V method is also useful for measuring the doping profile vs depth in thin samples; this technique is based on the depletion approximation, and utilized the capacitance of an MOS capacitor biased in the depletion condition to obtain plots of $1/C^2$ vs V. The slopes of these curves are proportional to the impurity concentration at the edge of the space-charge layer. However, this technique is limited by the inversion phenomenon.

The pulsed MOS C-V method, in which a short-duration voltage pulse is used to replace the steady dc reverse bias, was introduced as a means to measure the doping profile over a large distance into the Si region. As the general technology of MOS devices progressed, it became much simpler and more convenient to study the pulse effect by monitoring the capacitance of an MOS capacitor as a function of time. Using this technique, it was shown that the bulk generation lifetime could be obtained. Zerbst (Ref 16) developed a technique which allowed both the generation lifetime and the surface generation velocity to be extracted from the capacitance-time decay curve.

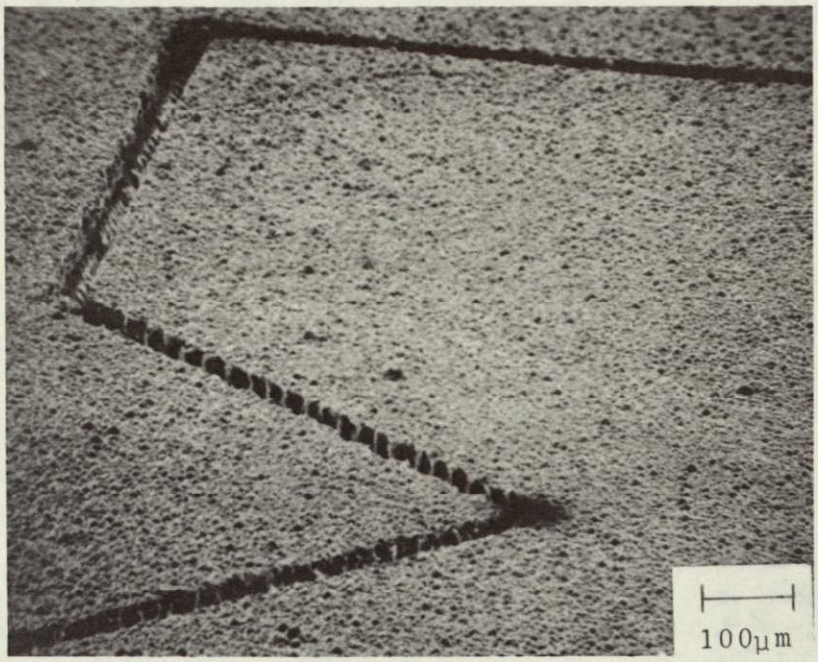

(a)

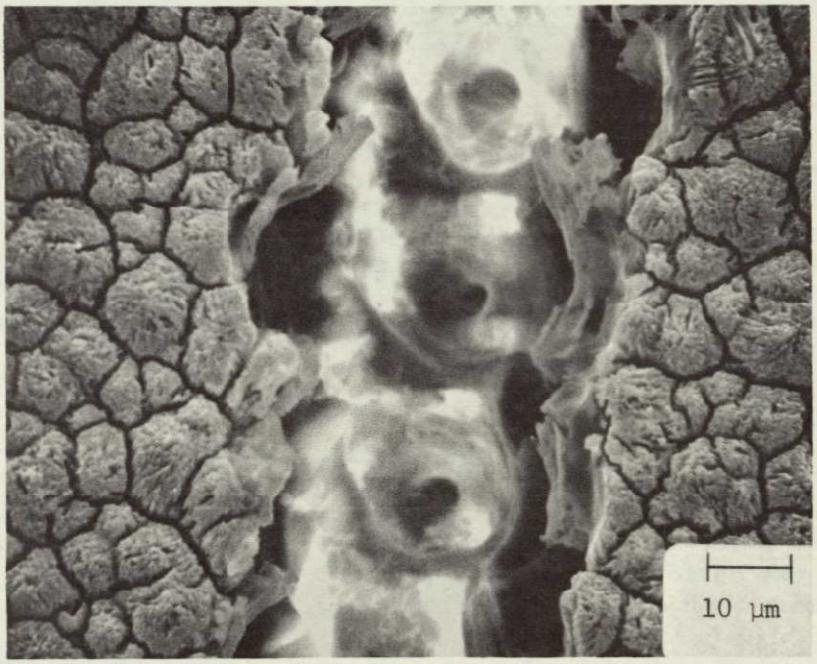

(b)

Figure 2-33. SEM Photographs of Channel Produced in Si Film by Pulsed Laser Scribing. (a) Defining the Bridge Pattern; (b) Vertical View of Channel and Exposed Polycrystalline Alumina Substrate.

A simplified schematic diagram of the apparatus that was used for C-V measurements is shown in Figure 2-34. For the C-t measurements the x-y recorder was simply replaced by a storage oscilloscope. Samples of Si on sapphire, B-doped in the mid-10^{17} cm^{-3} range, were processed into an array of isolated MOS structures - each surrounded by an ohmic contact region - on which the C-V-t method was successfully applied. Minority carrier lifetimes the order of 10^{-7} sec were measured in these 25μm epitaxial samples. However, very few samples prepared in the program were characterized in this manner.

Spreading resistance measurements were also used in evaluating the electrical properties of both the epitaxial Si films and the polycrystalline Si films. The highly specialized spreading resistance (SR) apparatus is not available at Rockwell, but a specialty laboratory - Solecon Laboratories - that works exclusively with this analytical method is located in Costa Mesa, CA, only a short distance from the Rockwell facility in Anaheim. Rapid-response service at this experienced and highly-qualified laboratory was obtained on numerous samples throughout the contract program.

There was some question early in the program as to the validity of this type of measurement on polycrystalline Si material. A resistivity limitation of 10^3-10^4 ohm-cm characterizes the method and the apparatus; films with effective resistivities less than that should be susceptible to spreading resistance analysis, with good spatial resolution. The significance of the absolute values of resistance obtained with the two-point SR probe in polycrystalline materials with grains having dimensions similar to the probe separation may well be in doubt. However, strong trends or any severe departures from a smooth continuous variation in resistivity as a function of depth into the layer - such as might be encountered with an impurity layer or a major change in grain size in the interior - are revealed by the SR profile, which is obtained by making measurements on a low-angle bevel extending through the entire layer.

It was found in practice that the SR probe measurement provided data that were very consistent with the results of measurements made by the van der Pauw method or the Hall bridge method; it also proved to be a valuable procedure for examining the variation in electrical properties in the interior of the films, as discussed in later sections.

2.3.8 Early Evaluation of Selected Candidate Substrate Materials by Si CVD Experiments

Some of the substrates on hand at the start of the contract were used in preliminary CVD screening experiments early in the program. For example, Figure 2-35 shows the obvious contamination of CVD Si film growth on a single-crystal sapphire monitor wafer caused by the adjacent wafer, consisting of an ASM743 lead borosilicate glaze on an ASM614 alumina substrate, present during Si deposition in He carrier gas at ~825°C. Figure 2-36 shows the excessive bowing of Corning Code 7059 glass when a Si film was deposited on it in He at 700°C; the film is in tension at room temperature in this case. Additional Si deposition experiments with this glass are described in Section 2.3.9.

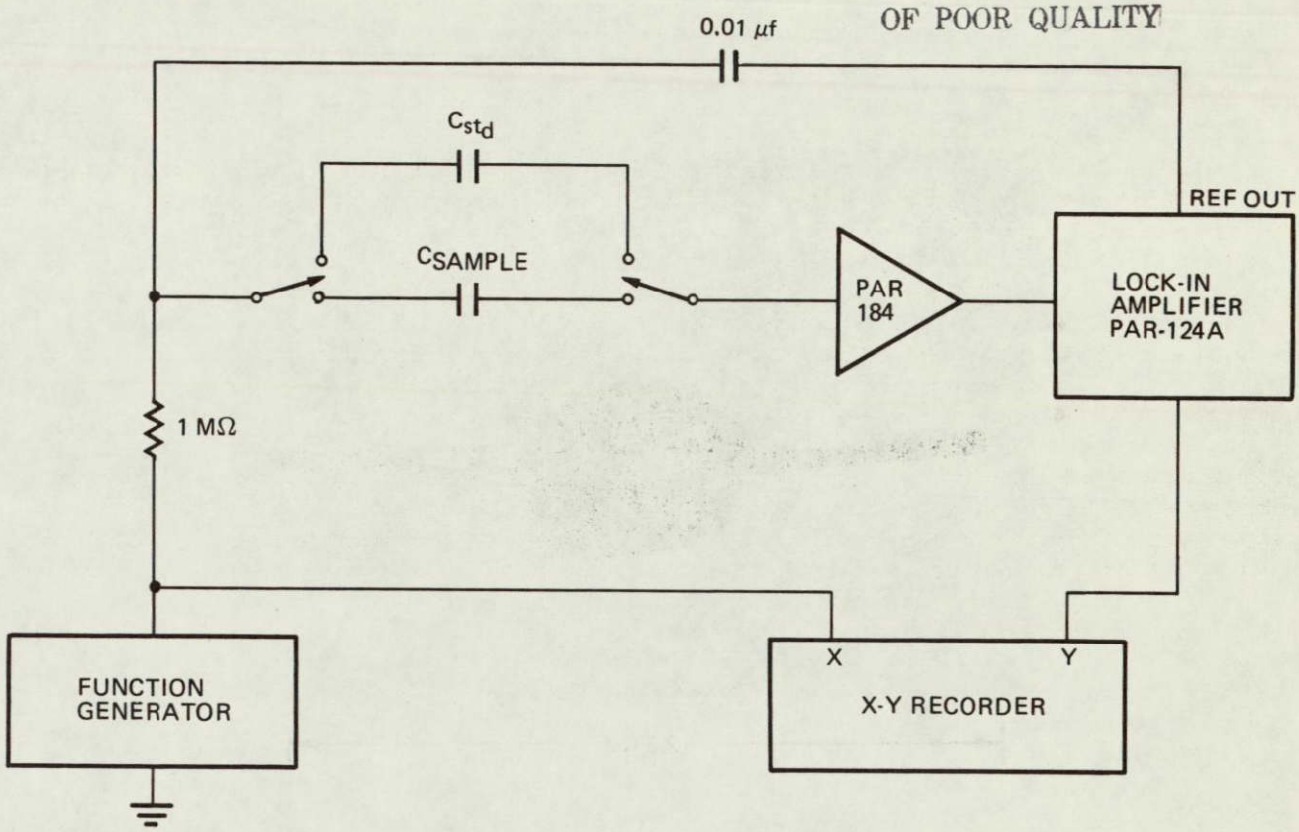

Figure 2-34. Schematic Diagram of Apparatus for MOS Capacitance-Voltage Measurements

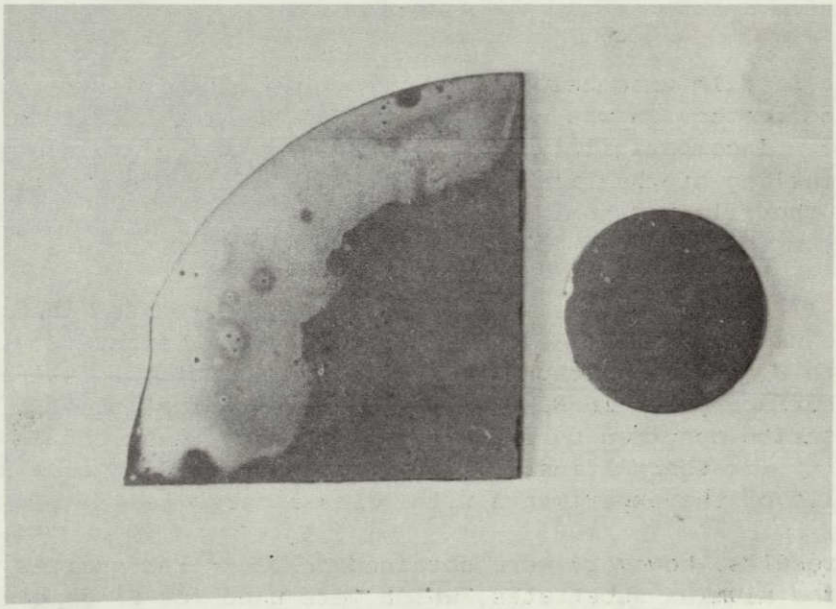

Figure 2-35. Evidence of Contamination of CVD Si Film Growth on Sapphire (Large Wafer) Caused by Nearby Glazed Alumina Substrate (Lead Borosilicate on ASM614) during Deposition in He at 827°C

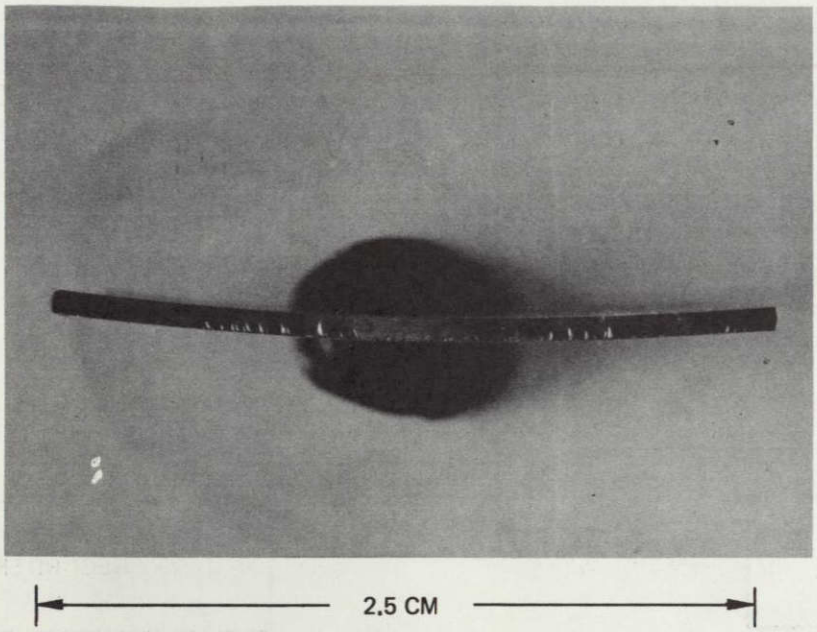

Figure 2-36. Edge View Showing Bowing of Composite of CVD Si on Code 7059 Glass after Deposition in He at 700°C. Si Film on Upper (Concave) Surface

The deposited Si film also helped to reveal nonuniformities found in some of the substrates tested, as was evidenced by Si CVD growth on cordierite (Figure 2-37). Incompatibility of the Si film with a glaze also manifested itself in wrinkling of the film-glaze composite after growth, as shown in Figure 2-38; the film was nominally 14μm thick in this case and was grown in He at ~700°C, rather than at ~825°C as was the deposit shown in Figure 2-35.

Corning Code 1723 aluminosilicate glass also failed to meet the requirements for substrate use for CVD Si, even at relatively low temperatures. This glass failed in both H_2 and He atmospheres; amorphous structural features were found on the film surface grown in H_2 at 850°C, and contamination of the companion sapphire substrate occurred during Si deposition in He at 850°C. There was even reactivity (or thermal instability) observed at 620°C in a He atmosphere. Further details of the experiments with glasses are given below.

Encouraging results, however, were obtained in the first quarter with fired polycrystalline alumina substrates, which were used for Si deposition at temperatures above 1000°C. These materials exhibit some preferred orientation in their polycrystalline structures, and the Si films grown on these were also preferentially oriented. The alumina substrates used first were those of the highest purity: MRC Superstrate, Coors ADS995, and 3M ASM805. The latter was found to have the best as-fired surface of the alumina substrates examined early in the program. Si grown by CVD on this material and on sapphire at

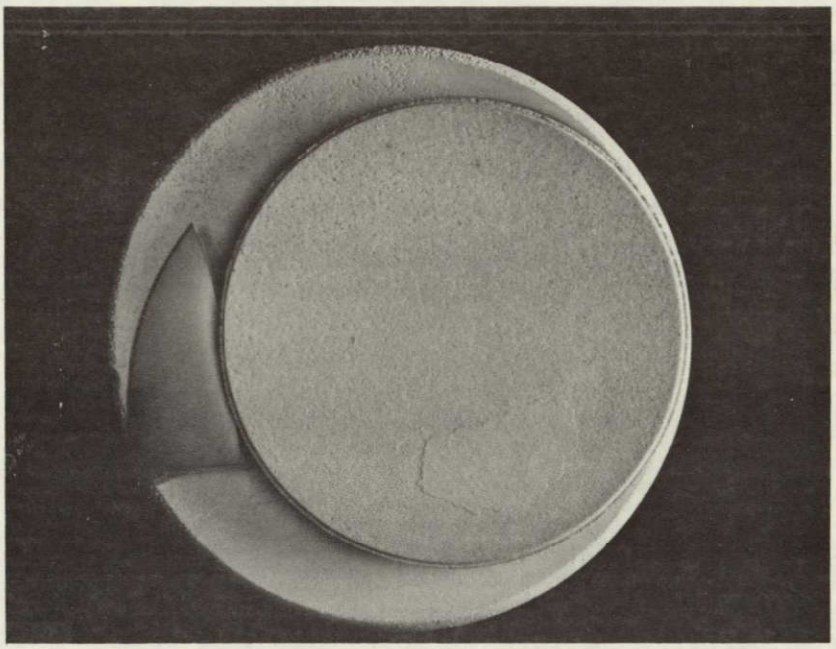

Figure 2-37. Nonuniformity in ASM701 (Cordierite) Substrate Revealed by Si CVD Film Growth in He on 3.5-cm-dia Substrate

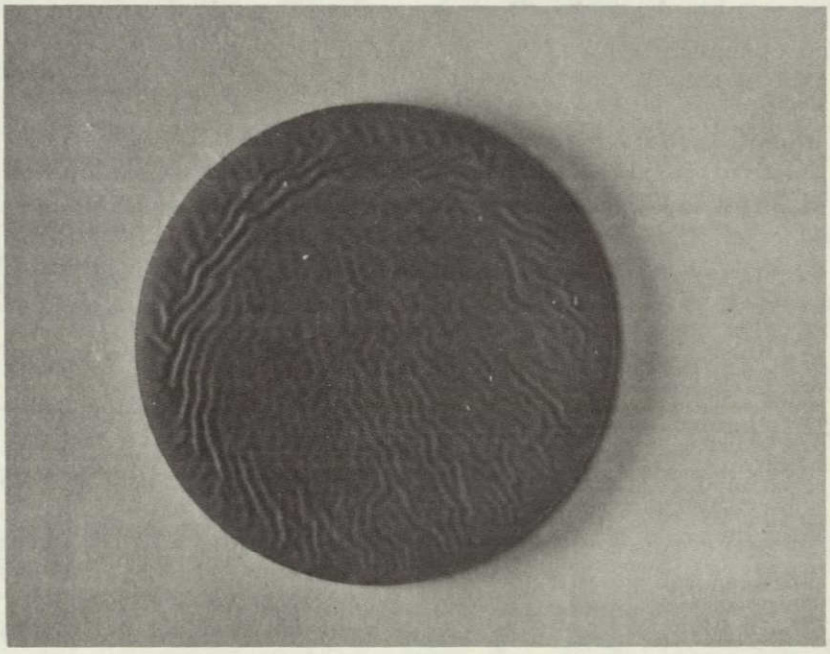

Figure 2-38. Wrinkled CVD Si Film 14μm Thick Grown on Glazed Alumina Substrate (Lead-borosilicate Glaze 743 on ASM614) in He at 700°C

1025°C produced single-crystal growth on the sapphire and a film having reflective sheen on the alumina. No obvious form of impurity contamination in the film on the sapphire was in evidence in those experiments.

Based on those preliminary results and the early availability of this and similar substrate materials received from MRC and Coors, the aluminas were selected for some of the first studies of CVD parameters in the work of Task 3 (see Section 1), as well as for detailed characterization of the substrate materials themselves.

However, because the glasses more closely qualify as low-cost substrates in the context of this contract, the description of Si CVD film growth experiments with glass substrates will be given first.

2.3.9 Si CVD on Glasses

Initial exploratory deposition experiments with Corning Code 7059 barium aluminoborosilicate glass were done early in the first quarter, prior to the first trip to visit potential suppliers, and at that time deposition parameters were arbitrarily chosen. At a SiH_4 flow rate of 25 ccpm, a He flow of 6 ℓpm, and a temperature of 700°C, a highly reflective film of Si was grown for 25 min on this glass, but considerable bowing of the film-substrate composite in a concave-upward direction occurred, as was shown in Figure 2-36, indicative of appreciable tensile stress in the film.

Based on the relative magnitudes of the TECs for Si and 7059 glass (see Figure 2-4), bowing in the opposite direction would be expected if differential thermal contraction alone were responsible. However, the composite was observed to bow in the same direction during the growth process, prior to cooling. Thus, other causes directly related to the physical and/or chemical stability of the glass at temperatures around 700°C were probably involved.

A second similar experiment showed that the 7059 glass did not distort detectably prior to Si film deposition at 700°C. No bowing was observed in He, for example, at 600, 650, or 700°C after 30 minutes at each temperature, but concave-upward bowing was obvious after only a few minutes of Si growth at 700°C. The distortion therefore resulted from reaction of the glass surface with the SiH_4 or its products of decomposition. This incompatibility probably rules out Code 7059 glass as a simple non-composite low-cost substrate for Si growth by SiH_4 pyrolysis.

The Corning Code 1723 aluminosilicate glass, which was specially prepared in plate form (it is normally available only in blown-ware, tubing, and rod), was also evaluated early in the program for its compatibility with Si grown from SiH_4, in both H_2 and He atmospheres. Si grown in a H_2 carrier at 850°C (~60 deg C below the softening point) resulted in a film with "worm-like" structure, indicating probable local melting or chemical reaction of the glass, and some obvious contamination of the companion sapphire substrate. Bowing was in evidence in a convex-upward direction following deposition, prior to

cooling to room temperature, for the 17μm-thick film on the 750μm-thick substrate. Due to differences in TEC for the two materials this bowing might be expected to increase, producing compressive stresses in the Si.

With this same glass at a growth temperature of 850°C in a He atmosphere, a Si film ~26μm thick was produced which consisted of a mixture of large and small grains; the Si film grown simultaneously on sapphire gave evidence of having been contaminated by the neighboring glass substrate.

Si growth in He at ~620°C, which is below the strain point of the glass (665°C), produced a very reflective film on the glass, but the film grown simultaneously on the sapphire monitor wafer peeled during handling, again suggesting contamination of the Si and/or sapphire by volatile products from the glass. At high magnification, bubbles of various sizes were observed in the Si film and/or at the film-glass interface, by both optical microscope and SEM examination (Figure 2-39). These results indicated that this glass also is probably not satisfactory as a substrate for the growth of Si sheet by SiH_4 pyrolysis.

Early exploratory Si CVD compatibility experiments carried out with the three glasses Corning Code 1715, Owens-Illinois GS211, and Owens-Illinois GS213 also indicated serious instabilities when H_2 was used as the carrier gas. For example, all three substrates failed the SiH_4-in-H_2 growth tests at ~850°C, evidenced by whisker type growth on the substrate surfaces and/or major contamination of the Si film grown on the companion sapphire substrate. As an illustration, Figure 2-40 is an SEM photograph of the surface of the Si deposit grown on glass GS211 at ~850°C in H_2 (4 ℓpm flow rate), with a SiH_4 flow rate of 25 ccpm. In addition to the obviously defective deposit on the glass, the Si growth on the neighboring sapphire was seriously affected by some contaminant, presumably resulting from the glass reaction with the CVD environment.

However, in a SiH_4-in-He environment at about the same temperature the Si films deposited on the three glasses appeared to be quite normal; contamination of the companion sapphire substrate did not appear in any of the three cases.

The Si depositions on 1715 glass were done in the temperature range ~860 to ~1000°C. The He flow rate was 6 ℓpm and the SiH_4 flow rate 25 ccpm in each of the experiments. The Si film grew at a rate of ~0.6μm/min to a thickness of ~6μm in the experiment at ~860°C; ~1.4μm/min to a thickness of ~14μm at 914°C; ~1.0μm/min to a thickness of ~16μm at 955°C; and ~1.0μm/min to a thickness of ~20μm at 1000°C.

The films grown on this glass at the three higher temperatures each had a dull finish at the conclusion of the experiment. The film surface was heavily textured in all four cases, but the nature of the surface features was quite different for the four samples, as shown by optical microscope and SEM examination. The SEM photographs for the 6μm deposit prepared at a low growth rate at ~860°C show a film surface with suprisingly well-ordered crystallographically faceted features producing good reflectivity at certain viewing angles to the normal. The surface of this sample is shown in Figure 2-41. The surface texture has a re-

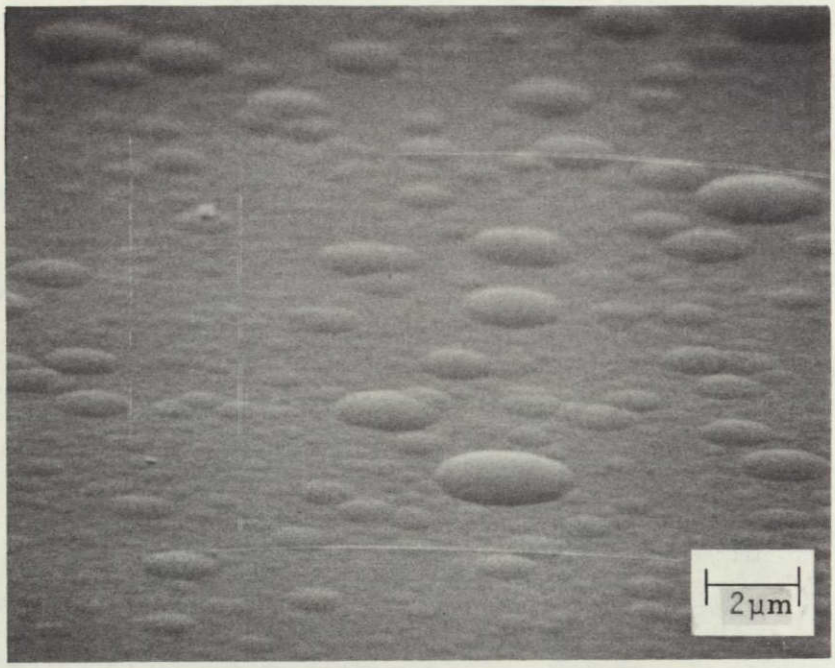

Figure 2-39. Bubbles Formed at Interface of CVD Si Film Grown on Corning Code 1723 Glass Substrate at ~650°C in He

Figure 2-40. SEM Photograph of CVD Si Deposit on O-I Glass GS211 at ~850°C in H_2 Atmosphere

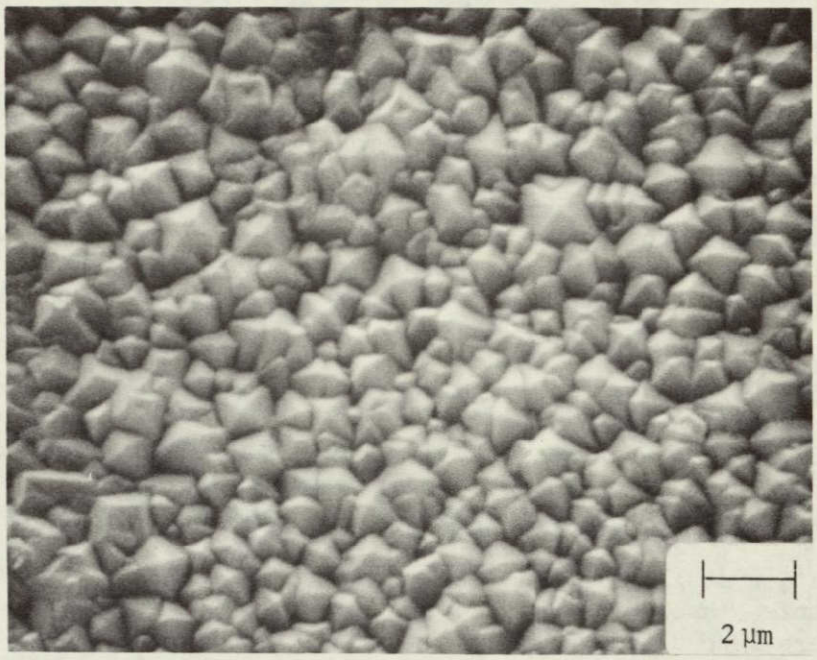

(a)

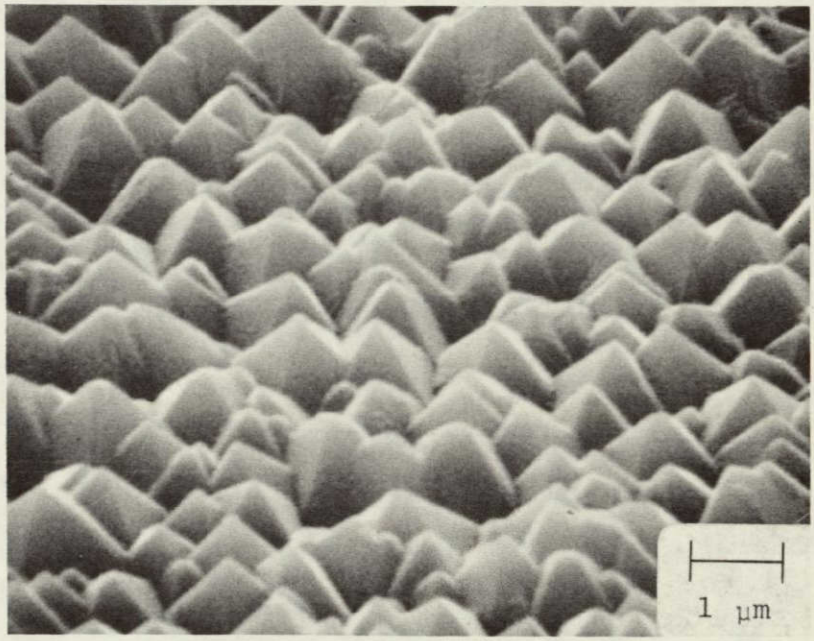

(b)

Figure 2-41. SEM Photographs of Surface of CVD Si Film Grown on Corning Code 1715 Glass by SiH_4 Pyrolysis in He at ~860°C. a) View at Normal Incidence; b) View at 45 deg to Surface

semblance to that observed on some of the ordered polycrystalline Si films grown on several of the relatively fine-grained polycrystalline alumina materials (see Section 2.3.10).

At the higher deposition temperatures, however, the surface texture of the films grown on 1715 glass became coarser and more "three-dimensional" in appearance, with numerous bulbous projections. The Si film deposited on 1000°C, for example, grew at a rate almost 50 percent faster than the one grown at ~860°C and was ~20μm thick, rather than ~6μm. SEM examination showed a much different surface texture, with little obvious faceting on the relatively tall surface features (Figure 2-42), which accounts for the dull appearance of the film.

The experiments with Owens-Illinois glasses GS211 and GS213 with He carrier gas were also done with a He flow rate of 6 ℓpm and a SiH_4 flow rate of 25 ccpm. The film on GS211 deposited at ~850°C grew at a rate of ~1.7μm/min to a thickness of ~35μm, while that on GS213 was deposited at 860°C at a rate of ~2μm/min to a thickness of ~50μm. In both cases deeply textured surfaces resulted on the Si deposit, producing a very dull appearing finish.

SEM examination of the film on GS211 indicated somewhat irregular pyramidal growth features, averaging about 4μm across with moderate faceting (Figure 2-43). There were also what appeared to be large clusters or "chunks" of Si distributed about the surface, indicating a less orderly growth process than was observed at the same deposition temperature on Corning Code 1715 glass. Electrical measurements on the undoped film on this glass indicated a much higher conductivity than that found for the other undoped Si-on-glass films, as discussed in the next section, suggesting the possibility of a high density of imperfections of some type - possibly an impurity acquired from the glass.

Further evidence of systematic structural differences among the films deposited on these glasses in the ~850-1000°C temperature range was obtained by x-ray diffraction analysis, and is discussed in the following section. The structural differences indicated both by the x-ray evidence and by the variations in surface texture described above could be in part a result of the change in the dominant layer growth mechanism in this temperature range in He, as was suggested relative to the observed maximum in the growth rate vs temperature curve for He carrier gas (see Figure 2-29).

Further details of the properties of undoped and doped Si films grown on these glasses in He atmospheres are given in the next two sections.

2.3.9.1 Structural and Electrical Properties of Undoped CVD Si Films on Glasses

A group of four undoped Si films deposited by SiH_4 pyrolysis in a He atmosphere on substrates of Corning Code 1715 glass (calcium aluminosilicate) was characterized for structural and electrical properties. The He flow rate was 6 ℓpm and the SiH_4 rate was 25 ccpm in the four depositions, carried out at temperatures of 858, 914, 955, and 1000°C. The four films are listed in Table 2-10.

The film grown at ~860°C was observed to have a dark and somewhat granular appearance due to the microscopic faceting of the surface, as was discussed

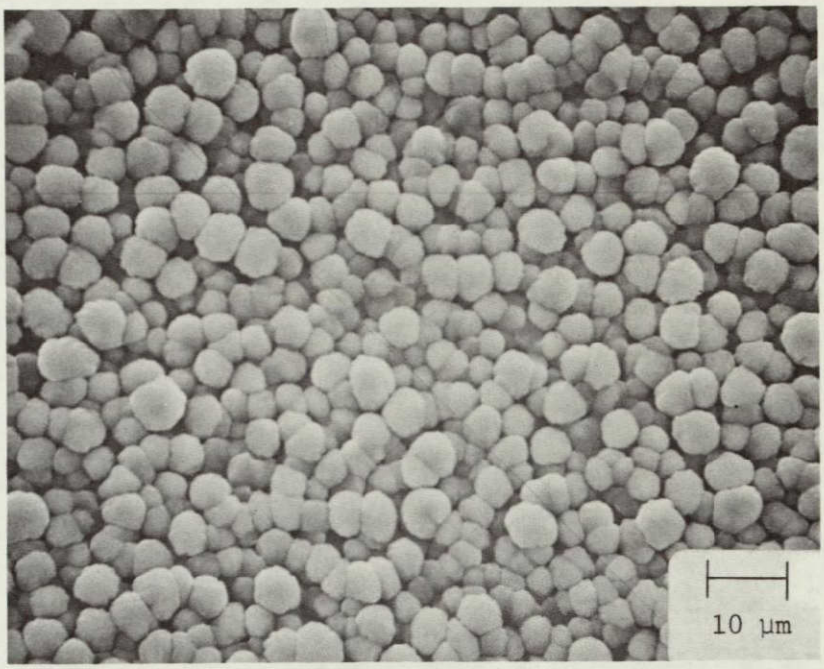

(a)

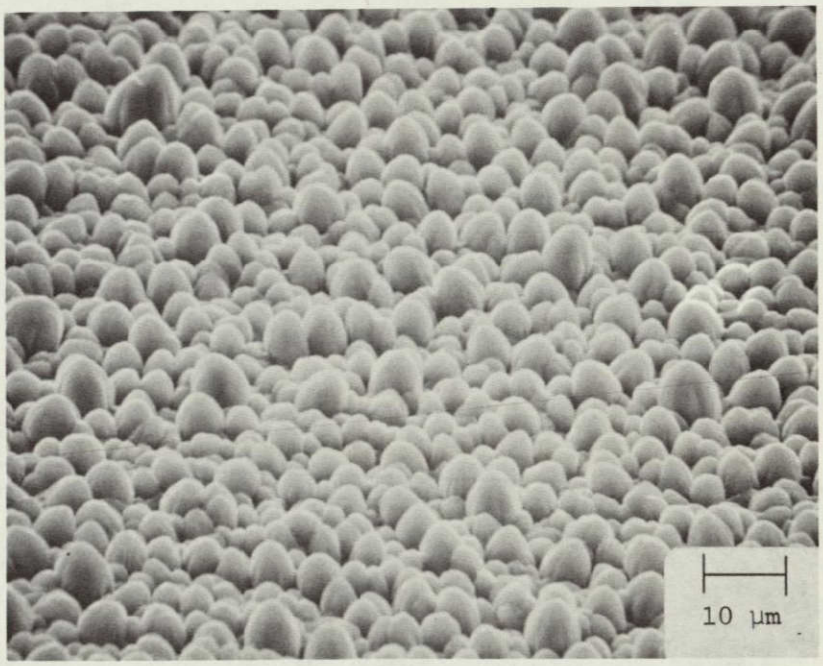

(b)

Figure 2-42. SEM Photographs of Surface of CVD Si Deposited on Corning Code 1715 Glass by SiH_4 Pyrolysis at 1000°C in He. a) View at Normal Incidence; b) View at 45 deg to Surface

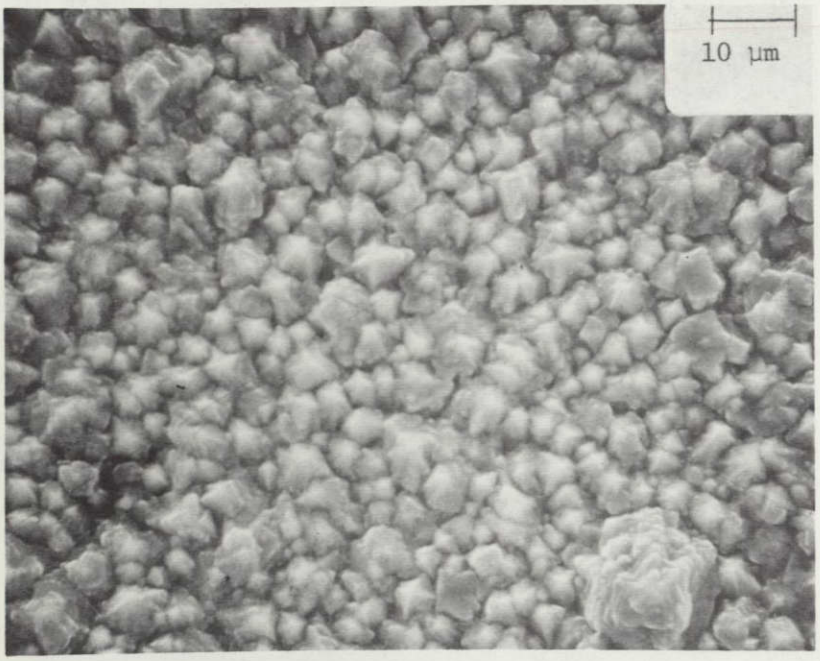

(a)

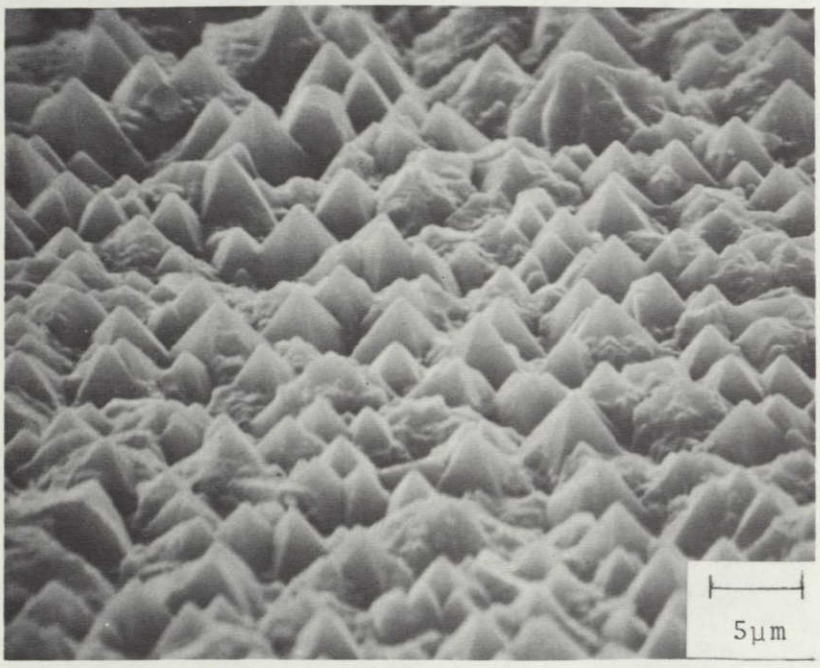

(b)

Figure 2-43. SEM Photographs of Surface of Si Film Deposited on Owe Illinois GS211 Glass by SiH_4 Pyrolysis at ~860°C in He. a) View at Normal Incidence; b) View at 45 deg to Surface

Table 2-10. Structural Properties of CVD Si Films Grown by SiH_4 Pyrolysis in He on Corning Code 1715 Glass

DEPOS. TEMP. (°C)	AVERAGE FILM THICKNESS (μm)	DEPOSITION RATE (μm/min)	AVE. HORIZ. DIMENSION OF SURFACE FEATURES (μm)	PREFERRED CRYSTAL ORIENTATION BY X-RAY ANALYSIS*
858	5.9	0.6	0.9	VS {100}; FS {111}; A {110}
914	14	1.4	3.5	FS {100}; FS {111}; P {110}
955	16	1.0	4.0	P {100}; P {111}; FS {110}
1000	20	1.0	3.3	P {100}; P {111}; P {110}

*VS = very strong,

*FS = fairly strong,

*P = preferred, but only moderately;

*A = not detected.

above. Examination of the specimen by SEM revealed a surface of fairly regular approximately tetrahedral features that appeared to be ~0.9μm in average dimension in a direction parallel to the film-substrate interface, as indicated in the table. The orientation of the facets was not determined.

SEM photographs of the film surface at two different magnifications, one at normal incidence and one at a 45 deg viewing angle with the sample surface, were shown in Figure 2-41. The regular faceting of the surface features is clearly visible in the normal incidence view of Figure 2-41a. The oblique view in Figure 2-41b shows the steep sides of the largely tetrahedral features. This film had external characteristics quite similar to some of the Si films obtained earlier in the program on relatively fine-grained polycrystalline alumina substrates. It is striking that such characteristics were obtained on an amorphous substrate; these results offered considerable encouragement for continued work with this glass substrate material.

Analysis of the x-ray diffraction line profiles for this film indicated a very strong preferred {100} orientation, consistent with the external tetrahedral surface morphology observed in the SEM examination. There was also evidence of stronger {111} orientation than is characteristic of random polycrystalline Si. The {110} orientation was not detected in this film.

The other three films on 1715 glass were also examined. X-ray diffraction analysis of these films - in terms of the relative intensities of the (111), (220), (311), and (400) lines - was carried out using both graphical analysis of the diffractometer traces and numerical results obtained from the angle-mode programmer attachment for the diffractometer. The analyses clearly showed a steady decrease in the amount of preferred {100} orientation with increasing growth temperature, although even at 1000°C this orientation was more prevalent than in a randomly oriented polycrystalline Si sample. Conversely, the {110} orientation, not preferred in the film grown at ~860°C, increased in prevalence with increasing growth temperature to 955°C, and then decreased somewhat at 1000°C.

Similar evidence of a maximum in the degree of preferred {110} orientation in this same general deposition temperature range and film thickness range was observed by Kamins and Cass (Ref 8) for CVD Si polycrystalline films deposited on thermally oxidized Si wafers. The {111} orientation, appearing as a preferred orientation in the film deposited at ~860°C, also appeared to decrease steadily with increasing deposition temperature - a result different from that found by Kamins and Cass for Si on SiO_2. (See Table 2-10.)

Examination of the same three specimens in the SEM showed surface features somewhat like those found on the film grown at ~860°C. However, the average horizontal dimension of the regular surface features was found to be 3.5, 4.0, and 3.3μm for the films deposited on 1715 glass at 914, 955, and 1000°C, respectively (Table 2-10). It should be noted that the film grown at ~860°C was only about 6μm thick, while the other three were two to three times as thick. If, as earlier evidence indicated, individual grains tend to increase in horizontal dimension as the film thickness increases, then some of the difference between the observed surface-feature dimension for the 860°C film (~0.9μm) and that of the other three films (3-4μm) could be attributed to the thickness difference.

The difference in the surface characteristics of the films deposited at the higher temperatures is shown by the SEM photographs of the 1000°C film, which were shown in Figure 2-42. Considerably coarser surface features are evident, there are numerous tall bulbous projections, and faceting of the surface features is almost absent.

The two films deposited at the intermediate temperatures (914, 955°C) exhibited surface structures intermediate between those shown in Figures 2-41 and 2-42. The film deposited at 955°C resembled that deposited at 1000°C (Figure 2-42), while that grown at 914°C still exhibited some faceting, although not nearly as pronounced as that shown in Figure 2-41.

Electrical measurements were made on the four undoped Si films on Corning Code 1715 glass, using a Hall bridge pattern on all films and the van der Pauw method on all but the film grown at 860°C. The van der Pauw method was used first; then a Hall bridge pattern was photolithographically etched into the Si film in the center of the region in which the van der Pauw measurements were made. Resistivity in all four was high, ranging monotonically from 2.8×10^5 ohm-cm in the film grown at ~860°C down to 8.1×10^4 ohm-cm in the film grown at 1000°C. All films were p type as grown, with measured carrier concentrations in the range from 5×10^{11} to 1×10^{13} cm^{-3}. The films grown at the two intermediate temperatures (914 and 955°C) exhibited the highest carrier mobilities and the lowest carrier concentrations. Results of these measurements are given in Table 2-11. Differences in the measured values of the parameters obtained by the van der Pauw and the bridge methods largely follow the pattern indicated in the discussion in Section 2.3.7.4, even for the polycrystalline films involved here.

Also included in the table are the results of electrical measurements on an undoped Si film deposited at ~860°C on Owens-Illinois glass GS211. The film was deposited in He carrier gas at a flow rate of 6 ℓpm with the SiH_4 flow rate 25 ccpm, resulting in an average thickness of ~35μm. This undoped polycrystalline film was much more conducting than those on the Corning glass; a p-type carrier concentration $\geq 10^{15} cm^{-3}$ indicates a fairly high density of structural defects or, more likely, a significant impurity content in the film - presumably from the glass, as mentioned earlier.

X-ray diffraction analysis of the film grown on GS211 indicated strong {110} preferred orientation, and the {100} orientation was stronger than in a random polycrystalline Si sample but not predominant. Figure 2-43 showed SEM photographs of the surface of the film deposited on the GS211 glass. The deeply textured surface is seen to be more irregular than that found on the Si film deposited at the same temperature on Corning Code 1715 glass (Figure 2-41). The surface features have an average horizontal dimension of about 4μm, essentially the same size as the surface features observed on the three thick (14-20μm) Si films grown on Corning Code 1715 glass at the higher temperatures (Table 2-10), yet they resemble the tetrahedral morphology seen in Figure 2-41b. The large chunks of Si (or other material) referred to earlier are quite visible in Figure 2-43a.

All of the Si-on-glass films discussed above have a general surface character similar to the rosette type of structure observed on Si films grown on polycrystalline as-fired alumina substrates. Significantly different, however, is the greater degree of crystallographic faceting found in the films on glass and the larger angles made by these facets with respect to the nominal substrate surface plane.

Results obtained with polycrystalline Si films deposited on Corning Code 1715 glass early in the program indicated that variations in preferred orientation occur both with film thickness and with deposition temperature. Studies of

Table 2-11. Electrical Properties of CVD Si Films* Grown by SiH_4 Pyrolysis† on Glass Substrates in He Carrier Gas††

SUBSTRATE	DEPOS TEMP (°C)	AVE FILM THICKNESS (μm)	METHOD OF MEAS**	RESISTIVITY (ohm-cm)	CARRIER CONC.* (cm^{-3})	CARRIER MOBILITY (cm^2/V-sec)
Corning 1715 Glass	858	5.9	HB	2.8×10^5	1.1×10^{13}	2.0
	914	14	vdP	1.3×10^5	5.8×10^{11}	82
			HB	1.1×10^5	5.0×10^{11}	111
	955	16	vdP	1.0×10^5	7.7×10^{11}	81
			HB	4.5×10^4	1.5×10^{12}	95
	1000	20	vdP	7.3×10^4	1.1×10^{13}	7.7
			HB	8.1×10^4	1.8×10^{12}	43
Owens-Illinois GS211 Glass	861	35	vdP	82.5	3.5×10^{16}	2.2
			HB	2×10^3	1.0×10^{15}	3.1

* All films p type; all undoped

† SiH_4 flow rate 25 ccpm

†† He flow rate 6 ℓpm

** HB = Hall bridge; vdP = van der Pauw

polycrystalline Si on other amorphous substrate materials by other investigators (Refs 8,12) have given similar results. To investigate this dependence further, because of its possible influence on the photovoltaic properties of the polycrystalline films, two groups of undoped film samples on glasses were prepared, one deposited at ~850°C and one at ~950°C (both in He), each involving films in three different thickness ranges (1000-2000Å , 1.5-2.5μm, and 6-10μm). RED analysis was then used in the evaluation of the properties of these films. Substrates of Corning Code 1715, Owens-Illinois GS211, and Owens-Illinois GS213 glasses and single-crystal ($01\bar{1}2$)-oriented sapphire were used. The specific objective was to determine if any differences in preferred orientation could be detected among films grown at a given temperature in the three thickness ranges or between films of similar thickness grown at the two different temperatures.

The RED patterns obtained for the three thicknesses of films grown at ~850°C in He are shown in Figures 2-44 through 2-47 for films on substrates of 1715, GS211, and GS213 glasses and single-crystal sapphire, respectively. There is evidence of preferred orientation in the thinnest film and more strongly preferred orientation in the thicker films, for the case of all three glass substrates.

The thinnest films (0.1-0.2μm) on all three glasses exhibited surprisingly good structural quality, with the degree of preferred orientation in the films on GS211 and GS213 glasses significantly greater than in the film on 1715 glass. The latter showed only slight evidence of any preferred orientation. Thicker films (~1.6μm) were structurally better in all three polycrystalline cases, the increase in preferred orientation being most noticeable in the film on 1715 glass; the two films were structurally similar on the other two glasses, that on GS213 exhibiting slightly stronger preferred orientation than the film on GS211.

The thickest films showed still greater preferred orientation in all three polycrystalline cases, again with the greatest improvement occurring in the film on 1715 glass; the RED pattern in the latter case resembles that of a twinned epitaxial sample. In all three thickness ranges the films on the companion sapphire substrates appeared epitaxial, with excellent structural perfection indicated by the RED patterns.

Figures 2-48 through 2-51 show the RED patterns obtained for the four sets of films grown at ~950°C (observed) in He. These films were generally not as good structurally--with the exception of the films on sapphire, which appeared as even better epitaxial single-crystal layers (at all three thicknesses) than those grown at ~850°C. The ~0.15μm film on 1715 glass (Figure 2-48a) produced a pattern with only a few polycrystalline rings on a background of a near continuum; the patterns from the films on GS213 and GS211 consisted of prominent polycrystalline rings with no evidence of the segmenting that is associated with strong preferred orientation, thus distinguishing these films from the ~0.1μm films grown on these two glasses at ~850°C.

Figure 2-44. RED Patterns for CVD Si Films Grown on Corning Code 1715 Glass at ~850°C in He, in Thickness Ranges a) 0.1-0.2μm, b) 1.7-2.5μm, c) 8-9μm.

Figure 2-45. RED Patterns for CVD Si Films Grown on Owens-Illinois GS211 Glass at ~850°C in He, in Thickness Ranges a) 0.1-0.2μm, b) 1.7-2.5μm, c) 8-9μm.

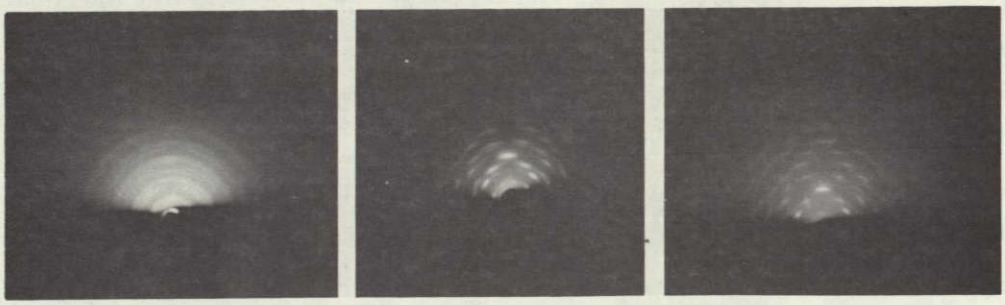

Figure 2-46. RED Patterns for CVD Si Films Grown on Owens-Illinois GS213 Glass at ~850°C in He, in Thickness Ranges a) 0.1-0.2μm, b) 1.7-2.5μm, c) 8-9μm.

Figure 2-47. RED Patterns for CVD Si Films Grown on $(01\bar{1}2)$-oriented Sapphire at ~850°C in He, in Thickness Ranges a) 0.1-0.2μm, b) 1.7-2.5μm, c) 8-9μm.

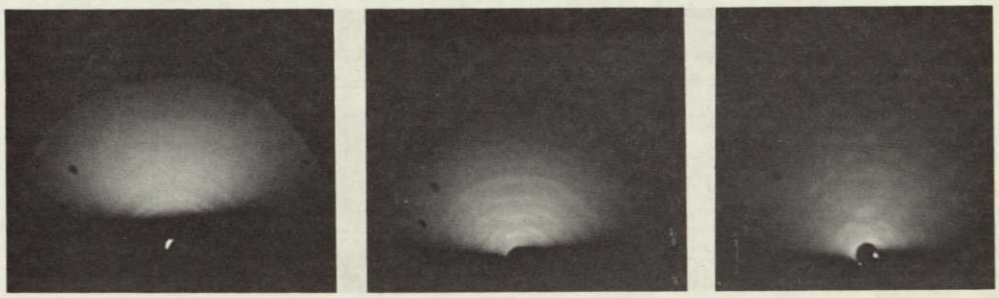

(a) (b) (c)

Figure 2-48. RED Patterns for CVD Si Films Grown on Corning Code 1715 Glass at ~950°C in He, in Thickness Ranges a) 0.3-0.4μm, b) 1.7-2.3μm, c) 3-6μm.

(a) (b) (c)

Figure 2-49. RED Patterns for CVD Si Films Grown on Owens-Illinois GS211 Glass at ~950°C in He, in Thickness Ranges a) 0.3-0.4μm, b) 1.7-2.3μm, c) 3-6μm.

(a) (b) (c)

Figure 2-50. RED Patterns for CVD Si Films Grown on Owens-Illinois GS213 Glass at ~950°C in He, in Thickness Ranges a) 0.3-0.4μm, b) 1.7-2.3μm, c) 3-6μm.

(a) (b) (c)

Figure 2-51. RED Patterns for CVD Si Films Grown on $(01\bar{1}2)$-oriented Sapphire at ~950°C in He, in Thickness Ranges a) 0.3-0.4μm, b) 1.7-2.3μm, c) 3-6μm.

The thicker films (~1.7μm) on all three glasses showed segmenting in the rings of the RED patterns, with the films of GS213 and GS211 again exhibiting slightly more of the effect than did the film on 1715 glass. In this instance all three films exhibited the change from continuous rings to segmented rings corresponding to a thickness change from ~0.1μm to ~1.7μm, whereas at ~850°C growth temperature only the film on 1715 glass went through this transition. Generally, however, the ring patterns were much less distinct for the films grown at 950°C than for those at 850°C, indicating the possibility of a less ordered growth at all stages for the higher temperature.

The thickest films grown at ~950°C (3-6μm) produced RED patterns even less sharply defined than those for the 1.7μm films, although it appeared that the indistinct rings were segmented more abruptly than in the patterns produced by the intermediate-thickness films. One interpretation of this result is that the preferred orientations were relatively more sharply established in the thickest films but all other crystallites were nearly randomly oriented, with perhaps even some pseudo-amorphous regions occurring.

Whereas the RED method samples only a very thin region of the film near the upper (last-grown) surface, x-ray diffraction analysis produces patterns that are formed by contributions from diffracted beams from regions up to many micrometers below the surface. X-ray diffraction analysis of the thinnest films (0.15-0.18μm) grown at 855-860°C indicated a highly polycrystalline structure in the three films on glass, with the {100} planes about equally (but not strongly) preferred on all three substrates and the {110} planes only slightly preferentially oriented on the GS211 and GS213 glasses but not on 1715 glass. These results are not inconsistent with the evidence obtained by RED analysis, although the film thicknesses were not large enough to generate strong intensities in the x-ray spectrum.

The thicker films (1.7-2.5μm) on all three glasses exhibited preferred {100} orientation, strongest in the film on GS211 glass and weaker (but about equal) in the films on 1715 and GS213 glasses. In all three cases this preferred orientation was significantly stronger than was observed in the very thin films. The {110} planes did not appear as preferentially oriented in these intermediate thickness films; in fact, the (220) line was nearly absent in the spectrum for the film on GS213 glass.

The thickest films (7.9-9.3μm) on the three glasses exhibited very strong {100} preferred orientation--about the same in all three cases. In addition, the film on 1715 glass exhibited moderately strong {110} preferred orientation, consistent with the evidence obtained by RED analysis that the thick film on 1715 glass was highly oriented (although polycrystalline).

In all three thickness ranges the films grown at ~850°C on sapphire exhibited (111), (220), and (400) diffraction lines, but the (311) line was missing in each case. The relative intensity of the (400) line, associated with the {100} planes, increased with film thickness and was extremely strong, as might be expected for films that are nearly completely epitaxial but have some misoriented or polycrystalline content.

structural quality was about the same for the three substrates, although both {100} and {110} preferred orientations were present in films grown at the higher temperature. The temperature dependence of preferred orientation in these films is obviously a complex function; further detailed study is required to define it completely.

During the fifth quarter of the program Owens-Illinois supplied three billets of experimental glasses (7 cm diam x 6.5 cm thick), designated EE-2, EE-5, and GS-238 (see Table 2-2 for pertinent properties). These billets were processed by a Rockwell glass fabricating laboratory into polished substrates about 750μm (0.030 in.) thick. Final polishing to a "felt" finish with CeO_2 produced surfaces which appeared to be void-free and superior to those previously supplied by the manufacturer. Substrates of these glasses that were cleaned with a Caro's etch were compared with those cleaned only with organic solvents; SEM photographs showed that the surfaces were essentially identical in the two cases, so Caro's etch was used in the "standard" substrate cleaning procedure thereafter.

A preliminary evaluation of the three new Owens-Illinois glasses was then undertaken. In one experiment polished samples of EE-2, EE-5, and GS238 glasses were used (together with a sapphire monitor wafer) for deposition of undoped Si by pyrolysis of SiH_4 (flow rate ~11.5 ccpm) in He (1.5 ℓpm) at ~845°C (observed) for 30 min, resulting in a layer ~24μm thick on the Si and corresponding to a growth rate of ~0.8μm/min. The growth progressed well, without incident, and the films on all three glasses appeared to be uniform and clean and relatively reflective. There was no evidence of any cross-contamination from the glasses to the sapphire substrate, on which the film appeared to nucleate properly and grow without perturbation. Resistivities were all $1\text{-}2\times10^5$ ohm-cm except for that of the layer on EE-5 glass, which was $\sim2\times10^4$ ohm-cm. Carrier concentrations were about 10^{12} cm^{-3}, except for the film on EE-5 in which the value was $\sim6\times10^{13}$ cm^{-3}.

Additional experiments were done with these same glasses and substrates of GS213 glass, to provide a known reference substrate in addition to the customary sapphire. Deposition was done at ~860°C (observed) with a lower SiH_4 flow rate (~10 ccpm) and a He flow rate of 1.5 ℓpm for 80 min, resulting in a film ~38μm thick on the sapphire (growth rate ~0.5μm/min). This run also progressed well, with no evidence of significant contamination or other problems of film nucleation and growth. There was indication of some differences in growth features of the films on two of the glasses (EE-2 and EE-5) near the edges of the substrates, but this may have been the result of thermal gradients or reactant gas flow patterns near the periphery of the sample pedestal.

The three glasses were also found not to be stable to the Si CVD growth process in H_2; this environment resulted in severely perturbed growth, including whisker-like formations and other phenomena common to films grown on other glasses in H_2 atmospheres.

X-ray diffraction analysis of the polycrystalline films grown at ~850°C in He showed there to be moderately strong {110} preferred orientation on all three of the new glasses, in the films grown with a SiH_4 flow rate of ~11.5 ccpm and film thicknesses of about 25μm. The amount of preferred orientation was about the same on GS238 and EE-2 and slightly less for the film on EE-5. There was also definite preferred {100} orientation, although not as strong as the {110}; it was again less prominent in the film on EE-5 than in the other two samples. The film grown simultaneously on $(01\bar{1}2)$ sapphire in this experiment was not epitaxial; a Laue back-reflection diffraction pattern indicated polycrystalline structure, but the diffractometer analysis showed very strong {100} preferred orientation, as would be expected, together with about the same preferred {110} orientation as observed in the film grown simultaneously on the EE-5 glass substrate.

Spreading resistance (SR) probe scans* through the thickness of the films confirmed their high resistivity, but clearly showed that the resistivity increased nearly linearly with depth into the film by about an order of magnitude in all four cases. For all films but that on EE-5 glass the resistivity indicated by the SR scan at the film-substrate interface was very nearly the value given by the van der Pauw measurements ($1\text{-}2\times10^5$ ohm-cm); for the film on EE-5 glass the SR scan indicated a surface resistivity somewhat lower than that found in the other films, and the van der Pauw result was also lower ($\sim2\times10^4$ ohm-cm), although the resistivity at the interface was $\sim10^5$ ohm-cm as for the other three films.

A set of undoped films grown on the same three glasses and sapphire plus a substrate of Owens-Illinois GS213 glass, with a SiH_4 flow rate of 10 ccpm and a temperature of 858°C, were in the thickness range 30-40μm. Carrier concentrations measured by the van der Pauw method had been found to be in the $2\times10^{11}\text{-}8\times10^{12}$ cm^{-3} range, and resistivities were again $2\times10^4\text{-}2\times10^5$ ohm-cm. SR probe scans on these films also showed a nearly linear increase in resistivity with depth into the film by approximately an order of magnitude, with the resistivity at the interface being essentially equal to the value obtained by the van der Pauw measurement, as above. Again, however, the film on EE-5 glass was an exception, with the van der Pauw result intermediate between the SR resistivity value at the surface and that at the interface.

These observed resistivity variations with depth were consistent with earlier observations on Si films grown on other glasses and with the possible presence of a donor impurity occurring in increasing concentration near the interface.

The films grown in the last-mentioned experiment on the four glasses and sapphire were also analyzed for preferred orientation. Extremely strong {110} preferred orientation was found in the films on all four glasses in this experiment - over two orders of magnitude more prominent than found in the previous set of films. In this instance the orientation was strongest in the film on the EE-5 glass and least in the film on EE-2 glass, but still extremely strong. Again there was {100} preferred orientation observed, as well - about the same in the film on GS238 as in the previous experiment but over an order of magnitude stronger in the films on EE-5 and EE-2. The film on GS213 also exhibited preferred {100} orientation, stronger than that on GS238 but slightly less than that on EE-5 and EE-2.

*Measurements made by Solecon Laboratories, Costa Mesa, CA

2.3.9.2 Properties of B-doped CVD Si Films on Glasses

After preliminary data were obtained for B doping of Si films in He carrier gas at deposition temperatures of ~850°C, a series of experiments was undertaken to grow doped Si films on several candidate glass substrate materials, in each case also employing a single-crystal sapphire monitor substrate for simultaneous Si deposition.

The results of measurements of the electrical properties of some of these films are given in Table 2-12. All of the films in the table (except as noted) were grown under the same deposition conditions (SiH_4 flow rate 10 ccpm, He carrier gas flow rate 1.5 ℓpm, observed deposition temperature ~850°C).

Depressed growth rates were observed on the sapphire substrates in all of these experiments and for the glass substrates in all but experiments 164 and 171. The apparent growth rate on the glass ranged from 1.2 to over 2.0 times that on the single-crystal sapphire substrate in this series of depositions. Furthermore, the measured carrier concentrations were in most cases larger in the polycrystalline film on glass than in the simultaneously grown film on single-crystal sapphire, by factors ranging from 1.8 (experiment 168) to 5.4 (experiment 164). Only in experiments 171 and 172 were the measured carrier concentrations in the films on the glasses less than those measured in the films on sapphire, and only in experiment 171 was the resistivity of the film on glass less than that of the film on sapphire.

Although the Si films grown on sapphire at ~850°C were not completely epitaxial they would, under optimum growth conditions at this temperature, be expected to be at least strongly oriented crystallographically. It might be expected that a higher free carrier concentration would be found in such films than in highly polycrystalline films simultaneously grown on amorphous glass surfaces. The fact that this was not observed lends some weight to the suspicion that an impurity from the glass substrates used in these experiments adversely affected the Si film nucleation and/or growth process on the sapphire substrates, and probably also influenced the growth process and effective doping concentration in the films on the glasses as well.

Further evidence of such a possibility was obtained in spreading resistance measurements made on the films grown in experiments 164, 165, and 166. In experiment 164 substrates of Corning Code 1715 glass and single-crystal $(01\bar{1}2)$-oriented sapphire were used, with a B_2H_6 flow rate of 50 ccpm for 45 min resulting in films of approximately 27 and 17μm thickness, respectively (Table 2-12). A spreading resistance probe scan on a 0.05 rad bevel through the film on the glass substrate (32μm probe spacing, 20g probe load, 10μm increment between probe readings) produced the resistivity-vs-thickness plot of Figure 2-52a, upper curve. The data shown were obtained from the measured spreading resistance data by application of a correction factor based on the behavior of bulk single-crystal Si; it had been found previously in uniformly doped polycrystalline Si films that the resistivity values obtained by this method were in very good agreement with those obtained on the same films by four-terminal measurements of resistivity.

Table 2-12. Electrical Properties (van der Pauw Method) of CVD Si Films Grown by SiH_4 Pyrolysis* in He (1.5 ℓpm) on $(01\bar{1}2)$ Sapphire and Various Glass Substrates

Expt. No.	Obs. Depos. Temp. (°C)	B_2H_6† Flow Rate (ccpm)	Substrate Material**	Film Thick. (μm)	Growth Rate (μm/min)	Resist. (ohm-cm)	Carrier Conc. (cm^{-3})	Mobility (cm^2/V-sec)
164	850	50	Corning 1715 glass	27.2	0.60	8.0	5.4×10^{17}	1.4
			$(01\bar{1}2)$ sapph.	16.8	0.37	1.03	1.0×10^{17}	61.
165	856	500	Corning 1715 glass	14.2	0.32	0.20	2.6×10^{18}	12.
			$(01\bar{1}2)$ sapph.	12.0	0.27	0.13	1.4×10^{18}	35.
166	858	500	O-I GS211 glass	15.4	0.34	0.12	2.8×10^{18}	18.
			$(01\bar{1}2)$ sapph.	9.2	0.20	0.081	1.4×10^{18}	57.
167	851	50	O-I GS211 glass	19.0	0.38	0.37	1.2×10^{18}	14.
			$(01\bar{1}2)$ sapph.	10.7	0.21	0.26	3.9×10^{17}	61.
168	858	500	O-I GS213 glass	15.8	0.35	0.37	1.6×10^{18}	10.
			$(01\bar{1}2)$ sapph.	10.0	0.22	0.096	9.0×10^{17}	73.
169	856	50	O-I GS213 glass	29.0	0.32	6.3	2.5×10^{17}	40.
			$(01\bar{1}2)$ sapph.	17.8	0.20	0.44	1.3×10^{17}	108.
171	835	50	O-I GS210 glass	55.9	0.62	0.26	9.3×10^{17}	25.
			$(01\bar{1}2)$ sapph.	27.0	0.30	0.49	1.1×10^{18}	11.
172	839	50	O-I GS186 glass	38.0	0.42	14.0	1.2×10^{17}	3.8
			$(01\bar{1}2)$ sapph.	23.0	0.26	0.65	1.5×10^{17}	65.

*SiH_4 flow rate 10 ccpm

**All substrates polished

†B_2H_6 46 ppm in He

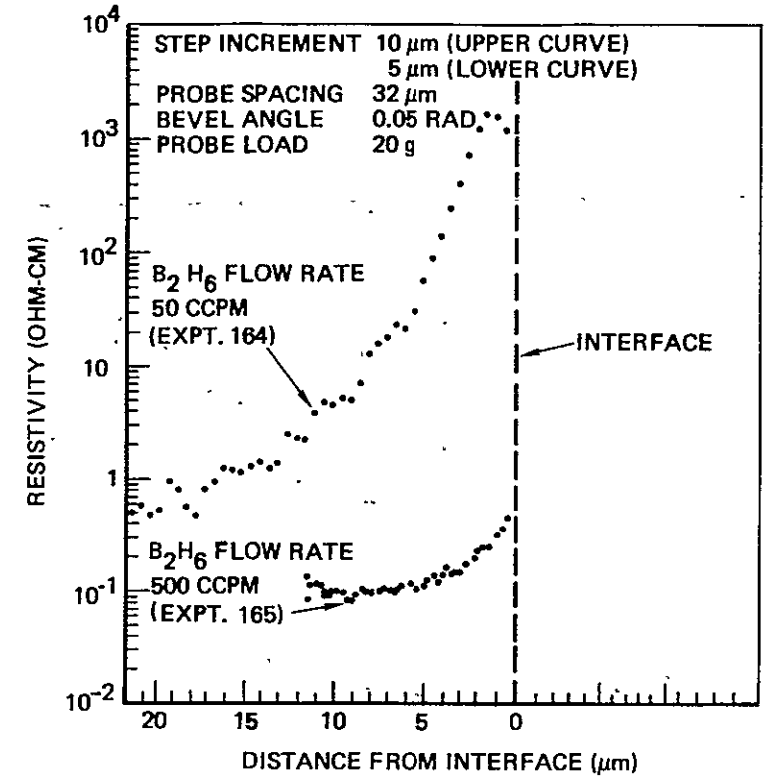

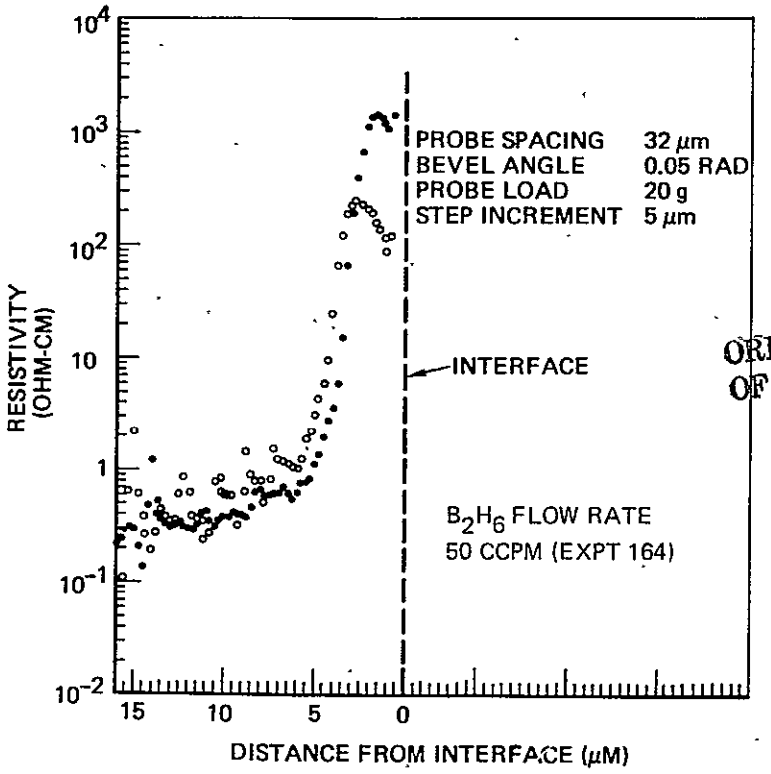

Figure 2-52. Spreading Resistance Probe Scans through Thickness of Doped CVD Si Films on (a) Corning Code 1715 Glass, and (b) Single-crystal Sapphire Substrates, for Two Different Boron Impurity Additions

Measurement of resistivity in another portion of this same film by the van der Pauw method indicated a value of 8 ohm-cm (Table 2-12), but it is clear from the SR scan that a large variation in resistivity with thickness occurs beginning ~8μm below the surface, covering a range from ~1 ohm-cm to over 10^3 ohm-cm at the Si-glass interface. A similar resistivity plot obtained on another Si film grown on Corning Code 1715 glass under essentially the same conditions except for the B_2H_6 flow rate (experiment 165, 500 ccpm) is also shown in Figure 2-52a. Although the deposition time was the same in both experiments there was a significant difference in the growth rate, so the film thicknesses were different in the two cases, as indicated in the figure.

Of significance is the fact that the resistivity of the more heavily doped film (order of magnitude difference in the measured carrier concentrations in the companion films on sapphire, as shown in Table 2-12) is much more uniform as a function of distance from the interface, although there is nearly an order of magnitude difference between the value near the surface (~0.1 ohm-cm) and that at the interface (0.6-1.0 ohm-cm). Furthermore, the SR probe values for this sample are quite consistent with the result obtained by the four-terminal method (0.2 ohm-cm), as given in the table.

Figure 2-52b shows the resistivity as a function of distance from the interface, obtained by spreading resistance measurements on two different bevels, for the film grown on sapphire simultaneously with that on glass in experiment 164 (upper curve, Figure 2-52a). One set of points was obtained at the edge of the sapphire substrate that adjoined the glass substrate during the deposition, while the other was obtained on another edge at a point ~6mm from the location of the first measurement (and thus that much farther from the glass substrate during the experiment).

Comparison of the plots for the two films shows several features of interest. First, the resistivity in the region of the interface is essentially the same for the film on glass as it is for the film on sapphire at the location nearest the glass substrate. Second, the resistivity at the interface in the film on sapphire is considerably larger in the location near the glass substrate than it is in the other region. Third, at both locations in the film on sapphire the resistivity drops rapidly at a distance greater than 2 or 3μm from the interface, decreasing to ~1 ohm-cm at a distance of 5 or 6μm from the sapphire interface and then slowly decreasing to a value of 0.3-0.4 ohm-cm at the surface. This value is somewhat less than that obtained by the four-terminal method, results of which are given in the table. The latter measurement provides a value that is an average over a significant part of the thickness of the film, accounting for the magnitude obtained. The resistivity variation with depth in the film on glass, however, becomes significant only a few micrometers below the surface, as indicated above.

In experiment 166 (Table 2-12) substrates of Owens-Illinois GS211 glass and single-crystal sapphire were used, again with a B_2H_6 flow rate of 500 ccpm, and films of about 15 and 9μm, respectively, were obtained. Measured carrier concentrations (van der Pauw method) were nearly the same - on both substrates - as those obtained in experiment 165, and there were only slight differences in resistivities as measured by the four-terminal method. The spreading

C-2

resistance measurement on the film grown on sapphire in this experiment showed only slight variation in resistivity with depth into the film, ranging from ~0.1 ohm-cm at the surface to an average of ~0.06-0.07 ohm-cm throughout most of the film, in very good agreement with the four-terminal value of 0.08 ohm-cm (Table 2-12). No excursion to very high resistivity at the interface was observed for this film on sapphire.

The spreading resistance results for the experiments with Corning Code 1715 glass appear to be consistent with the possible presence in the CVD Si films of some compensating donor impurity that might enter the film from the substrate, in the case of the film on glass, or indirectly from the glass through the vapor phase, in the case of the film on sapphire. This glass is a calcium aluminosilicate known to contain various amounts of other impurities. However, it is not clear which of these impurities - if any - would be likely to produce the observed effects in Si films deposited at temperatures of ~850°C for relatively short times. It is possible that other causes, such as residual surface contamination on the glass substrate or charge depletion effects associated with the presence of an insulating substrate, could be responsible for the observed effects.

X-ray diffraction analysis was used for identifying preferred orientation tendencies in doped polycrystalline Si films grown on these glasses in the 850°C temperature range. In an experiment in which a mixture of 1.5 ℓpm of He and 1.5 ℓpm of H_2 was used as the carrier gas to test the stability of two of the glasses in such an atmosphere at ~860°C (with a SiH_4 flow rate of 10 ccpm and a B_2H_6 flow rate of 50 ccpm) Si films were grown on polished substrates of Corning Code 1715 and Owens-Illinois GS211 glasses and single-crystal sapphire for 45 min, producing films approximately 20μm thick. X-ray analysis showed the film on the 1715 glass to be very strongly preferentially oriented with {100} planes parallel to the interface. There was also a moderate {111} preferred orientation, although it was much less prominent than the {100} dominant orientation; the {110} planes were also present but the line intensity (the (220) line) was weaker than that of the {311} planes. Thus, the distribution of principal low-index planes was quite similar to that found earlier in the program for undoped Si films grown on this glass in the 850-860°C temperature range.

The film grown on GS211 glass in this experiment also showed strong {100} preferred orientation, although it was not as dominant as in the film on 1715 glass. Also, there was not the evidence of {111} preferred orientation seen in the film on 1715 glass. The {110} planes, which had been found as a strong preferred orientation in an undoped film grown on GS211 glass earlier in the program , were also present but only to about the extent representative of a randomly oriented sample. Thus, the orientation tendencies of this doped film on GS211 glass appeared to be different from those seen earlier in an undoped film grown in a He (only) atmosphere.

To investigate this point further, a He (only) carrier gas (at 1.5 ℓpm) was used to grow Si simultaneously on GS211 glass and single-crystal sapphire substrates at ~860°C, with a B_2H_6 dopant flow rate of 300 ccpm. Again a

strong {100} preferred orientation was found by x-ray diffraction analysis, and again the diffraction line indicative of {110} planes was present but in about the relative intensity representative of a randomly oriented film.

The question of possible influence of the added B impurity concentration on the crystallographic orientation tendencies of these films was raised by the above results. Some evidence for such an effect had been observed previously in doped polycrystalline Si films grown on polycrystalline alumina substrates, such as Vistal (see Section 2.3.10).

A doped Si film grown on a substrate of Owens-Illinois GS210 glass (experiment 171, Table 2-12) at a temperature of 835°C (SiH_4 flow rate 10 ccpm, He carrier gas flow rate 1.5 ℓpm, B_2H_6 dopant gas flow rate 50 ccpm) was found by x-ray analysis also to exhibit strong {100} preferred orientation. This orientation tendency was not as strong as that observed in the films on GS211 glass and far less than that characteristic of films grown on Corning 1715 glass in this same temperature range. The deposition on GS210 was continued for 90 min, resulting in a 56μm film on the glass but only about half of that thickness on the companion sapphire substrate. It is interesting that the film grown simultaneously on the sapphire substrate in this experiment exhibited orientation characteristics not greatly different from those of a randomly-oriented film; only a tendency toward {100} orientation was noted, and the measured hole mobility was only 11 cm^2/V-sec.

In experiment 172 (Table 2-12) a 38μm film was grown on substrates of Owens-Illinois GS186 glass at a temperature of ~840°C for a period of 90 min; the SiH_4 and He flow rates had their customary values, and the B_2H_6 flow rate was again 50 ccpm. Once again, very strong {100} preferred orientation was observed in the film, and in this instance the diffraction line representative of {110} planes appeared somewhat more prominent than it would be for a randomly oriented film.

The possibility of variations in apparent preferred orientation with azimuth angle in the plane of the film-substrate interface was examined briefly for these polycrystalline films on glass. Films on GS211, GS210, and GS186 glasses were analyzed in this way. In all three cases some variations in diffraction line intensity ratios were found as the film was rotated in azimuth 45 and 90 deg from the position used initially for the diffractometer scan. However, in none of the instances was the ratio variation observed to be both systematic with angle and significant in magnitude. Thus, the observations concerning preferred orientation tendencies in these films appeared to be valid and not biased by other effects - such as those that would be present if there were a high incidence of very large crystal grains in the films, as in Si growth on refired Vistal alumina substrates, for example (see Section 2.3.10).

It thus seems clear that CVD Si films grown on various glasses by the SiH_4 pyrolysis reaction in a He carrier gas in the 850°C temperature region tend to crystallize with a strong {100} preferred orientation whether undoped or B-doped, at least when grown to thicknesses the order of 15μm or more.

Later in the program, when additional data on B doping of polycrystalline Si films grown in He at ~850°C were being obtained prior to fabrication of polycrystalline solar cell structures, another set of Si films on glasses was examined for the effects discussed in the preceding paragraphs. Substrates of Corning Code 1715, Owens-Illinois GS213, and Owens-Illinois GS211 glasses were used, along with the usual $(01\bar{1}2)$-oriented sapphire substrate in each run. The films were grown with a He flow rate of 1.5 ℓpm, SiH_4 at 11.5 ccpm, and B_2H_6 (46 ppm in He) flow rates ranging from 5 to 1000 ccpm.

Observed film growth rates on the sapphire substrates were in the range 0.3-0.4μm/min, whereas the growth rates obtained on sapphire in a preceding set of doping concentration experiments under essentially the same deposition conditions but without the glasses present were in the range 0.5-0.7μm/min. This result is consistent with the earlier observations about film growth rates for the SiH_4 pyrolysis process in the presence of certain glasses. The growth rates observed on the sapphire substrates were also less than those occurring for the films grown simultaneously on the glasses--typically half to two-thirds of the rate for the glasses, although variations were considerable.

The tendency for somewhat higher carrier concentrations to be measured in B-doped polycrystalline films grown on glasses in He at ~850°C than in the simultaneously grown films on sapphire substrates was again seen in this group of samples. Since very good crystal structure (i.e., essentially epitaxial growth) was found in this set of films on sapphire (by x-ray analysis) it would be expected that the available carrier concentration associated with added B impurity in any polycrystalline film grown at the same time would be less than that measured in the epitaxial film. Since this was again not found to be the case, it appears that other electrically active centers of some kind were probably involved, again suggesting the influence of an impurity from the glass substrate.

Both van der Pauw and SR determinations of layer resistivities showed that the polycrystalline films on the glasses in this set of samples had consistently higher resistivities than did the simultaneously grown films on sapphire, also as observed in the earlier results, except for one case in which a low B doping concentration was involved (diborane flow rate 5 ccpm) and the two films had very similar resistivity profiles throughout their thicknesses. The SR scans obtained on pairs of films simultaneously grown on substrates of Owens-Illinois GS211 glass and sapphire at three different B doping levels (diborane flow rates of 5, 150, and 1000 ccpm) are shown in Figure 2-53.

The SR scans in Figure 2-53a show the similarity in the resistivity profiles for the polycrystalline film and that grown on sapphire for the low doping case mentioned above. Figure 2-53b shows the large difference in resistivity for the two films obtained with a diborane flow rate of 150 ccpm. This large difference is believed to be associated primarily with a major difference in the effective carrier mobilities in the two films; separate van der Pauw measurements indicated significantly larger carrier concentration in the polycrystalline film on glass than in the film on sapphire. The large difference in thickness of the two films is also seen in this figure.

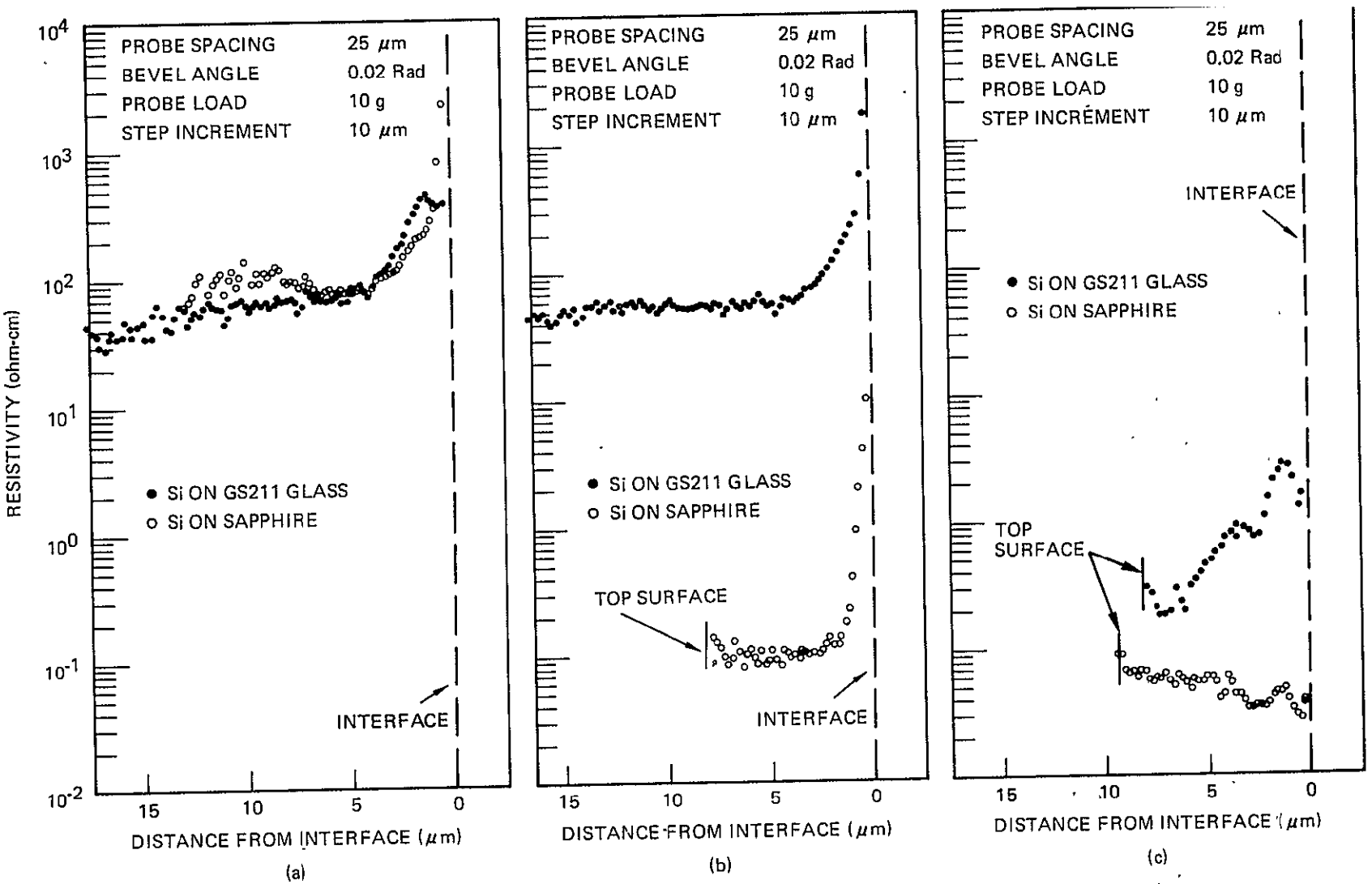

Figure 2-53. Spreading Resistance Probe Scans Showing Resistivity as Function of Distance from Interface for Three Pairs of CVD Si Films Grown Simultaneously on GS211 Glass and $(01\bar{1}2)$ Sapphire at ~850°C in He, for Diborane Flow Rates of a) 5 ccpm, b) 150 ccpm, c) 1000 ccpm.

Figure 2-53c shows the SR scans for the two films obtained with a very large diborane flow rate (1000 ccpm). Again the resistivity of the film on glass exceeds that of the film on sapphire, especially near the interface. The scans indicate fairly uniform resistivity with depth in the film on sapphire but a steady trend toward higher resistivity as the interface is approached in the film on glass (with several localized fluctuations).

The entire question of the possible influence of impurities in the glass substrates on the properties of the CVD Si films remains unresolved. There is some indication, in the SR scans for the three films on GS211 glass in Figure 2-53, for a resistivity variation with depth that could be associated with the presence of a donor impurity occurring in increasing concentration nearer the interface, but the effect is not nearly as pronounced as in films grown under similar conditions on Corning Code 1715 glass.

These experiments in which B-doped p-type Si films were grown simultaneously on glass and sapphire substrates also gave some evidence that diborane flow rates above about 300 ccpm failed to increase significantly the available hole concentration in the films on the sapphire substrates, using the 46 ppm B_2H_6-in-He source that had been employed in all of the p-type doping experiments on this program. This indicated either that a saturation concentration of the Si film with B had been reached (in the mid-10^{18} cm^{-3} net hole range) or that the concentration of B_2H_6 in the dopant source tank was insufficient to produce a higher B concentration in the Si film for the other parameters (SiH_4 flow rate and carrier gas flow rate) being used. In the former instance, the apparent saturation could be associated in some way with the presence of impurities in the glasses. It might also indicate that it will be difficult to achieve usable hole concentrations greater than mid-10^{18} cm^{-3} in polycrystalline Si films on glass substrates.

Finally, several experiments were undertaken during the fifth quarter of the program to grow Si films on the three new Owens-Illinois glasses (EE-2, EE-5, and GS-238) in He at temperatures higher than the usual ~850°C, to determine if higher B doping concentrations could be obtained in the polycrystalline films than had previously been achieved with the available source tank of B_2H_6. Substrates of GS213 glass were also included in the experiments for comparison purposes.

The Si films grown on GS213 glass at an observed temperature of 897°C, with a B_2H_6 flow rate of 500 ccpm, and at an observed temperature of 925°C, with the same B_2H_6 flow rate, were examined by x-ray diffractometry. The film grown at 897°C was about 10μm thick and had a measured carrier concentration of ~$9x10^{17}$ cm^{-3} (van der Pauw), and was found to exhibit slight {110} preferred orientation. The film grown at 925°C was over 20μm thick, was found by van der Pauw measurement to have a carrier concentration of ~$2x10^{17}$ cm^{-3}, and exhibited strong {110} preferred orientation in addition to some {100} preferred orientation. This variation in the preferred orientation tendencies of polycrystalline Si films on glass substrates with changes in growth temperature (and perhaps also with B doping concentration) was observed with at least one other glass (Corning Code 1715) used in this program.

2.3.10 Si CVD on Polycrystalline Aluminas

Si CVD experiments using polycrystalline alumina substrates of various types were carried out throughout the course of the program. The complexity of polycrystalline Si growth on polycrystalline alumina surfaces was found to be considerable, and the TEC of alumina does lead to some bowing of the Si-alumina composite when very thick films (>50μm) are grown on substrates the order of 600μm thick.

However, the alumina substrates, both single-crystal (sapphire) and polycrystalline, continued to be the most available and hardy substrates for baseline film growth experiments and for evaluation of the effects of changes in growth parameters on film properties. Unfortunately, there appears to be little present indication or belief--on the part of manufacturers and/or suppliers--that the costs per unit area of high-purity polycrystalline aluminas are likely to be reduced to sufficiently low levels to meet the requirements of the LSSA Project, even in the very large quantities envisioned for future production for the project.*

Further, the work of this contract has indicated that there may be troublesome impurity problems in several of the structurally most attractive aluminas. There is also some evidence that the differences in the significant (for solar cells) properties of the polycrystalline Si films deposited on several of the polycrystalline aluminas of interest may not be large, and may be relatively independent of the surface condition (i.e., polished or as fired). There is no question, however, about the value of the aluminas (especially those with large crystal grains) in studies of Si CVD growth parameters and--especially--mechanisms of film nucleation, island growth, and crystallite orientation.

The investigations of Si films grown on various polycrystalline alumina substrate materials in this program are summarized in this section.

2.3.10.1 Undoped Si Films

Early in the program films of Si were grown simultaneously on as-manufactured surfaces of ASM805, ADS995, and MRC Superstrate. Temperatures of 1025 and ~1100°C and carrier gases of H_2 and He were used, to permit a comparison of film structural properties for the several sets of conditions. In each case the film deposition process was preceded by a high-temperature (1250°C) etch of the substrate in H_2. The high deposition temperatures were selected to enhance grain growth, with 1025°C considered low enough to minimize any autodoping tendency by the alumina substrates.

It was found that films ~20um thick deposited in H_2 were considerably smoother and more uniform in appearance and in surface texture than films about 6μm thick grown in He.

---

*If this situation should change at some future time, due to significant developments in alumina processing technologies or to other factors not now anticipated, then polycrystalline aluminas of sufficiently high purity would become very important candidates for use in fabricating polycrystalline solar cells by the CVD process.

The degree of preferred orientation was different on a given substrate for the films grown in H_2 at 1025°C and those grown at ~1100°C. Thus, the film on ASM805 was very strongly {110} oriented at 1025°C and less strongly oriented to those planes at 1100°C. The film on Superstrate was strongly {110} oriented at 1025°C and only moderately oriented to these planes at ~1100°C, with evidence of {111} preferred orientation at 1100°C as well. The film on ADS995 was only slightly oriented preferentially to the {110} planes at 1025°C and even less so at 1100°C.

SEM examination of the films grown in H_2 on the different aluminas at 1025°C showed the film surfaces to be almost identical in appearance, as shown in Figure 2-54, with characteristic surface features having nearly the same average size (measured parallel to the interface) of ~4μm. However, the film on ADS995 also exhibited some crystallographic faceting of the surface features that was not seen on the other two films, as shown in Figure 2-55, even though the x-ray analyses indicated it to be the least preferentially-oriented of the three films.

X-ray analysis of diffraction line widths for particle-size line broadening effects indicated no broadening in the films grown at ~1100°C but some detectable broadening in two of the films grown at ~1025°C. The film on Superstrate appeared to have an average grain size of ~0.1μm, while that on ADS995 was the order of 0.04μm by the x-ray analysis. The relatively small difference in deposition temperature of these two groups of films thus appeared to produce a detectable difference in the average grain size in two of the three cases, based on a comparison involving the two methods of grain size determination. It is not clear that the difference in the dimensions of the surface features as seen in the SEM and the average size of the crystal grains as determined by x-ray analysis represents a valid distinction in grain size for these two sets of films.

In another early set of experiments thick Si films were grown on three as-manufactured ASM805 substrates in separate experiments at ~1025°C in H_2 (4 ℓpm); two of the films were 20-25μm thick, one grown at ~1.6μm/min and the other at ~3.3μm/min, while the third film was ~40μm thick and grown at ~3.3μm/min. These experiments were intended to indicate what differences in film properties might be associated either with growth rate or with film thickness.

X-ray diffraction analysis of the three samples indicate a slight amount of line broadening in all three cases, consistent with the earlier observation of some line broadening for films grown on polycrystalline aluminas at ~1025°C but not at ~1100°C. However, in the earlier films the broadening was found in the Si films on ADS995 and Superstrate aluminas but not in the Si grown on ASM805. The results in all three thick films on ASM805 indicated a grain size of about 0.05μm, similar to the earlier x-ray result on the other substrates.

The same three Si film samples were examined by SEM techniques. The surfaces of the two thinner films, which were grown at rates differing by a factor of about 2, were identical in appearance (Figure 2-56a), with surface rosette features of ~3.0 and ~2.8μm average dimension for the films grown at ~3.3 and ~1.6μm/min, respectively. The film grown at ~3.3μm/min to a thickness of ~40μm had significantly larger surface features, averaging ~5.2μm (Figure 2-56b).

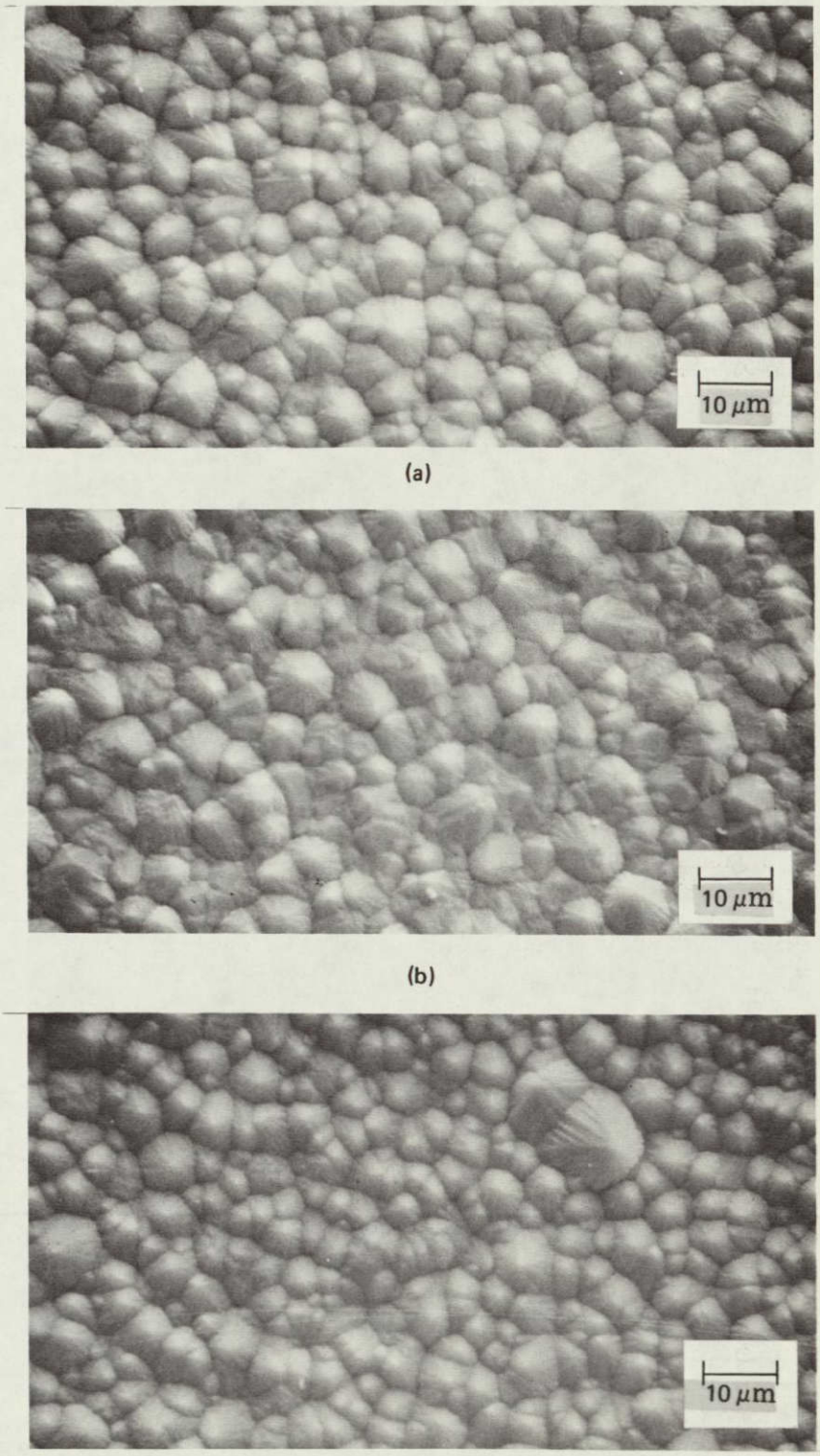

Figure 2-54. Rosette Surface Features of CVD Si Films Grown on Fired Polycrystalline Alumina Substrates in H_2 at 1025°C by SiH_4 Pyrolysis (a) on MRC Superstrate; (b) on ADS995 (Coors); (c) on ASM805 (3M)

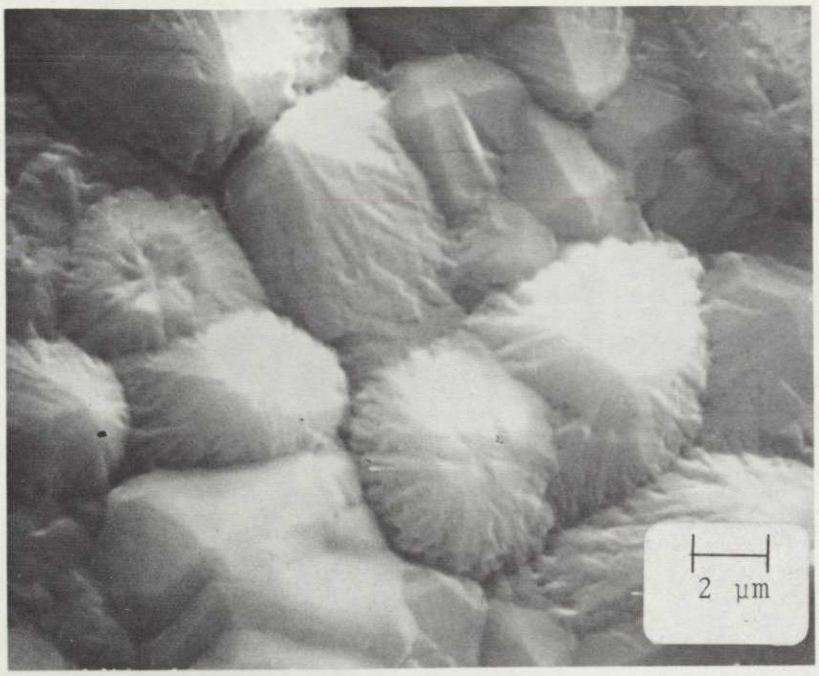

(a)

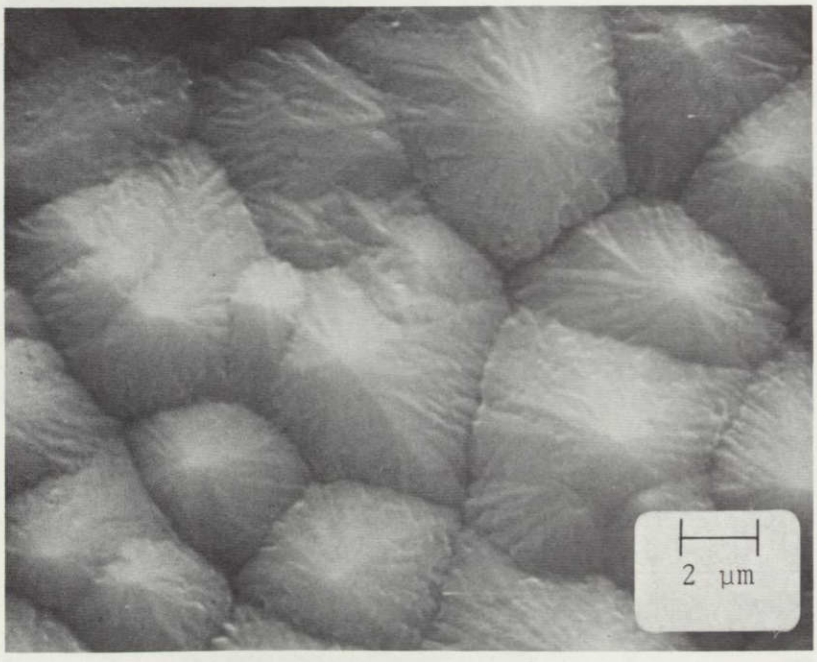

(b)

Figure 2-55. High Magnification Views of Rosette Surface Structures on CVD Si Films Grown on (a) ADS 995 (Coors) and (b) ASM805 (3M), by SiH_4 Pyrolysis in H_2 at 1025°C. Note Faceting in (a).

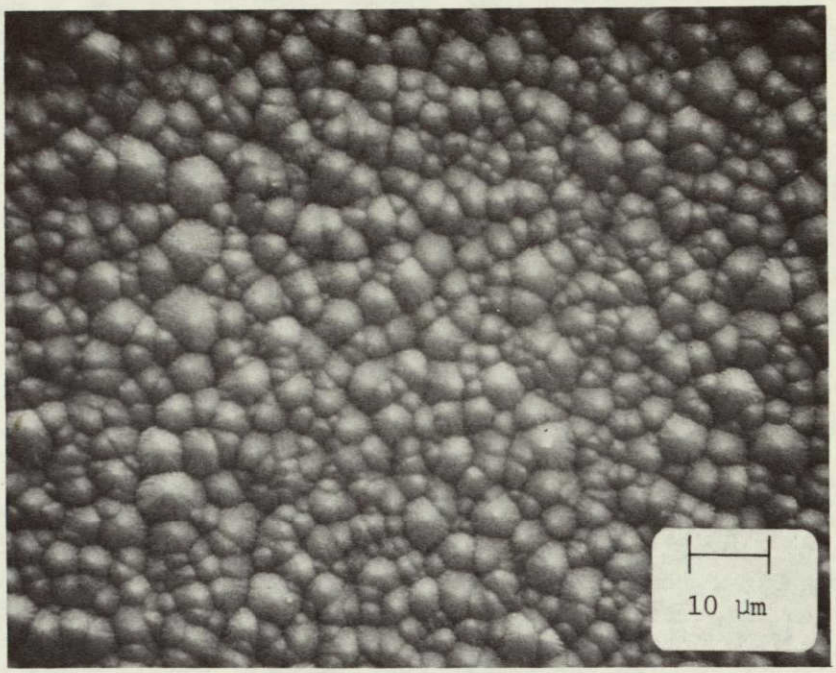

(a)

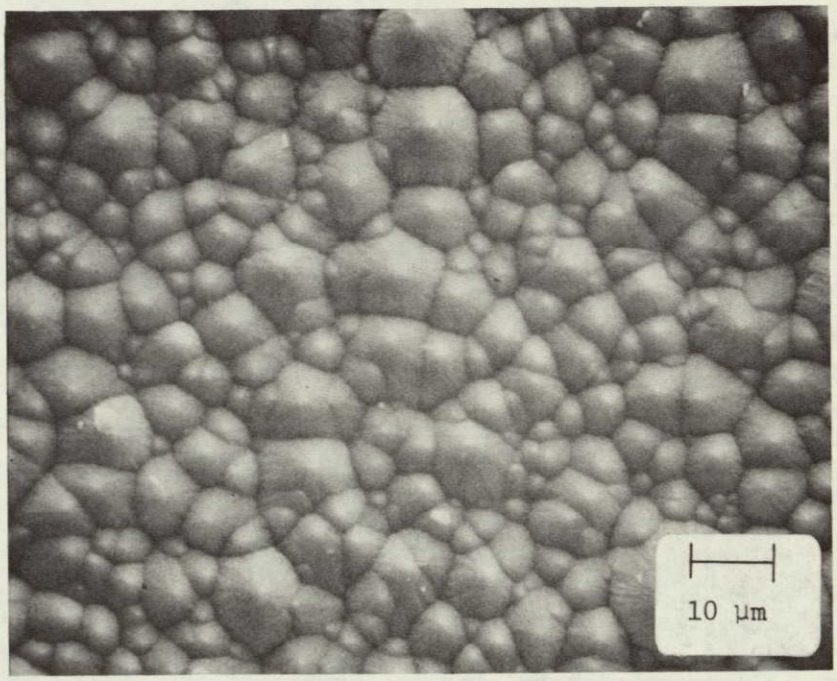

(b)

Figure 2-56. Rosette Surface Structures on CVD Si Films Grown on ASM805 Substrates in H_2 at ~1025°C at Approximately Equal Rates (>3μm/min). (a) Film Thickness ~20μm. (b) Film Thickness ~40μm.

Evaluation of the amount of preferred orientation in the set of three films again established very strong preferred {110} orientation in all three, the amount appearing to increase with film thickness, providing confirmation of the tendency of ASM805 alumina to induce {110} Si growth. Also, the thickest film (~40μm) gave no {100} reflection whatever, whereas in the two thinner ones the {100} reflections were relatively stronger than would be observed in a randomly oriented sample.

As-broken cross sections suggested columnar growth structure in the films, as well as some kind of transition layer in the part of the film adjoining the alumina substrate, especially in the 40μm film (Figure 2-57).

To further elucidate the structure in these films the samples were etched for 1 min at 65°C in a 1:1 KOH-saturated H_2O:isopropyl alcohol mixture. This etch is highly anisotropic, typically etching the {100} or {110} surfaces 10 to 400 times the rate it etches {111} surfaces. After etching, the surfaces revealed the anticipated columnar structure (Figure 2-58). In addition, two other effects were visible. Certain areas exhibited faster etching to form "caves," and the top half of the film etched significantly faster than the layer adjacent to the alumina interface. This could indicate a significant difference in the average crystallographic orientation of the grains in the upper part of the polycrystalline film with respect to those nearer the alumina-film interface, with the former being more strongly {110}-oriented. It might also simply be related to a difference in the etching rate near the interface due to the effect of the nearby Al_2O_3 material.

Another portion of the same 40μm film on ASM805 was mounted for a standard metallographic cross section. Following a final step using 0.05μm Al_2O_3 abrasive slurry on a silk polishing surface, the sample was etched in the KOH etch at 80°C for ~1 min to delineate structural features. Figure 2-59 shows a region of this cross section after etching. The etching has delineated the vertical or columnar growth pattern and has also revealed apparent voids or "caves," most of them horizontally disposed and probably the same feature as was observed in the broken cross sections examined in the SEM. The composite photomicrograph shown in Figure 2-60 gives more detail of the region in the center of Figure 2-59, further revealing the apparent columnar growth pattern of the Si film on ASM805 alumina. Finally, examination of this metallographic cross-section sample in the SEM resulted in the photographs of Figure 2-61. These show a nearby region of the cross section at two different magnifications.

Si CVD experiments using established procedures were also performed to compare as-fired ASM805 alumina substrates with refired material supplied by the 3M Company. The first films were grown on substrates which were cleaned only with organic solvents and H_2O rinses; the films were covered with growth whiskers, consistent with the presence of some surface contamination. Another film grown on a refired substrate which was acid-cleaned was found to be essentially free of whiskers, but the growth on the sapphire companion wafer appeared partially contaminated, indicating either the purity of the refired alumina was adversely affected by the firing process or the technique used in preparing the refired material for deposition needed improvement.

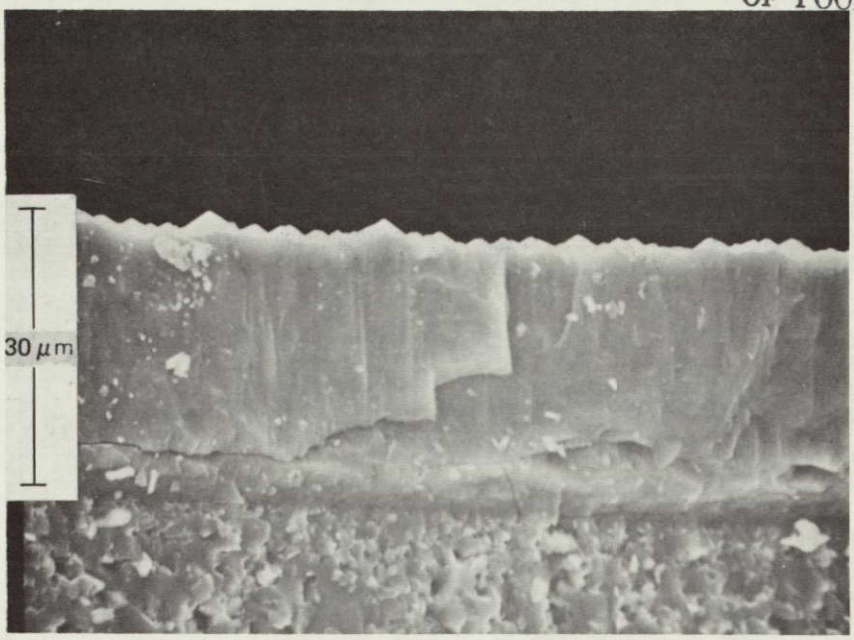

(a)

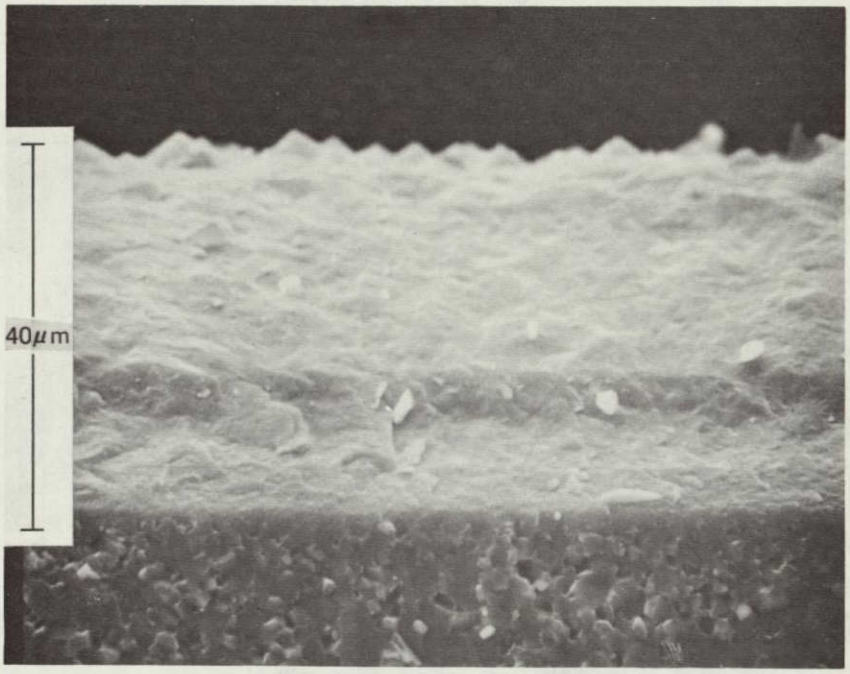

(b)

Figure 2-57. SEM Photographs of Cleaved Cross Sections of CVD Si Films Grown on ASM805 Substrates in H_2 at ~1025°C at Different Rates. (a) Rate <2μm/min, Thickness 24-30μm. (b) Rate >3μm/min, Thickness ~40μm.

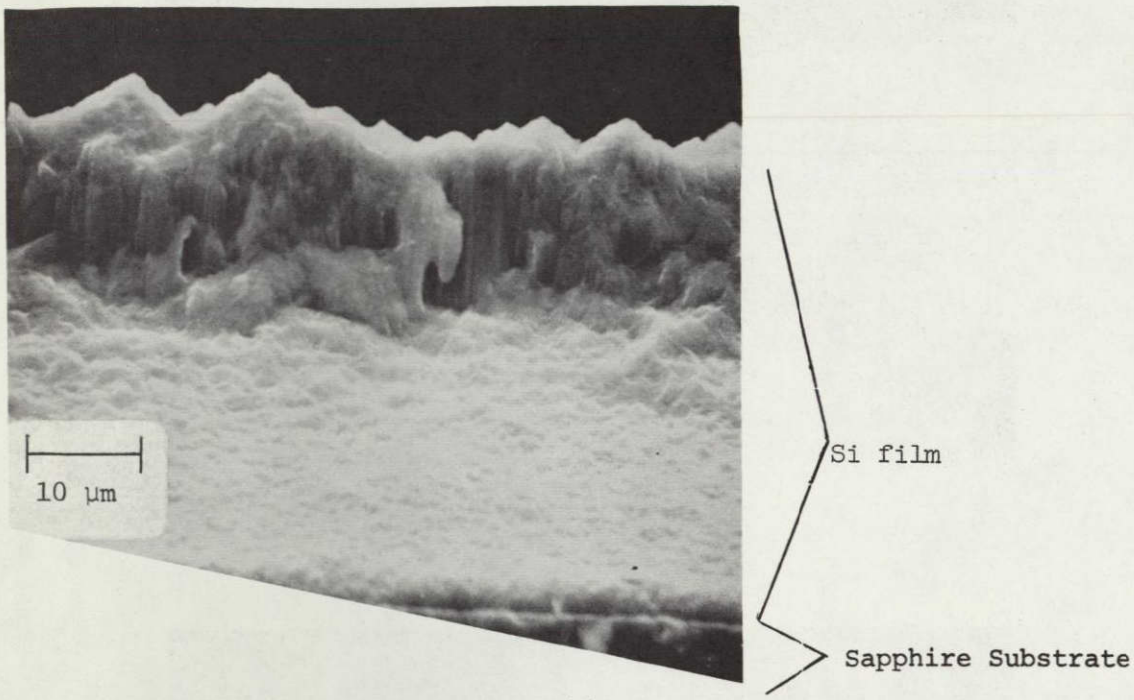

(a)

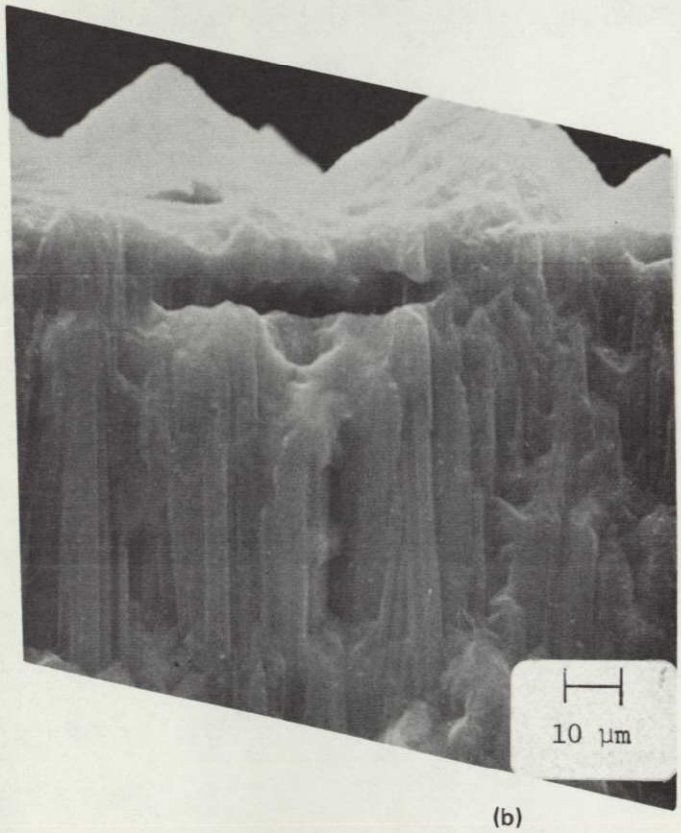

(b)

Figure 2-58. Appearance of Cleaved Cross Section of 40µm-thick CVD Si Film of Figure 2-57b after KOH Etching. (a) 1500X, (b) 3000X.

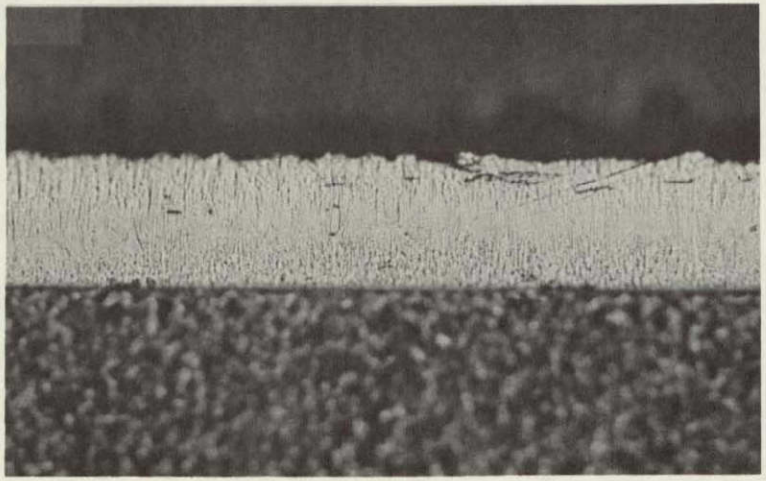

Figure 2-59. Metallographic Cross Section of 40µm-Thick CVD Si Film of Figure 2-57b, after Polishing and KOH Etching. (Polycrystalline alumina substrate is at bottom of photomicrograph.)

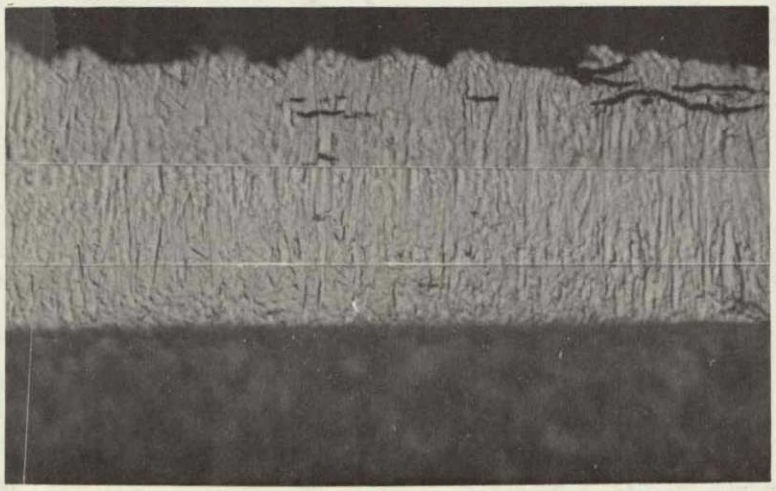

Figure 2-60. Composite Photomicrograph Showing Detail of Central Region of Figure 2-59 (40µm-thick CVD Si Film on ASM805 Alumina)

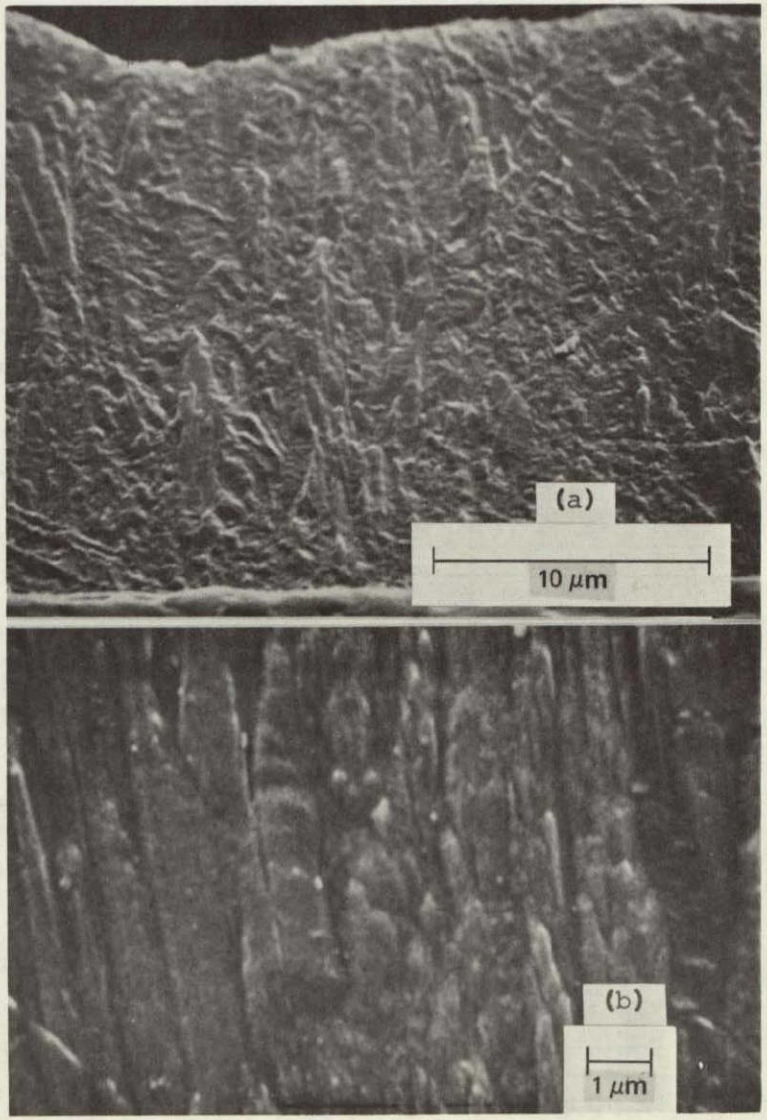

Figure 2-61. SEM Photographs of Metallographic Cross Section of Figures 2-59 and 2-60 at Two Different Magnifications. CVD Si-on-ASM805 Sample of Figure 2-57b, Showing Apparent Columnar Growth

It was subsequently determined that there may have been an impurity introduced into the alumina during the refiring process by the manufacturer. The substrates were stacked for refiring in a furnace with a support and cover of lower purity than the ASM805, and contamination could have occurred from the support and/or the cover. Although the refired ASM805 appeared to contain larger grain sizes, the average appearance of the Si overgrowth on the refired surface resembled that of films grown on the as-fired ASM805 material.

X-ray diffraction analysis of a film or refired ASM805 showed a very strong {110} preferred orientation, similar to that observed in Si films grown on the normally processed ASM805 substrates but much more pronounced. No evidence of {100} orientation was found in the x-ray data.

As a result of additional processing of this sample in preparation for electrical measurements, further information regarding grain size was obtained. Extensive etching with a modified Sirtl etch (used to produce Hall-effect bridge patterns defined by photomask techniques) produced deep trenches in the boundaries separating the three-dimensional rosette-like surface features that had been previously observed so clearly in SEM examination of various films deposited on polycrystalline alumina (Figure 2-62). The etching also resulted in some attack of the surfaces of the individual "mounds" or surface features. This is believed due to dislocations, stacking faults, or twin boundaries within the Si grains, with the etched trenches coinciding with true grain boundaries. That is, the external surface morphology appeared to accurately represent the size and shape of individual Si crystal grains in that portion of the film.

Figure 2-62 shows the surface of this Si film in the as-deposited condition as observed by SEM examination. The two photographs are at the same magnification; Figure 62a is for normal incidence and Figure 2-62b is made at a 45 deg viewing angle. Figure 2-63 shows the surface of the same Si film after the heavy etching described above, with the deep trenches around each mound clearly delineated in Figure 2-63a and the attack of the individual mounds shown distinctly in Figure 2-63b.

Efforts to define the grain boundaries in the interior of this Si layer by etching a vertical cross-section through the layer were less conclusive. Both fractured and lapped/polished sections exhibited prominent artifacts prior to etching. After etching, additional features - also believed to be artifacts - were delineated which obscured the grain boundary structure.

Spreading resistance measurements made on this undoped sample (before etching), with appropriate corrections applied for film thickness, gave the data shown in Figure 2-64, which indicate good uniformity as a function of depth into the layer. There is evidence of a gradual decrease in net p-type carrier concentration as the film-substrate interface is approached; the approximate location of the interface for that portion of the sample measured is indicated by the vertical dashed line at ~51μm depth. The measurements were made on a ~5-deg bevel, with a probe spacing of 30μm and 10μm between data points on the bevel. The ordinate scale of effective net carrier concentration is arbitrary

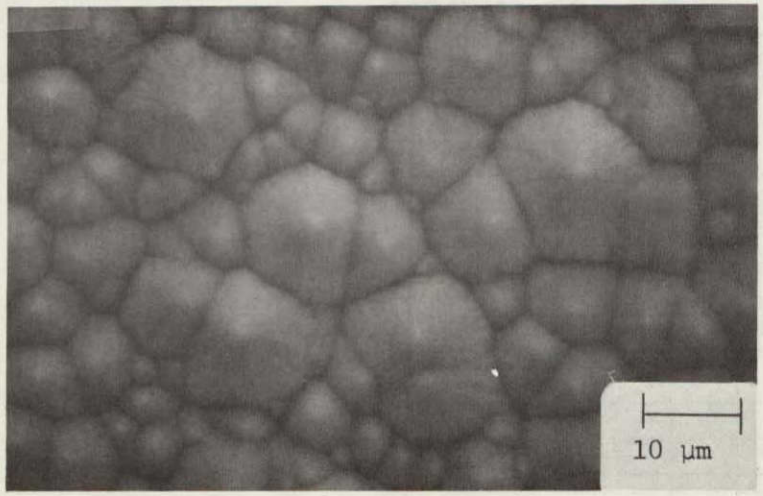

(a)

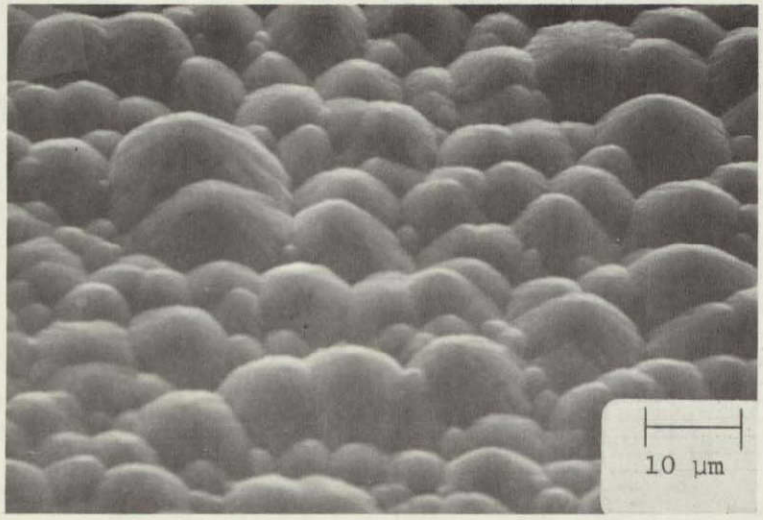

(b)

Figure 2-62. SEM Photographs of CVD Si Film on Refired ASM805 (a) at Normal Incidence and (b) at 45 deg to Sample Surface.

(a)

(b)

Figure 2-63. SEM Photographs of Film in Figure 2-62 after Extensive Etching in Modified Sirtl Etch.

for this particular SR probe trace; no attempt was made to convert the resistance data accurately. The trend of the data is the important thing in this figure, and the slight decrease in net hole concentration as the interface is approached could be indicative of a compensating donor impurity or other imperfection associated with the substrate or with the interface itself.

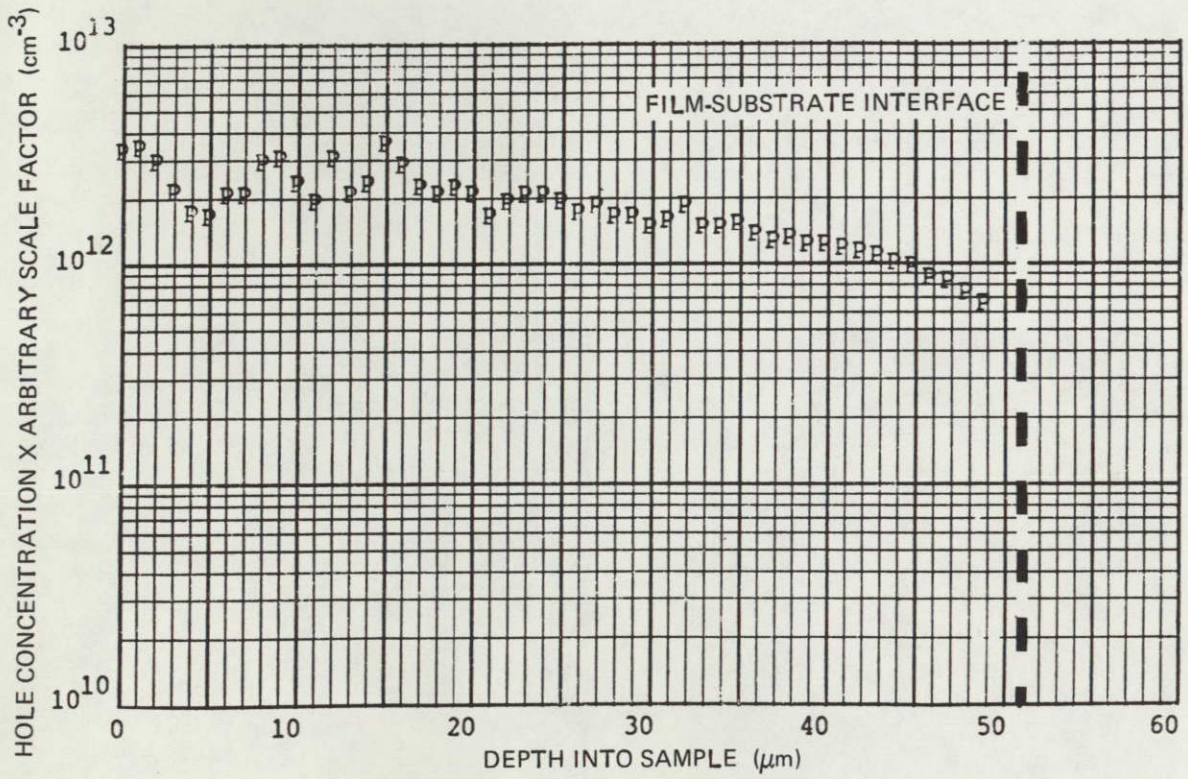

Figure 2-64. Hole Concentration (arbitrary scale factor) as Function of Depth in Si CVD Film of Figure 2-62 and 2-63, Measured by Spreading Resistance Method. (Bevel angle ~5 deg, probe spacing 30μm, spacing between measurements 10μm.)

A series of Si CVD experiments was carried out using substrates of Vistal alumina having each of four different histories of refiring beyond the normal processing used for commercial-grade Vistal. Because of the large crystal grains in these refired materials it was expected that they would provide useful surfaces for study of the interdependence of Si CVD parameters as well as for preparation of polycrystalline film samples for evaluation.

A comparison of the surfaces of the Si films on the four polished Vistal substrates is shown at low magnification in the optical photomicrographs in Figure 2-65. This sequence gives a good indication of both the relative total area coverage and the size of the highly reflective individual epitaxial regions (seen as white areas in the photographs) on the four surfaces. Also clearly shown (especially in the films on Vistal 3 and 4) are other growth regions on individual substrate crystal grains which may also be epitaxial but are more heavily faceted and therefore not as reflective; these are the defined regions seen in various shades of gray in the figure. Many of these gray or black regions, of course, may be polycrystalline rather than epitaxial.

These undoped Si films were grown at ~1025°C in H_2 (4 ℓpm) with SiH_4 flow rates of 25 ccpm; growth rates were ~3μm/min and thicknesses 18-20μm. In each case a pre-deposition treatment in H_2 at 1250°C for 15 min was used. Both polished and as-manufactured surfaces of all four Vistals were used in this series of depositions, with a sapphire monitor substrate in each experiment.

SEM photomicrographs of a Si film 18μm thick deposited on a polished Vistal 4 substrate are shown in Figure 2-66. Figure 2-66a shows a region of the film surface at relatively low magnification. Several very large grains are visible in the field, although most of the film surface appears fine-grained. The large grain in the center is nearly 200μm long in its largest dimension. Figure 2-66b shows at higher magnification the intersection of that grain with another more obviously epitaxial grain. The film replicates the large grain structure of the substrate, although the surface boundaries between grains - except for the prominent epitaxial grains - are subtle and difficult to detect in some of these figures.

The surface of the Si film grown simultaneously on an as-fired Vistal 4 substrate is shown in the SEM photographs in Figure 2-67, both of which were made at normal incidence. The film again replicates the grain boundary structure of the substrate; this is more readily visible in the case of the unpolished substrate involved here. Some very large grains are evident in this film, as in the film on the polished substrate. However, many of the areas outlined by what appear to be grain boundaries propagated through the film from the substrate are merely regions of relatively fine-grained polycrystalline Si growth such as is seen on other alumina substrates. This is evident in Figure 2-67b, which shows a region that appears to be epitaxial and other areas exhibiting typical polycrystalline surface features.

The results obtained with the other three groups of Vistal substrates--both polished and as-fired--were similar to those described for Vistal 4, but with correspondingly different grain sizes.

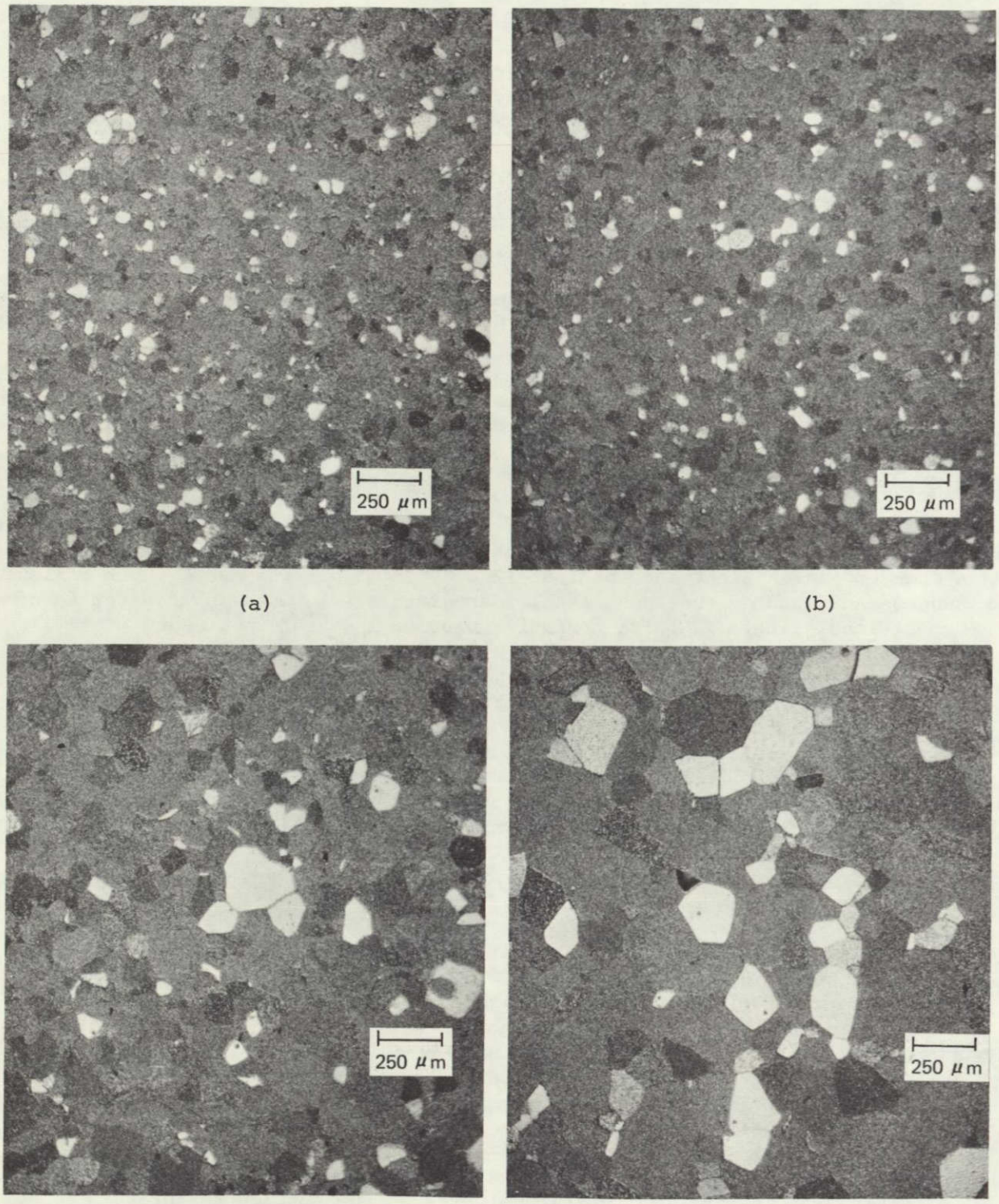

(a) (b)

(c) (d)

Figure 2-65. Optical Photomicrographs of CVD Si Films on Polished Substrates of (a) Vistal 1, (b) Vistal 2, (c) Vistal 3, (d) Vistal 4, at Low Magnification

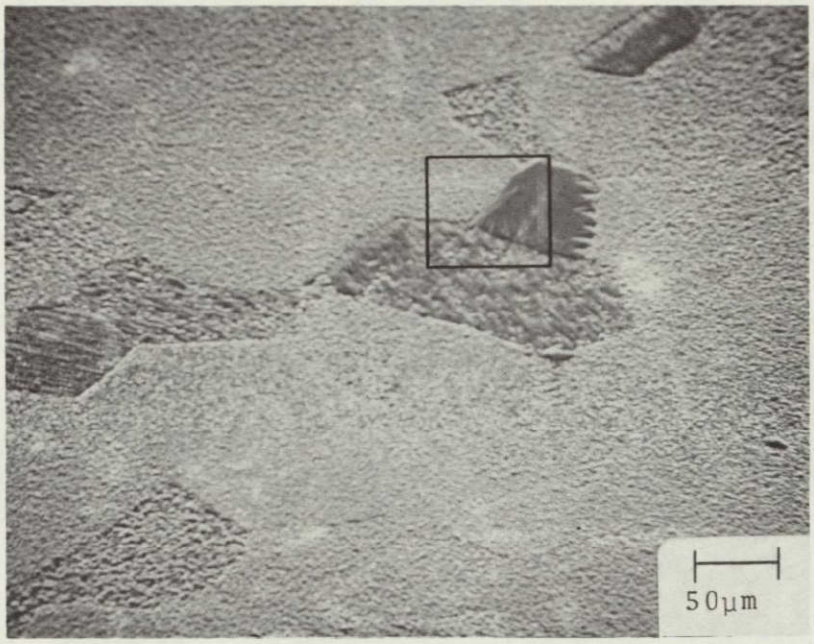

(a)

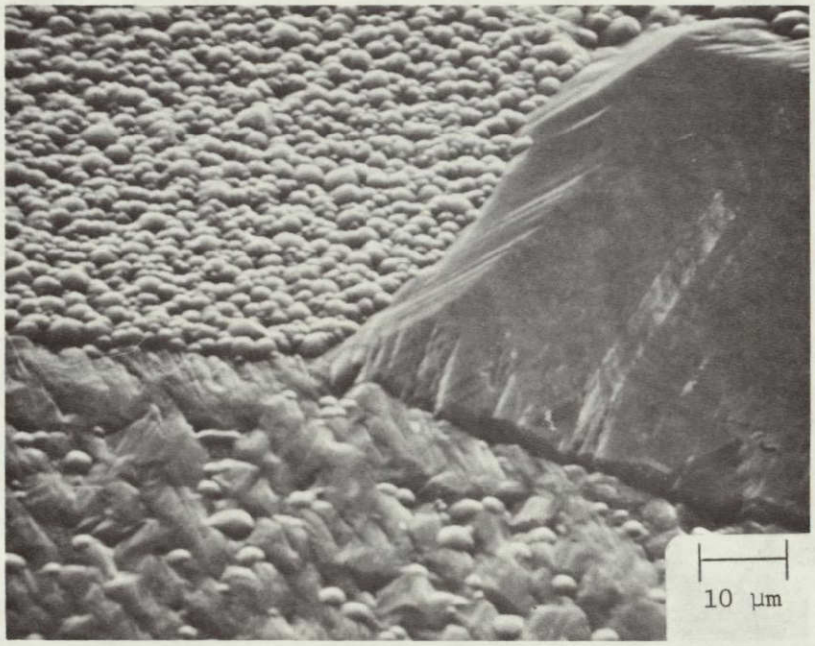

(b)

Figure 2-66. SEM Photographs of CVD Si Film on Polished Vistal 4, at Two Different Magnifications. (Viewing angle 45 deg with sample surface)

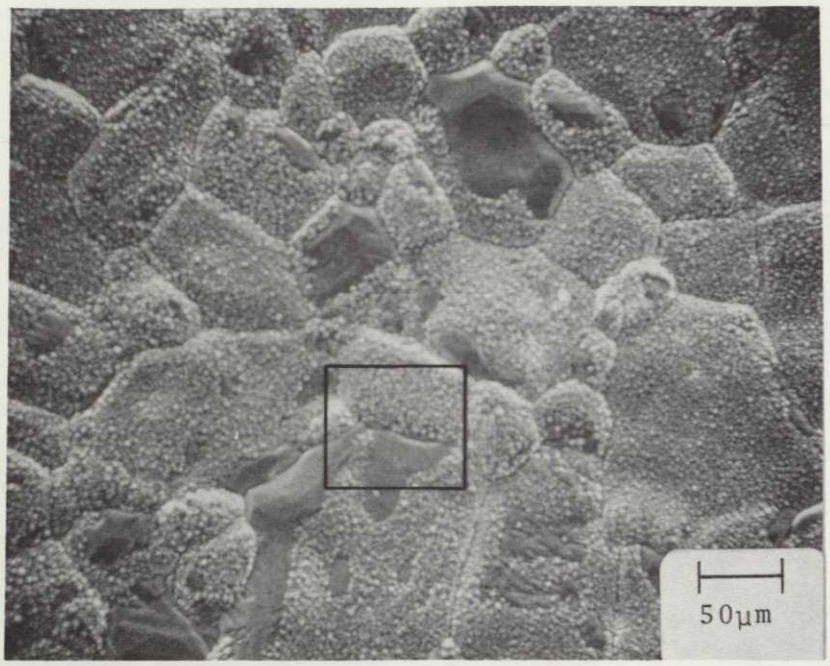

(a)

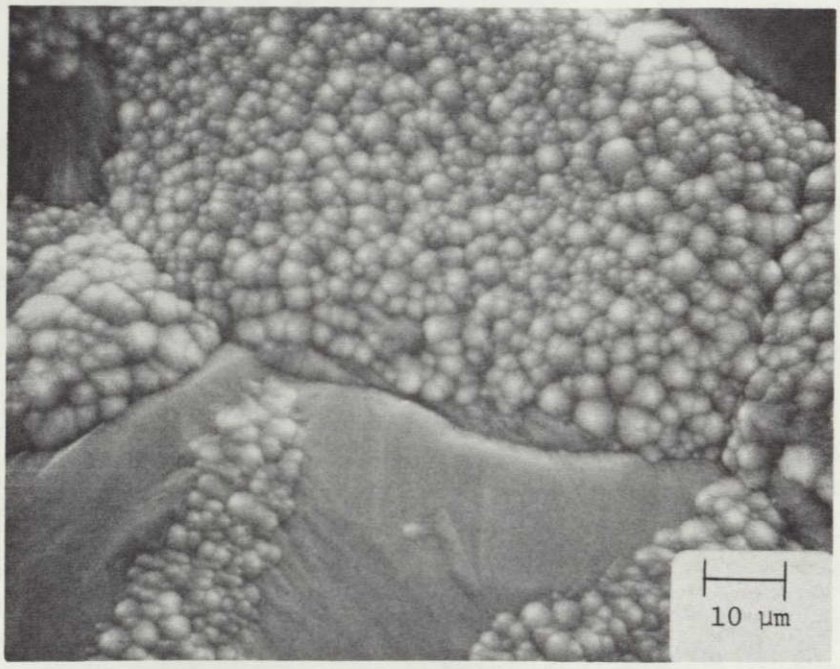

(b)

Figure 2-67. SEM Photographs of CVD Si Films on As-fired Vistal 4 Polycrystalline Alumina Substrate, at Two Different Magnifications. (Viewing at normal incidence.)

The surface roughness of the Si deposits on the Vistals was found to be considerably better on the films grown on the polished surfaces than on the unpolished surfaces. Dektak profilometer traces, shown in Figure 2-68 for a film on Vistal 4, reveal at least a factor of 5 improvement in surface roughness for these 18μm-thick films.

X-ray diffraction analysis of the two films on Vistal 4 alumina showed strong {110} preferred orientation in both instances, although it appeared very much stronger in the film grown on the polished substrate. In addition, strong {100} preferred orientation was present in the film on the polished substrate, while this reflection in the other film was only slightly greater in intensity than what would be expected for a randomly oriented polycrystalline film. Evidence of line broadening was found in the x-ray analyses, indicating average grain sizes ~0.1μm, apparently in conflict with the external appearance of the film. However, the numerous large epitaxial or near-epitaxial islands are evidently immersed in a sea of much smaller Si grains, so the smaller grain size obtained by x-ray analysis (which produces an average for essentially the entire Si film thickness) may not be as inaccurate as it seems at first glance.

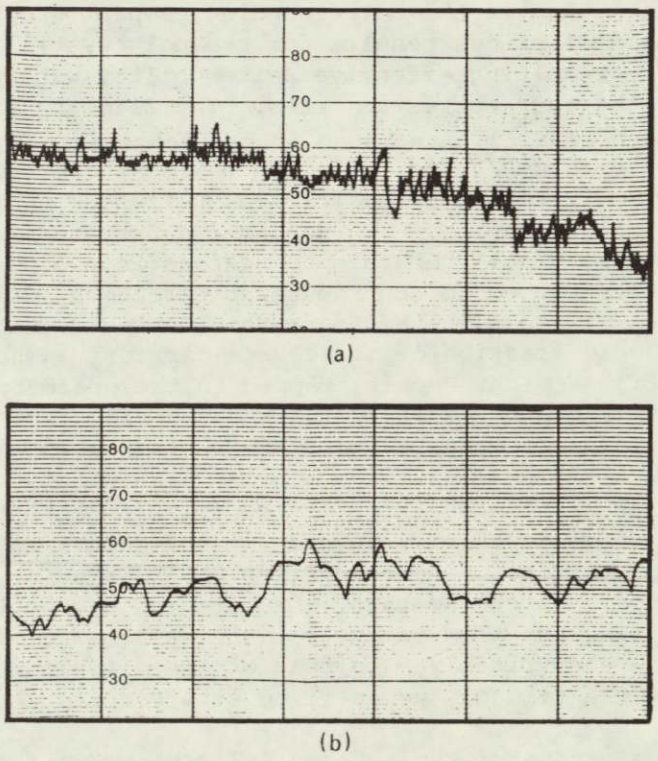

Figure 2-68. Dektak Profilometer Traces of Surfaces of CVD Si Films Deposited by SiH_4 Pyrolysis on (a) Polished Vistal 4 (four consecutive firings at ~1800°C for 6 hr) and (b) As-fired Vistal 4. (Note different vertical scales.)

The electrical properties of the set of undoped Si films grown on Vistal substrates of four different firing histories were measured by both the Hall bridge and the van der Pauw methods. The results of the measurements by both methods, along with the properties of the corresponding epitaxial films grown simultaneously on single-crystal $(01\bar{1}2)$ sapphire, are given in Table 2-13. As indicated in the table, the background doping level, based on the measured properties of the epitaxial films on sapphire, continued in the low 10^{14} cm^{-3} concentration range.

The Hall bridge measurements confirmed the previous van der Pauw results that the resistivities of the undoped polycrystalline films on Vistal substrates, whether polished or as fired, were in the $1\text{-}4 \times 10^{5}$ ohm-cm range. (The Hall bridge results for the films on Vistal 1 appear of doubtful validity; no explanation for the deviation was found.) These values were two to three orders of magnitude larger than those for the corresponding epitaxial films grown simultaneously on single-crystal sapphire substrates.

The measured carrier concentrations for the polycrystalline films were all about 10^{12} cm^{-3}, generally somewhat larger for the film on the as-fired substrate than for that on the corresponding polished substrate and consistently 1½ to 2 orders of magnitude smaller in the polycrystalline films (on either type of Vistal surface) than in the corresponding companion epitaxial film (again disregarding the Hall bridge results for the polycrystalline films in experiment 94). The resulting effective Hall mobility was in the range 132-161 cm^2/V-sec for the four epitaxial films. The films on Vistal tended to have mobilities much smaller than those in the companion epitaxial films, falling in the range 10-34 cm^2/V-sec, with those with larger grains generally exhibiting higher mobilities and the films on polished substrates tending to have higher mobilities than those on as-fired substrates. This is consistent with expectations, since the grain boundaries in the polycrystalline Si films would be expected to contribute an effective resistance factor separate from that associated with the intragrain doping density. Also, it is likely that an appreciable fraction of the charge carriers - whatever their source in an undoped film - might become trapped in the grain boundaries of the polycrystalline film. The net result is the reduced effective carrier mobility observed in the films on the smaller-grained substrates.

The general similarity in electrical properties of the films on both types of Vistal surface is not surprising, especially in view of the general similarity of the external structural properties of the two films as observed in the SEM and the optical microscope. On the average, the integrated effect of the polycrystalline array comprising the film on the polished substrate might be expected to be very similar - electrically - to that of the different polycrystalline array comprising the film on the as-fired substrate.

Spreading resistance (SR) evaluation of the undoped films grown in three of these four experiments provided some indication that an electrically-active impurity may be present in the refired Vistal substrates. The SR probe scan down a small-angle bevel through the entire film thickness for the epitaxial films grown on sapphire in experiments 92, 93, and 94 (see Table 2-13) indi-

Table 2-13. Electrical Properties of Undoped P-type Si Films Deposited by SiH_4* Pyrolysis in H_2 (4ℓpm) on ($01\bar{1}2$) Single-crystal Sapphire and Vistal Alumina Substrates

EXPT. NO.	DEPOS. TEMP. (°C)	SUBSTRATE		FILM THICK. (μm)	METHOD OF MEAS.†	RESIS-TIVITY (ohm-cm)	CARRIER CONC. (cm^{-3})	HALL MOBILITY (cm^2/V-sec)
		MATERIAL	SURFACE					
91	1031	Sapphire	Polished	17.3	HB	1.6×10^{2}	2.8×10^{14}	144
		Vistal 4	Polished	17.9	vdP	2.4×10^{4}	8.6×10^{13}	3
					HB	2.4×10^{5}	1.0×10^{12}	26
		Vistal 4	As fired	17.9	vdP	2.8×10^{4}	7.6×10^{12}	30
					HB	9.2×10^{4}	2.0×10^{12}	34
92	1021	Sapphire	Polished	18.1	vdP	1.5×10^{2}	5.1×10^{14}	81
					HB	1.4×10^{2}	2.8×10^{14}	161
		Vistal 3	Polished	17.5	vdP	3.5×10^{5}	7.3×10^{11}	24
					HB	3.5×10^{5}	7.1×10^{11}	25
		Vistal 3	As fired	17.0	vdP	3.8×10^{5}	9.0×10^{11}	18
					HB	1.6×10^{5}	1.7×10^{12}	22
93	1024	Sapphire	Polished	17.9	vdP	5.3×10^{3}	5.1×10^{13}	23
					HB	2.2×10^{2}	2.1×10^{14}	135
		Vistal 2	Polished	18.0	vdP	3.5×10^{5}	1.2×10^{12}	15
					HB	(Bridge pattern damaged in etching)		
		Vistal 2	As fired	18.0	vdP	1.2×10^{5}	5.0×10^{12}	10
					HB	1.2×10^{5}	3.5×10^{12}	15
94	1025	Sapphire	Polished	18.0	vdP	9.0×10^{2}	1.6×10^{14}	45
					HB	4.9×10^{2}	9.7×10^{13}	132
		Vistal 1	Polished	17.0	vdP	2.6×10^{5}	1.2×10^{12}	20
					HB	7.1×10^{2}**	8.0×10^{14}** (n-type)	11**
		Vistal 1	As fired	16.0	vdP	1.5×10^{5}	3.5×10^{12}	12.
					HB	5.3×10^{3}**	7.2×10^{13}**	16**

*SiH_4 flow rate 25 ccpm
†vdP = van der Pauw method; HB = Hall bridge method
**Validity of these Hall bridge results in doubt (cause unknown)

cated a wide-range variation in measured resistivity as a function of distance from the film-substrate interface for these undoped films. For example, the resistivity (obtained from SR probe values by applying a correction factor based on properties of single-crystal Si) of the epitaxial film of experiment 92 varied gradually from ~20 ohm-cm at the surface to ~45 ohm-cm at a depth of 10μm, and then rapidly to ~10^5 ohm-cm at the interface. The simultaneously grown polycrystalline films on polished and as-fired Vistal 3 were grossly uniform in resistivity, averaging approximately $6x10^4$ ohm-cm to a depth of 15-16μm and rising to ~10^5 ohm-cm at the interface. Local values varied within the range $5-8x10^4$ ohm-cm for the film on the polished substrate and the range $4-8x10^4$ ohm-cm for the film on the as-fired substrate. These variations were such that they may have been associated with individual (perhaps epitaxial) large grains in the film; this possibility was not verified in the films of this experiment, however.

Similarly, the undoped epitaxial film prepared in experiment 93 (Table 2-13) was found by SR probe scan to vary continuously from 10^2 ohm-cm at the surface to $3x10^4$ ohm-cm at the interface, while the polycrystalline film on polished Vistal 2 increased (fairly uniformly) from $4-5x10^4$ ohm-cm at the surface to ~10^5 ohm-cm at the interface, and the film on as-fired Vistal 2 varied from ~$3x10^4$ ohm-cm at the surface to 10^5 ohm-cm at the interface. Again the traces for the polycrystalline films showed some fine structure that might be associated with individual crystal grains in the film; this effect was again more pronounced in the film grown on the as-fired substrate.

Finally, the SR probe scan in the undoped epitaxial film of experiment 94 (Table 2-13) also showed an increase in resistivity from ~45 ohm-cm at the surface to about 100 ohm-cm at a depth of 10μm, and then a rapid increase to $4x10^4$ ohm-cm at the interface. The simultaneously grown polycrystalline films on Vistal 1 ranged from ~$5x10^4$ ohm-cm at the surface to ~$2x10^5$ ohm-cm at the interface for the film on the polished substrate and from $2-3x10^4$ ohm-cm at the surface to ~10^5 ohm-cm at the interface for the film on the as-fired Vistal 1. In this instance, again, the resistivity of the film on the as-fired substrate exhibited more internal variation than did the one on the polished alumina substrate.

The results described above could be associated with a compensating electrically active donor center occurring in the deposited Si film in a concentration that increases nearer the film-substrate interface. This donor center might be a physical imperfection induced at the interface in early growth stages but is more likely a donor impurity that entered the growing film from the Vistal substrate.

The SR probe was also used to identify individual crystal grains and grain boundaries in the undoped Si polycrystalline films grown on Vistal substrates. A low-angle bevel was polished along one entire edge of one piece of the film-substrate composite, and the SR probe scan was made along nearly the entire bevel length in a line parallel to the intersection of the bevel and the top surface of the film, at a position corresponding to a depth slightly (several μm) below the original film surface. The SR probe readout trace (in terms of

measured resistance in ohms) exhibited strong excursions for each of the examined films grown on Vistal substrates, and these excursions were interpreted to represent resistivity variations associated with individual crystal grains and grain boundaries. The intervals between probe readout peaks (or valleys) were largest for the films on Vistal 3 and smallest for the film on Vistal 1, consistent with the grain size differences observed by SEM analysis.

2.3.10.2 Boron-doped P-type Films

As indicated earlier in the report, a study was made of the impurity doping characteristics of polycrystalline CVD Si films grown by SiH_4 pyrolysis on various substrates. Hall bridge and van der Pauw measurements were employed to determine the active carrier (hole) concentrations in polycrystalline B-doped films grown with various amounts of dopant, in the form of B_2H_6 (46 ppm in He), added to the carrier gas stream during growth. The measured carrier concentration in the epitaxial film grown simultaneously on the companion single-crystal $(01\bar{1}2)$ sapphire substrate was taken as the measure of the actual doping impurity concentration added to a given set of films grown at the same time. Polycrystalline alumina substrates of several types were used for these experiments.

It was found that a large and rapid decrease in measured carrier concentration occurs as the added doping impurity is decreased in the range from ~$3x10^{18}$ to ~10^{16} cm^{-3}. This result appears consistent with some of the conclusions advanced by Seto (Ref 17) for B ion-implanted polycrystalline Si.

Although there is a lack of data for the dopant concentration range from $4x10^{16}$ to $3x10^{17}$ cm^{-3}, clear indication of the nature of this doping behavior is given by the data plotted in Figure 2-69. The available carrier concentrations, measured by both van der Pauw and Hall bridge methods, in B-doped p-type polycrystalline Si CVD films deposited by SiH_4 pyrolysis at ~1025°C on polycrystalline alumina substrates are shown as a function of the B impurity concentration added during film growth, measured as indicated above.

At very low added B concentrations (the order of the background impurity doping level in the reactor-- ~$5x10^{14}$ cm^{-3}), the available carrier concentration in the polycrystalline films is in the low 10^{12} cm^{-3} range. For increasing B impurity additions the available concentration increases but at a slow rate until the 10^{16} cm^{-3} range, above which a very rapid rise in the available carrier concentration in the polycrystalline film occurs as the impurity concentration is further increased. At a doping concentration of 10^{18} cm^{-3} the carrier concentration in the polycrystalline film is ~$5x10^{17}$ cm^{-3}, or 50 percent of the added doping concentration. At 10^{19} cm^{-3} doping concentration the measured carrier concentration in the polycrystalline film is also 10^{19} cm^{-3}; carrier concentrations in the polycrystalline films are then essentially the same as those in the epitaxial films, although there are still significant differences in the carrier mobilities in the two cases in the 10^{19} cm^{-3} range.

The results appear to be independent of the specific polycrystalline alumina substrate used, that is, independent of the grain size in the polycrystalline film in the size range involved in these studies. However, as grain sizes approach 200μm and larger, as occurs when substrates of refired Vistal alumina

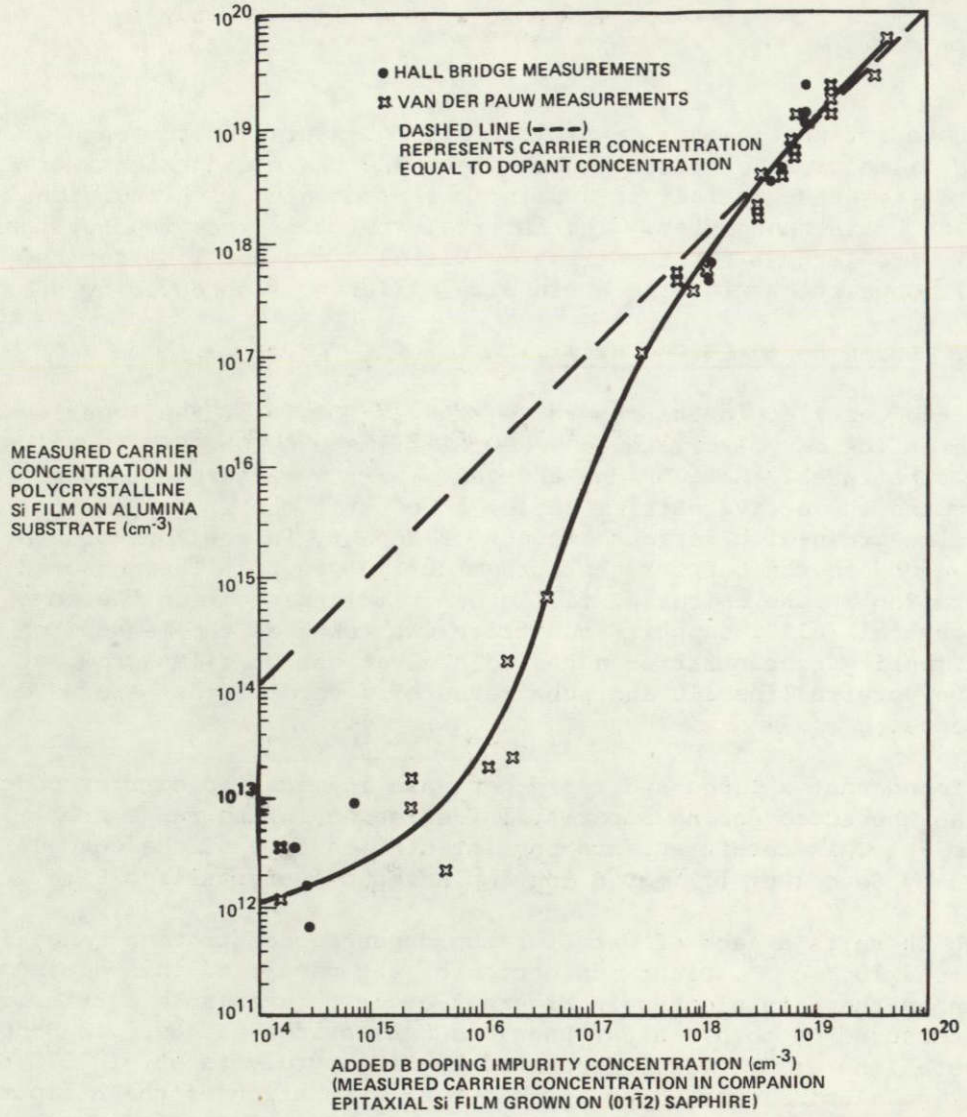

Figure 2-69. Measured Carrier Concentration in B-doped Polycrystalline Si Films Grown by SiH_4 Pyrolysis at ~1025°C on Polycrystalline Alumina Substrates as Function of B Concentration Added during Growth (determined by measurement of carrier concentration in companion epitaxial Si films).

are used for Si film growth, the relative importance of the properties of the individual crystal grains and those of the grain boundaries would be expected to change.

The data given in Figure 2-69 are similar to those of Cowher and Sedgwick (Ref 18) and of Seto (Ref 17), although different in detail. Additional results obtained with these polycrystalline Si films and further discussion of the observed properties in terms of possible models of transport processes will be given elsewhere.*

---

*R. P. Ruth et al, to be published. A preliminary account of these results was given at the 19th Electronic Materials Conference, Ithaca, NY, June 29-July 1, 1977, Paper No. H7.

Spreading resistance (SR) measurements made on some B-doped Si films grown on polycrystalline alumina substrates and their companion sapphire substrates provided further information on the possibility of impurities from certain aluminas interfering with growth of films of desired properties. As an example, very lightly doped films grown simultaneously on single-crystal sapphire and as-manufactured MRC Superstrate alumina at 1025°C, with SiH_4 flow rate 10 ccpm, H_2 flow rate 1.5 ℓpm, and B_2H_6 flow rate 0.5 ccpm, were found by van der Pauw and Hall bridge measurements to have average active carrier concentrations of ~$1x10^{16}$ and ~$2x10^{13}$ cm^{-3}, respectively, and resistivities of ~6 ohm-cm and ~$2x10^4$ ohm-cm, respectively.

The SR probe scan of the epitaxial film on sapphire as a function of depth into the film shows an average resistivity of about 10 ohm-cm (although there is considerable scatter in the data) from the surface to a depth of about 15μm, below which a rapid increase in resistivity occurs through the final 3 or 4μm, approaching a value in excess of 10^3 ohm-cm at the interface (Figure 2-70, lower curve). The resistivity throughout most of the thickness is fairly close to the value obtained by the four-terminal methods. When the SR probe values for ρ are converted to carrier densities, by means of the bulk crystal correction program, the value for the upper 15μm of the film is ~10^{15} cm^{-3}, an order of magnitude lower than the thickness-averaged value obtained by the Hall-effect methods.

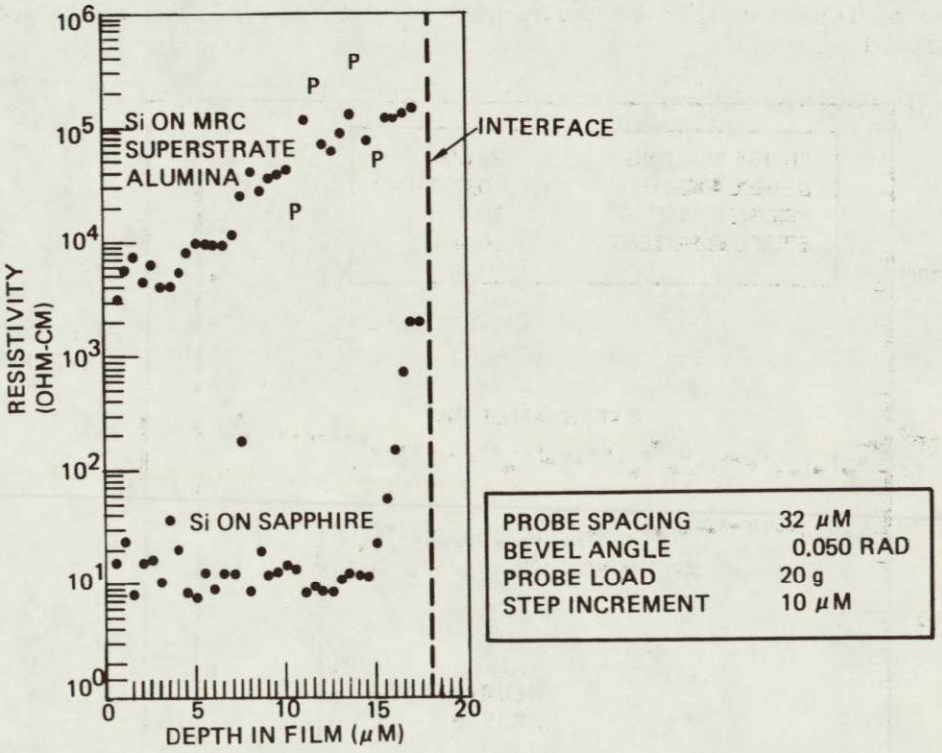

Figure 2-70. Resistivity as Function of Depth, Obtained from Spreading Resistance Probe Scans, for Lightly-doped Si Films Grown by SiH_4 Pyrolysis on Substrates of As-manufactured MRC Superstrate Alumina and Single-crystal Sapphire at 1025°C in H_2

There is also considerable scatter in the resistivity data obtained with the SR probe as a function of depth into the polycrystalline film grown on the alumina substrate in this experiment, as shown in the upper set of points in Figure 2-70. The resistivity begins increasing almost immediately from ~4×10^3 ohm-cm at the surface to ~2×10^4 ohm-cm at a depth of ~7.5μm and finally to 2×10^5 ohm-cm or more in the interfacial region. This is consistent with the thickness-averaged value of ~2×10^4 ohm-cm obtained by the other methods.

These results are consistent with the presence of some impurity escaping from the alumina substrate and continuing to permeate the growing Si film on the alumina but in decreasing local density as the film thickness increases. Similarly, this same impurity may have access to the Si film on the sapphire in significant amounts only in the earlier stages of its growth, accounting partly for the differences in the two plots. Other possible explanations for the observed behavior exist, however, as was pointed out earier.

The epitaxial Si films grown on single-crystal sapphire substrates simultaneously with the polycrystalline Si films on MRC Superstrate alumina substrates in two other experiments involving higher B doping concentrations were also analyzed by spreading resistance measurements. The SR probe scan in one case (experiment 183, Figure 2-71) shows a very uniform resistivity of ~0.03 ohm-cm throughout the film thickness, with no indication of a significant increase in the interfacial region. The resistivity determined on another piece of the same sample by four-terminal measurements was 0.02 ohm-cm, in good agreement with the SR value.

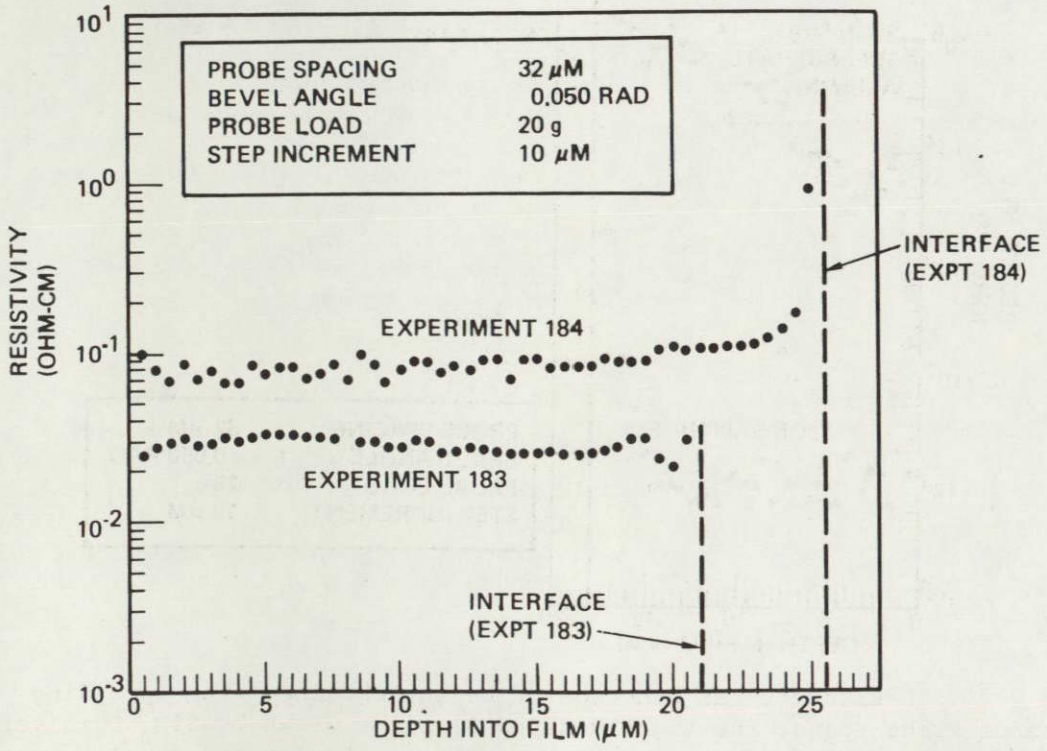

Figure 2-71. Resistivity as Function of Depth, Obtained from Spreading Resistance Probe Scans, for Heavily-doped Epitaxial Si Films Grown by SiH_4 Pyrolysis on Single-crystal Sapphire Substrates at 1025°C in H_2.

The epitaxial Si films grown on sapphire in the other experiment produced the SR probe scan also shown (upper set of data points) in Figure 2-71. Although the scatter of the data for this sample is somewhat greater than for the other film, the resistivity is again very uniform with depth to a point 2-3μm from the interface, averaging ~0.09 ohm-cm throughout, with the exception of the increase by about an order of magnitude near the interface. The average resistivity of this film as determined by the four-terminal method was also 0.09 ohm-cm.

Although the effect was not prominent in this sample, it appears that the resistivity plot faintly shows the characteristics that are very prominent in the plot of resistivity vs depth for the lightly-doped epitaxial film on sapphire in Figure 2-70. Additional investigations are necessary to determine if these effects are, in fact, caused by impurities entering the Si films during growth from the surface or the interior of the substrates being used.

An experiment undertaken in the third quarter involved the simultaneous deposition of B-doped Si films on three substrates of Vistal 3 - in the as-fired condition, lapped, and polished - along with a sapphire monitor wafer. The films were heavily doped (~2×10^{19} cm^{-3}, by measurement of the film on sapphire) and were grown at 1028°C at rates of 2.6 to 3.5μm/min, with thicknesses of 21 to 28μm. X-ray diffraction analysis indicated very strong {110} preferred orientation in all three films on Vistal, consistent with earlier observations. The film on the polished Vistal 3 exhibited by far the strongest {110} orientation, with the film on the as-fired substrate next; the film on the lapped substrate was relatively much weaker in the {110} orientation, yet nonetheless highly oriented in that plane. The film on the polished substrate also exhibited a strong {100} orientation (although relatively much less than the very strong {110} orientation), whereas this plane was only slightly preferred in the film on the lapped substrate and essentially in random-orientation prominence in the film on the as-fired substrate.

The electrical properties of the films on the three Vistal substrates, obtained by both van der Pauw and Hall bridge techniques, are given in Table 2-14. Close agreement of the results for the two methods is evident, although the usual relative magnitudes, as described earlier, do exist. Carrier concentrations and resistivities measured in all four films are nearly the same, both tending to be only slightly larger in the polycrystalline films than in the epitaxial film. The effective Hall mobilities in the polycrystalline films are alike and about 60 percent of that in the film on sapphire, measured by either method. These measurements provide correlation (at the high-doping-concentration end of the range) of the electrical properties in epitaxial and polycrystalline Si films as a function of added impurity concentration, and tend to confirm the observations of other investigators - that differences in electrical properties between epitaxial and polycrystalline films become smaller as doping levels are increased, as discussed in connection with Figure 2-69.

This same set of Si films was examined by the spreading resistance method to investigate the degree of uniformity of doping with distance from the film-substrate interface. The epitaxial film resistivity varied only slightly

Table 2-14. Electrical Properties of B-doped p-type Si Films Deposited Simultaneously by SiH_4* Pyrolysis at 1028°C in H_2 (4 ℓpm) on Single-crystal $(01\bar{1}2)^4$ Sapphire and Vistal 3 Alumina Substrates

Substrate		Film Thick. (μm)	Method of Meas.**	Resistivity (ohm-cm)	Carrier Conc. (cm^{-3})	Hall Mobility (cm^2/V-sec)
Material	Surface					
Sapphire	Polished	23	vdP	1.2×10^{-2}	1.4×10^{19}	40
			HB	1.2×10^{-2}	8.5×10^{18}	64
Vistal 3	Polished	25	vdP	1.6×10^{-2}	1.6×10^{19}	26
			HB	1.3x10	1.2×10^{19}	42
Vistal 3	As fired	21	vdP	1.2×10^{-2}	2.1×10^{19}	25
			HB	0.9×10^{-2}	2.1×10^{19}	34
Vistal 3	Lapped	28	vdP	2.0×10^{-2}	1.2×10^{19}	25
			HB	1.6×10^{-2}	1.0×10^{19}	38

*SiH_4 flow rate 25 ccpm

**vdP = van der Pauw method; HB = Hall bridge method

(and quite uniformly) throughout its thickness - from ~0.012 ohm-cm near the surface to ~0.020 near the interface. The polycrystalline films on Vistal substrates were also uniformly doped, with about the same measured resistivities as found in the epitaxial film - again only slightly higher than the latter.

It is interesting that the SR probe results in terms of resistivity for the polycrystalline films agreed very closely with the results obtained directly on these films by the van der Pauw technique, despite the fact that the computer-applied correction factor that was used in converting the SR probe resistance readings to corresponding resistivity values is based on the properties of {111}-oriented single-crystal Si. Also, it is not surprising that there is no evidence of the compensating donor at the film-substrate interface as observed in the undoped films on Vistal - presumably because of the high B doping density in these films.

The SR probe was also used successfully to identify individual crystal grains and grain boundaries in the Si film grown on the polished Vistal 3 substrate of the experiment of Table 2-14. A bevel was polished along one entire edge (~6mm long) of one quarter of the original film-substrate composite, and the SR probe scan was made along nearly the entire bevel length in a line parallel to the top of the bevel, at a position corresponding to a depth several μm below the film surface.

Optical photomicrographs were made of the entire bevel length to show the "tracks" made by the two-point SR probe (spacing between probe points 29μm, step-distance between readings 10μm). EBIC-mode SEM photographs were also made of the entire bevel length to delineate the large individual grains found in the Si films on this substrate material. These two sets of photographs were then assembled to make two composite views of the entire bevel length.

Figure 2-72 shows the two composite photographs aligned side-by-side, with individual crystal grains in the beveled Si film clearly visible and the tracks of the SR double-point probe (two styli 29μm apart) evident along nearly the full length of the bevel. A scale is also mounted alongside to facilitate identification of regions in the SR readout trace, shown in Figure 2-73. This makes it possible to correlate distinct steps in the measured resistance with easily discernible crystal grain boundaries in the SEM photographs.

Some of the separate epitaxial regions/grains in this film were 100 to 200μm across, as earlier examination by other means had shown. The measured interprobe resistance value along the entire ~5mm scan length was approximately 25 ohms and nearly constant except in the interior of large epitaxial regions, where it dropped consistently to ~20 ohms. When converted (approximately) to corresponding resistivities, the difference in the two values is quite similar to the observed difference in the resistivities of the three polycrystalline films, on the one hand, and that of the epitaxial film on sapphire grown simultaneously in this experiment, on the other.

In other experiments polished alumina substrates were used, along with the usual sapphire monitor wafer, for deposition of B-doped Si at a rate of ~3μm/min at 1025°C, at different doping levels, to permit comparison of film properties on the three high-purity aluminas of greatest interest in this program - ASM805, MRC Superstrate, and Vistal. X-ray diffraction data indicated the {110} orientation to be very strongly preferred in the films on Superstrate and ASM805, and also preferred - but much less strongly - in a film on Vistal 3. The latter also exhibited equally strong {100} orientation, but this orientation appeared only in random-orientation prominence in the films on Superstrate and ASM805.

These results confirmed the earlier findings for preferred orientations in undoped Si films grown on ASM805 and MRC Superstrate aluminas, both as to the presence of strong {110} orientation and as to the absence of any preferred {100} orientation. The results also confirmed earlier observations on undoped Si films on polished refired Vistals, namely, that films on polished Vistal 4 and Vistal 3 exhibit a strong {100} orientation tendency in addition to the strong {110} preferred orientation.

The electrical properties of films doped to the 10^{17}-10^{18} cm^{-3} range were found to be quite similar on the different substrates. Measurements on the film on sapphire indicated a carrier concentration of $3x10^{18}$ cm^{-3} and a mobility of 74 cm^2/V-sec (by the van der Pauw technique). Similar measure-

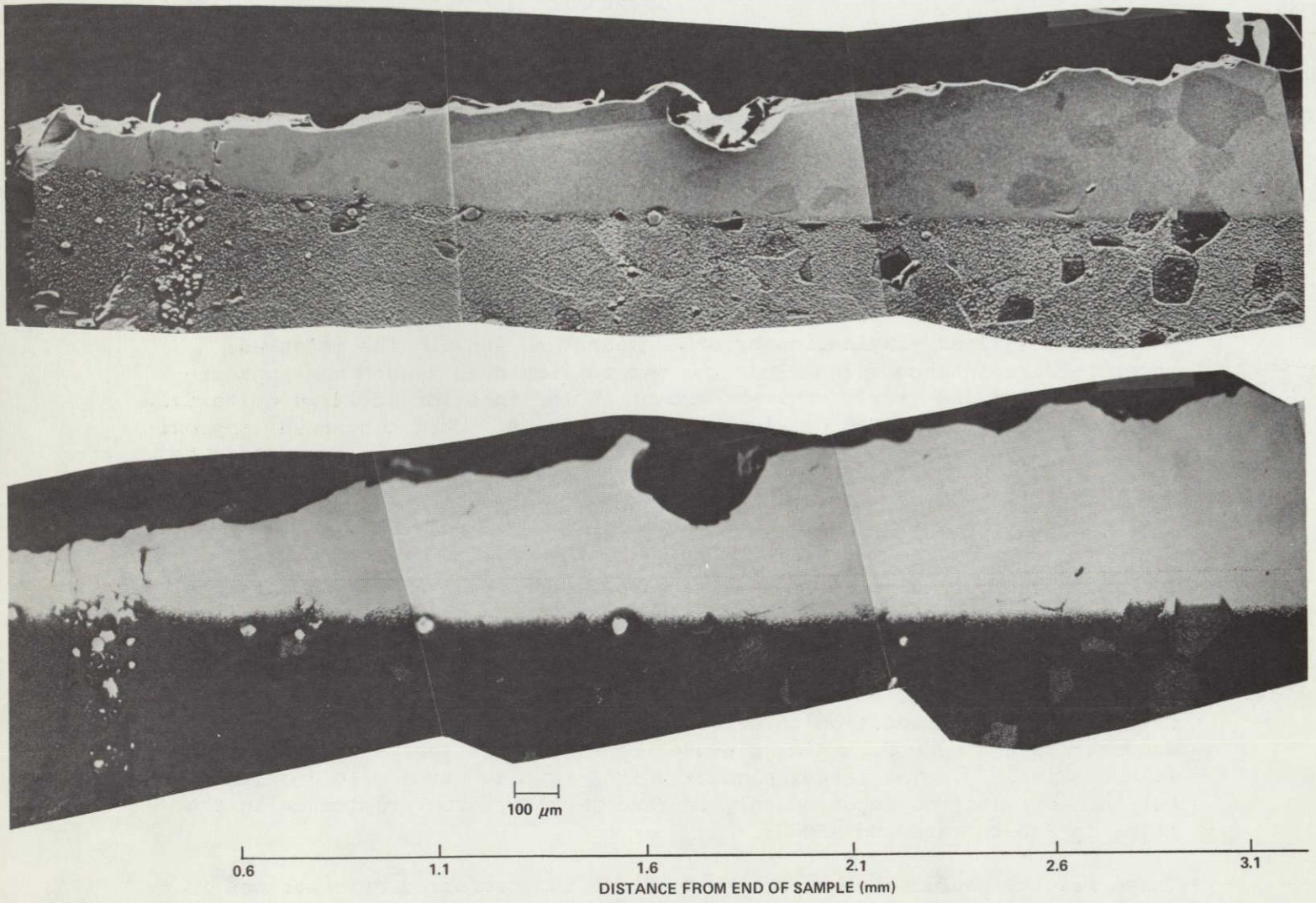

Figure 2-72. Composite Optical and SEM/EBIC Micrographs Showing Individual Grains in Doped CVD Si Films on Polished Vistal 3 and SR Probe Tracks on Bevel through Film.

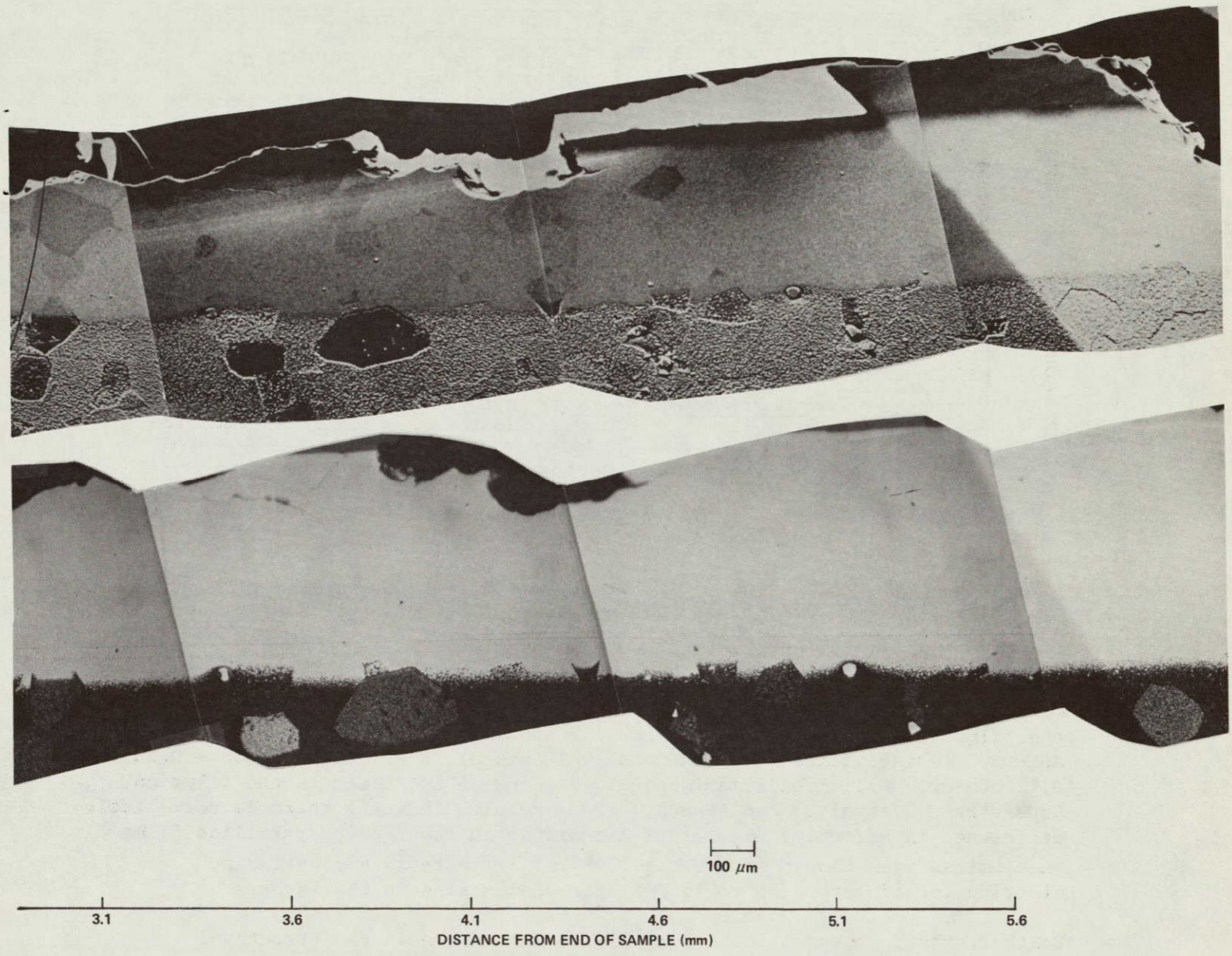

Figure 2-72 (Cont)

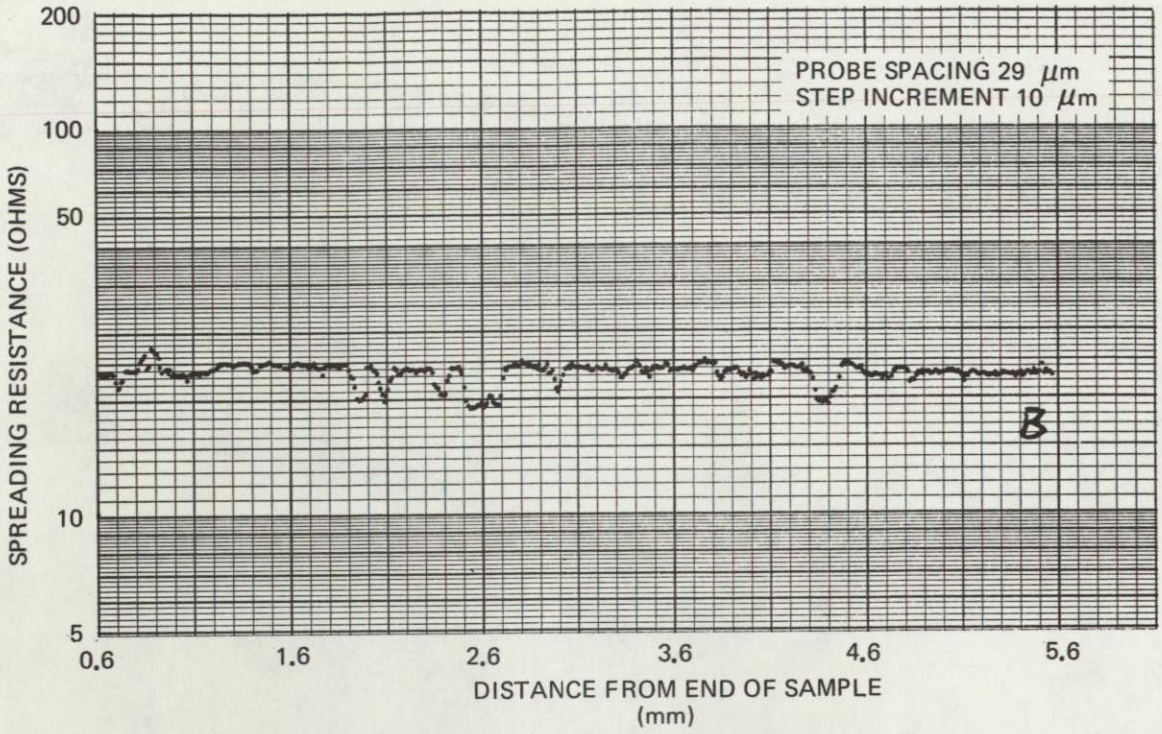

Figure 2-73. SR Probe Scan along Bevel in Doped CVD Si Film on Polished Vistal 3

ments on the other films indicated carrier concentrations of 1.5×10^{18} cm^{-3} in the films on Superstrate and on Vistal 3 and 2.0×10^{18} cm^{-3} in the film on ASM805. Resistivities were essentially identical in all three cases - 0.12 to 0.13 ohm-cm. Hall mobilities were 33, 34, and 26 cm^2/V-sec in the films on Superstrate, Vistal 3, and ASM805. These results indicate there is very little difference in effective electrical properties in doped polycrystalline films on aluminas even though in one case (Vistal 3) there is a significant distribution of large (50 to 150μm) epitaxial grains in the layer.

Further, there appeared to be very little difference in the structural and electrical properties of B-doped Si films deposited on MRC Superstrate whether the substrate was in the polished or the as-fired condition. The results of electrical measurements on these films and on the film grown simultaneously on $(01\bar{1}2)$-oriented sapphire are shown in Table 2-15. The bridge measurements on the epitaxial film on single-crystal sapphire indicate that the flow rate of B_2H_6-in-He that was used produced a net carrier concentration of ~10^{18} cm^{-3}; the observed Hall mobility in this film was 125 cm^2/V-sec. The measurements on the two films on the polycrystalline substrates were made by the van der Pauw method, because the samples were subsequently to be sent to OCLI for solar cell fabrication and the entire sample area was to be preserved for that purpose. The resistivities of the polycrystalline Si films were nearly the same, and more than an order of magnitude larger than that of the companion film on sapphire. The measured carrier concentrations were

nearly identical in the polycrystalline films and about half of the value in the single-crystal film. As a result, the effective Hall mobilities in the two films on MRC alumina were only a fraction of that found in the film on sapphire.

The fact that the electrical properties as well as the structural properties are quite similar in these films raises the question as to the real value of the extra processing - that is, the mechanical polishing - invested in the one substrate. Since there was also relatively little difference in the apparent surface roughness of the films on the polished and the as-fired substrates, even the presumed advantage of having a smoother film surface for subsequent device processing and contacting may not be valid for this particular substrate material.

Another deposition experiment of the same type involved simultaneous deposition of doped Si on substrates of polished Superstrate, as-fired ASM805, and single-crystal polished $(01\bar{1}2)$ sapphire. The films were grown in H_2 (4 ℓpm) at 1033°C with a SiH_4 flow rate of 10 ccpm and a B_2H_6-in-He flow rate of 500 ccpm to produce heavy B-doping in the films.

SEM examination of the film surfaces on the ASM805 alumina showed that the surface features were very similar to those seen on undoped Si films grown on this material earlier. Little if any distinct faceting could be seen on the pyramidal features that comprised most of the surface.

X-ray diffraction analysis of the two polycrystalline doped films again showed very strong {110} preferred orientation in the film on the polished Superstrate, as was the case in the experiment described above, although the effect was much greater in this film. The {100} planes again appeared as a second preferred orientation in the film on the polished Superstrate. The film on as-fired ASM805 also exhibited strong {110} preferred orientation, but the {100} planes were not detected at all.

Results of electrical measurements on the three films grown in this experiment are given in Table 2-16. Because of the high concentration of diborane introduced into the reactant gas stream in this experiment, the measured hole concentration in the epitaxial Si film grown on the single-crystal sapphire substrate was very high - about 2×10^{19} cm^{-3} as measured with the Hall bridge. The Hall mobility found for this film on sapphire was 31 $cm^2/V\text{-}sec$, a reasonable value for Si on sapphire in the 10^{19}-10^{20} cm^{-3} doping range involved.

The characteristics of the films on the two polycrystalline aluminas were measured by the van der Pauw method. The resistivities of both films are similar and are somewhat larger than the resistivity of the Si film on sapphire as measured by the van der Pauw method, The net carrier concentration measured by the van der Pauw method in these films was about 2×10^{19} cm^{-3} in both cases, resulting in effective Hall mobilities of about 30 $cm^2/V\text{-}sec$. Although there appear to be some minor inconsistencies, the results generally agree with those for heavily doped films on Vistal 3 substrates as recorded in Table 2-14.

Table 2-16. Electrical Properties of B-doped CVD Si Films Deposited by SiH_4 Pyrolysis in H_2 (4 ℓpm) Simultaneously on Single-crystal Sapphire and Polycrystalline Superstrate and ASM805 Aluminas

SUBSTRATE MATERIAL AND SURFACE CONDITION	SiH_4 FLOW RATE (ccpm)	B_2H_6-IN-He FLOW RATE (ccpm)	DEPOS TEMP (°C)	APPROX FILM THICK (μm)	RESISTIVITY (ohm-cm)		HOLE CONCENTRATION (cm^{-3})		HALL MOBILITY (cm^2/V-sec)	
					van der Pauw	Hall Bridge	van der Pauw	Hall Bridge	van der Pauw	Hall Bridge
(01$\bar{1}$2) sapphire (polished)	10	500	1033	25	0.0050	0.012	3.3×10^{19}	1.7×10^{19}	37	31
MRC Superstrate alumina (polished)	10	500	1033	25	0.0094	–	2.0×10^{19}	–	32	–
3M ASM805 alumina (as fired)	10	500	1033	25	0.0087	–	2.4×10^{19}	–	30	–

Two separate experiments, that were designed to supply properly doped polycrystalline Si films on alumina substrates for experimental solar cell fabrication by OCLI, resulted in some data that gave more evidence of a possible impurity escaping from the substrate during Si deposition. Si films had been grown in these experiments on as-fired ASM805 substrates at a rate of ~3μm/min by pyrolysis of SiH_4 (flow rate 25 ccpm) in H_2 (flow rate 4 ℓpm) at temperatures of 1022 and 1025°C, respectively, with B doping from B_2H_6 flowing at rates of 75 and 10 ccpm, respectively. Measurements on the two epitaxial films on sapphire monitor wafers indicated carrier concentrations of 5.2×10^{18} and 9.5×10^{17} cm^{-3}, respectively. Measurements (by the van der Pauw method) on the polycrystalline films on as-fired ASM805 substrates indicated carrier concentrations 55 to 70 percent of the above values and resistivities of 0.085 and 0.83 ohm-cm, respectively.

Spreading resistance evaluation of these doped films was accomplished by a probe scan down a bevel through the entire film thickness. The scan for the more heavily doped film is shown in Figure 2-74a. The resistivity is fairly uniform at 0.035 to 0.040 ohm-cm to a depth of 15μm, at which point it gradually increases to a value of 0.8 to 0.9 ohm-cm at the film-substrate interface. The probe scan of the more lightly doped polycrystalline film is shown in Figure 2-74b. It shows almost no region of uniform resistivity as a function of depth, instead increasing almost continuously from about 0.15 ohm-cm at the surface to 8 to 10 ohm-cm at the interface with the alumina substrate. The observed properties in the two cases are consistent with the possible entry into the growing film of a compensating donor impurity, presumably by diffusion, from the substrate.

2.3.10.3 Very Thick Si Films

The properties of very thick (75-90μm) Si films grown on polycrystalline alumina and single-crystal sapphire substrates were investigated to obtain an indication of the problems that might be encountered later in preparing CVD Si films of thickness adequate to absorb most of the usable solar spectrum in a solar cell structure.

A major point of interest in the growth of very thick films is the extent to which grain sizes in polycrystalline films grown by the CVD process increase with thickness. Various indications have been found in this program that this does, in fact, occur - at least on some substrates. It is important to ascertain if this is a generally occurring phenomenon or one that takes place only on certain substrate materials.

A second important aspect of thick film growth on dissimilar substrate materials is the extent to which physical distortion of the film-substrate composite occurs after deposition and cooling to room temperature, as a result of thermal contraction differences between the two materials. This distortion most often takes the form of bowing or buckling of the composite, with the deposited film in tension or compression depending upon the algebraic sign of the difference in thermal expansion coefficient (TEC) values for the two materials. In more extreme cases the differences in thermal contraction

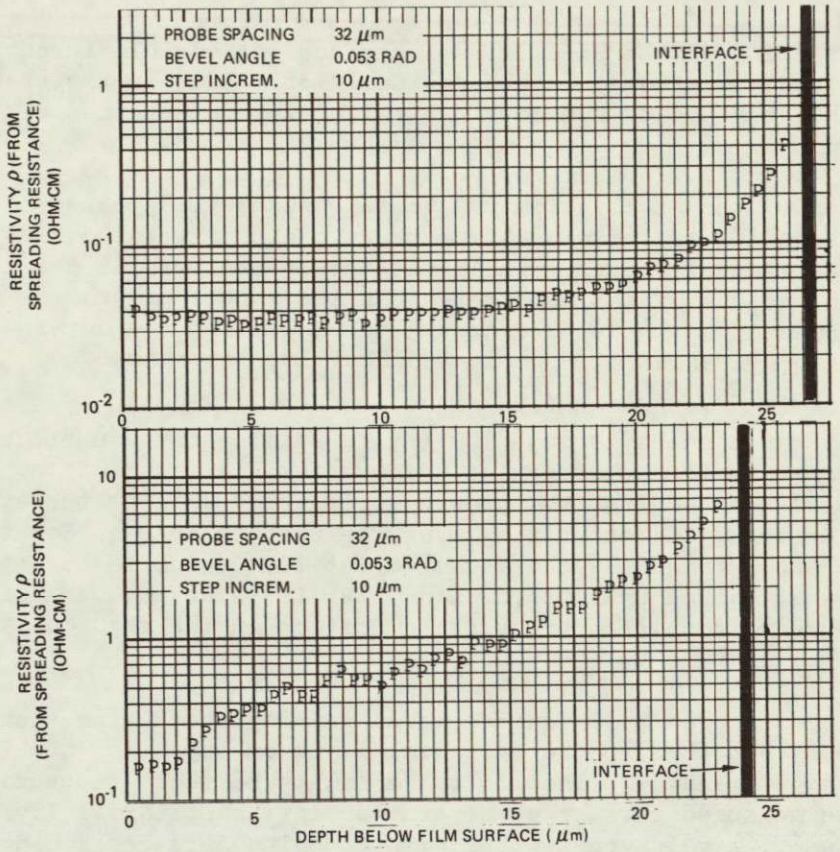

Figure 2-74. Spreading Resistance Probe Scans through Thickness of Doped CVD Si Films on As-fired ASM805 Substrates. a) $p \approx 4 \times 10^{18}$ cm^{-3}, b) $p \approx 5 \times 10^{17}$ cm^{-3} (Measured on polycrystalline films by van der Pauw method)

behavior result in locally severe stresses that cause the film to separate from the substrate, either intact or in small pieces, or to remain bonded to the substrate and cause small sections of the substrate material to break away from the main portion.

The first experiment involved deposition of B-doped Si simultaneously on substrates of polished Vistal polycrystalline alumina and polished single-crystal $(01\bar{1}2)$-oriented sapphire. The films were grown by SiH_4 pyrolysis at ~1030°C (observed) in H_2 (1.5 ℓpm), with the SiH_4 flow rate ~10 ccpm and the diborane flow rate 6 ccpm. Both substrates were subjected to the usual pre-deposition treatment of baking at 1250°C in H_2 (1.5 ℓpm) for 15 min. Deposition for 100 min resulted in a relatively smooth layer 75-80μm thick on the sapphire and a strongly faceted and relatively rough layer 85-90μm thick on the Vistal, corresponding to average growth rates of ~0.8 and ~0.9μm/min, respectively.

The Si/sapphire composite was only very slightly bowed, while the Si/Vistal composite was extensively bowed, convex upward as would be expected for the relative magnitude of the TEC values for Si and alumina. (Quantitative measurement of the amount of distortion was not undertaken.) In addition,

considerable crazing of the Si-alumina interface was visible through the transparent Vistal substrate; the basic "cell" or module in the crazing pattern appeared to embrace numerous crystal grains rather than a single grain.

Various regions of the Si layer on the Vistal substrate appeared to be epitaxial, corresponding to individual substrate grains crystallographically favorable for epitaxial growth, similar to the characteristics of thinner films grown on various Vistal substrates earlier in the program. The film on sapphire appeared somewhat "overgrown" but exhibited the outward appearance of an epitaxial (100)-oriented Si film, as expected.

Spreading resistance scans through the entire film on both substrates indicated a perturbation in the otherwise uniform resistivity profile, centered at a distance of 14-17μm from the growth interface. This perturbation appeared as an increase in resistivity over the uniform average for the rest of the layer, and extended over a region about 10μm thick in both films. It is not known what caused this fluctuation, but it is assumed that it was associated with some unidentified transient condition in the reactant gas flow.

The resistivity measured by SR in the layer on polycrystalline alumina was slightly higher than that in the epitaxial layer on sapphire (the latter layer was found by x-ray examination to be highly perfect structurally), as expected. The measured carrier concentration in the epitaxial layer was about 1×10^{18} cm^{-3}, a value consistent with B doping data described earlier for growth of thinner Si layers in H_2 at ~1025°C.

SEM examination of the surface of the layer grown on Vistal alumina produced the photographs shown in Figure 2-75. The two views--taken at the same magnification but at an angle of 45 deg and normal to the surface, respectively--clearly show the variety of surface features occurring as well as the high incidence of features with transverse dimensions exceeding 25μm. The extremely rough texture of the surface is further emphasized by the SEM photographs in Figure 2-76, which show unpolished fracture cross sections of the layer and the polycrystalline substrate in two different regions. In the center of Figure 2-76a is a region in which the Si layer filled a sizable void in the initial surface of the alumina substrate. Figure 2-76b, showing a region near the edge of the small piece being examined, further emphasizes the rough but faceted texture of the layer and also shows a large crack in the layer itself. It is not known if this crack resulted from fracturing the small piece of the sample used for examination in the SEM or if it had occurred previously, as a result of the thermally induced stresses near the interface.

The presence of defects of some kind near the interface (i.e., within about 10μm) in the Si layer on the Vistal alumina had been indicated by the SR scan through the full thickness of the layer. This was more clearly demonstrated, however, by two SR scans at constant depths in the layer--one ~10μm below the top surface and one ~15μm from the interface (Figure 2-77); both scans extended for distances of several millimeters parallel to the layer-substrate interface.

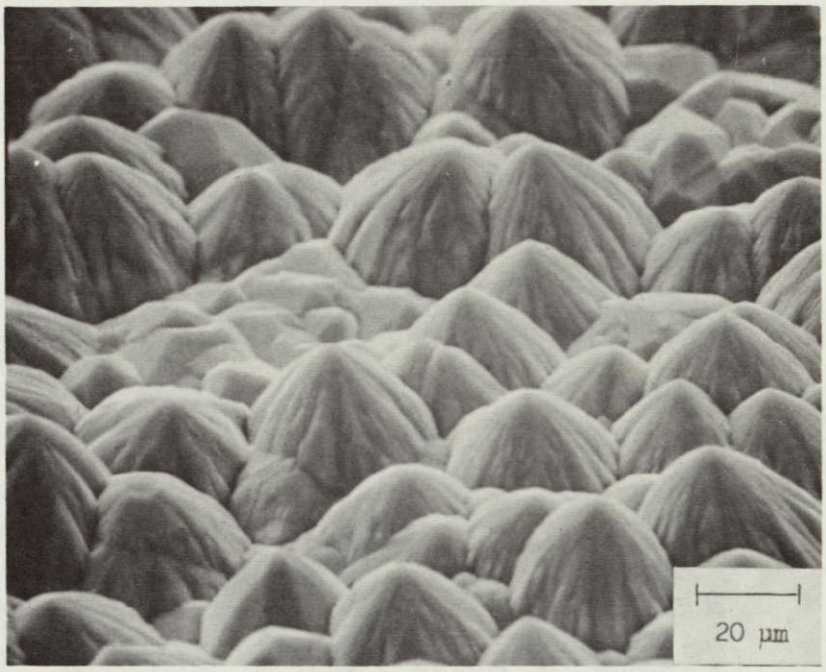

(a)

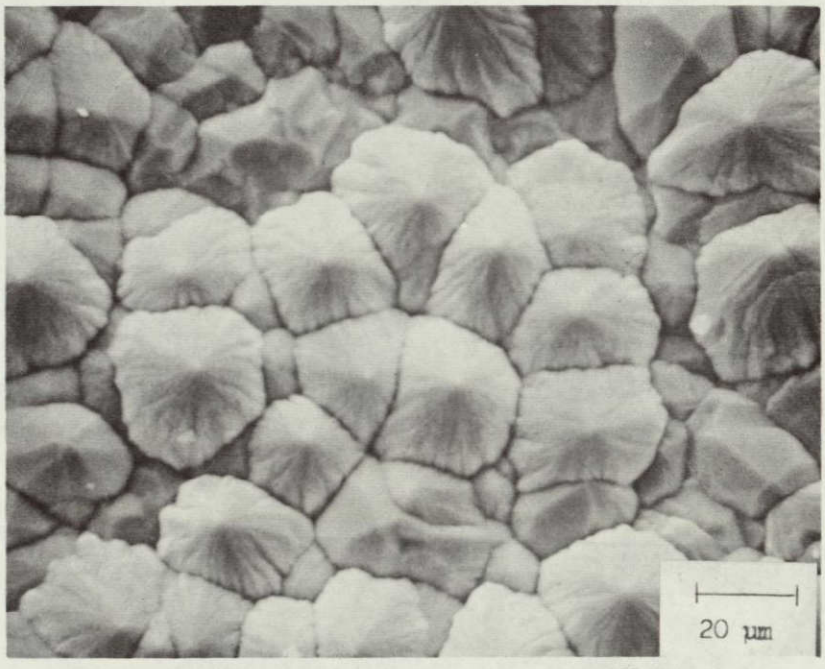

(b)

Figure 2-75. SEM Photographs of Surface of 85-90µm Thick Doped CVD Si Layer Grown on Polycrystalline Alumina (Vistal) Substrate at ~1030°C in H_2. a) View at 45 deg Angle with Surface, b) Perpendicular View.

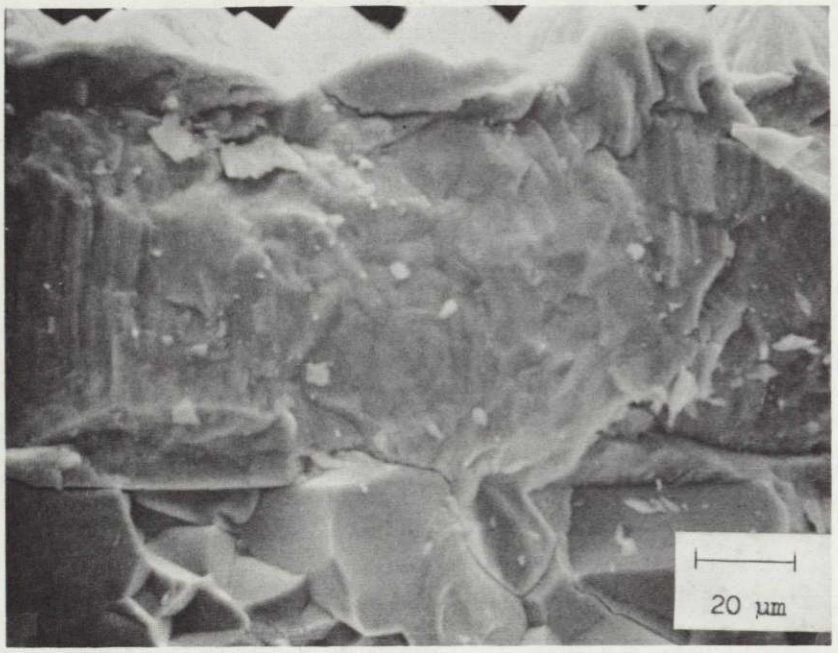

(a)

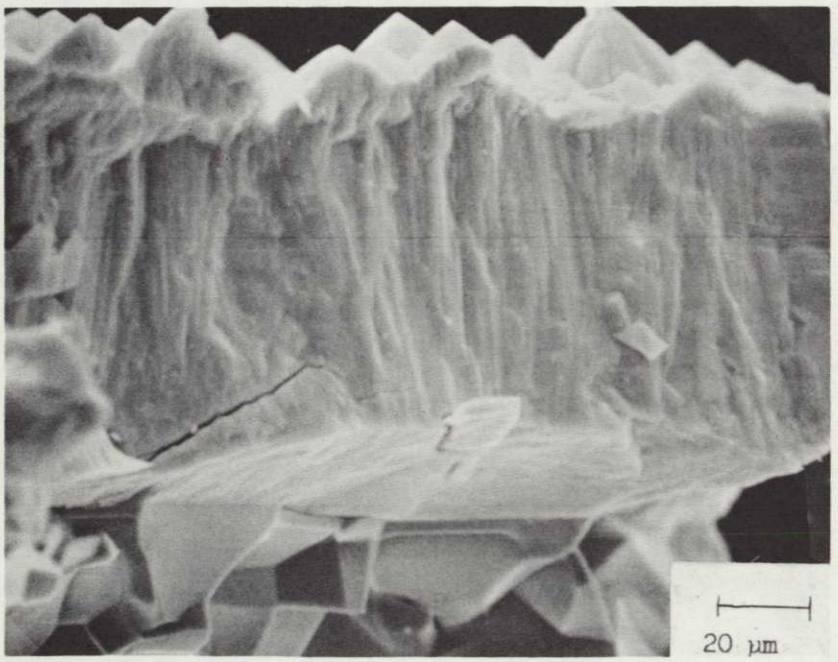

(b)

Figure 2-76. SEM Photographs of Unpolished Fracture Cross Sections of Sample of Figure 2-75, Showing Rough Surface Texture and a) Si Growth into Voids in Substrate Surface and b) Crack in Layer near Interface.

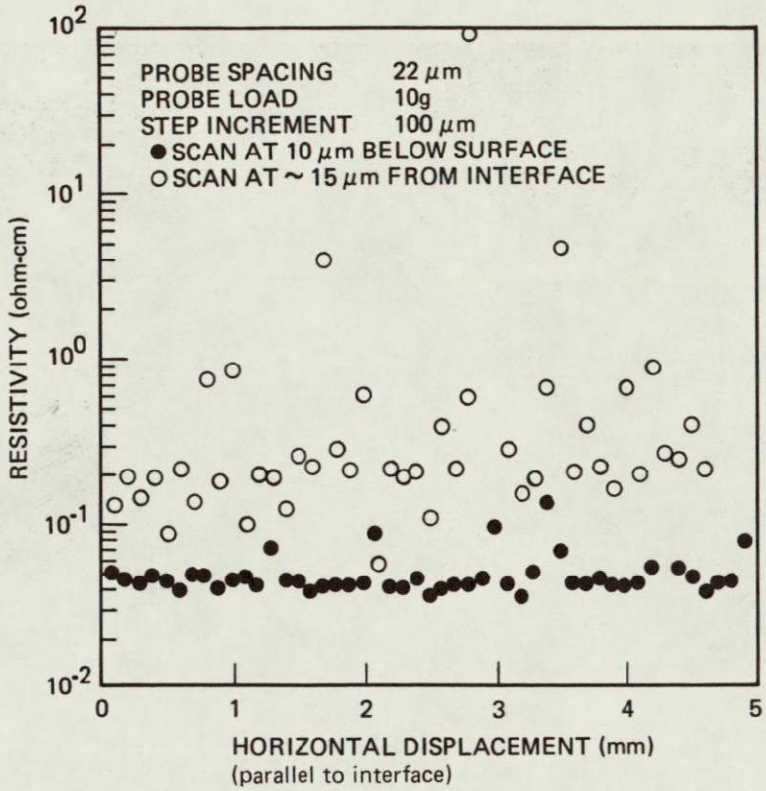

Figure 2-77. Spreading Resistance Probe Scans Showing Resistivity as Function of Horizontal Displacement Parallel to Interface, at Two Constant Depths in Layer of Figure 2-75. a) ~10μm below Surface, b) ~15μm from Interface.

The scan at 10μm depth shows a very uniform resistivity of ~0.04 ohm-cm across the sample, consistent with the SR scan of resistivity versus depth which had indicated a nearly constant value of resistivity for the upper 50μm of the polycrystalline layer. The excursions to higher resistivity values at five different locations in the 5mm-long scan are associated with grain boundaries in the Si layer that probably correlated with grain boundaries in the initial polycrystalline substrate surface.

The scan made at a distance of ~15μm from the interface indicates an average resistivity of ~0.2 ohm-cm - again consistent with the resistivity found at this depth (in the perturbed region mentioned earlier) in the SR scan through the thickness of the layer. However, at this depth there are extreme excursions in resistivity that are associated with numerous voids, cracks, and other defects, some of which were visible in the optical microscope along the beveled surface near the interface.

In contrast, the surface of the thick epitaxial layer grown on the sapphire substrate is shown in the SEM photograph in Figure 2-78a, a view normal to the layer surface. The crystallographic facets are seen to be largely overgrown, and the relatively smooth surface of the layer is shown clearly in the SEM photograph of an unpolished fracture cross section in Figure 2-78b.

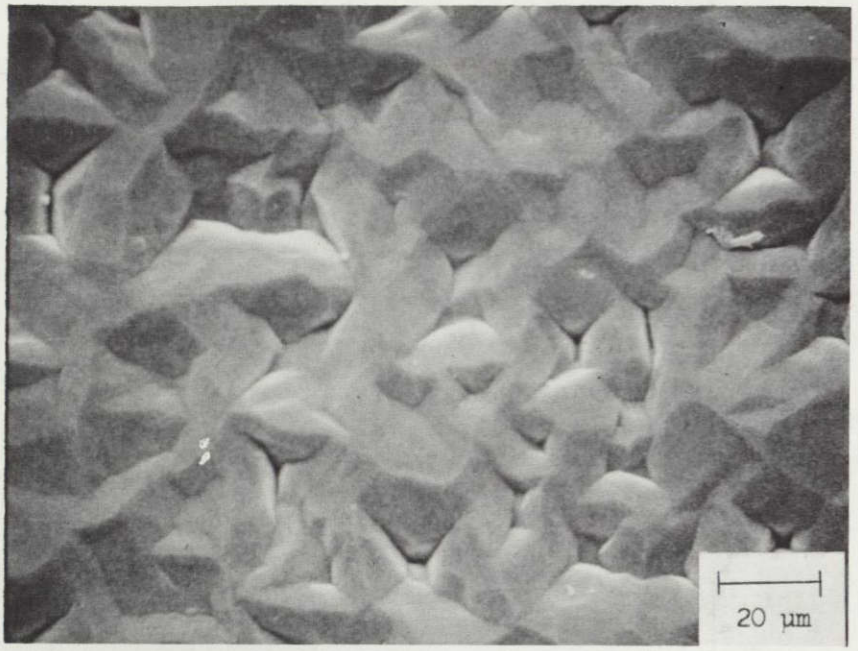

(a)

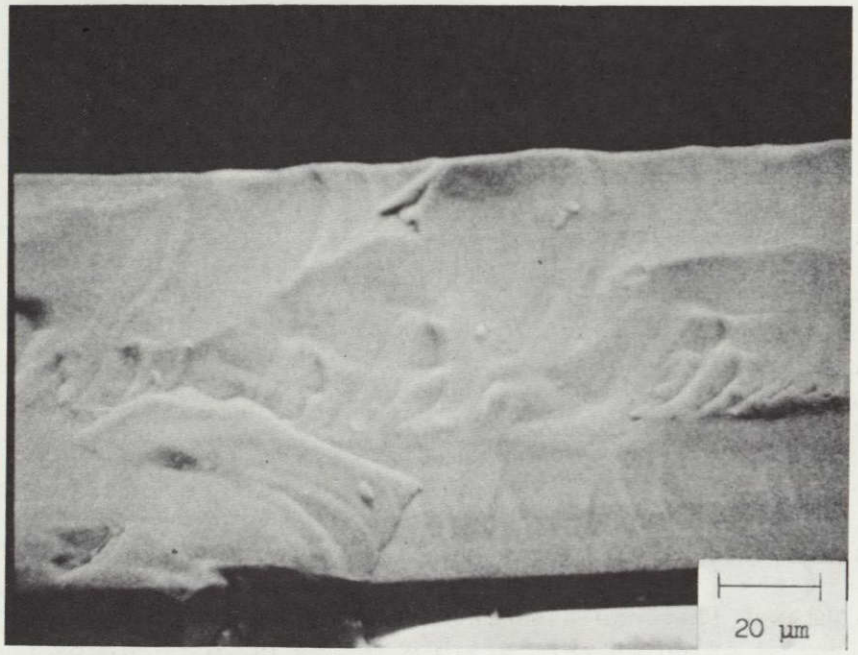

(b)

Figure 2-78. SEM Photographs of 75-80µm Thick Doped CVD Si Layer Grown on (01$\bar{1}$2) Sapphire Simultaneously with Sample of Figure 2-75. a) View Normal to Surface, b) Unpolished Fracture Cross Section.

2.3.11 Si CVD on Miscellaneous Substrates

Although the emphasis in this program was on the use of glass and polycrystalline alumina substrates (Sections 2.3.9 and 2.3.10), some experiments were done with other substrate materials. Most such experiments were of a preliminary exploratory nature, to evaluate the stability of the substrate material in the Si CVD environment.

Some CVD experiments were done with relatively thin samples of zircon ($ZrO_2 \cdot SiO_2$) received from Kyocera (Z360, Table 2-4) and the 3M Company (ASM475, Table 2-4) late in the second quarter. A preliminary evaluation of these materials was accomplished in a Si CVD experiment employing parameters known to be satisfactory for Si deposition on polycrystalline aluminas previously tested. The substrates were solvent- and acid-cleaned and subjected to a pre-deposition etch in H_2 at 1250°C in the reactor before Si growth by SiH_4 pyrolysis at ~1025°C. Whisker-like growth was obtained, as shown in the SEM photograph of Figure 2-79, indicating zircon is not as hardy as alumina in the Si CVD environment when H_2 is used. Si film deposition in He at 1025°C produced better results on these substrates, but still not good planar growth, as shown in Figure 2-80.

Mullite (see Table 2-4) was found to fare somewhat better as a substrate in a He atmosphere than in H_2 for growth of Si at ~1030°C, even though the substrate material appeared to be quite porous. The resulting Si crystallites were more regular in shape than those formed on zircon but still were non-uniform, and appeared as cucumber-like protuberances when viewed at an acute angle to the surface, as shown in the SEM photographs in Figure 2-81. X-ray analysis of this n-type high-resistivity film indicated a moderately strong {110} preferred orientation occurred.

These results tend to indicate that mullite is not well suited to the CVD process, primarily because of its porosity in the forms available during the program. There was also evidence of some discoloration in the mullite as a result of the CVD environment, probably associated with impurities in the material.*

Some preliminary screening experiments were done with glass-ceramics (see Table 2-2), but the limited supply of suitable samples of these materials prohibited an extensive evaluation. Some samples of Corning Code 9606 glass-ceramic became available during the third quarter, and some tests of the stability of this material in the CVD environment were conducted at that time. A Si deposit grown in H_2 at 860°C was whisker-like (Figure 2-82), similar to the Si growth on zircon in H_2 at 1025°C (Figure 2-79). In He the Si growth displayed some crystallographic order but was marked by flower-like rosette platelets emanating from the film surface, as shown in Figure 2-83. The non-uniformity of the film shown in the latter figure may have been associated with the surface problem previously discussed (Section 2.2.4 and Figure 2-15). X-ray diffraction analysis of this deposit showed a very strong {110} preferred orientation.

---

*Interest in mullite as a substrate material for another process for obtaining polycrystalline Si layers for possible low-cost solar cells (the so-called dip-coating process under development on the LSSA Project by Honeywell) has resulted in some efforts by one or two ceramic manufacturers to improve the properties of mullite. If sufficiently improved material becomes available it should be re-examined for use in CVD Si growth.

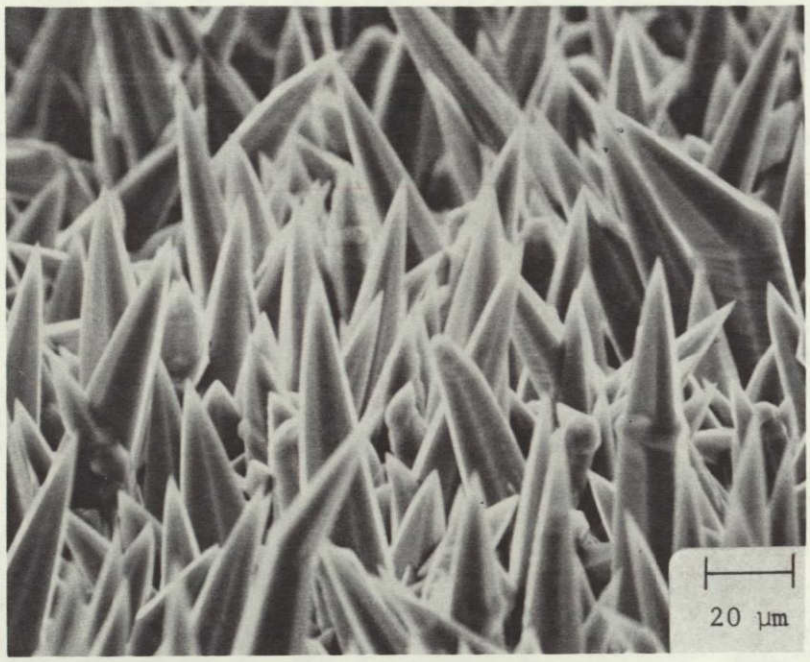

Figure 2-79. SEM Photograph of Whisker-like Deposit of Si on Zircon. Grown by SiH_4 Pyrolysis at 1025°C in H_2 Atmosphere.

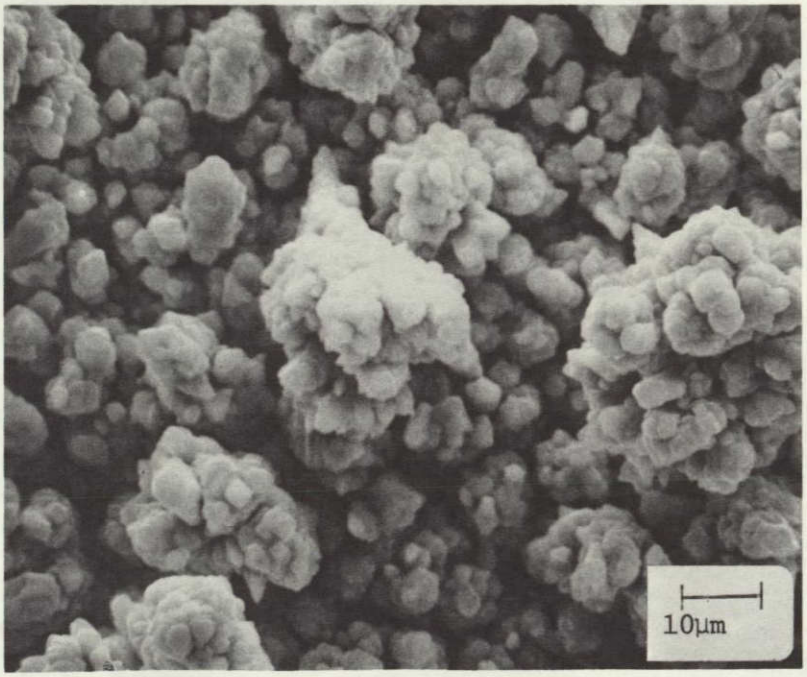

Figure 2-80. SEM Photograph at Normal Incidence of Surface of Si Film Grown on Zircon by SiH_4 Pyrolysis at 1025°C in He

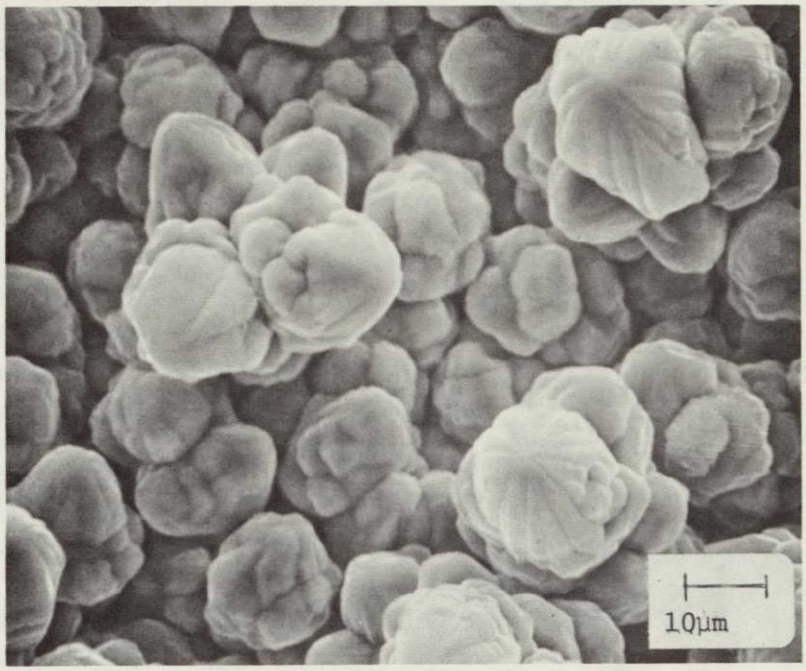

(a)

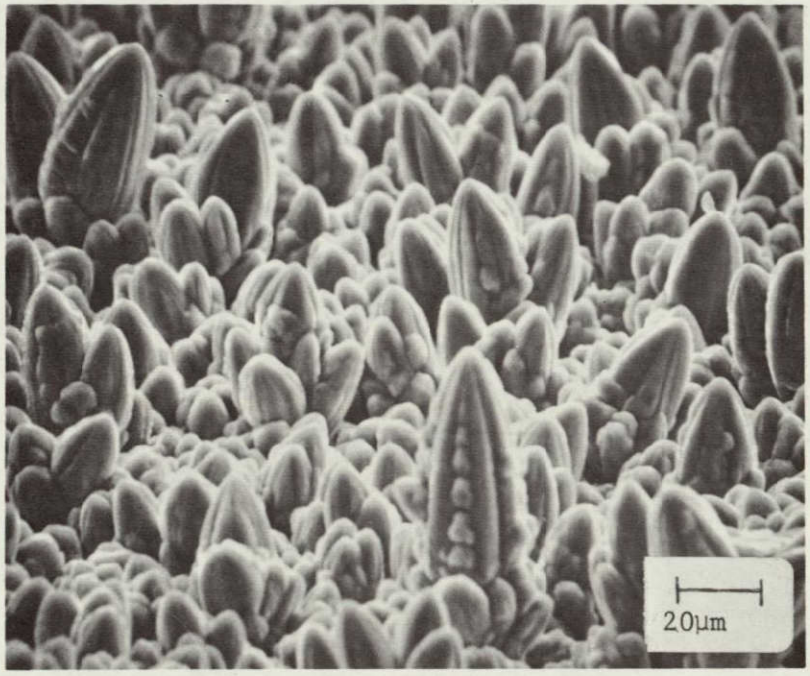

(b)

Figure 2-81. SEM Photographs of CVD Si Grown on Mullite Substrate by SiH_4 Pyrolysis in He at ~1030°C. a) Viewed at Normal Incidence, b) at 30 deg with Sample Surface

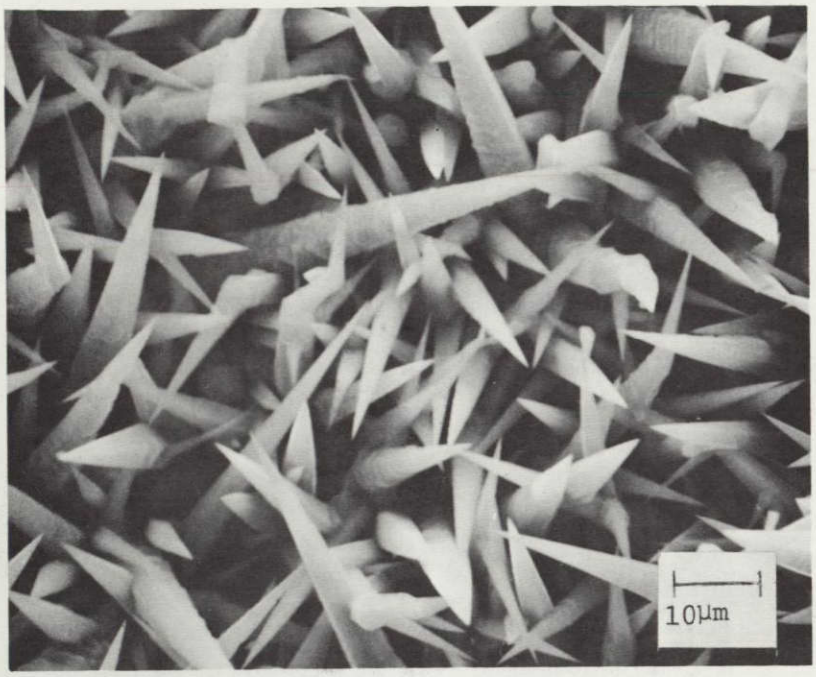

Figure 2-82. SEM Photograph of CVD Si Film Grown by SiH_4 Pyrolysis at ~860°C in H_2 on Substrate of Corning Code 9606 Glass-ceramic. (Viewed at normal incidence.)

Some experiments were also undertaken to examine the stability in the CVD process environment and the effects on the Si film properties of a metal substrate material. Among other things, such a substrate - produced on some other supporting material by a suitable deposition technique - would be of great value in achieving adequate ohmic contact to the back side of a thin-film solar cell structure. Because of its almost negligible solubility in Si at the temperatures used for Si CVD on glass substrates and its ready availability, Ti was used in the first experiments, even though it has other major disadvantages as an impurity in Si devices. Layers of several different thicknesses were deposited by sputtering onto Corning Code 7059 glass substrates in a separate apparatus. Si films were then grown on the Ti surfaces at ~850°C in He; Ti films ~1500Å thick were used in the first experiments. The composite samples were bowed after deposition, with the Si film in compression. It is interesting that this distortion is the opposite of that observed when Si was grown directly on 7059 glass (see Figure 2-36), indicating that the Ti layer protected the glass from the reaction in the CVD environment that produced the concave-upward bowing of the bare substrate.

X-ray diffraction analysis of the Si film indicated a moderate {110} preferred orientation. Electrical measurements were not made on the film. Energy dispersive x-ray analysis in the SEM showed no evidence of Ti in the film, although low concentration levels would not have been detected by this method of analysis.

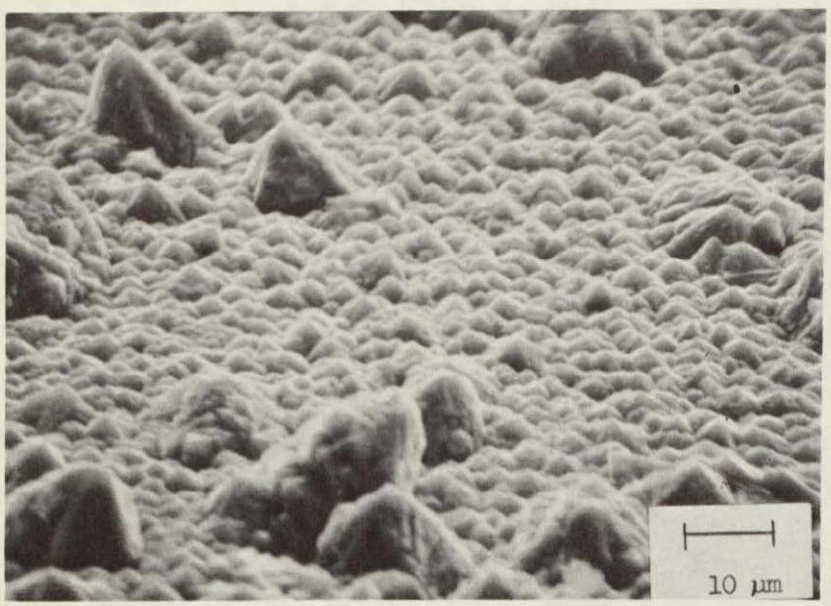

(a)

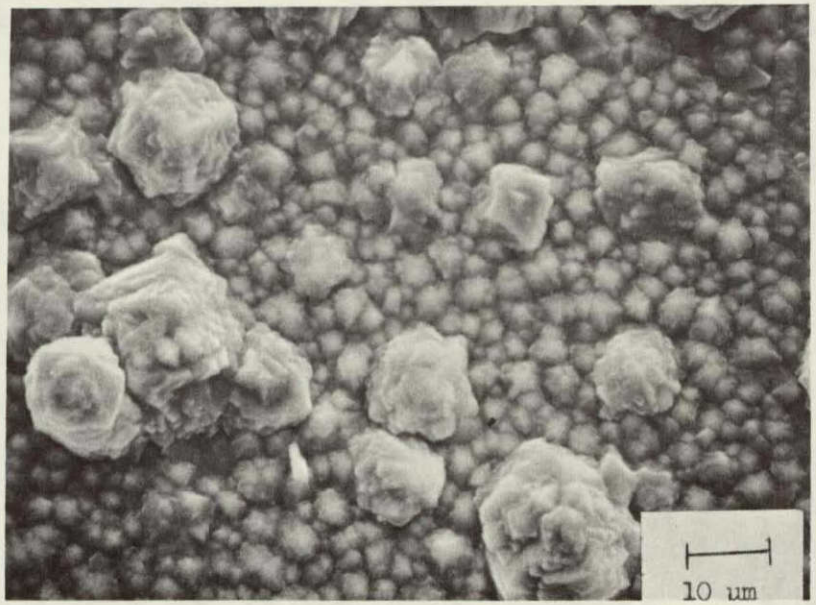

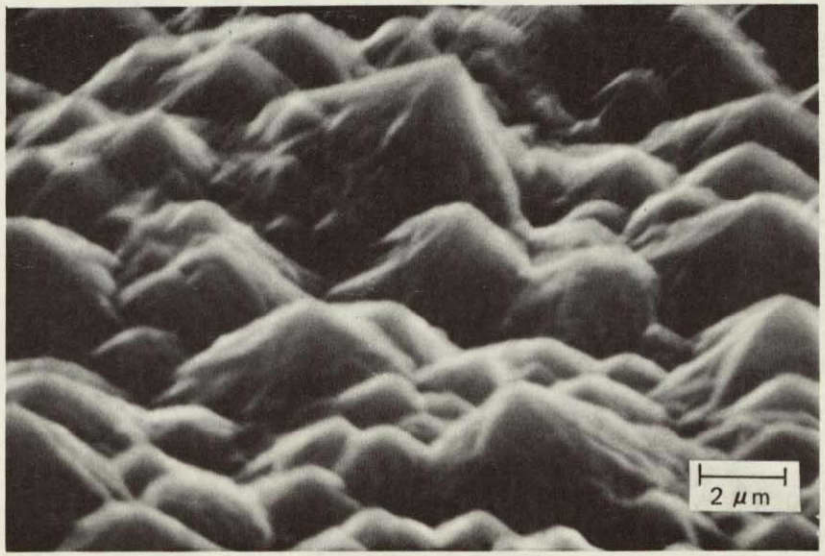

(c)

Figure 2-83. SEM Photographs of CVD Si Film Grown by SiH_4 Pyrolysis at ~840°C in He on Substrate of Corning Code 9606 Glass-ceramic. a) and c) Viewed at 30 deg with Surface, b) Normal Incidence

This preliminary examination of a metal-glass composite substrate did appear to indicate that such a combination might be satisfactory for Si CVD film growth, particularly if a more suitable metal were used, although no further work was done with these composite structures during this program. However, additional investigations of polycrystalline Si for solar cell applications, as recommended in Section 3 of this report, should include evaluation of metal-glass composites in certain configurations especially for purposes of providing base-layer contact in solar cell structures.

An exploratory Si deposition experiment was also done with a glazed nickel-steel supplied by Chi-Vit Corp. (see Table 2-2). The coating was an alkaline-earth aluminosilicate glass. In order to avoid contamination of the SiC-covered carbon pedestal used in the experiments with the aluminas at that time, a pedestal of old vintage was used in direct contact with the steel base. During the heating of the pedestal and substrate, however, a part of the SiC layer separated from the carbon pedestal and sprayed the substrate with debris. Rather than abort the experiment, a Si film was grown on the glaze at ~850°C in a He atmosphere, despite the contamination. The film was found to be adherent to the glaze. A second experiment was then done in which the Si film was deposited in a He atmosphere at 860°C. In that experiment there was considerable wrinkling of the film near the edge of the substrate, and the composite was bowed, with the film in compression, at room temperature. During storage for several days after the deposition the highly-stressed film separated completely from the substrate and shattered into numerous small pieces.

A proprietary glass prepared by the Atomics International Division of Rockwell as a glaze on ASM805 polycrystalline alumina was also tested as a substrate for Si deposition in He at ~800°C. The resulting film-substrate composite survived the deposition process and appeared satisfactory at the conclusion of the deposition. However, upon standing following removal from the reactor this film also failed under the stresses present and separated completely from the substrate, shattering into a multitude of small flakes.

Compatibility with Si CVD growth was examined for two different glazes prepared by Ferro Corporation, Specialty Glass Products Division (Cleveland, OH). Testing was performed under standard CVD growth conditions and also under high-temperature "fluid" conditions, as described below.

These glazes were standard production glazes, designated RX3638-1 and RX3638-2, and were prepared by Ferro on several substrates of 96- and 99.5-percent-purity polycrystalline alumina substrates supplied by Rockwell. RX3638-1 (No. 1) is a lead-free, alkali-containing low-temperature-fired glaze with a TEC value of ~7.1×10^{-6} per deg C, and RX3638-2 (No. 2) is both lead-free and alkali-free, with a TEC of ~7.7×10^{-6} per deg C. The compositions of these glazes are proprietary with Ferro.

Si growth in He at ~860°C on the alkali-free glaze (No. 2) was adherent, but for growth at 950°C in He flaking of the film was evident. Glaze No. 1 (alkali-containing) bubbled when heated to 850°C in He, and the bubbles persisted even when the (observed) temperature was increased to 1050°C. Si growth on the resulting molten surface remained only partially adherent.

However, when H_2 was used as the gas atmosphere in an experiment with both glazes in the chamber the surfaces of both remained smooth at 1025°C; both appeared to be molten. Exposure to SiH_4 in H_2 at 1025°C resulted in partially reflective films at the growth temperature. On cooling, the film on the alkali-containing glaze rippled severely, but the film on the alkali-free glaze contained some large crystallites (up to 20μm across). SEM photographs of the film surfaces are shown in Figure 2-84.

A thinner film (~2μm) grown later on glaze No. 2 wrinkled, however, suggesting considerable strain was present in the films grown on both of the glazes. It was not clear if the large crystallites obtained on glaze No. 2 were the result of the influence of the substrate or were caused by possible contaminin-ants in the gas phase. This question has not been resolved.

2.3.12 Nucleation and Early-stage Growth of CVD Si on Various Substrates Using SiH_4 Pyrolysis

An examination of the early stages of the growth of Si layers on the substrates of interest was considered important so that the effects of growth conditions on individual island formation and on subsequent growth behavior at the Si-substrate interface could be estimated. It is known, for example, that remelt-ing of polycrystalline Si can lead to large grain sizes (Refs 19,20), but the melting point of Si (1425°C) is higher than the softening point of the glasses used in this program and reactivity at such temperatures is very extensive with the ceramics, such as alumina. Therefore, the initial experiments with early growth phenomena were directed toward determining conditions that would lead to only partial coverage of the substrate under "normal" growth condi-tions.

It was determined that essentially complete Si coverage of single-crystal sapphire was achieved in ~0.1 sec using normal growth conditions (SiH_4 flow rate of 10 ccpm at 1025°C). Figure 2-85a shows a CVD Si deposit on single-crystal $(01\bar{1}2)$-oriented sapphire after ~0.1 sec growth at 1025°C with a SiH_4 flow rate of 10 ccpm in H_2 carrier gas. The individual Si islands have nearly coalesced, so that the layer is nearly continuous. Growth that appears quite similar occurs on refired polished Vistal 4 (large-grained polycrystalline Al_2O_3), with more dense growth occurring at the boundary between two different grains in the substrate (Figure 2-85b).

For less than 0.1 sec of Si film growth, only partial coverage is in evidence (Figure 2-86) for growth on a refired polished Vistal substrate. It is noted that certain grains of the polycrystalline substrate possess a greater density of Si islands than others. That is, the crystallographic orientations of the grains have a major effect on initial nucleation density. The greatest density of islands tends to occur at the grain boundaries, perhaps due to surface migration of atoms and/or nuclei and subsequent clustering at steps in the surface at the grain boundaries. There is also evidence seen of island congregation at steps in the surface of a grain in regions removed from the boundaries, as shown in Figure 2-87 for Si growth at a lower SiH_4 flow rate (2 ccpm) at 1025°C.

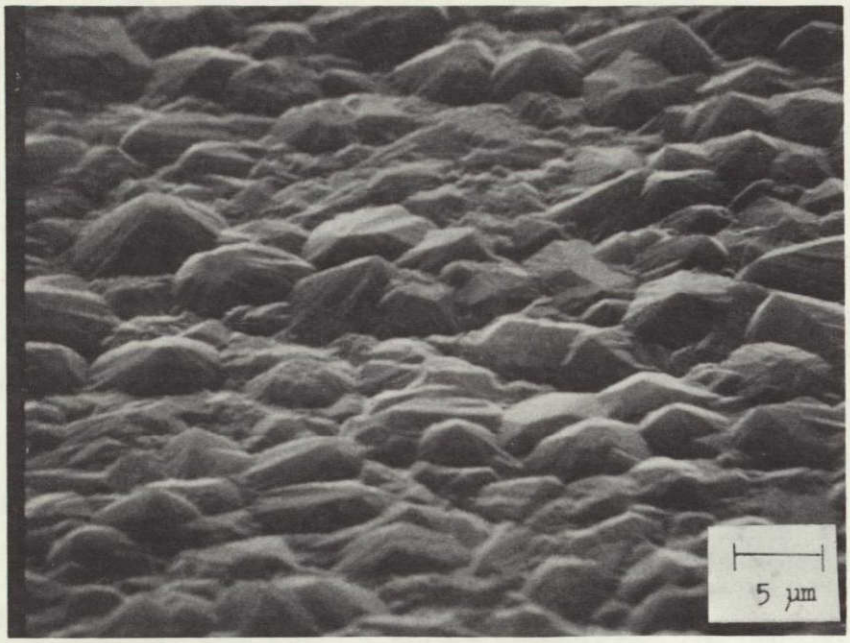

(a)

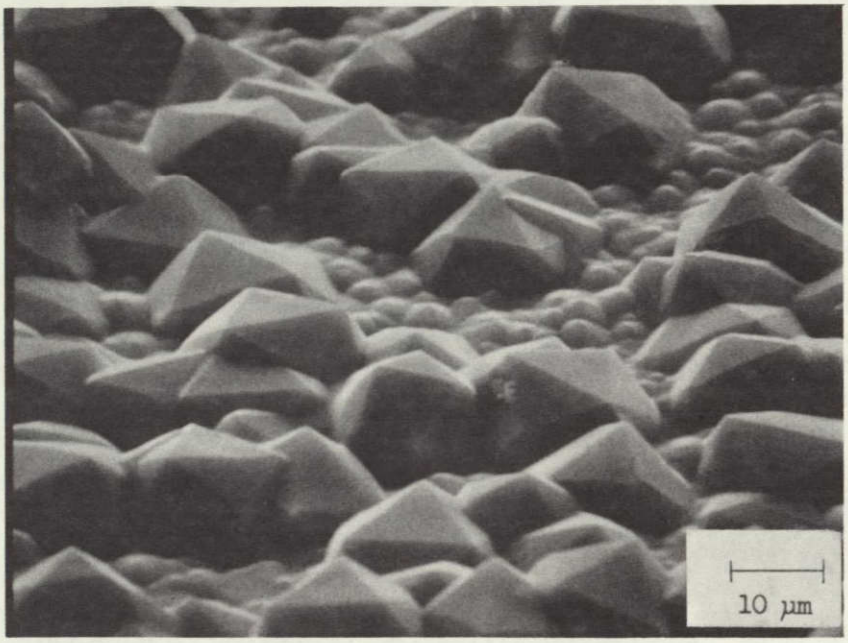

(b)

Figure 2-84. SEM Photographs of Surfaces of CVD Si Layers Deposited on Two Different Pb-free Ferro Glazes at ~1025°C in H_2. a) Film on Glaze Containing Alkali, b) Film on Alkali-free Glaze.

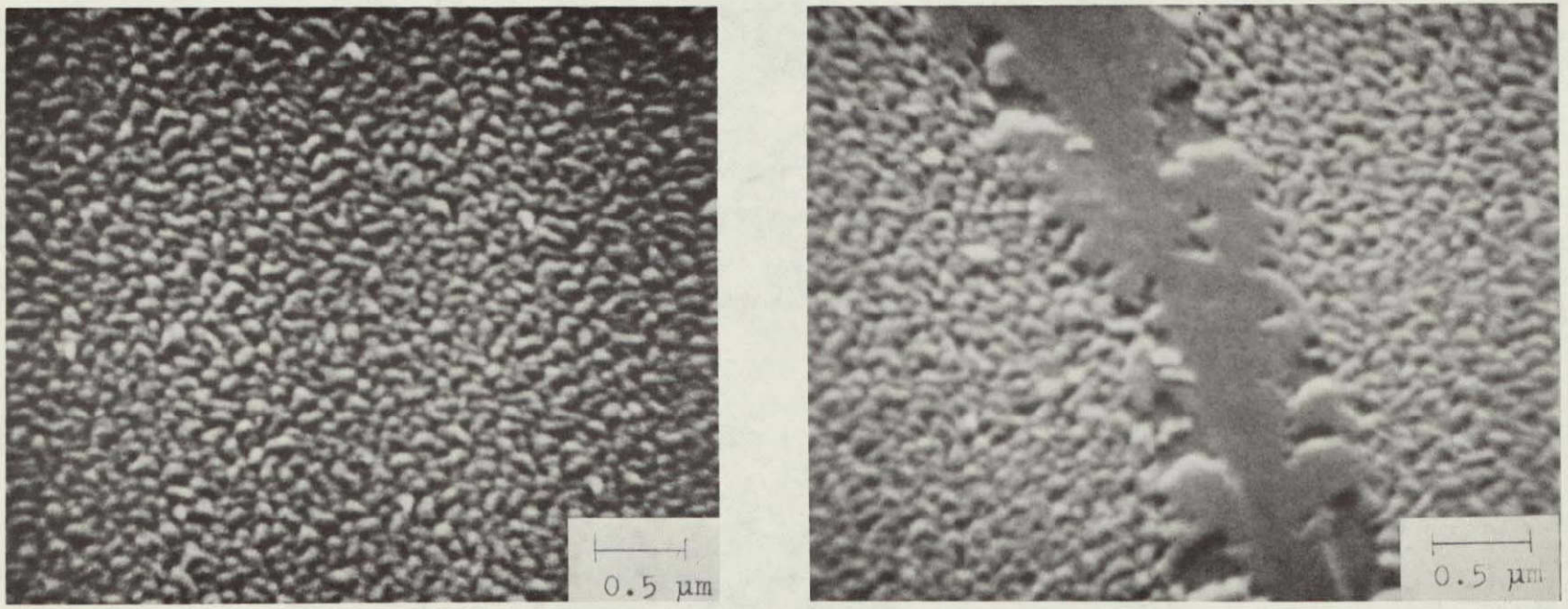

(a) (b)

Figure 2-85. SEM Photographs of Early Growth of CVD Si on Alumina. a) Deposit on Single-crystal $(01\bar{1}2)$-oriented Sapphire; b) Deposit on 4-times-refired Polished Vistal (Polycrystalline Alumina). (SiH_4 flow rate 10 ccpm for ~0.1 sec at 1025°C in H_2 carrier gas.)

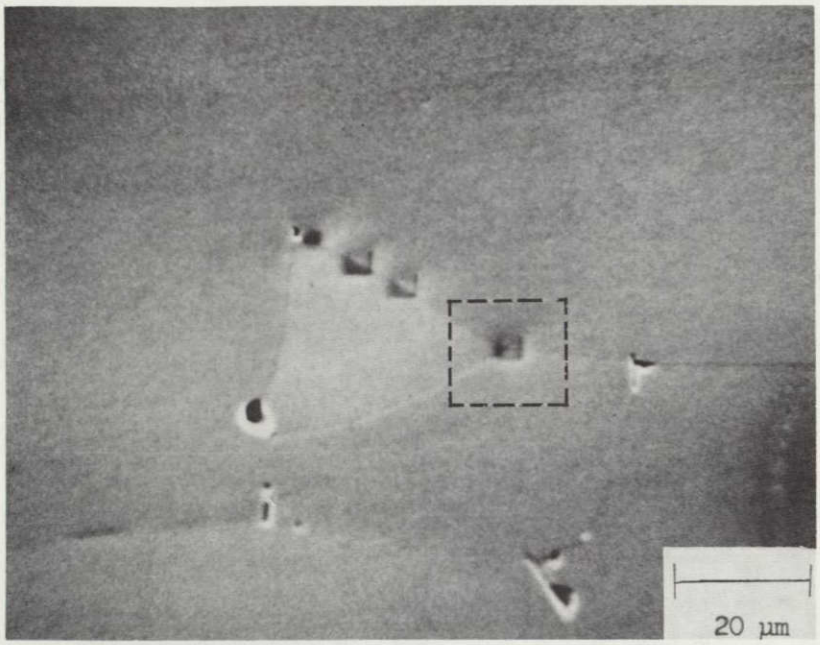

(a)

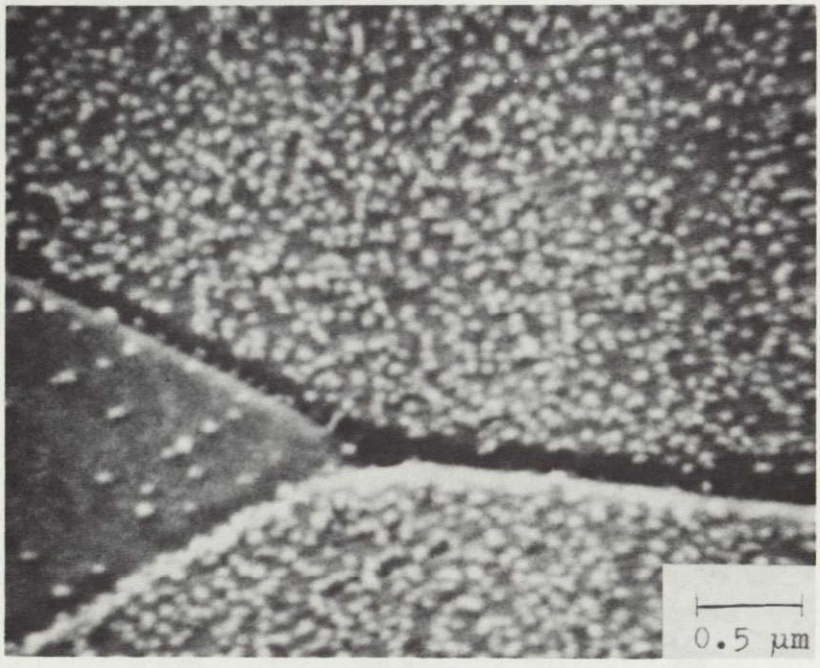

(b)

Figure 2-86. SEM Photographs of Early Growth of CVD Si on Polished 4-times-refired Vistal (Polycrystalline Alumina). Area Shown in (b) Marked by Rectangular Outline in (a). (SiH_4 flow 10 ccpm for <0.1 sec in H_2 carrier gas, at 1025°C)

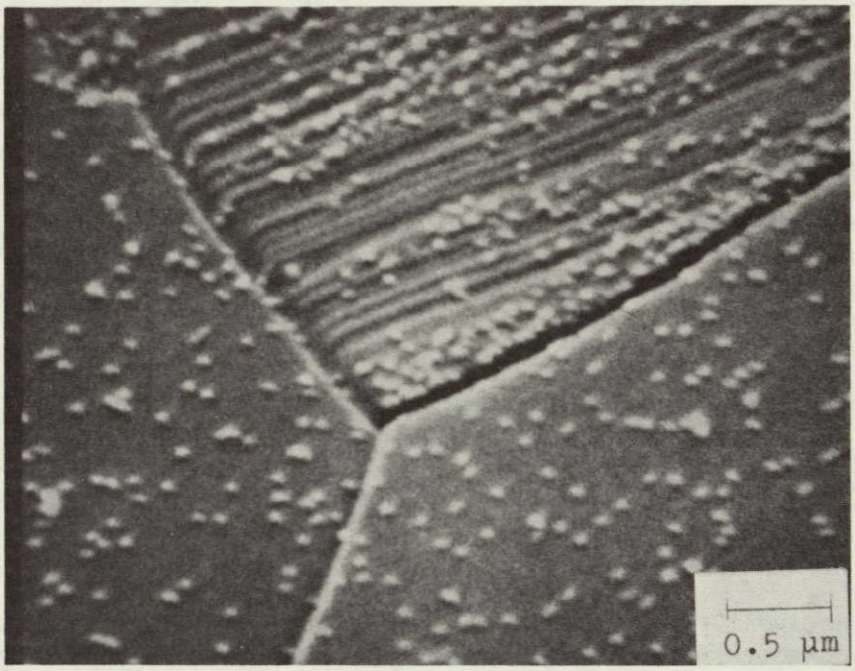

Figure 2-87. SEM Photograph of Early Growth of CVD Si on Polished 4-times-refired Vistal (Polycrystalline Alumina). (SiH_4 flow rate 2 ccpm for 0.1 sec at 1025°C in H_2 carrier gas)

These observations further establish that refired large-grained Vistal alumina can be used effectively to provide an informative picture of post-nucleation and early-stage growth processes that occur for Si deposited by CVD, even on fine-grained low-cost alumina surfaces. This is because the large individual grains of Al_2O_3 in the Vistal tend to provide local conditions that are probably much the same as those existing not only on a larger scale on a single-crystal sapphire surface of that same orientation but also on a smaller scale on an individual grain in a fine-grained low-cost alumina (neglecting effects of impurities escaping from grain boundaries or voids in the polycrystalline case).

Nucleation and island growth experiments were also performed on glass substrates, first using typical growth parameters for Si on glasses - nominally 850°C and a SiH_4 flow rate of 10 ccpm in He carrier gas. On exposure to SiH_4 for 1 sec, growth was evidenced by slight darkening of the substrates. Slight color change was also in evidence after 0.1 sec of growth. However, it was not possible to detect, by normal SEM examination, the presence of the

same type of three-dimensional islands as were found for film growth at 1025°C in H_2 on Vistal and sapphire, except in isolated regions where the substrate surface may have been contaminated. It is possible that on the amorphous glass surface at 850°C the early stage of Si growth is also predominantly amorphous, rather than polycrystalline, and that only in thicker films is the polycrystalline structure in evidence.

In these early experiments with glass substrates there were some indications that the substrate may not have been completely covered even after 6 sec of Si deposition in He at 850°C. A two-step growth process at 850°C (6 sec in He atmosphere followed by 30 min in H_2 atmosphere) led to the same type of needle and whisker growth previously observed on Corning Code 1715 and Owens-Illinois GS211 glasses after Si growth in a H_2 atmosphere. This suggested that the coverage was incomplete following the first step of the growth process (or that the Si was pervious to H_2).

In later experiments, partial-coverage layers of Si on substrates of Owens-Illinois GS213 and EE-2 and Corning Code 1715 glasses - as well as on sapphire monitor wafers - were prepared at temperatures of ~850°C in He, but with lower SiH_4 flow rates (~5 ccpm). Those samples were examined in the SEM, prior to the preparation of surface replicas to obtain enhanced resolution for examination either in the SEM or in the transmission electron microscope.

The reflective 12-sec deposits exhibited well-developed individual "islands" that appeared to be just beginning general coalescence, as shown in Figure 2-88, although the resolution of the SEM did not permit definite identification of any open spaces among the islands except perhaps on the EE-2 glass substrate (Figure 2-88d). Average island (or surface feature) size ranged downward from the order of 0.1-0.2μm for the deposit on sapphire, to perhaps 0.05-0.1μm for the deposit on EE-2 glass, 0.05μm for that on GS213 glass, and 0.02-0.05μm for that on 1715 glass.

A similar set of deposits grown for 3 sec exhibited yellow coloration, were quite transparent, and appeared to have much smaller islands or surface features, ranging downward from 0.04-0.08μm for the film on sapphire to less than 0.03μm for the deposit on EE-2 glass, with the feature size on GS213 and 1715 substrates appearing about the same and slightly smaller than that on sapphire.

The 1-sec deposits still showed very small individual features, but the features appeared quite uniform in size and shape on a given substrate (rather than elongated, as those in the 12-sec deposits appeared to be), and were perhaps only a quarter of the apparent size of those in the 3-sec deposits. The size of the features in the deposit on sapphire was again the largest, but it was very difficult to distinguish size differences among the other three deposits.

A second set of deposits was grown on the same three glasses for a 3-sec period. Immediately thereafter, the deposits were annealed <u>in situ</u> for 30 min. at the growth temperature (855°C) while in place on the sample pedestal and with the He flow continuing at 1.5 ℓpm. These deposits appeared very similar to those grown for 1 sec (with no annealing), including the apparent island size on each of the substrates. It is not clear if this effect was really caused by the annealing process or if there was a significant uncontrolled difference in the actual deposition times among the three experiments in question.

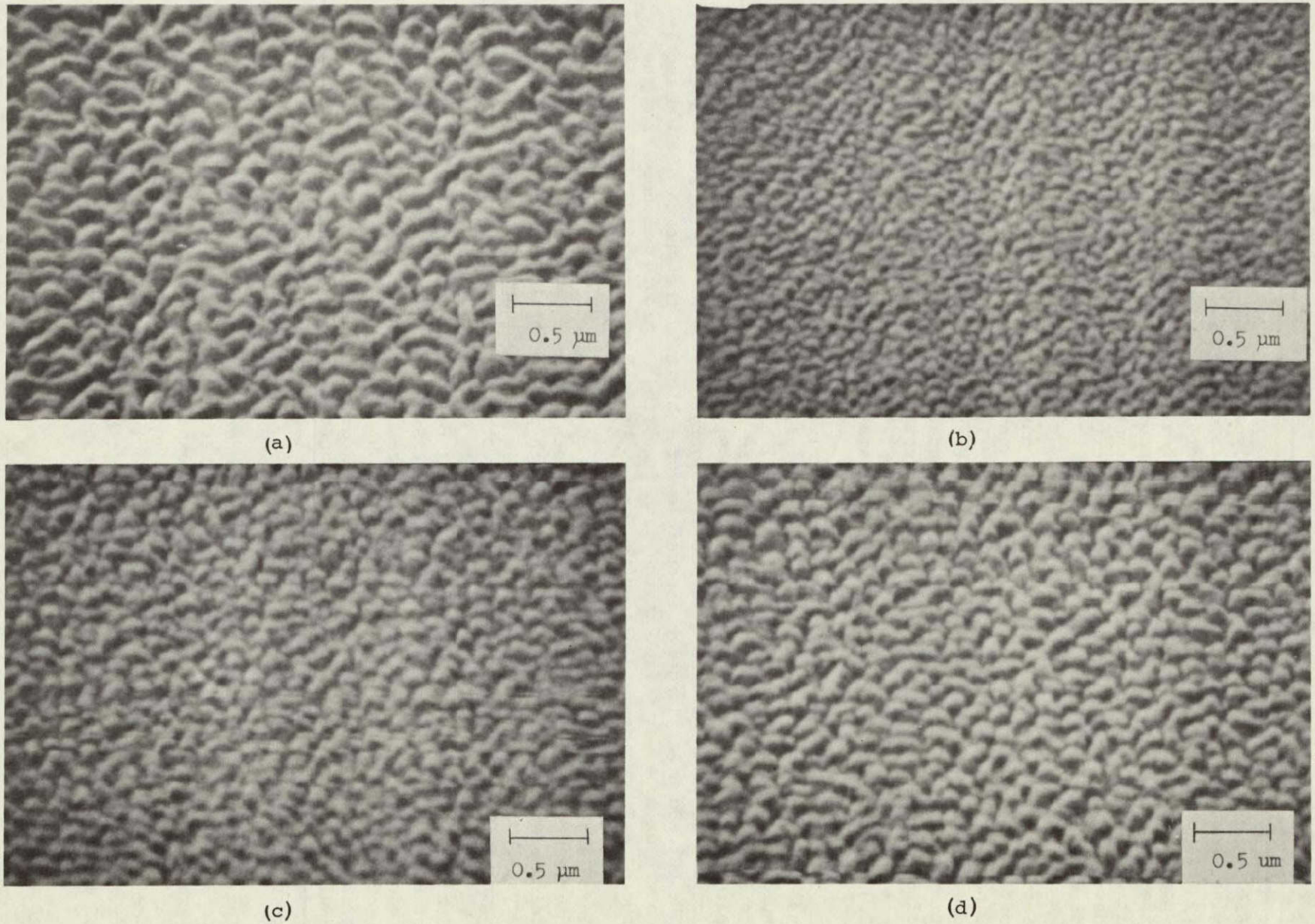

Figure 2-88. SEM Photographs of Partial-coverage Si Deposits Grown for 12 sec on Four Different Substrate Materials by SiH_4 Pyrolysis in He at 855°C, showing Individual Islands of Si. Substrates a) $(01\bar{1}2)$ Sapphire; b) Corning Code 1715 Glass; c) Owens-Illinois GS213 Glass; d) Owens-Illinois EE-2 Glass.

RED patterns obtained for the several polycrystalline films on each of the glass substrates indicated that the degree of preferred orientation detected by this particular method of analysis increased distinctly for the longer deposition times. This may simply have been a sampling phenomenon, since the deposits did not appear to be continuous, but it seems more likely that it was a real measure of an increased amount of preferred orientation that developed as the island size (i.e., effective amount of material present) increased.

Further investigation of these effects, considered to be very important and offering a possible method for obtaining enhanced grain sizes in polycrystalline Si films on glasses, was planned for later in the program. However, it did not prove to be possible to carry out those experiments with the remaining time and funds of the contract. Recommendations for continued investigations of these phenomena are included in the Section 3 discussion.

2.3.13 Growth of CVD Si Films by Pyrolysis of SiH_4-HCℓ Mixtures

An investigation was undertaken to determine if SiH_4-HCℓ mixtures could be used to enhance grain growth in polycrystalline Si films grown on low-cost substrates. Previous studies at Rockwell had demonstrated that by adding HCℓ to $SiCℓ_4$ it was possible to encapsulate an amorphous SiO_2 region between two patches of bare Si with a highly twinned Si deposit, x-ray diffraction examination of which gave no evidence of polycrystalline structure (Ref 21). The HCℓ added was largely responsible for inhibiting the growth of Si directly on the oxide layer while, at the same time, the Si growth extended from the two bare Si regions and joined to form a "bridge" over the SiO_2.

In this program it was intended that the HCℓ added to the Si source would preferentially attack the smaller Si crystals formed on amorphous or polycrystalline substrates, resulting in Si growth preferentially on the larger Si crystals which survived the attack by HCℓ, thereby leading to a greater proportion of larger grains that should grow further during the continuing deposition.

Studies by Bloem (Ref 22) in a horizontal reactor have shown that the addition of HCℓ to SiH_4 greatly enhanced epitaxial Si growth rates, presumably by reduction of the gas phase nucleation rate, but this effect occurs at relatively high temperatures; at lower temperatures he found that the etching reaction predominates. Since growth from SiH_4 and etching by HCℓ proceed independently (Ref 22), reactant mixtures of SiH_4 and HCℓ at a given temperature which result in a reduced Si growth rate and preferential removal of small crystals could provide films with enhanced grain size.

The first experiments were designed to determine the effect of HCℓ additions to SiH_4 on the growth rate of Si in the vertical reactor. Sapphire substrates were used in the initial experiments to expedite film thickness (i.e., growth rate) measurements by the IR technique, and H_2 was used as the carrier gas. Additions of HCℓ to SiH_4 flows of 25 ccpm (MFC readings) were made, and Si films were grown at ~1025°C. At the first HCℓ concentration used (flow rate of 10 ccpm) a slight increase in growth rate was observed, but with progressive

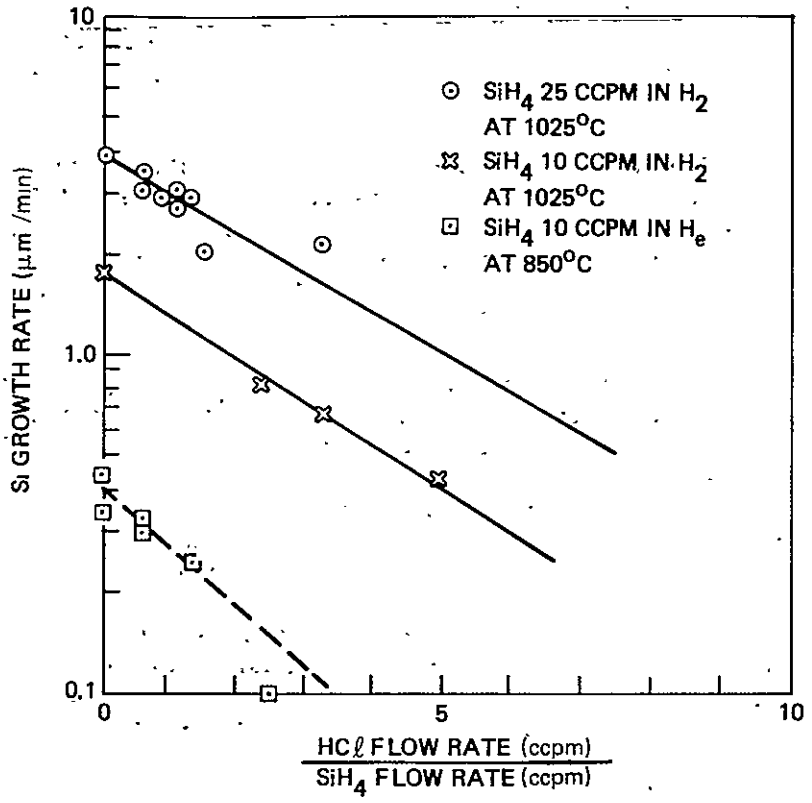

Figure 2-89. Changes in Si CVD Growth Rate Caused by Various Additions of HCℓ to SiH_4

in thickness across the pedestal diameter when the total H_2 flow was 4 ℓpm. At a SiH_4 flow rate of 10 ccpm the Si growth rate was 1.5μm/min; with HCℓ flowing at 100 ccpm, the net Si growth rate was slightly negative, the film grown in the first thin layer (12 sec deposition time) having almost disappeared in 13 min of exposure to the SiH_4-HCℓ mixture.

Double-layer films were grown in H_2 at HCℓ flow rates of 25, 30, and 50 ccpm, but it did not appear that any extensive enlargement of average grain size occurred with these parameters.

X-ray analysis of 12-sec polycrystalline Si growths (approximately 0.5μm thick) on substrates of as-fired ASM805, as-fired Superstrate, and polished Superstrate, grown at 1025°C in H_2 (4 ℓpm) with a SiH_4 flow rate of 25 ccpm as a preliminary to the double-layer experiments, indicated completely random orientations in all three cases. However, the thick (20-25μm) layer grown on such a thin layer in the presence of HCℓ had developed distinct preferred orientation in the {110} plane, and in at least one case the preferred orien-

tation was very strong. Whether this orientation developed as a consequence of the HCℓ present or simply as a result of the CVD Si layer continuing its growth to greater thicknesses, as was observed before, was not determined.

The conclusion of this series of experiments, therefore, was that no improvement in either overall film quality or average grain size occurred in films on alumina substrates prepared by this particular two-step process relative to those same properties in films of comparable thickness grown in a single step without HCℓ.

Si deposition experiments using SiH_4-HCℓ mixtures were also carried out with substrates of Corning Code 1715 and Owens-Illinois GS211 and GS213 glasses. Growth rates for undoped Si films deposited in He were first established for a rotameter reading corresponding to 10 ccpm flow of SiH_4 at observed deposition temperatures of ~850 and ~950°C without HCℓ in the system. In each experiment a single-crystal sapphire substrate accompanied the same three glasses.

At 850°C the growth rates of these relatively thin films on the sapphire substrates were 0.3-0.4μm/min for the above parameters; at ~950°C they were 0.12-0.17μm/min. The values at ~850°C were slightly higher than the rates observed (0.2-0.3μm/min) for doped films grown on sapphire substrates in the presence of the same glasses in an earlier series of experiments involving similar deposition parameters (Section 2.3.1.2), but still below the average growth rate of ~0.5μm/min observed for these deposition parameters when sapphire substrates alone were used.

Undoped films in three different thickness ranges - 0.1-0.2μm, 1.5-2.5μm, and 6-10μm - were then prepared in He at ~850 and ~950°C. The polycrystalline films were analyzed by reflection electron diffraction and x-ray diffraction procedures to examine the extent of preferred orientation variation with film thickness and deposition temperature.

Experiments were then initiated to establish net Si growth rates in a He atmosphere in the presence of various concentrations of HCℓ at the growth temperature typically used for film growth on glasses, i.e., ~850°C. Sapphire substrates were used for these experiments, done in preparation for the subsequent examination of the HCℓ two-step process for growth of Si on glasses. At a concentration (i.e., flow rate) ratio for HCℓ:SiH_4 of about 4:1 the Si deposition rate and the film etch rate (due to HCℓ) were essentially offsetting - that is, the net growth rate was approximately zero. At a 25:1 ratio, Si growth was slightly less than 1/3 its usual rate at ~850°C, and at 1.4:1 the Si growth rate was about 2/3 its value in the absence of HCℓ. The results of these experiments are included in the data given in Figure 2-89. Since RED examination of the films grown on these glasses at ~950°C had shown them to be inferior structurally to those grown at ~850°C, no HCℓ etch-rate information was sought at the higher temperature.

To examine the effect of the HCℓ two-step deposition process on the properties of Si films grown on glasses a set of double-layer samples similar to those grown on the polycrystalline aluminas (see above) was prepared, again involving two different HCℓ concentrations for growth of the upper layer of each thickness.

One set of double layers consisted of a bottom layer nominally 1-2μm thick and a thicker top layer (nominally 6-10μm thick) grown in the presence of HCℓ flowing through the deposition chamber at ~8 and ~25 ccpm. Substrates of GS211, GS213, and 1715 glasses and single-crystal sapphire were used. X-ray diffraction analysis of the composite layers on GS211 and 1715 glass indicated essentially random orientation of the polycrystalline Si on both substrates for the low HCℓ flow rate and slightly preferred {100} orientation for the higher HCℓ flow rate, the preferred orientation being more prominent in the film on GS211 glass. However, the extent of preferred orientation did not even approach that observed in films grown to about the same thickness on the same glasses at ~850°C in the absence of HCℓ. The companion double layers grown on sapphire in these same experiments exhibited about the same relative x-ray diffraction line intensities as did the film of comparable total thickness (~7.9μm) grown without HCℓ, although the (400) line was relatively less intense for both of the double-layer samples.

A second set of double-layer samples, with the bottom layer 0.1-0.3μm thick and a top layer 1-2μm thick, the latter again grown with HCℓ flows of 8 and 25 ccpm, was also prepared. X-ray diffraction analysis of these samples again showed that essentially random polycrystalline Si was formed on both GS211 and 1715 glass substrates for the low HCℓ flow rate and on 1715 glass for the higher HCℓ flow rate. The double layer grown on GS211 glass with the higher HCℓ flow rate exhibited a slight tendency for preferred orientation of both {100} and {110} planes; single layers of about the same thickness grown on this same glass at ~850°C without HCℓ had significantly more {100} preferred orientation and essentially no evidence of {110} preferred orientation.

The companion double layers grown on sapphire substrates were somewhat different from the film of similar thickness (~1.7μm) grown without the HCℓ. Both of the double layers exhibited considerably more x-ray evidence of {110} planes than did the single layer, and the double layer grown with 25 ccpm of HCℓ flowing during the second step was also much more strongly {100} oriented than was the one with 8 ccpm of HCℓ flowing during growth of the upper portion. The reason for these differences is not clear.

Only the films grown on GS213 glass and sapphire substrates in the presence of HCℓ had surfaces sufficiently smooth, as grown, for RED analysis. Whisker growth was evident on the surface of the film grown on 1715 glass, and the surface of the top layer on the GS211 glass substrate was quite irregular. Comparison of the RED patterns obtained for the four double-layer films on GS213 glass and the single-crystal sapphire substrates with the corresponding patterns for single layers produced without HCℓ clearly showed major differences in film quality near the surface for both substrates. Highly twinned growth was indicated on the sapphire substrates for the HCℓ two-step process, for example.

SEM examination of fracture cross-sections of the four double layers on the companion sapphire substrates permitted confirming measurements of the total thickness of the composite layers, and also delineated the boundary between the two sequentially grown layers. For example, in the thicker sample (14μm) grown with an HCℓ flow rate of 25 ccpm for the upper layer the first-grown

layer was ~4μm thick and the second layer ~10μm. SEM examination of the surface of this sample indicated strongly faceted, highly crystallographic surface features averaging 2μm across, essentially the same as the dimensions of the surface features on the single layer of comparable thickness grown without HCℓ on the GS213 glass substrate.

The thinner sample (~1.3μm) grown on sapphire with 8 ccpm of HCℓ flowing through the chamber during deposition of the top layer consisted of a bottom layer 0.2-0.3μm thick and a top layer ~1.0μm thick. SEM examination of the surface of this sample revealed much less well-defined surface facets and an average dimension for the surface features of about 0.5μm, only slightly different from the dimensions of surface features on the single layer grown to comparable thickness on GS213 glass at ~850°C without HCℓ.

The apparent stability of the three glasses to the HCℓ two-step process, based on general observations during these experiments and on the observed structure of the upper layers formed with HCℓ present, is greatest for GS213 and least for Code 1715 glass. The overall conclusion is that the two-step process involving HCℓ at ~850°C in He clearly produces films of poorer structural quality on glasses than those grown directly from SiH_4 in a single step without HCℓ, under otherwise similar conditions. This result is similar to that obtained for growth on polycrystalline alumina substrates at 1025°C in H_2, as discussed earlier.

2.3.14 Growth of Epitaxial CVD Si Films Using Dichlorosilane Process

Near the end of the program a series of epitaxial Si films ~20μm thick was grown by the dichlorosilane process in the AMC Model AMV-800 CVD reactor in the Advanced Device Research Laboratory of the Rockwell Electronics Research Center. A series of five such deposition experiments was carried out, with a variety of Si single-crystal substrates providing the base for high quality epitaxial growth.

The dichlorosilane pyrolysis process for Si CVD film growth proceeds according to the following simplified reaction:

$$SiH_2Cl_2 \rightarrow Si + 2HCl \quad .$$

The pyrolysis proceeds at temperatures (typically 1000-1150°C) similar to those used for SiH_4 pyrolysis, and very high growth rates can be achieved - up to ~20μm/min in a H_2 atmosphere - throughout most of the temperature range of interest for epitaxy. Specifically, the growth rate is relatively independent of deposition temperature in the range 1000-1175°C and also shows little variation with crystallographic orientation of the substrate (Ref 23).

One of the main reasons for interest in the dichlorosilane process in this program was the fact that HCℓ is produced as a product of the pyrolysis. The two-step HCℓ process involving Si CVD growth by SiH_4 pyrolysis did not appear to produce the hoped-for enhanced grain size in continuous polycrystalline Si films due to HCℓ etching effects (see Section 2.3.13), but since the

HCℓ liberated by the dichlorosilane pyrolysis would be energetically different from that added in the SiH_4 process it was thought that different results might be obtained. Unfortunately, as indicated earlier, the effects of HCℓ etching on non-continuous (i.e., partial-coverage) polycrystalline Si films on various low-cost substrates with either the SiH_4 or the dichlorosilane process were not investigated experimentally because of time limitations in this program. Additional studies of these phenomena are recommended, as indicated in Section 3 of this report.

In the Si CVD experiments that were done with the dichlorosilane process all of the single-crystal substrates were vapor-phase etched in HCℓ in the deposition chamber at temperatures of 1175-1180°C for ~2 min before film growth. The Si films were deposited at ~1075°C at growth rates of ~0.7μm/min.

P-type films doped with boron (from B_2H_6) to concentrations ranging from ~$1x10^{15}$ to ~$1x10^{18}$ cm^{-3} were prepared in these experiments. Six types of Si substrates were used in various combinations in the experiments: 1) 2¼ in. diam. chemically polished (etched) wafers of p-type 1-3 ohm-cm (100)Si solar cell material (from OCLI); 2) same, but only partially "polished" by a slow chemical etch that leaves a relatively rough "fine-grained" surface; 3) 2x4 cm chemically polished (etched) standard solar cell blanks of p-type 1-3 ohm-cm (100)Si (from OCLI); 4) same, but optically polished by standard techniques used for preparing solar cell blanks (from OCLI); 5) 2 in. diam. optically polished wafers of p-type ~10 ohm-cm (100) device-quality Si (from Monsanto); and 6) same, but n-type material (from Monsanto).

A group of these Si films was processed by OCLI into solar cells, for comparison with those fabricated in similarly doped epitaxial Si films grown by SiH_4 pyrolysis. These results are discussed in Section 2.4.

2.4 PREPARATION AND EVALUATION OF SOLAR CELL STRUCTURES IN CVD Si SHEET MATERIAL (TASKS 4 AND 6)

Experimentation with various candidate low-cost substrate materials, as described in Section 2.2, and investigations of CVD parameters and various special procedures for the purpose of achieving improved properties in the polycrystalline Si films grown on these substrate materials, as described in Section 2.3, continued throughout most of the program. The results of those studies could often be adequately determined by the various materials characterization techniques employed routinely.

However, since the overall objective of the contract was to investigate and develop the Si CVD technique specifically for application to low-cost large-area solar cell array fabrication - and eventually to large-scale production - it was also necessary to maintain a flow of Si sheet samples through the solar cell fabrication process, so that a measure of the suitability of the Si sheet material for that specific application would be provided at any given time during the conduct of the work.

As indicated in the Introduction, the processing of Si sheet material into solar cell structures throughout this program was done by the Photoelectronics Group of OCLI. This arrangement was made so that well-established standard cell processing methods would be applied in a routine manner to the Si sheet samples generated in the deposition experiments at Rockwell, thus providing good assurance that observed variations in photovoltaic performance of the experimental cell structures would be attributable to variations in the sheet material properties rather than to uncontrolled or unidentified variations in the processing itself.

However, it was recognized that the Si sheet samples prepared at Rockwell would be very non-standard in properties and configuration, relative to the standard single-crystal Si solar cell blanks normally used in solar cell processing lines such as those at OCLI. Thus, the experimental cell processing was carried out by the OCLI Research and Development Group, still employing conventional processing techniques but introducing variations as required, according to the specific properties and configurational characteristics of the particular group of Si sheet samples involved.

Of over 350 Si CVD experiments done in the reactor system (Section 2.1 and Figure 2-2) during the course of the program at most approximately 50 utilized standard (established) CVD procedures strictly for preparation of sheet samples for analysis, processing, demonstration, or delivery to JPL. All other experiments were exploratory in nature and thus produced samples that were correspondingly experimental.

The contract Statement of Work stipulated that the contractor shall "fabricate and evaluate solar cells with a minimum of 1 cm^2 area" and that "techniques for producing solar cells from these films shall be, to the maximum extent possible, previously developed procedures." It was further stipulated that "one solar cell, on the average, shall be made per week during this program."

The interpretation given throughout the contract to the requirement for use of previously developed procedures was that conventional diffusion processing to produce p-n junctions in appropriately doped base material should be used routinely on the Si sheet samples whenever possible, to the exclusion of other junction formation techniques such as ion implantation doping and in situ growth, even though such alternative procedures - although not developed to the point of being standard methods for solar cell fabrication - might well be more advantageous for the polycrystalline and/or heavily defected samples prepared in this program. Consequently, most of the experimental solar cells fabricated and evaluated in this contract were made by impurity diffusion methods followed by appropriate adaptations of standard contacting techniques.

Fortunately, during the final six months of the contract, on the basis of a contract modification made at Rockwell's request, it was also specified that some experimental cell structures should be made by in situ growth of p-n junctions, with two appropriately doped regions being deposited by Si CVD in succession in the reactor. The photovoltaic performance of such grown-junction structures was to be compared with that of structures involving essentially identical CVD-grown base regions and subsequently diffused (rather than deposited) upper layers to produce the necessary junctions.

It was further specified that these grown-junction cells would be made on polycrystalline alumina substrates, along with companion cells made on single-crystal sapphire substrates to provide a "standard" performance reference for comparison purposes. It was intended that similar polycrystalline grown-junction structures would be made on other low-cost substrate materials (especially glasses) in a subsequent phase of the work, as a logical next step in the investigations. Recommendations for such studies are discussed further in Section 3.

This section contains a detailed summary of the growth, fabrication, and photovoltaic characterization of experimental solar cell structures that were prepared in CVD Si sheet material on a variety of substrates. At all stages of the investigations involving polycrystalline Si solar cells there were epitaxial Si cell structures prepared on single-crystal sapphire substrates as "control devices," to provide an indication of the integrity of the overall growth and fabrication procedure in use on that particular batch of samples and to give a measure of the performance "ceiling" that might be expected of the polycrystalline (and thus inferior) Si cells fabricated at the same time. These epitaxial Si-on-sapphire "baseline reference" devices are included in all of the following discussions.

Groups of experimental cells produced and evaluated throughout the program are described in chronological sequence, to emphasize the way in which the work progressed.

2.4.1 Standard Solar Cell Processing Procedures

Details of the handling, processing, and measurement techniques applied to any one sample at OCLI were varied to accommodate the characteristics and/or limitations of the sample. However, there was a standard sequence of procedures that was generally followed to whatever extent possible. Standard solar

cell processing methods were used to allow best correlation of results with those obtained with conventional bulk single-crystal Si cells that were always processed along with the Si sheet samples to serve as controls.

The Si sheet samples received by OCLI were first routinely checked for surface characteristics, thickness, conductivity type, and resistivity by standard methods. In some cases a preferential etch was applied to delineate individual crystallites in selected areas; various surface treatments were used, if necessary, to prepare the sample for p-n junction formation.

A junction was then formed by diffusion of phosphorus into the p-type sheet material.* The temperature and time used for the diffusion (which employed a $POCl_3$ source) were modified slightly from time to time, depending upon the samples being processed, but were usually adjusted to produce junctions 0.3-0.6μm deep into the p-type sheet material. Diffusion oxides were then removed and open-structure ohmic contacts were applied, using conventional deposition methods. The junctions were then isolated to reduce edge-leakage, and in a few cases antireflection coatings were applied to permit more accurate measurement of photovoltaic conversion efficiency; usually, however, the antireflection coatings were omitted.

With illumination from a defined light source, such as the AM0 or the AM1 spectrum from a solar simulator, the conventional photovoltaic parameters I_{sc}, V_{oc}, P_{max}, CFF, and power conversion efficiency were determined. The diffusion lengths of minority carriers in the completed cell structures were estimated or determined, when possible, by a photovoltaic method using a monochromatic light source. For samples in which the uniformity of photoresponse was of special interest (for example, to examine effects of grain boundaries) a photocurrent scan of the surface of the sheet could be made using a small-diameter light spot to compare the output of various regions of the sample.

In most instances an array of small-diameter mesa diodes was formed on the junction structures by etching techniques. The diodes were evaluated separately to indicate the degree of homogeneity in the sample and to correlate the electrical properties with any visible structural features (e.g., grain boundaries). Diode measurements included the photovoltaic parameters I_{sc} and V_{oc} and dark and light forward diode characteristics. Other measurements were made as required, depending upon the particular samples involved.

Any significant departures from these standard procedures that were used on any particular group of samples are identified in the subsequent descriptions.

Reports of all data and related observations concerning the sheet samples were supplied to Rockwell by OCLI. Technical consultation on the correla-

---

*For reasons discussed earlier, the polycrystalline Si sheet material used for the base region of experimental junction-type solar cells in this program was always prepared to be p type, with the front (incident-light) region being made n type by subsequent processing.

tions between observed sheet properties and the details of the CVD sheet growth process occurred regularly as part of the working arrangement.

2.4.2 Cell Structures Fabricated and Characterized in First Nine Months of Program

Eight samples were prepared and submitted to OCLI during the first quarter of the program. These eight samples, with the pertinent deposition parameters and film properties, are listed in Table 2-17. All samples were undoped.

Three of the first four Si films were deposited on single-crystal $(01\bar{1}2)$-oriented sapphire substrates that were 500μm thick. The fourth film was deposited on a multi-crystalline sapphire substrate containing numerous large and elongated individual grains, with some of the grain-boundary intersections with the polished surface being nearly parallel. No attempt was made to establish the crystallographic orientations of the individual grains, although the 525μm-thick wafer was cut with a nominal $(01\bar{1}2)$ orientation. This substrate provided a Si film with numerous relatively large single-crystal regions and numerous grain boundaries, to present a film of intermediate difficulty for the standard solar cell processing to be undertaken by OCLI. The first four samples prepared and sent to OCLI were deliberately selected to represent a wide variety of film characteristics, so that the nature of some of the problems to be encountered in processing subsequent samples could be ascertained early in the program.

The fifth sample was another undoped epitaxial Si film grown on $(01\bar{1}2)$-oriented sapphire in H_2 at ~1025°C. This sample was intended for double diffusion processing to produce a photovoltaic junction. The other three samples consisted of sizeable pieces of thick Si films grown on ASM805 alumina substrates in H_2 at ~1025°C at two different growth rates, to thicknesses of about 20 and 40μm.

Results obtained on the first four samples during the first quarter were not encouraging. Considerable difficulty was encountered in processing the samples at OCLI because they were quite thin (~3μm, except for OCLI-4) and were undoped. Both OCLI-3 and -4 were found to be slightly n-type, whereas OCLI-1 and -2 had such high resistivity that they did not permit conductivity-type detection even with a very sensitive probe. On the strength of that evidence, however, all four samples were B-diffused (1050°C for 15 min) to attempt to form a p-n junction in the base material. Mesas were formed by etching, but no evidence of any rectification or photovoltage was found in the first evaluation.

The first four samples had been heavily stained as a result of the B diffusion (extensive cleaning did not remove the stains). However, two sets of small mesas (~0.02 cm^2) were etched into the surfaces of all four samples, in two separate procedures using different etch rates in order to control properly the amount of material removed. Again no photovoltage was observed under illumination, with mechanical-contact probes on the mesa tops and on the remaining Si between mesas. A very high effective resistance (~1 megohm) was observed for the mesa structures.

Table 2-17. CVD Si Sheet Samples* Submitted to OCLI during First Quarter for Solar Cell Processing

SAMPLE NO.	SUBSTRATE AND THICKNESS (μm)	OBSERVED DEPOS. TEMP. (°C)	CARRIER GAS AND FLOW RATE (ℓpm)	SiH_4 FLOW RATE (ccpm)	FILM THICKNESS (μm)	AVERAGE GROWTH RATE (μm/min)	SAMPLE DIMENSIONS (cm) AND APPROX AREA (cm^2)	FILM STRUCTURE AND/OR SURFACE TEXTURE
OCLI-1	(01$\bar{1}$2) Aℓ_2O_3† 500	605	H_2 4	10	3.5	~0.02	r≈1.9** (3.6)	Poly; Random Orientation
OCLI-2	(01$\bar{1}$2) Aℓ_2O_3† 500	860	H_2 4	10	2.6	~0.5	r≈1.9** (3.0)	Poly; Preferred {110} Oriented
OCLI-3	(01$\bar{1}$2) Aℓ_2O_3† 500	1032	H_2 4	5	3.0	~2.0	r≈1.9** (2.5)	Epitaxial
OCLI-4	Multicrystalline Aℓ_2O_3† 525	1025	H_2 4	10	8.6	~1.7	2.2 x 1.9 (oval) (3.3)	Epitaxial in Separate Grains
OCLI-5	(01$\bar{1}$2) Aℓ_2O_3† 500	1030	H_2 4	5	10	~2.0	r≈1.8** (2.5)	Epitaxial
OCLI-6	ASM805 Alumina ~ 640	1025	H_2 4	25	20	~3.3	1.5 x 2.0 (3.0)	Poly: Preferred {110} Oriented
OCLI-7	ASM805 Alumina ~ 640	1021	H_2 4	10	24	~1.6	1.4 x 1.9 (2.7)	Poly: Preferred {110} Oriented
OCLI-8	ASM805 Alumina ~640	1030	H_2 4	25	40	~3.3	1.8 x 1.6 (2.9)	Poly; Preferred {110} Oriented

* All Si films undoped.

† These substrates not subjected to high-temperature H_2 etch before deposition.

** These samples approximately 90 deg sector of circle of radius r cm.

Regions of the diffused layers left protected in forming the first two sets of small mesas were then etched to form relatively large-area mesas (~0.8 cm^2), and contacts were vacuum-deposited on the mesas and the exposed bottom region of the Si layer. Again no photovoltage was observed on probing the mesas under illumination.

It was concluded that the undoped nature of these thin layers had precluded successful formation of a single-diffusion junction that would exhibit a photovoltage. The effective diffusion rates of the common dopants (B and P) in Si having the varied structural properties represented in this set of samples was not known at the time; some experimentation was required to establish such information. A separate film-doping step should probably have been undertaken (using P) before the B diffusion for junction formation was carried out, to achieve a fairly uniform low doping level throughout the layer.

Results on the other four samples (OCLI-5,6,7 and 8) indicated that a photovoltaic effect was observed. Sample OCLI-5 as received by OCLI tested p-type by thermal probing, so a shallow n^+ layer was formed by P diffusion at 875°C for 20 min. Small mesas were formed on part of the diffused surface by masking and etching. Under moderately intense illumination from a tungsten lamp, and with mechanical-contact probes on the mesas and the lower region of the deposited layer, a photovoltage of ~200mV was obtained with a low photocurrent. Using a contactless rf method to measure the effective resistivity, a value of sheet resistance of ~100,000 ohms per square was obtained for this device.

Larger mesas were then formed on the remaining n^+ diffused layer, and vacuum-deposited Aℓ contacts were applied to the mesa tops and the exposed base-region (p-type)Si. Under tungsten-lamp illumination, with the diode reverse-biased to permit determination of the photocurrent, a current density of ~1.5 mA/cm^2 and a photovoltage of ~230mV were measured. It was estimated that a much-reduced internal resistance might permit a curve fill factor of ~0.5 and a conversion efficiency the order of 0.2 percent (determined by direct comparison with a conventional single-crystal cell) for a cell of the type fabricated in this first group.

These first attempts to apply standard solar cell processing methods to CVD Si films indicated at the time that it might indeed become nessary to develop and/or apply other specialized methods - for example, junction growth by CVD or ion implantation doping instead of, or in addition to, diffusion doping for junction formation - to these polycrystalline films in order to get adequate indication of their ultimate suitability for solar cell fabrication. However, as indicated earlier, standard diffusion processing continued to be used for most of the program while attempts were being made to achieve polycrystalline Si sheet material having improved properties.

Another six samples of CVD Si sheet were submitted to OCLI during the second quarter. These samples are listed in Table 2-18, along with their deposition parameters and other pertinent properties. All of the Si films were B-doped,

Table 2-18. B-doped CVD Si Sheet Samples Submitted to OCLI during Second Quarter for Solar Cell Processing and Measurement

SAMPLE NO.	SUBSTRATE MATERIAL AND THICKNESS (μm)	DEPOS. TEMP (°C)	CARRIER GAS AND FLOW RATE (ℓpm)	SiH_4 FLOW RATE (ccpm)	DOPANT GAS* FLOW RATE (ccpm)	FILM THICK-NESS (μm)	AVE. GROWTH RATE (μm/min)	FILM RESIS-TIVITY (ohm-cm)	HOLE CONCEN-TRATION (cm^{-3})	HALL MOBILITY (cm^2/V-sec)	SAMPLE DIMENSIONS (cm) AND APPROX AREA (cm^2)	FILM STRUCTURE AND/OR SURFACE TEXTURE
OCLI-9	$(01\bar{1}2)$ Al_2O_3 375	1022	H_2 4	10	0.91	18	1.8	0.26†	1.3×10^{17}†	187†	1.0 x 1.1 1.1	Epitaxial
OCLI-10	$(01\bar{1}2)$ Al_2O_3 300	1025	H_2 4	10	9.1	18	1.8	0.070†	6.1×10^{17}†	145†	1.15 x 1.0 1.15	Epitaxial
OCLI-11	$(01\bar{1}2)$ Al_2O_3 300	1023	H_2 4	10	9.1	20	1.9	0.063†	6.8×10^{17}†	146†	1.0 x 0.9 0.9	Epitaxial
OCLI-12	$(01\bar{1}2)$ Al_2O_3 300	1025	H_2 4	10	9.1	19	1.9	0.052†	9.5×10^{17}†	125†	1.0 x 0.95 0.95	Epitaxial
OCLI-13	MRC Superstrate alumina (as fired) 700	1025	H_2 4	10	9.1	20	2.0	0.76**	5.0×10^{17}**	16**	1.3 x 1.2 1.6	Poly; preferred {110} oriented
OCLI-14	MRC Superstrate alumina (polished) 675	1025	H_2 4	10	9.1	20	2.0	0.86**	4.8×10^{17}**	15**	1.4 x 1.4 2.0	Poly; preferred {110} oriented

*Films B-doped from B_2H_6-in-He (46 ppm)
†Measured by Hall bridge method
**Measured by van der Pauw method

with measured active carrier concentrations in the range from 10^{17} to 10^{18} cm^{-3}. Four of the samples were CVD films on single-crystal $(01\bar{1}2)$-oriented sapphire substrates and thus were epitaxial; Hall mobilities for these films were in the range from 125 to 187 cm^2/V-sec. The other two samples were polycrystalline CVD films grown on polycrystalline alumina (MRC Superstrate) substrates - one in the as-fired condition and one polished at Rockwell prior to its use as a substrate. The films on these two samples both exhibited strong {110} preferred orientation. All six films were in the thickness range 10 to 20μm, and all film surfaces were in the as-grown condition, i.e., neither polished nor etched.

Because all of the samples of this group were p-type, with measured carrier concentrations in a range acceptable for base region material for Si solar cells, a standard P diffusion was carried out to form the p-n junctions. This used a $POCl_3$ source, as usual, and was done at 900°C for 10 min. P-type 1 ohm-cm control slices of single-crystal Si were included in the processing. After diffusion the diffusion glass was removed, and all samples then were found to be n type by thermal probe testing.

By means of suitable masking, a large mesa was etched in each sample (1:10 $HF:HNO_3$ for 30 sec), with 6 to 8μm of Si being removed around the mesas. With moderate-intensity tungsten-lamp illumination (~100 mw/cm^2) and only mechanical-probe contacts preliminary V_{oc} readings were obtained, after which V_{oc} was also obtained for two of the Si sheet cells and the control cell in the AMO simulator (with no attempt to control sample temperature). The open-circuit photovoltages obtained in these two preliminary measurements are shown in the first two rows of Table 2-19, which gives the values for V_{oc}, I_{sc}, curve fill factor (CFF), and L_e (diffusion length of minority carriers - electrons - in the p-type base region of the cell) for these six experimental cell structures after successive steps in processing and reprocessing.

Simple stripe or U-shaped Ti-Ag contacts were then applied to the mesa tops and to the exposed base Si and the responses were obtained in the AMO simulator, again without temperature control. The results are given in the third, fourth, and fifth rows of Table 2-19. Since it appeared that the contacts were not properly adherent they were removed and reapplied. The responses to the moderate tungsten-lamp illumination obtained with the new contacts are given in rows 6 and 7 of the table; no real improvement was observed. Since all of the Si sheet samples exhibited high dark reverse-leakage currents the mesas were all re-masked and re-etched; again no improvement was observed.

Because of the poor curve shapes obtained (CFF, row 5), the samples were heat-treated at 550°C for 5 min to attempt to reduce contact series resistances by sintering. Again the responses were measured, with the results given in rows 8-13, inclusive, in Table 2-19. On the basis of the known minority carrier diffusion length (~100μm) in the control sample and the photocurrent responses given in the table, estimates of the approximate diffusion lengths in the Si sheet samples were made, and these are listed in row 14 of Table 2-19.

Table 2-19. Photovoltaic Properties of Solar Cell Structures** in Si Sheet Samples OCLI-9, 10, 11, 12, 13, and 14 after Various Processing Steps

MEASUREMENT/PROPERTY	SAMPLE							REMARKS
	Control† (1 ohm-cm s.c. Si)	OCLI-9	OCLI-10	OCLI-11	OCLI-12	OCLI-13	OCLI-14	
1. V_{oc} (mV) (~100 mw/cm^2 W Lamp)	490	283	355	347	278	48	43	Mechanical probe contacts
2. V_{oc} (mV) (AMO Solar Simulator)	535	NM*	440	NM*	NM*	80	NM*	Mechanical probe contacts; no temp. control
3. V_{oc} (mV) (AMO Solar Simulator)	560	290	415	340	270	43	40	Ti-Ag contacts; no temp. control; contacts evidently poorly bonded
4. I_{sc} (ma)	11.8	0.87	3.85	0.8	2.6	0.4	0.34	
5. CFF	–	Concave	0.30	Concave	0.25	0.25	0.25	
6. V_{oc} (mV) (~100 mw/cm^2 W Lamp)	523	260	342	175	119	26	23	New contacts
7. I_{sc} (ma)	6.2	0.23	0.56	0.28	0.36	0.022	0.020	
8. V_{oc} (mV) (~100 mw/cm^2 W Lamp)	525	280	230	110	78	32	25	After annealing at 550°C for 5 min.
9. I_{sc} (ma)	6.6	1.04	0.67	0.60	0.56	0.79	0.86	
10. V_{oc} (mV) (~130 mw/cm^2 W Lamp)	570	345	360	236	125	82	77	As above
11. I_{sc} (ma)	21.6	6.9	3.7	3.9	3.9	5.8	3.4	
12. V_{oc} (mV) (AM1 Solar Simulator)	525	325	340	230	NM*	62	65	As above
13. I_{sc} (ma)	23	2.9	1.6	2.0	NM*	0.8	0.75	
14. L_e (μm)	100	~2	~1	~1	~1	~2	~1	Estimates based on control sample and photocurrent responses

** None of the structures was anti-reflection coated.
† Nominal efficiency 10 percent
* NM = Not measured

Sample OCLI-10 had the best curve shape (CFF) of the sheet samples in this group, although it was obviously not good on an absolute scale. The estimated AM0 efficiency for this cell was ~0.5 percent; this would increase to ~0.65 percent if an AR coating were applied. (None of the samples of this group was AR-coated, however.) Additional attempts to reprocess samples OCLI-9 and 14 - including complete removal of the contacts and the diffused layers on the mesa, and rediffusion and recontacting - were ineffective in producing any improvement in performance. Sample OCLI-12, which had exhibited very poor performance, was found by bevel-and-stain techniques to have a junction depth of ~0.4μm, so its poor performance was due to other factors.

The variation in V_{oc} in the Si sheet cells on sapphire (samples OCLI-9, 10, 11, 12) can perhaps be correlated with the variation in the base material doping concentration (see Table 2-18). The greatly reduced V_{oc} values for the small-grained polycrystalline cells (OCLI-13 and -14) on MRC Superstrate alumina substrates are probably related to factors such as the high reverse saturation current density in junctions formed in polycrystalline material, not an unexpected result.

During the third quarter of the program ten more of the samples prepared in Si CVD experiments were delivered to OCLI for processing and evaluation. These are listed in Table 2-20, with their deposition parameters and relevant properties. Six of them (OCLI-18-23, inclusive) were doped epitaxial samples on single-crystal sapphire, to provide Si sheet solar cell structures that would exhibit photovoltaic performance that would represent an upper limit that could be expected from any similarly processed polycrystalline Si sheet material on low-cost substrates. The other four samples consisted of three B-doped and one undoped polycrystalline Si films grown on polycrystalline alumina substrates; two of them were deposited on polished MRC Superstrate and two on as-fired ASM805 (3M Co.). It was expected that the significantly larger samples in this group would facilitate handling and processing at OCLI and generally provide more information of value to the program. The undoped sample (OCLI-15) was not processed into a solar cell, based on the difficulties encountered with such samples earlier in the program.

Samples OCLI-18 and 19 were processed first, along with the usual high-lifetime single-crystal Si control sample. Both sheet samples were etched lightly (1:6:10 $HF:HNO_3:CH_3COOH$, for 20 sec) before processing, to remove any shallow defective layer and/or surface contamination. They were then P-diffused at 900°C for 14 min, using a $POCl_3$ source. The resulting glass was removed after diffusion by immersion in HF; the samples were found then to be n type by probe test.

Etch-resistant tape was then used to permit etching a large digitated mesa covering about half the area of each sample; about 5μm of Si was removed by the etching (1:10 $HF:HNO_3$ for 25 sec), resulting in p-type material in all regions among the mesa fingers. The samples were then cleaned, and Ti-Ag was deposited by vacuum deposition over the total sample area; no post-

Table 2-20. B-doped CVD Si Sheet Samples Submitted to OCLI during Third Quarter for Solar Cell Processing and Measurement

SAMPLE NO.	SUBSTRATE MATERIAL AND THICKNESS (μm)	DEPOS TEMP (^{o}C)	CARRIER GAS AND FLOW RATE (lpm)	SiH_4 FLOW RATE (ccpm)	DOPANT GAS* FLOW RATE (ccpm)	FILM THICK-NESS (μm)	AVE. GROWTH RATE (μm/min)	FILM RESIS-TIVITY (ohm-cm)	HOLE CONCEN-TRATION (cm^{-3})	HALL MOBILITY (cm^2/V-sec)	SAMPLE DIMENSIONS (cm) AND APPROX AREA (cm^2)	FILM STRUCTURE AND/OR SURFACE TEXTURE
OCLI-15	MRC Superstrate alumina (polished) 700	1031	H_2 4	10	None	33	1.6	2.8×10^{5} **	5.5×10^{11}**	41**	1.2x1.1 1.3	Poly: preferred {110} oriented
OCLI-16	3M ASM805 alumina (as fired) 700	1022	H_2 4	25	75	25	3.1	0.04†	3.2×10^{18}†	47†	1.8x1.7 3.1	Poly; preferred {110} oriented
OCLI-17	3M ASM805 alumina (as fired) 625	1025	H_2 4	25	10	25	3.2	0.5†	5.8×10^{17}†	22†	1.7x1.7 2.9	Poly; preferred {110} oriented
OCLI-18	$(01\bar{1}2)A\ell_2O_3$ 575	1023	H_2 4	25	10	25	3.2	0.08**	6.6×10^{17}**	114**	3.1x2.4 7.4	Epitaxial
OCLI-19	$(01\bar{1}2)A\ell_2O_3$ 500	1022	H_2 4	25	5	26	3.2	0.1**	5×10^{17}**	125**	2.5x2.2 5.5	Epitaxial
OCLI-20	$(01\bar{1}2)A\ell_2O_3$ 550	1024	H_2 4	25	10	20††	2.5	NM***	$\sim10^{17}$††	NM***	2.3x2.0 4.6	Epitaxial
OCLI-21	$(01\bar{1}2)A\ell_2O_3$ 550	1027	H_2 4	25	10	20††	2.5	NM***	$\sim10^{17}$††	NM***	3.4x1.1 3.7	Epitaxial
OCLI-22	$(01\bar{1}2)A\ell_2O_3$ 500	1030	H_2 4	25	10	20††	2.5	NM***	$\sim10^{17}$††	NM***	2.5x1.7 4.2	Epitaxial
OCLI-23	$(01\bar{1}2)A\ell_2O_3$ 375	1024	H_2 4	25	10	20††	2.5	NM***	$\sim10^{17}$††	NM***	1.5x1.0 1.5	Epitaxial
OCLI-24	MRC Superstrate alumina (polished) 700	1030	H_2 4	25	1.96	20††	2.5	NM***	$>10^{16}$††	NM***	1.5x0.9 1.3	Poly; preferred {110} oriented

*Films B-doped from B_2H_6-in-He (46 ppm)

†Measured by Hall bridge method

**Measured by van der Pauw method

††Estimate from CVD parameters

***NM = Not measured

deposition heat treatment was used. Wax masking was used to remove the metal from the edges of the mesas, leaving two interdigitated contact areas - one for the mesa top and one for the p-type Si in the base region, as shown in the diagram of Figure 2-90a. No AR coating was applied at that stage of the processing to any of the samples, one of which is shown in the photograph in Figure 2-90b.

The two epitaxial sheet samples and the single-crystal control sample (Control No. 1) were then tested in the AM0 solar simulator. Results of these measurements are given in rows 1 through 5 in Table 2-21. The open-circuit photovoltages of the two Si sheet cells compared reasonably well with that of the control sample, but the short-circuit current densities and the maximum power per unit area delivered to the load were quite low for the sheet cells relative to the single-crystal control cell.

It is interesting to note, however, that the curve fill-factor was very low and about equal for all three cells. The fact that the Ti-Ag contacts were not heat-treated for any one of the three cells was probably the main cause of this. The power conversion efficiency is seen to be low for both of the Si sheet cells, but it was also quite low for the control cell. This indicates that the front-contact arrangement was far from satisfactory for the control cell and that there may have been other aspects of the processing that could have been modified to obtain improved cell performance in the sheet samples as well as the single-crystal control material. It should again be emphasized that the control cells were deliberately subjected to the same processing as that experienced by the sheet samples, to provide the best comparison basis.

Measurements were also made of the photocurrent density under illumination by the AM0 simulator tungsten lamp alone and the simulator xenon lamp alone; these results are given in rows 6 and 7 of the table. The results show that the response at longer wavelengths (tungsten lamp, $\lambda > 0.6\mu m$) in the sheet cells was especially poor; that at shorter wavelengths was relatively better, as would be expected.

The three samples were then exposed to monochromatic illumination ($\lambda \approx 0.92\mu m$) from an LED, with the junction back-biased in order to get a measure of the generated photocurrent due to the illumination over the arbitrary area of the light spot used. The results so obtained are entered in row 8 of Table 2-21. On the basis of an assumed minority carrier diffusion length of ~100μm in the single-crystal control sample, the diffusion lengths in the two sheet samples appeared to be about 3μm, as shown in row 9 of the table. This result was verified for numerous locations over the surface of each of the sheet cells, indicating uniformity of this characteristic.

The two sheet samples were then coated with SiO to reduce reflection losses, and the performance in the AM0 solar simulator was again determined. The results are given in rows 10 through 14 of Table 2-21. The improved performance of both cells is striking; in particular, the improved curve fill-factor of OCLI-18 and the increased power conversion efficiency of both cells tend to indicate that the proper modifications in contact design and overall processing could produce even further improvements in performance. However, the photocurrent generation indicated by the response to the tungsten lamp (row 15) still corresponds to a short diffusion length, as suggested above.

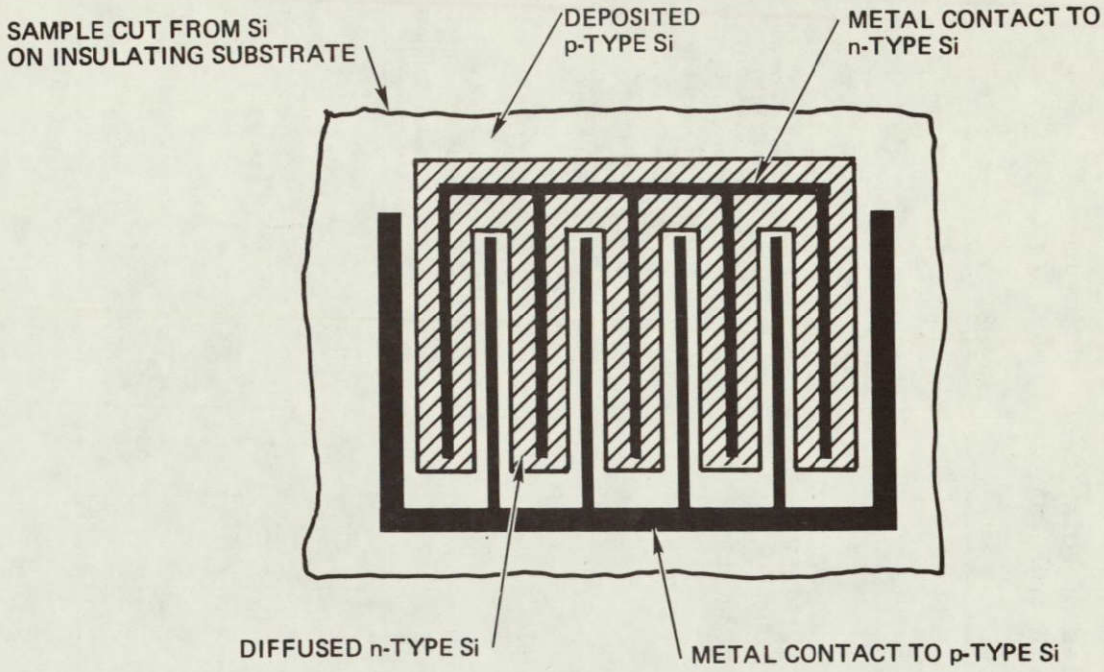

(a)

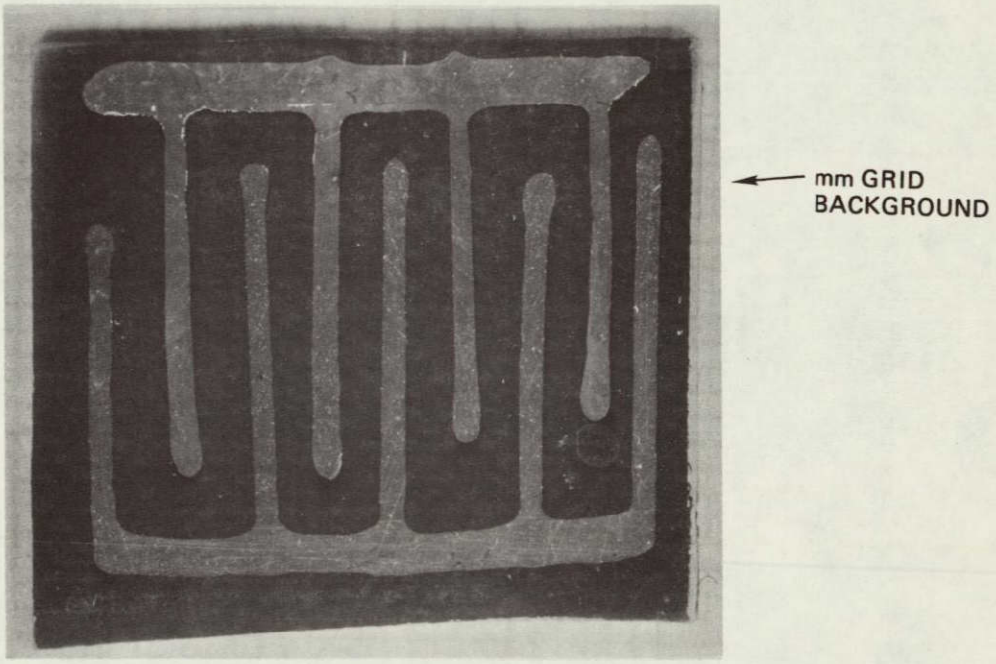

(b)

Figure 2-90. Interdigitated Solar Cell Structure Formed by Mesa Etching n/p Si Sheet Samples OCLI-16 through 24. a) Schematic of Structure, b) Photograph of Representative Sample, Showing Tape-defined Mesa Pattern.

Table 2-21. Measurements of Photovoltaic Properties of Solar Cell Structures in Si Sheet Samples OCLI-16 through 24*

MEASUREMENT/PROPERTY	SAMPLE												REMARKS
	Control No. 1 (2 ohm-cm s.c. Si)	OCLI-18	OCLI-19	Control No. 2 (2 ohm-cm s.c. Ci)	OCLI-17	OCLI-20	OCLI-21	Control No. 3 (2 ohm-cm s.c. Si)	OCLI-16	OCLI-22	OCLI-23	OCLI-24	
Active cell area (cm^2)	1.5	2.54	2.68	2.35	1.6	2.8	2.25	~0.4	~0.4	~0.4	~0.4	~0.4	
Uncoated samples													
1. V_{oc} (mV) (AMO Solar Simulator)	490	400	360	470	56	350	420	350	10	200	330	VL†	No control of sample temp; Ti-Ag contacts nor heat treated; I_{sc} partly limited by readout series resistance.
2. I_{sc} (mA/cm^2)	16	6.1	7.8	14.5	–	–	–	15.4	1	UR**	5.0	VL†	
3. Load power delivered (mw/cm^2)	2.25	0.82	0.81	1.55	–	–	–	UR**	–	UR**	UR**	VL†	
4. CFF	0.29	0.33	0.29	0.23	–	–	–	–	–	–	–	–	
5. Power conversion efficiency (%)	1.6	0.6	0.6	1.1	–	–	–	–	–	–	–	–	Based on 140 mw/cm^2 insolation
6. I_{sc} (mA/cm^2) (W Lamp alone)	12	2.4	3.0	12.1	–	–	–	UR**	–	UR**	UR**	VL†	Illumination mainly at $\lambda > 0.6\ \mu m$
7. I_{sc} (mA/cm^2) (Xe Lamp alone)	7.3	3.9	4.8	–	–	–	–	–	–	–	–	–	Illumination mainly at $\lambda < 0.6\ \mu m$
8. I_g (mA) (LED at $\lambda = 0.92\ \mu m$)	0.8	0.06	0.06	0.85	–	0.12	0.07	–	–	–	–	–	Junction back-biased; area is that of light spot.
9. L_e (μm)	100 (est)	~3	~3	~100 (est)	≤1	~4	~2	–	–	–	–		Estimates based on control sample and photocurrent responses.
Samples coated with SiO (AR coating)													
10. V_{oc}(mV) (AMO Solar Simulator)	–	415	450	–	70	445	–	–	290	–	–	–	As in rows 1–4.
11. I_{sc} (mA/cm^2)	–	8.3	12.2	–	0.69	3.12	8.62	–	–	7.5	–	–	
12. Load power delivered (mw/cm^2)	–	1.8	2.35	–	–	0.26	1.47	–	–	–	–	–	
13. CFF	–	0.52	0.43	–	–	0.23	0.38	–	–	–	–	–	
14. Power conversion efficiency (5)	–	1.3	1.7	–	–	0.2	1.1	–	–	–	–	–	As in row 5
15. I_{sc} (mA/cm^2) (W Lamp alone)	–	3.5	4.3	–	–	–	3.4	–	–	–	–	–	As in row 6

*Blank spaces: No measurement made

**UR = Uncertain reading – very low and unsteady

†VL = Very low reading – essentially zero

factor. The tungsten-lamp response of OCLI-21 after coating (row 15) again confirmed the long-wavelength response deficiency associated with short diffusion lengths in the Si film samples.

The remaining four Si sheet samples listed in Table 2-20 (OCLI-16,22,23,24) were also processed separately. OCLI-16 was a polycrystalline film on ASM805 as-fired alumina, OCLI-24 was a polycrystalline film on polished MRC Superstrate alumina, and OCLI-22 and 23 were epitaxial films on sapphire. These four samples were processed identically to the preceding group of three, except that separate n^+ islands (rather than connected n^+ islands as for OCLI-17, 20, and 21) were defined by acid-resistant tape masking and etching.

Results of limited measurements made on these four samples and the separate single-crystal control sample (Control No. 3) are also summarized in Table 2-21. Generally the same conclusions apply to these results as to those obtained for the other samples in this group, as discussed above.

On the basis of these measurements it appeared unlikely that Si sheet cell efficiencies better than about two percent could be expected, even if series resistance problems were solved so that curve fill factors would be better. The apparently low diffusion lengths (short lifetimes) seemed the most likely cause of this limitation. This problem is well known in Si-on-sapphire, and it should be noted that none of the recognized precautions for reducing the effects of lifetime killers in Si-on-sapphire - such as the use of a heavily doped adjoining getter layer (in this case a p^+ layer under the p-type grown layer) - was used in preparing the Si sheet samples discussed above.

However, as was indicated earlier (Section 2.3), some measurements by the C-V-t method on similar B-doped epitaxial Si films on sapphire, also without the gettering underlayer, had indicated lifetimes of about 10^{-7} sec, corresponding to calculated minority carrier diffusion lengths (using assumed carrier mobility values for the films in question) in excess of 10μm. This apparent discrepancy raised several questions about the basic properties of the films and about the effects of the OCLI solar cell processing on these basic properties.

That is, if the apparently short minority carrier diffusion lengths observed in the experimental solar cells described above were characteristic of the as-grown epitaxial films on sapphire, rather than induced in some way as a result of the device processing, then some corrective measures would have to be taken before the performance of these epitaxial cells could be considered to represent an upper limit on the performance of cells in the less perfect Si sheet material (on low-cost substrates). At the early stage in the program typified by the results given in Table 2-21, however, it seemed more likely that other shortcomings of the film properties or of the cell processing itself were responsible for the poor performance observed both in the epitaxial cells and in the polycrystalline cells fabricated up to that time in the program.

2.4.3 Cell Structures Fabricated and Characterized during Fourth and Fifth Quarters

In the fourth quarter 11 additional Si sheet samples grown by the CVD process were delivered to OCLI for processing and evaluation. These are listed in Table 2-22 with their deposition parameters and relevant properties. Included were two polycrystalline films on Corning Code 1715 glass, two polycrystalline films on Owens-Illinois GS211 glass, two polycrystalline films on Owens-Illinois GS213 glass, one polycrystalline film on Owens-Illinois GS186 glass, one polycrystalline film on as-manufactured MRC Superstrate polycrystalline alumina, and two double-layer samples (OCLI-34 and 35) on single-crystal sapphire substrates, each consisting of a relatively thick p-type layer of medium B doping concentration ($\sim 5 \times 10^{17}$ cm^{-3}) on a thin (4-7μm) p^+ layer ($\sim 10^{19}$ cm^{-3}).

The double-layer p/p^+ samples on sapphire were prepared with two different thicknesses of the p^+ film (4 and 6-7μm), to determine the effect of p^+ film thickness on carrier lifetime properties and subsequent solar cell properties. The results were to be used as a baseline reference for similar structures produced on lower-cost substrates and to help develop solar cell fabrication techniques for films grown on low-cost insulating substrates.

To avoid possible contamination of the sapphire by any neighboring substrates of other materials, the p/p^+ structures submitted to OCLI were produced in runs using only sapphire substrates. Preliminary determination of the conditions necessary to produce the desired p^+ and p doping levels with B was made by simultaneous growth on sapphire and high-resistivity Si, followed by measurement of electrical properties with a four-point probe. The p/p^+ structure was then formed on sapphire by consecutive Si film growths without removing the substrate from the reactor or exposing the sample in any way to the laboratory atmosphere between the two growths.

A spreading resistance probe scan was made on a small piece of the double layer CVD Si sample from which another piece was cut and sent to OCLI as sample OCLI-35 (see Table 2-22). The results of this scan, expressed both as resistivity and as carrier concentration as functions of depth into the composite film, are shown in Figure 2-91. The resistivity (and thus the calculated carrier density) is seen to be very uniform in the thicker upper layer; the calculated carrier concentration ($\sim 8 \times 10^{17}$ cm^{-3}) is somewhat higher than that estimated on the basis of deposition parameters (Table 2-22). In the heavily doped bottom layer the measured resistivity averages 0.002 ohm-cm, while the calculated carrier density is $5\text{-}6 \times 10^{19}$ cm^{-3} in this region. This doping concentration should have been more than adequate for affecting the minority carrier lifetime properties of the upper p-type region through gettering action of the acceptor centers, the purpose for which this particular composite structure was intended.

Seven of the samples listed in Table 2-22 (OCLI-25,26,28,29,32,33, and one half of OCLI-35) as well as two single-crystal 2 ohm-cm Si control blanks (No. A1 and No. A2) were processed as "batch A" into solar cells by the

Table 2-22. B-doped CVD Si Sheet Samples Submitted to OCLI during Fourth Quarter for Solar Cell Processing and Measurement

SAMPLE NO.	SUBSTRATE MATERIAL AND THICKNESS (μm)	OBSERV. DEPOS. TEMP. (^{o}C)	CARRIER GAS AND FLOW RATE (ℓpm)	SiH_4 FLOW RATE (ccpm)	DOPANT GAS* FLOW RATE (ccpm)	FILM THICKNESS (μm)	AVE. GROWTH RATE (μm/min)	FILM RESISTIVITY (ohm-cm)	HOLE CONCENTRATION (cm^{-3})	HALL MOBILITY (cm^2/V-sec)	SAMPLE DIMENSIONS (cm) AND APPROX. AREA (cm^2)	FILM STRUCTURE AND/OR SURFACE TEXTURE
OCLI-25	Corning Code 1715 glass 800	850	He 1.5	10	50	30	~0.6	8†	3.0×10^{17}†	2.6†	1.1x0.9 0.99	Poly; {100} preferred orientation
OCLI-26	Corning Code 1715 glass 800	865	He 1.5	10	500	~11	0.24	0.20**	2.6×10^{18}**	12**	1.5x1.0 1.5	Poly; {100} preferred orientation
OCLI-27	Owens-Illinois GS211 glass 1050	851	He 1.5	10	50	~19	0.38	0.37**	1.2×10^{18}**	14**	1.2x1.3 1.6	Poly; {100} preferred orientation
OCLI-28	Owens-Illinois GS213 glass 1025	858	He 1.5	10	500	~16	0.36	0.37**	1.6×10^{18}**	10**	1.2x1.2 1.4.	Poly; {100} preferred orientation
OCLI-29	Owens-Illinois GS213 glass 1025	856	He 1.5	10	50	29	0.32	6.3**	2.5×10^{16}**	40**	1.3x1.1 1.4	Poly; {100} preferred orientation
OCLI-30	Owens-Illinois GS186 glass 1025	839	He 1.5	10	50	38	0.42	14**	1.2×10^{17}**	3.8**	1.2x1.2 1.4	Poly; {100} preferred orientation
OCLI-31	Owens-Illinois GS211 glass 1050	861	He 1.5	10	300	27***	0.3***	0.5***	10^{18}***	10***	1.2x1.1 1.3	Poly; {100} preferred orientation
OCLI-32	(01$\bar{1}$2) $A\ell_2O_3$ (Polished) 750	1025	H_2 1.5	10	5	25	1.4	0.12***	6×10^{17}**	88**	1.2x0.8 0.96	Epitaxial
OCLI-33	MRC Superstrate Alumina (as mfd) 875	1025	H_2 1.5	10	5	25	1.4	2.3†	2.6×10^{17}†	11†	1.2x0.8 0.96	Poly; {110} preferred orientation
OCLI-34	(01$\bar{1}$2) $A\ell_2O_3$ (Polished) 750	1025	H_2 1.5	10	1) 300†† 2) 6††	1)4*** 2)17***	1)1.3*** 2)1.3***	1) 0.005*** 2)0.1***	1) 10^{19}*** 2)5×10^{17}***	1) 35*** 2) 90***	2.3x1.2 2.8	Epitaxial (both layers)
OCLI-35	(01$\bar{1}$2) $A\ell_2O_3$ (Polished) 750	1031	H_2 1.5	10	1) 295†† 2) 6††	1)6*** 2)21***	1)1.1*** 2)1.5***	1)0.005*** 2)0.1***	1)2×10^{19}*** 2)5×10^{17}***	1) 35*** 2) 90***	2.3x1.3 3.0	Epitaxial (both layers)

*Films B-doped from B_2H_6-in-He (46 ppm)

†Measured by Hall bridge method
**Measured by van der Pauw method
††Double layer: No. 1 deposited first, then No. 2
***Estimate, based on CVD parameters and other factors.

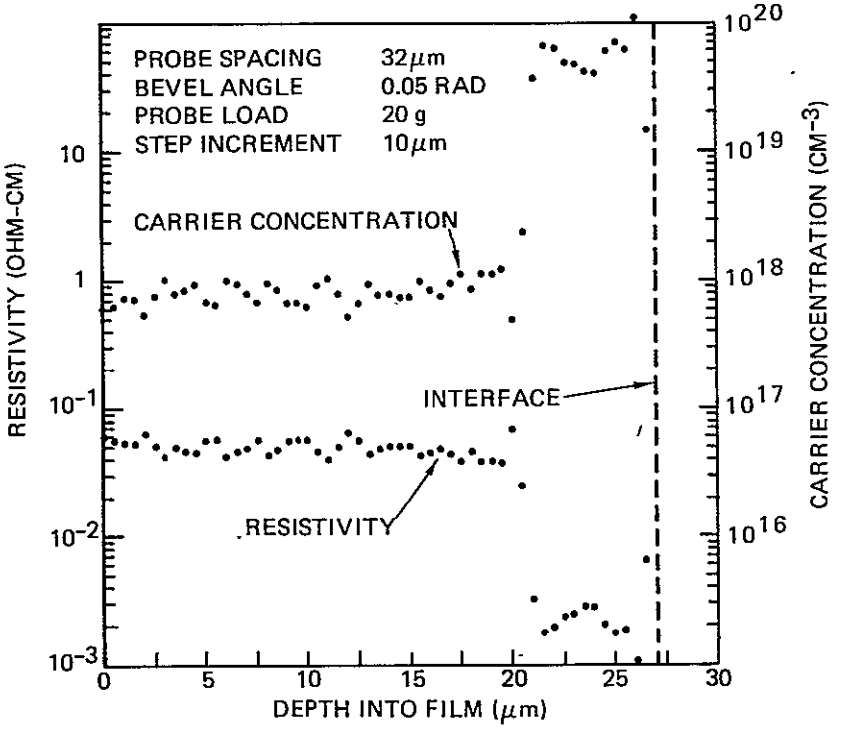

Figure 2-91. Spreading Resistance Probe Scan Showing Resistivity (and Calculated Carrier Concentration) as Function of Depth in Composite p/p^+ CVD Si Sample OCLI-35, Grown on Sapphire Substrate by SiH_4 Pyrolysis at 1031°C in H_2.

following procedure. All traces of previously applied metal contact pads or other surface debris were removed, followed by a standard degreasing (trichloroethane and N_2 blow-dry); no pre-diffusion surface etch was used. All samples were then P-diffused simultaneously at 840°C for 15 min, using a $POCl_3$ source. All surface glasses were removed after diffusion by immersion in a 1:10 $HF:H_2O$ etch for 30 sec, followed by a thorough wash and N_2 blow-dry. All samples probed n type at that stage.

A typical solar cell finger-type coarse-grid contact pattern of Ti-Ag was then deposited by vacuum evaporation through an aperture mask onto all samples. Etch-resistant tape was then used to cover a "picture-frame" around the edge of each sample. By means of wax masking, small areas about 1mm in diameter were defined within the frame, and mesas were then formed by etching in 1:10 $HF:HNO_3$ long enough to remove 4-5μm of the Si film in the exposed regions. Approximately half of the mesas were crossed by a contact stripe of the deposited grid pattern. The tape frame was then removed, the mesas were masked, and the frame region was etched for ~20 sec. The region among the mesas was probed to confirm that it was uniformly p type, as was

the contact frame. Ti-Ag was then vacuum-deposited onto the contact frame region, with the entire central mesa area masked. The Ti-Ag contacts were not sintered at this stage, however.

"Batch B," which included the remaining samples from the list in Table 2-22 and the other half of sample OCLI-35, plus two single-crystal Si control wafers (No. B1 and No. B2), was processed with only a slightly different procedure. Batch B samples were photoresist-masked and etched into rectangular 2mmx1mm mesas; mesa heights were ~5μm. The base-region contact for the batch B samples was a line contact along only one edge of the sample, rather than the full-frame contact used on the batch A samples. The contacts on three of the batch B samples (including one control sample) were sintered to determine if a significant change in measured properties resulted, but it did not. Figure 2-92 shows photographs of representative samples of batch A and batch B, showing the etched mesa-type solar cells in each case.

Measurements were made with several different kinds of illumination: 1) moderate intensity (approximately 1 sun) tungsten lamp; 2) high-intensity tungsten lamp; 3) LED, with ~0.9μm wavelength radiation; 4) tungsten lamp with filter wheel (for spectral response); 5) AM0 solar simulator, using both xenon and tungsten lamps; 6) xenon lamp of simulator; and 7) tungsten lamp of simulator. During illumination, mechanical probe contact was made to the mesa top and to the Ti-Ag ohmic base contact of the sample under test.

Open-circuit photovoltages V_{oc} were first obtained with the moderate-intensity (~1 sun) tungsten lamp. Results for both batches are summarized in Table 2-23; several mesa devices on each sample in batch A were measured, but only one device on each sample of batch B was measured. Only mesas free of the contact grid line were evaluated on the batch A samples.

These preliminary results indicated that fairly good uniformity of response from mesa to mesa on a given sample occurred for the samples of batch A, but that major differences in response were obtained from sample to sample in both batches, depending upon the properties of the CVD Si sheet material. In particular, the epitaxial sheet material on single-crystal sapphire substrates (OCLI-32 and 35-1) exhibited relatively high V_{oc} values, although not as high as the V_{oc} for the better of the two single-crystal Si control wafers. The polycrystalline samples showed much lower photovoltages, as might be expected. It appears that the more lightly doped films of the pairs of polycrystalline films on glasses exhibited better photovoltaic performance.

The measured mesas on the samples of batch B exhibited similar characteristics. The V_{oc} values for the epitaxial samples were 70-80 percent of those for the controls, while the polycrystalline samples had V_{oc} values the order of 10 percent of those of the controls.

Additional measurements were then made on both groups of samples using a high-intensity tungsten lamp, with an output roughly equivalent to 2 suns. The open-circuit voltage V_{oc} and the photogenerated increase in reverse current at -1V were measured under illumination, the latter taken as an indication of the short-circuit current I_{sc}. The results are given in Table 2-24 for three (sometimes two) different mesa devices on each sample in both groups.

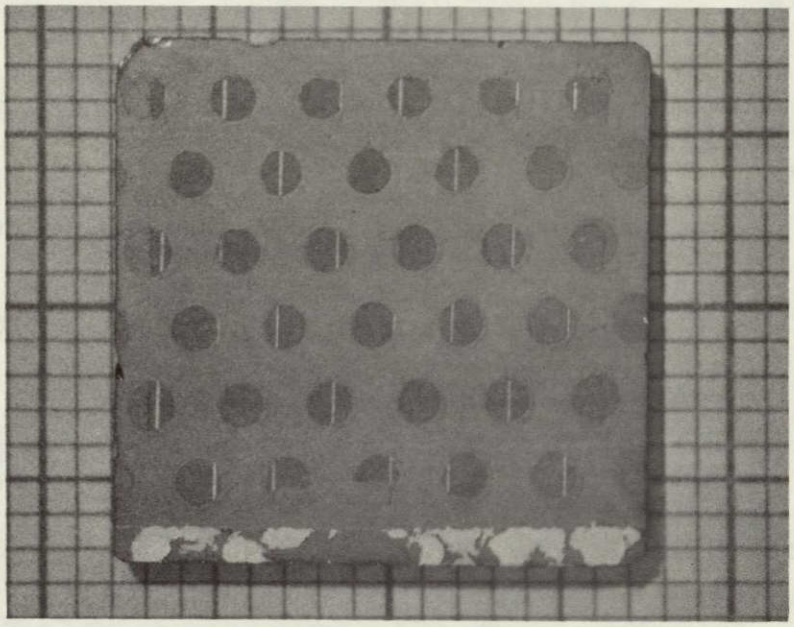

(a)

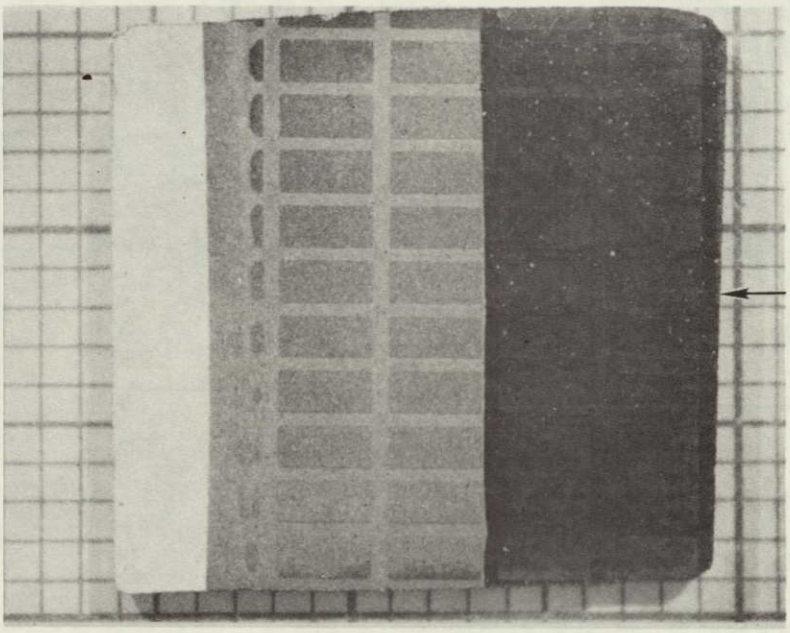

(b)

Figure 2-92. Etched Mesa-type Solar Cells in CVD Si Sheet Samples. (a) Batch A, Sample OCLI-28 (Polycrystalline Si on GS213 Glass); (b) Batch B, Sample OCLI-30 (Polycrystalline Si on GS186 Glass). Both Samples Shown on mm Grid Background.

Table 2-23. Photovoltage Response* of P-diffused n/p Mesa-type Solar Cells Fabricated in B-doped CVD Si Sheet Material on Various Substrates

SAMPLE				OPEN-CIRCUIT PHOTOVOLTAGE** V_{oc} (mV)					
Number	Substrate Material	Film Structure***	Carrier Concentr. (cm^{-3})						
Batch A									
OCLI-25	1715 glass	Poly.	3×10^{17}	145	126	114	106	99	71
OCLI-26	1715 glass	Poly.	3×10^{18}	12	7	5	4		
OCLI-28	GS213 glass	Poly.	2×10^{18}	30	29	27	21	16	14
OCLI-29	GS213 glass	Poly.	2×10^{16}	200	167	165	157	156	
OCLI-32	Sapphire	S.c.	6×10^{17}	330	310	307	304		
OCLI-33	Superstrate alumina (as fired)	Poly.	3×10^{17}	80	57	53	52		
OCLI-35-1	Sapphire	S.c.	$8 \times 10^{17}/5 \times 10^{19}$	475	446	442	429	426	
Control A1	S.c. Si †	–	$\sim 5 \times 10^{15}$		556	552	536	525	
Control A2	S.c. Si ††	–	$\sim 5 \times 10^{15}$		398	397	394	375	
Batch B									
OCLI-27	GS211 glass	Poly.	1×10^{18}		90				
OCLI-30	GS186 glass	Poly.	1×10^{17}		30				
OCLI-31	GS211 glass	Poly.	1×10^{18}		35				
OCLI-34	Sapphire	S.c.	$8 \times 10^{17}/2 \times 10^{19}$		400				
OCLI-35-2	Sapphire	S.c.	$8 \times 10^{17}/5 \times 10^{19}$		400				
Control B1	S.c. Si	–	$\sim 5 \times 10^{15}$		550				
Control B2	S.c. Si	–	$\sim 5 \times 10^{15}$		500				

*Moderate intensity (~1 sun) tungsten lamp source.
**Measured on one or more individual mesa devices, as indicated.
†Full backside contact
††"Picture-frame" front contact to base
***Poly = Polycrystalline; s.c. = single crystal

Short-circuit current densities J_{sc} were calculated in each case by using the nominal area of the individual mesas in batch A (7.0×10^{-3} cm^2) and in batch B (2.0×10^{-2} cm^2) without taking account of minor variations in actual area from mesa to mesa, differences in surface reflectivities for the various Si sheet materials, or shadowing by the measuring probe. The highest values of V_{oc} and J_{sc} for each sheet sample and for the control samples as a group are underlined in this table.

These results also illustrate the general uniformity of response among mesas on a given sample. The wide variation in V_{oc} values is evident, as in the preliminary V_{oc} measurements. Open-circuit voltages for the epitaxial films on sapphire, especially those with a p/p^+ deposited region, compared favorably with V_{oc} for the control wafers; the highest V_{oc} for an epitaxial film sample (OCLI-35-1) was 80 percent of the highest V_{oc} for a control sample, and exceeded considerably that of the poorest control sample (A2, Table 2-23) under comparable illumination conditions. V_{oc} values for the polycrystalline films were much lower, ranging from ~1 percent to ~45 percent of the V_{oc} for the poorest control sample, under comparable conditions. The V_{oc} values for some of the films on glass were significantly larger than that for the polycrystalline film on alumina (OCLI-33).

Photogenerated currents for the thin-film samples (including the epitaxial films on sapphire) were quite low, however. For comparable illumination (including some data not shown in these tables), generated short-circuit current densities for the cells in epitaxial films (irrespective of p/p^+ or single-layer-p base region) were from 13 to 23 percent of those in control cells. The cells in polycrystalline films on glasses produced current densities from ~3 to 29 percent of those in the control cells, while the cells in the polycrystalline film on alumina gave current densities ranging from 6 to 45 percent of those obtained with the control cells, under comparable illumination.

The best thin-film cells were those fabricated in an epitaxial film on sapphire, with a deposited p/p+ base region (OCLI-35-2). There was very good uniformity among the properties of individual mesas on most of the samples, but this sample was especially good in this respect. For 10 mesas measured at random under given illumination V_{oc} values averaged ~455mV, with a minimum of 430mV and a maximum of 475mV. The same 10 mesa devices produced an average generated short-circuit photocurrent of 184μA, with a minimum of 160μA and a maximum of 210μA.

The same consistency was demonstrated by forward and reverse I-V characteristics obtained for several mesa devices on the same sample. Figure 2-93 shows the I-V curves for OCLI-35-2 and Control B2, which were processed simultaneously in batch B. Figure 2-93a gives the dark and illuminated (tungsten lamp source) characteristics for four mesas on the single-crystal Si Control B2, and Figure 2-93b gives the corresponding characteristics for four mesas on OCLI-35-2, obtained under moderate-intensity (≥1 sun) illumination.

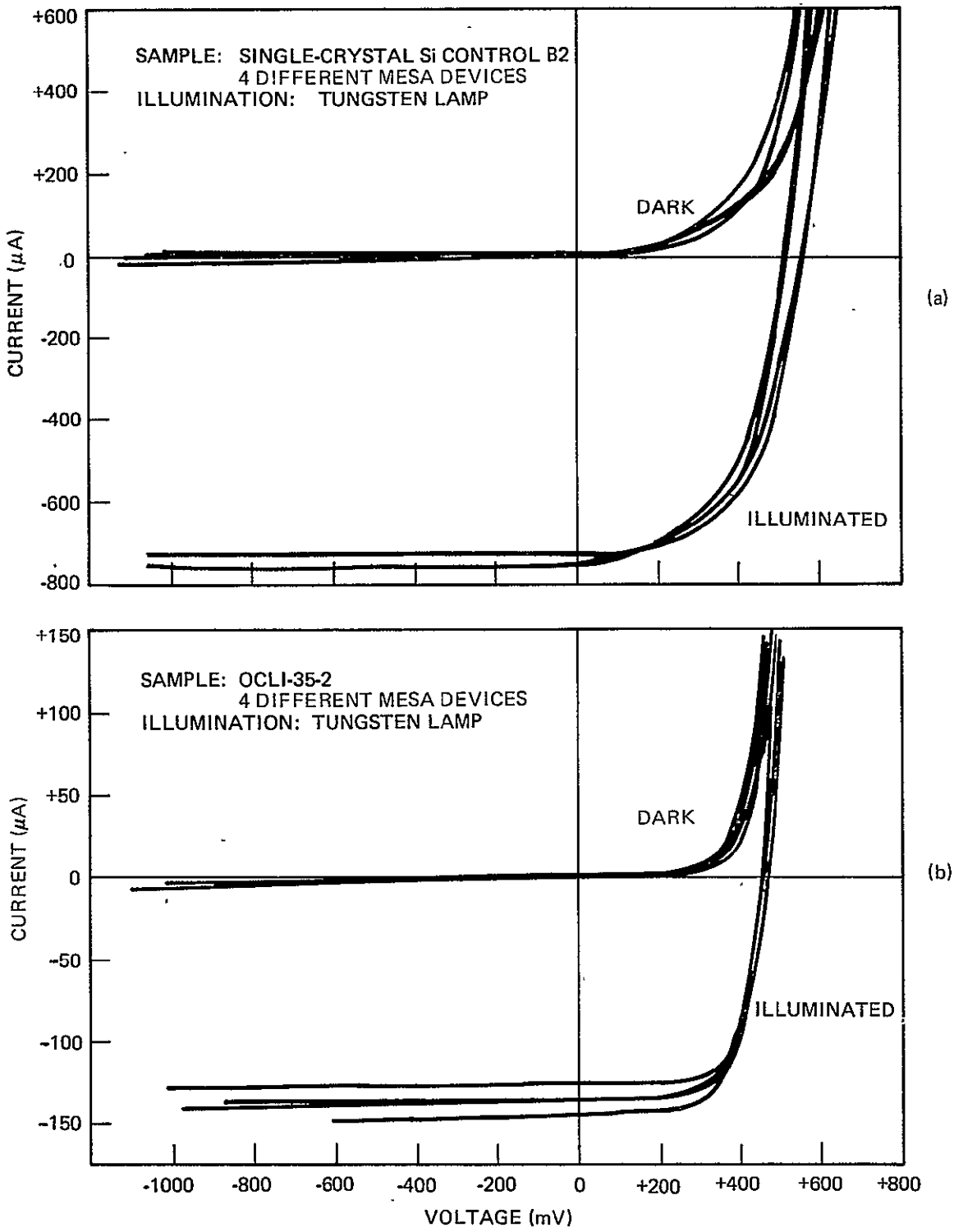

Figure 2-93. Dark and Light Forward and Reverse I-V Characteristics for 4 Separate Mesa Devices on Samples Processed Simultaneously in Batch B. a) Single-crystal Si Control Wafer B2, b) Si-on-sapphire Sample OCLI-35-2.

Photoresponse measurements were also made on most of the samples of this group using the 0.94μm wavelength radiation from a light-emitting diode (LED) as the illumination. Based on the assumption that the control samples had minority-carrier diffusion lengths L_n of ~100μm it was possible to deduce approximate values for L_n for the Si sheet samples. Values calculated in that manner are listed in Table 2-25; these have not been corrected for surface reflectivity effects or for variations in the LED intensity incident on the different mesas. The approximate values obtained, however, are indicative of the photovoltaic quality of the Si sheet samples relative to that of the single-crystal Si solar cell blanks. The epitaxial samples on sapphire (OCLI-32, 35-1, and 35-2) are seen to have L_n values from 3.5 to 4.3μm. The polycrystalline sheet samples on glasses have L_n values in the 0.5-5.5μm range, while the polycrystalline sample on as-fired MRC Superstrate alumina (OCLI-33) has L_n=5.5μm by this method.

Approximate spectral photoresponse measurements were made on samples OCLI-27, 30, and 35-2, as well as a control sample, using a tungsten lamp source with a filter wheel for illumination. The relative spectral response data are plotted in Figure 2-94 for two different mesa devices on each of the four samples. No corrections were made for reflectivity differences in presenting the data. The severe loss of long-wavelength response (i.e., for λ>0.7μm) for the three sheet samples is evident and is consistent with the low short-circuit photocurrent values obtained (Table 2-24) and the small values deduced for L_n (Table 2-25).

The relative spectral responses for these three samples at λ=0.8 and 0.9μm were used to calculate approximate values for L_n, again based on the assumed value of 100μm for the minority-carrier diffusion length in the control sample. These values are also given in Table 2-25 and are seen to be in close agreement with the approximate values for these three samples as deduced from the photoresponse measurements with the LED.

Finally, the same four samples were characterized using the AM0 solar simulator, which employs a xenon arc lamp for the short wavelength radiation and a tungsten lamp for the long wavelength portion of the simulated solar spectrum. The outputs of several mesa devices on each sample were measured. The fourth quadrant of the I-V characteristic under AM0 illumination for the best mesa device tested on each of the four samples is displayed in Figure 2-95. The curves for the control and for OCLI-35-2 have good shape. Those for polycrystalline sheet samples OCLI-27 (on GS211 glass) and OCLI-30 (on GS186 glass) are very poor, indicating severe carrier collection and/or junction shunting problems.

The measured values of V_{oc}, J_{sc}, and curve fill-factor (CFF) for the four samples, as taken from the I-V characteristics, are listed in Table 2-26. As indicated therein, the epitaxial sample (OCLI-35-2) has a larger CFF (0.66) than does the single-crystal control sample (0.60), consistent with the better loaded I-V characteristic displayed by the sheet sample (Figure 2-95). The CFF values for the polycrystalline sheet samples, on the other hand, are extremely low.

Table 2-25. Minority-carrier Diffusion Lengths L_n for P-diffused n/p Mesa-type Solar Cell Structures in B-doped CVD Si Sheet Material on Various Substrates

SAMPLE				MINORITY-CARRIER DIFFUSION LENGTH L_n (μm)		
Number	Substrate Material	Film Structure†	Carrier Concentr. (cm^{-3})	LED* ($\lambda = 0.94\,\mu m$)	Spectral Response** ($\lambda = 0.8\,\mu m$)	Spectral Response** ($\lambda = 0.9\,\mu m$)
Batch A						
OCLI-25	1715 glass	Poly.	3×10^{17}	4.5	–	–
OCLI-26	1715 glass	Poly.	3×10^{18}	0.5	–	–
OCLI-28	GS213 glass	Poly.	2×10^{18}	0.9	–	–
OCLI-29	GS213 glass	Poly.	2×10^{16}	5.5	–	–
OCLI-32	Sapphire	S.c.	6×10^{17}	4.3	–	–
OCLI-33	Superstrate alumina (as fired)	Poly.	3×10^{17}	5.5	–	–
OCLI-35-1	Sapphire	S.c.	$8 \times 10^{17}/5 \times 10^{19}$	3.5	–	–
Control A1	S.c. Si	–	$\sim 5 \times 10^{15}$	–	–	–
Control A2	S.c. Si	–	$\sim 5 \times 10^{15}$	100 (assumed)	–	–
Batch B						
OCLI-27	GS211 glass	Poly.	1×10^{18}	1.2	1.5	0.8
OCLI-30	GS186 glass	Poly.	1×10^{17}	1.1	0.4	0.3
OCLI-31	GS211 glass	Poly.	1×10^{18}	–	–	–
OCLI-34	Sapphire	S.c.	$8 \times 10^{17}/2 \times 10^{19}$	–	–	–
OCLI-35-2	Sapphire	S.c.	$8 \times 10^{17}/5 \times 10^{19}$	3.6	2.2	1.8
Control B1	S.c. Si	–	$\sim 5 \times 10^{15}$	–	–	–
Control B2	S.c. Si	–	$\sim 5 \times 10^{15}$	100 (assumed)	100 (assumed)	100 (assumed)

*L_n estimated from I_{sc} values for sheet samples relative to those for control samples for illumination by LED ($\lambda = 0.94\mu m$).

**L_n calculated from relative spectral responses at $\lambda = 0.8\mu m$ and $\lambda = 0.9\mu m$ for sheet samples relative to that for control sample, using tungsten lamp and filter wheel as illumination source. Si absorption coefficients used in calculation: $\alpha_{0.8\mu m} = 950\ cm^{-1}$ and $\alpha_{0.9\mu m} = 350\ cm^{-1}$.

†Poly = polycrystalline; s.c. = single crystal.

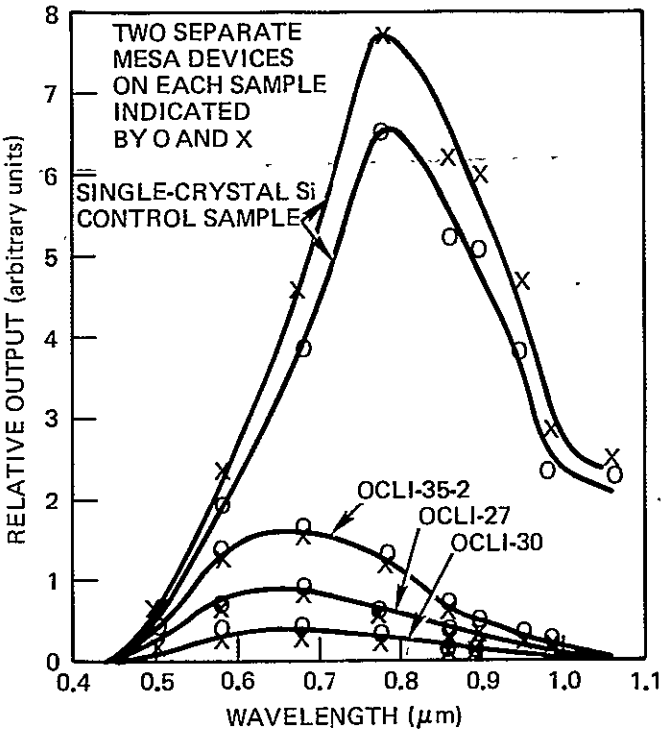

Figure 2-94. Relative Photovoltaic Spectral Response for 2 Separate Mesa Devices on Samples OCLI-35-2, OCLI-27, OCLI-30, and Single-crystal Si Control Cell.

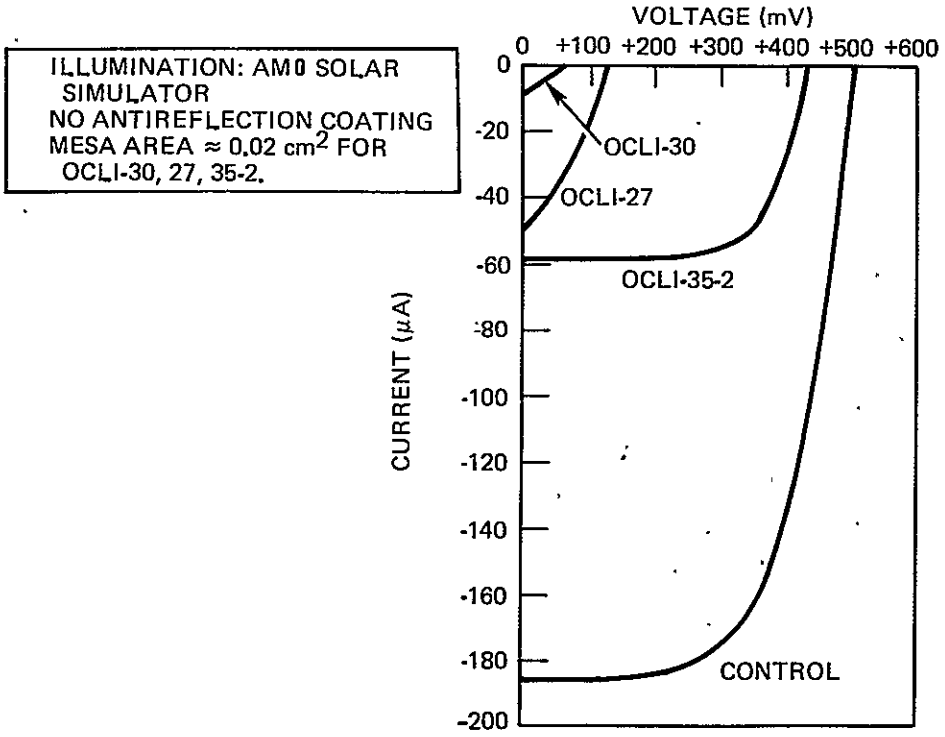

Figure 2-95. Fourth Quadrant of I-V Characteristic for Individual Mesa Devices on Samples OCLI-30, OCLI-27, OCLI-35-2, and Single-crystal Si Control, for AM0 Solar Simulator Illumination.

Table 2-26. Photovoltaic Properties for Individual Mesa Solar Cells* in Three CVD Si Sheet Samples and Single-crystal Si Control Sample, from I-V Characteristics of Figure 2-95 (AM0 Solar Simulator Illumination)

SAMPLE	V_{oc} (mV)	I_{sc} (μA)	P_{max} (μw)	CFF
OCLI-27	130	48.5	2.0	0.32
OCLI-30	65	8.8	0.16	0.28
OCLI-35-2	430	58.	16.4	0.66
Control	510	185.	57.0	0.60

*Mesa area approximately 0.02 cm^2, except control sample.

The power delivered to the load by the mesa devices on the epitaxial sample was about 30 percent of that delivered by the control sample under AM0 illumination; thus, if the control cell efficiency is assumed to be ~12 percent, the cells in the epitaxial sample had efficiencies of about 3.5 percent. The efficiencies in the two polycrystalline samples, on the same basis, were well below 1 percent.

These results indicated that improved photovoltaic performance was obtained when p/p^+, rather than just p, base regions were used in the CVD Si films. The low generated photocurrents, especially when examined as a function of wavelength, indicated poor diffusion lengths in the films. The high open-circuit voltages, on the other hand, were somewhat surprising in view of the poor current responses. The relatively large V_{oc} values obtained in several of the polycrystalline sheet samples on glass substrates indicated a fairly good p-n junction had been formed in this small-grain material. The data collected did not appear to indicate that high series resistance alone was responsible for the low measured photocurrents in the polycrystalline cells, but it seemed logical that a closer-spaced grid pattern that would contact more of the individual grains would improve the situation somewhat.

The results obtained with the experimental cells fabricated in the group of samples described above as well as in earlier groups had fallen short of expectations. With every group of Si sheet samples that had been processed there had also been control wafers of long-lifetime single-crystal Si of 2-3 ohm-cm resistivity processed simultaneously, to provide an indication of the general success of the processing sequence as well as a standard against which to compare the performance of the Si sheet devices. In some instances the photovoltaic performance of the devices in the control slices was also short of expectations, and appropriate allowances were thus made for the observed characteristics of the cells formed in the sheet material.

It thus continued to appear as if some general underlying problem, either in the fundamental properties of the Si sheet samples themselves or perhaps in the cell processing at OCLI, may have been causing the results in question.

To attempt to resolve the situation another group of samples, prepared during the fifth quarter of the program, was submitted to OCLI for solar cell fabrication. These samples were prepared on substrates of several glasses, single-crystal Si, and single-crystal sapphire, with a variety of B doping levels and both single-layer and double-layer (p/p^+) construction. The composite samples had three different ratios of thicknesses of the p and the p^+ regions. The deposition experiments were designed to provide a range of sample properties that might--when photovoltaic characteristics were obtained on the resulting devices--help to clarify some of the technical questions raised by the earlier results.

The specific sample structures prepared included the following: (1) uniformly doped p-type epitaxial Si films with carrier concentrations in the 10^{17}-10^{18} cm^{-3} range, on both p-type (100)-oriented single-crystal Si substrate wafers of solar cell quality (i.e., 2-3 ohm-cm resistivity and carrier diffusion lengths of ~100μm) and higher resistivity (≥10 ohm-cm) p-type (100)-oriented single-crystal Si wafers of good quality; (2) epitaxial double-layer p/p^+ Si sheet samples on sapphire substrates, with carrier concentrations in the 10^{18} and 10^{19} cm^{-3} ranges, respectively, and thickness ratios t_p/t_{p^+} of 1:3, 1:1, and 3:1 (to evaluate the effect of proximity of the p^+ region to the junction on the photovoltaic performance of the cells subsequently formed by diffusion); (3) similar double-layer p/p^+ structures on single-crystal Si wafers of the two types used in (1); and (4) uniformly doped p-type polycrystalline Si films with carrier concentrations in the 10^{17}-10^{18} cm^{-3} range on several different glasses.

Some difficulties were encountered in the first attempts to obtain good B-doped Si film growth on the p-type single-crystal Si substrate wafers (resistivity 2-3 ohm-cm) obtained from OCLI for these experiments. These wafers were (100)-oriented solar cell blanks (2 cm x 2 cm) that had been optically polished by standard procedures at OCLI. However, the first Si films deposited on these substrates were of very poor quality; it appeared that the substrate surfaces were not adequately cleaned for use in epitaxy. This was confirmed in several experiments in which clean uncontaminated Si films were grown simultaneously on companion substrates of (100)-oriented 10 ohm-cm p-type Si obtained from Rockwell supplies. Various cleaning procedures were used in attempting to produce an adequately clean surface on the solar cell blanks, but none was found to accomplish this. A second group of similar wafers was then obtained from OCLI, and those appeared to be relatively free of the persistent contaminant.* Epitaxial p-type films with measured carrier concentrations from

*Although not definitely established as the cause of the observed contaminant, it appeared that the individual plastic bags used for transfer of the first group of wafers to Rockwell were probably responsible for the cleaning problem.

10^{17} to $>5x10^{19}$ cm^{-3} were then successfully grown on substrates of both resistivities.

Because of the observed improvement in photovoltaic performance of earlier samples consisting of deposited p/p^+ composite films on sapphire substrates, several sets of such double-layer samples were prepared on Si substrates of both resistivities, as well as on sapphire. Since the extent of the influence of a p^+ gettering layer on the carrier lifetime (and thus diffusion length) in an adjoining p-type Si layer was not known quantitatively, these double layers were prepared with total thicknesses of 15-20μm and with the bottom (p^+) layer ~4μm, ~8μm, and ~12μm thick, placing the gettering layer respectively ~12μm, ~8μm, and ~4μm from the location of the p-n junction to be formed subsequently by diffusion of P into the p-type upper layer. Carrier concentrations in the p-type region were intended to be in the 10^{17}-10^{18} cm^{-3} range and those in the p^+ gettering layer were doped in excess of 10^{19} cm^{-3}. Evaluation of these composite structures after deposition, however, indicated that the doping level in the upper (p-type) region in many of the samples was higher than intended, i.e., greater than 10^{18} cm^{-3}.

The single-layer p-type Si sheet samples grown on substrates of single-crystal Si of two different resistivities at ~1025°C in H_2 (1.5 ℓpm) with a SiH_4 flow rate of ~10 ccpm were epitaxial, as expected. The problems encountered in cleaning the p-type 2 ohm-cm solar cell blanks prior to deposition, as mentioned above, resulted in some of the epitaxial layers having noticeable macroscopic as well as microscopic irregularities in surface characteristics and, presumably, in interior structural perfection.

The electrical properties of these single-layer samples were determined by van der Pauw measurements of the Hall effect and, in several instances, also by spreading resistance (SR) probe measurements. The latter method indicated somewhat (~50 percent) higher average resistivity values for a given film than was obtained by the van der Pauw method. Conversion of the SR resistivity values to carrier concentrations, using the standard correction for (100)-oriented bulk single-crystal Si, resulted in values less than those measured by the van der Pauw method by a factor of about 3. The SR scans through the thickness of the films indicated good uniformity of doping on both Si substrate materials, throughout the 10^{17}-10^{19} cm^{-3} concentration range.

The epitaxial double-layer p/p^+ samples grown on the two types of single-crystal Si and on $(01\bar{1}2)$-oriented sapphire substrates were deposited at ~1025°C in H_2 (1.5 ℓpm) with SiH_4 flow rates of ~10 ccpm. The p^+ regions were B-doped by means of diborane (46 ppm B_2H_6 in He) flow rates of 150 ccpm which resulted typically in measured carrier concentrations of $4\text{-}6x10^{19}$ cm^{-3}, irrespective of the substrate involved. The p-type upper regions of these double-layer samples were doped by diborane flow rates of 6 ccpm, resulting in measured carrier concentrations of $3\text{-}5x10^{18}$ cm^{-3}. As indicated earlier, it had originally been intended that the upper regions of these composite samples be doped to concentrations in the 10^{17} cm^{-3} range for use in solar cell fabrication.

The transition between the p^+ and the p regions in these samples was shown by SR probe scans to be very abrupt. Figure 2-96 shows the results of SR probe scans on bevels through the full thickness of the p and p^+ regions of three double-layer Si films grown on sapphire substrates with the above deposition parameters. Although the SR probe measures spreading resistance, which is converted to resistivity for plotting purposes, the data shown are in terms of the automatically calculated carrier concentrations (based on the standard correction for bulk (100)-oriented Si) plotted as functions of depth into the composite samples.

Each of the three different nominal values of the thickness ratio $t_p:t_{p^+}$ - 1:3, 1:1, and 3:1 - is represented in Figure 2-96. The data excursions to lower carrier concentration values at the lower side of the transition in each of the three plots are artifacts introduced by the automatic plotting equipment and are related to the correction for the finite sampling volume of the probe; the transition is too abrupt for the equipment to "follow" accurately. The procedure followed in growing the p-type layer on the completed p^+ layer involved simply a 2 min. carrier gas purge - without SiH_4 - between the two depositions.

Similar SR probe scans through three double layers grown on single-crystal Si substrates are shown in Figure 2-97. The three thickness ratios are again represented. Figure 2-97a is the data for a double layer with $t_p:t_{p^+} \approx 1:3$, grown on 2 ohm-cm Si. Figure 2-97b is the data for a double layer grown on 10 ohm-cm Si with the two regions about equal in thickness, while Figure 2-97c is for a sample on the same type of substrate but with $t_p:t_{p^+} \approx 3:1$. The artifacts on the low side of the concentration step are again seen to be present. The abruptness of the p-p^+ transition in these samples did not appear to be influenced by the nature of the substrate - whether sapphire, 10 ohm-cm Si, or 2 ohm-cm Si.

The several experiments to prepare uniformly doped p-type polycrystalline Si films on glasses for use in fabricating solar cell structures involved substrates of Corning Code 1715 and Owens-Illinois GS213 and GS211 glasses, together with the usual $(01\bar{1}2)$-oriented sapphire monitor substrate. Films were grown at ~850°C in 1.5 ℓpm of He, with a SiH_4 flow rate of ~11.5 ccpm and diborane-in-He flow rates of 5, 150, and 1000 ccpm. Just as had been found in earlier B doping experiments for Si film growth at ~850°C in He using sapphire substrates alone, so it was found in these experiments with glass as well as sapphire substrates, that there seemed to be an upper limit of $\sim 10^{18}$ cm^{-3} on the net hole concentration achievable in a film on sapphire under these growth conditions, whatever the added diborane concentration. Furthermore, the highest net active hole concentration that was obtained in any of the polycrystalline films grown on the glass substrates under the above deposition conditions was in the low- to mid-10^{18} cm^{-3} range. This upper limit, if found to hold rigidly, would prevent the fabrication of p/p^+ structures, for example, in Si films on glass substrates and would limit the variety of solar cell designs that could be successfully fabricated on glasses.

C-3

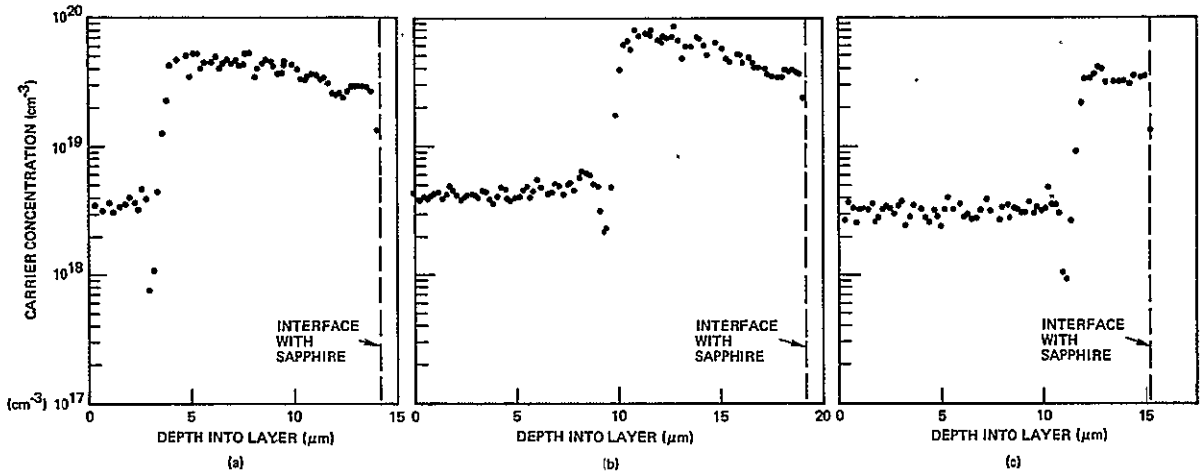

Figure 2-96. Spreading Resistance Probe Scans Showing Calculated Carrier Concentration versus Depth in Three p/p^+ Si Films Grown on Sapphire Substrates at ~1025°C in H_2. a) $t_p:t_{p^+} \approx 1:3$, b) $t_p:t_{p^+} \approx 1:1$, c) $t_p:t_{p^+} \approx 3:1$. (Probe spacing 22μm, probe load 20g, bevel angle 0.02 rad, step increment 10μm)

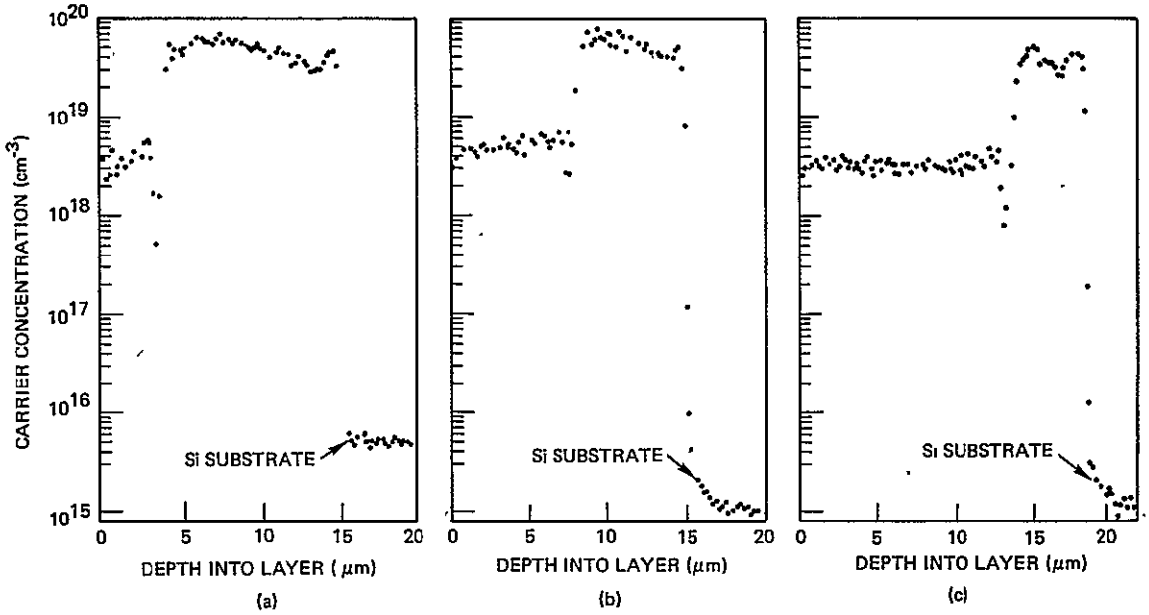

Figure 2-97. Spreading Resistance Probe Scans Showing Calculated Carrier Concentration versus Depth in Three p/p^+ Si Films Grown on Single-crystal Si Substrates at ~1025°C in H_2. a) $t_p:t_{p^+} \approx 1:3$, on 2 ohm-cm Si; b) $t_p:t_{p^+} \approx 1:1$, on 10 ohm-cm Si; c) $t_p:t_{p^+} \approx 3:1$, on 10 ohm-cm Si. (Probe spacing 17μm, probe load 20g, bevel angle 0.02 rad, step increment 10μm)

Both van der Pauw and SR determinations of layer resistivities showed that polycrystalline films on the glasses consistently had higher resistivities and higher carrier concentrations than did the simultaneously grown films on sapphire, as observed in earlier results. The SR scans obtained on pairs of films simultaneously grown on substrates of Owens-Illinois GS211 glass and sapphire at three different B doping levels (diborane flow rates of 5, 150, and 1000 ccpm) were shown in Figure 2-53, and illustrate some of these characteristics.

Of the group of 22 new Si sheet samples delivered to OCLI for possible solar cell fabrication, 15 were processed into solar cell structures during the fifth quarter. The samples included in the delivered group are listed in Table 2-27 together with their measured properties and the pertinent deposition parameters. In addition, the remaining pieces of each of the earlier p/p^+ Si sheet samples OCLI-34 and 35 (see Table 2-22) were included, to provide an opportunity to check on the reproducibility of cell processing and photovoltaic performance on two separate occasions with identical material. These samples are designed OCLI-34A and 35A and are also listed in Table 2-27.

The 15 samples processed into experimental cells at the time are designated by underline in Table 2-27. These include 13 sheet samples on single-crystal Si and two on single-crystal sapphire. Si wafers from two different sources were used as substrates in the preparation of the Si/Si samples. A group of (100)-oriented p-type 2 ohm-cm single-crystal Si wafers (2cm x 2cm) was obtained from OCLI; these were long-diffusion-length (L_n ~100μm) Czochralski-grown blanks used for the fabrication of high-efficiency diffused-junction single-crystal solar cells. Some of the blanks had been chemically-mechanically polished and some had been chemically polished (i.e., etched) only, in both cases at OCLI. In addition, 10 ohm-cm p-type (100)-oriented single-crystal Si wafers (5 cm dia) obtained from (and polished by) Monsanto for MOS/LSI device use at Rockwell were available for use as comparison substrates.

Three different nominal B doping levels are represented in the p-type epitaxial sheet samples OCLI-46 and 47, OCLI-36 and 39, and OCLI-42, 44, and 45 (Table 2-27). Each of the three groups involves optically polished single-crystal Si substrates from both of the above sources.

Three different thickness ratios (1:3, 1:1, 3:1) of the two regions in the p/p^+ double-layer B-doped structure are represented in the epitaxial sheet samples OCLI-50 and 51, OCLI-52 and 53, and OCLI-55 and 56. Each of the three pairs involves one sheet sample on an OCLI solar cell blank and one on a 10 ohm-cm Monsanto wafer.

Finally, OCLI-48 and 49 are double-layer p/p^+ samples grown on sapphire substrates, the first with a layer thickness ratio $t_p:t_{p+} = 1:3$ and the second with the ratio 1:1. As with the sheet samples involving single-crystal Si substrates, these also were epitaxial samples.

Table 2-27. B-doped CVD Si Sheet Samples Submitted to OCLI during Fifth Quarter for Solar Cell Processing and Measurement (See Note)

SAMPLE NO.	SUBSTRATE MATERIAL	OBSERV. DEPOS. TEMP (°C)	CARRIER GAS AND FLOW RATE (ℓpm)	SiH_4 FLOW RATE (ccpm)	DOPANT GAS* FLOW RATE (ccpm)	FILM THICK-NESS (μm)	AVE. GROWTH RATE (μm/min)	FILM RESIS-TIVITY (ohm-cm)	HOLE CONCEN-TRATION (cm^{-3})	HALL MOBILITY (cm^2/V-sec)	SAMPLE DIMENSIONS (cm) AND APPROX AREA (cm^2)	FILM STRUCTURE AND/OR SURFACE TEXTURE
OCLI-36	(100) S.C. Si 2 ohm-cm p-type (Mech. Polished)	1025	H_2 1.5	10	6	16.5	0.75	0.05†	~9×10^{17}††	NM	2.0x1.2 2.4	Epitaxial
OCLI-37	(100) S.C. Si 2 ohm-cm p-type (Mech. Polished)	1028	H_2 1.5	10	6	19***	0.9***	0.03***	2×10^{18}***	~90***	2.0 x 0.9 1.8	Epitaxial***
OCLI-38	(100) S.C. Si 2 ohm-cm p-type (Mech. Polished)	1028	H_2 1.5	10	6	19***	0.9***	0.03***	2×10^{18}***	~90***	2.0 x 1.0 2.0	Epitaxial***
OCLI-39	(100) S.C. Si 10 ohm-cm p-type (Mech. Polished)	1032	H_2 1.5	10	6	17***	0.8***	0.02***	4×10^{18}***	~75***	2.1 x 1.8 3.8	Epitaxial***
OCLI-40	(100) S.C. Si 2 ohm-cm p-type (Mech. Polished)	1029	H_2 1.5	10	6	19***	0.9***	0.05***	~2×10^{18}***	~75***	2.0 x 1.3 2.6	Epitaxial***
OCLI-41	(100) S.C. Si 2 ohm-cm p-type (Chem. Polished)	1029	H_2 1.5	10	6	19***	0.9***	0.05***	~2×10^{18}***	~75***	2.0 x 1.2 2.4	Epitaxial***
OCLI-42	(100) S.C. Si 2 ohm-cm p-type (Mech. Polished)	1026	H_2 1.5	10	18	15***	0.7***	~0.01***	~1×10^{19}***	~40***	2.0 x 1.1 2.2	Epitaxial***
OCLI-43	(100) S.C. Si 2 ohm-cm p-type (Chem. Polished)	1026	H_2 1.5	10	18	15***	0.7***	~0.01***	~1×10^{19}***	~40***	2.0 x 1.3 2.6	Epitaxial***
OCLI-44	(100) S.C. Si 2 ohm-cm p-type (Mech. Polished)	1031	H_2 1.5	8.8	18	16***	0.7***	~0.01***	~5×10^{18}***	~50***	2.0 x 1.4 2.8	Epitaxial***
OCLI-45	(100) S.C. Si 10 ohm-cm p-type (Mech. Polished)	1031	H_2 1.5	8.8	18	16	0.7	0.02†	3×10^{18}††	~50***	2.0 x 1.2 2.4	Epitaxial***
OCLI-46	(100) S.C. Si 2 ohm-cm p-type (Mech. Polished)	1027	H_2 1.5	8.8	1.9	19	0.9	0.09**	4×10^{17}**	190**	2.0 x 1.3 2.6	Epitaxial***
OCLI-47	(100) S.C. Si 10 ohm-cm p-type (Mech. Polished)	1027	H_2 1.5	8.8	1.9	17***	0.8***	0.20***	2×10^{17}***	170***	1.9 x 1.3 2.5	Epitaxial***
OCLI-48 (DL)	(01$\bar{1}$2) Sapphire (Polished)	1030	H_2 1.5	8.5	1) 150 2) 6	1) 10.5 2) 4	1) 0.7 2) 0.8	1)0.0025† 2)0.015†	1) 4×10^{19}††† 2)3.5×10^{18}††	1) NM 2) NM	2.0 x 1.4 2.8	Epitaxial*** (Both Layers)

NOTE: Samples processed into solar cell structures during quarter have number underlined

*Films B-doped from B_2H_6-in-He (46 ppm)

**Measured by van der Pauw method

***Estimate, based on deposition parameters and/or measurement on companion film grown simultaneously

†Measured by spreading resistance probe.

††Calculated from spreading resistance measurement.

NM = not measured. S.C. = single crystal

DL = double layer; 1) deposited first, 2) deposited second

Table 2-27 (Cont)

SAMPLE NO.	SUBSTRATE MATERIAL	OBSERV. DEPOS. TEMP. (°C)	CARRIER GAS AND FLOW RATE (ℓpm)	SiH_4 FLOW RATE (ccpm)	DOPANT GAS* FLOW RATE (ccpm)	FILM THICK-NESS (μm)	AVE. GROWTH RATE (μm/min)	FILM RESIS-RIVITY (ohm-cm)	HOLE CONCEN-TRATION (cm^{-3})	HALL MOBILITY (cm^2/V-sec)	SAMPLE DIMENSIONS (cm) AND APPROX AREA (cm^2)	FILM STRUCTURE AND/OR SURFACE TEXTURE
OCLI-49 (DL)	(01$\bar{1}$2) Sapphire (Polished)	1031	H_2 1.5	11.4	1) 150 2) 6	1) 9.0 2) 10.1	1) 0.9 2) 1.0	1)0.002† 2) 0.015†	1)5.5x10^{19}†† 2) 4.5x10^{18}††	1) NM 2) NM	2.0 x 1.5 3.0	Epitaxial*** (Both Layers)
OCLI-50 (DL)	(100) S.C. Si 2 ohm-cm p-type (Mech. Polished)	1025	H_2 1.5	11.4	1) 150 2) 6	1) 11.3 2) 4.2	1) 0.75 2) 0.8	1) 0.002† 2) 0.015†	1) 5x10^{19}†† 2) 4x10^{18}††	1) NM 2) NM	2.0 x 0.9 1.8	Epitaxial*** (Both Layers)
OCLI-51 (DL)	(100) S.C. Si 10 ohm-cm p-type (Mech. Polished)	1025	H_2 1.5	11.4	1) 150 2) 6	1) 13.3 2) 4.7	1) 0.9 2) 0.9	1) 0.002† 2) 0.016†	1) 5x10^{19}†† 2) 3.5x10^{18}††	1) NM 2) NM	1.3 x 1.2 1.5	Epitaxial*** (Both Layers)
OCLI-52 (DL)	(100) S.C. Si 2 ohm-cm p-type (Mech. Polished)	1023	H_2 1.5	11.3	1) 150 2) 6	1) 7.3 2) 8.7	1) 0.7 2) 0.9	1) 0.0015† 2) 0.012†	1) 7x10^{19}†† 2) 5.5x10^{18}††	1) NM 2) NM	2.0 x 1.5 3.0	Epitaxial*** (Both Layers)
OCLI-53 (DL)	(100) S.C. Si 10 ohm-cm p-type (Mech. Polished)	1023	H_2 1.5	11.3	1) 150 2) 6	1) 7. 2) 8.	1) 0.7 2) 0.8	1) 0.002† 2) 0.014†	1) 5.5x10^{19}†† 2) 5x10^{18}††	1) NM 2) NM	1.6 x 1.1 1.8	Epitaxial*** (Both Layers)
OCLI-54 (DL)	(01$\bar{1}$2) Sapphire (Polished)	1026	H_2 1.5	10.3	1) 150 2) 6	1) 3.6 2) 11.7	1) 0.7 2) 0.8	1) 0.0022† 2) 0.015†	1) 5x10^{19}†† 2) 4.5x10^{18}††	1) NM 2) NM	2.2 x 1.7 3.7	Epitaxial*** (Both Layers)
OCLI-55 (DL)	(100) S.C. Si 2 ohm-cm p-type (Mech. Polished)	1024	H_2 1.5	10.3	1) 150 2) 6	1) 4.0 2) 13	1) 0.8 2) 0.85	1) 0.002† 2) 0.014†	1) 5x10^{19}†† 2) 5x10^{18}††	1) NM 2) NM	2.0 x 1.3 2.6	Epitaxial*** (Both Layers)
OCLI-56 (DL)	(100) S.C. Si 10 ohm-cm p-type (Mech. Polished)	1024	H_2 1.5	10.3	1) 150 2) 6	1) 5.0 2) 14	1) 1.0 2) 0.9	1) 0.0025† 2) 0.017†	1) 4x10^{19}†† 2) 3.5 x 10^{18}††	1) NM 2) NM	1.8 x 1.6 2.9	Epitaxial*** (Both Layers)
OCLI-57 (DL)	(01$\bar{1}$2) Sapphire (Polished)	1030	H_2 1.5	10.4	1) 150 2) 6	1) 3.5 2) 11.5	2) 0.7 2) 0.8	1) 0.0025† 2) 0.016†	1) 3.5x10^{19}†† 2) 3.2x10^{18}††	1) NM 2) NM	2.2 x 1.8 4.0	Epitaxial*** (Both Layers)
OCLI-34A (DL)	(01$\bar{1}$2) Sapphire (Polished)	1025	H_2 1.5	10	1) 300 2) 6	1) 4*** 2) 17***	1) 1.3*** 2) 1.3***	1) 0.005*** 2) 0.1***	1) 1x10^{19}*** 2) 5x10^{17}***	1) NM 2) NM	Quarter Circle of Radius 1.9 cm 2.8	Epitaxial (Both Layers)
OCLI-35A (DL)	(0112) Sapphire (Polished)	1031	H_2 1.5	10	1) 295 2) 6	1) 6.5 2) 20.5	1) 1.1 2) 1.4	1) 0.0025† 2) 0.05†	1) 5x10^{19}†† 2) 8x10^{17}††	1) NM 2) NM	Quarter Circle of Radius 1.9 cm 2.8	Epitaxial (Both Layers)

NOTE: Samples processed into solar cell structures during quarter have number underlined

*Films B-doped from B_2H_6-in-He (46 ppm)

**Measured by van der Pauw method

***Estimate, based on deposition parameters and/or measurement on companion film grown simultaneously

†Measured by spreading resistance probe.

††Calculated from spreading resistance measurement.

NM = not measured. S.C. = single crystal

DL = double layer; 1) deposited first, 2) deposited second

The samples were processed according to the general procedure outlined in Section 2.4.1. After an initial thorough degreasing (trichloroethane, with N_2 blow-dry) the samples were P-diffused simultaneously with 4 control wafers (p-type 2 ohm-cm single-crystal 2cm x 2cm blanks) at 875°C for ~15 min using a $POCl_3$ source. This procedure was selected to produce a junction at a depth of ~0.35μm in the control wafers. After the surface glasses were removed (1 HF:10 H_2O etch for ~30 sec, followed by wash and blow-dry) the samples were all found to be n type at the surface.

A full-surface backside contact of Ti-Ag was then applied. A similar Ti-Ag front-surface contact in the form of the conventional comb-like finger-grid structure (3-4 lines per cm) was also applied. Both contacts were sintered (simultaneously) at ~500°C in a H_2 atmosphere for ~5 min. No antireflection coating was applied to any of the samples in this group, all of which were initially processed as single full-area solar cells.

Preliminary evaluation of these experimental solar cell structures was carried out using the AMO solar simulator. The results obtained in this series of measurements are summarized in Table 2-28; included are the corresponding responses of four single-crystal control cells processed and fabricated simultaneously with the sheet samples. The properties of the control cells compare favorably with the best single-crystal 2cm x 2cm n/p cells routinely produced at OCLI, so it appears that the processing and fabrication steps used with this group of samples were properly executed.

The differences in measured response for the three sets of cells fabricated in single-layer Si sheet material doped to three different concentration ranges are striking. Thus, samples OCLI-46 and 47, in which the Si layers were uniformly B-doped (simultaneously) to produce measured carrier concentrations of $4x10^{17}$ and $2x10^{17}$ cm^{-3}, respectively, gave good V_{oc} values of 470 and 534mV, respectively, compared with the average V_{oc} for the control samples of 580mV. Samples OCLI-36 and 39, in which the p-type Si layers were uniformly doped to produce measured carrier concentrations of ~$1x10^{18}$ and ~$3x10^{18}$ cm^{-3}, respectively, gave V_{oc} values of 120 and 131mV, respectively. Samples OCLI-42, 44, and 45, which were more heavily doped to produce carrier concentrations of nearly 10^{19} cm^{-3} (OCLI-42) and 5-9$x10^{18}$ cm^{-3} (OCLI-44 and 45, grown simultaneously), exhibited V_{oc} values of 16, 27, and 92mV, respectively, for the AMO test illumination. The measured short-circuit current densities obtained for these test conditions are seen to be similar for all of the samples in this group except OCLI-42 and 44, for which somewhat lower photogenerated current densities were observed.

These results clearly indicated that the more lightly doped p-type CVD Si produced far better photovoltaic response in junction devices formed by P diffusion under the conditions employed. This apparent sensitivity to acceptor doping level in the base material appeared considerably greater for the CVD sheet material than for comparably doped single-crystal Si wafers used for fabrication of conventional solar cells. It also appeared that CVD sheet material doped at concentrations below 10^{17} cm^{-3} should be included among those used for fabrication of experimental cell structures in this work. The results

Table 2-28. Photovoltaic Response* of P-diffused n/p Full-area Solar Cells Fabricated in B-doped CVD Si Sheet Material on Single-crystal Si and Sapphire Substrates

SAMPLE			PHOTOVOLTAIC RESPONSE*			
NUMBER	SUBSTRATE MATERIAL††	CARRIER CONC.** (cm^{-3})	V_{OC} (mV)	I_{SC} (mA)	APPROX. ACTIVE AREA† (cm^2)	J_{SC} (mA/cm^2)
OCLI-46	S.C. Si (2 ohm-cm)	$4x10^{17}$	470	34.8	2.2	15.8
OCLI-47	S.C. Si (10 ohm-cm)	$2x10^{17}$	534	36.7	2.1	17.5
OCLI-36	S.C. Si (2 ohm-cm)	$9x10^{17}$	120	35.1	2.2	16.0
OCLI-39	S.C. Si (10 ohm-cm)	$4x10^{18}$	131	59.7	3.5	17.1
OCLI-42	S.C. Si (2 ohm-cm)	$1x10^{19}$	16	26.2	2.0	13.1
OCLI-44	S.C. Si (2 ohm-cm)	$5x10^{18}$	27	37.1	2.6	14.3
OCLI-45	S.C. Si (10 ohm-cm)	$3x10^{18}$	92	33.4	2.0	16.7
OCLI-50	S.C. Si (2 ohm-cm)	$4x10^{18}/5x10^{19}$	82	23.4	1.4	16.7
OCLI-51	S.C. Si (10 ohm-cm)	$3.5x10^{18}/5x10^{19}$	84	20.6	1.3	15.8
OCLI-52	S.C. Si (2 ohm-cm)	$5.5x10^{18}/7x10^{19}$	30	20.8	1.2	17.3
OCLI-53	S.C. Si (10 ohm-cm)	$5x10^{18}/5.5x10^{19}$	58	23.8	1.4	17.0
OCLI-55	S.C. Si (2 ohm-cm)	$5x10^{18}/5x10^{19}$	30	36.7	2.4	15.3
OCLI-56	S.C. Si (10 ohm-cm)	$3.5x10^{18}/4x10^{19}$	89	43.6	2.7	16.1
OCLI-48	S.C. $(01\bar{1}2)$ Sapphire	$3.5x10^{18}/4x10^{19}$	56	~17.	2.6	~6.5
OCLI-49	S.C. $(01\bar{1}2)$ Sapphire	$4.5x10^{18}/5.5x10^{19}$	34	~1.5	2.8	~0.5
CONTROL 1	S.C. Si (2 ohm-cm)	$\sim 5x10^{15}$	580	100	3.4	29.4
CONTROL 2	S.C. Si (2 ohm-cm)	$\sim 5x10^{15}$	570	97	3.4	28.5
CONTROL 3	S.C. Si (2 ohm-cm)	$\sim 5x10^{15}$	575	99	3.4	29.1
CONTROL 4	S.C. Si (2 ohm-cm)	$\sim 5x10^{15}$	575	100	3.4	29.4

*AM0 solar simulator used as source of illumination
**See Table 2-27.
†No allowance made for grid-line coverage or contact-probe shadowing
††S.C. = single crystal,

also showed--for the three sets of single-layer samples--that better results were consistently obtained for CVD sheet material grown on the 10 ohm-cm single-crystal substrates than for layers grown on the high-lifetime 2 ohm-cm single-crystal substrates. There were several possible explanations for this result, one of which was the difficulty that was encountered in cleaning the OCLI substrate wafers adequately for use in epitaxy experiments, as discussed earlier.

The photovoltaic responses obtained with the cells fabricated in p/p^+ double-layer Si sheet material were poorer than had been expected. However, reference to the data in the table indicates the V_{oc} values for these samples (OCLI-50 and 51, 52 and 53, 55 and 56) are fairly consistent with the results obtained for the single-layer samples in which the doping concentration is in the same range as that in the upper (p-type) region of the p/p^+ double layers. The short-circuit current densities obtained with the cell structures fabricated in the double-layer samples were in the same range as those observed for the single-layer samples. Again the photovoltaic properties of the devices in sheet material grown on the 10 ohm-cm p-type single-crystal substrates exceeded those found for the devices in the layers grown on the 2 ohm-cm single-crystal substrates.

It is interesting that the difference in photovoltaic performance of devices in double-layer p/p^+ structures grown on the 2 ohm-cm substrates and those grown on the 10 ohm-cm substrates was greatest for the pair of samples (OCLI-55 and 56) for which the thickness ratio $t_p:t_{p+}$ was ~3:1, i.e., in which the p^+ layer was relatively thin and therefore fairly far from the p-n junction. The performance difference was less--but still quite significant--for the pair of samples (OCLI-52 and 53) for which the p and p^+ regions were about equal in thickness and in which the p^+ layer was about 8μm from the diffused junction.

The smallest difference in performance was for the two samples (OCLI-50 and 51) for which the $t_p:t_{p+}$ ratio was ~1:3, in which the p^+ region extended to about 4μm from the diffused junction. To determine if the apparent tendency for the p^+ layer to isolate the p-n junction (and thus its photovoltaic properties) from the influence of the properties of the substrate or if other factors present really dominate the situation requires additional experiments with other samples.

The pair of double-layer samples grown on sapphire substrates (OCLI-48 and 49, Table 2-28) resulted in diffused-junction cells exhibiting V_{oc} values similar to those for cells in double-layer samples on Si substrates for which the doping concentration in the p-type region was about the same (i.e., mid-10^{18} cm^{-3} range). There was no evidence in these full-area solar cells on sapphire of the large open-circuit photovoltages found in the mesa-type cell structures fabricated in double-layer Si sheet grown on sapphire, as in the group of samples discussed earlier (e.g., OCLI-34 and 35). In addition, short-circuit photocurrents were found to be very low for OCLI-48 and 49, again indicating major carrier collection and/or junction leakage problems.

Although there was evidence in these preliminary evaluations that properly doped epitaxial Si sheet material (e.g., OCLI-47) provided a base in which it was possible to form P-diffused junctions that exhibited very good open-circuit photovoltages, all of the full-area cells in this last group exhibited uniformly poor collected photocurrents. Furthermore, there was relatively little variation in the short-circuit current densities displayed by the sheet-sample devices for the test conditions used. The J_{sc} values (excluding those for the two samples on sapphire) were all in the range between 45 and 60 percent of the average of the short-circuit current densities produced by the four single-crystal Si control samples. This variation is very small compared with the variations in observed V_{oc} values. Thus, the evidence continued for the existence of factors limiting the charge collection efficiency in the Si sheet material and dominating the overall performance of the cells.

After completion of the evaluation of these full-area samples in the AMO simulator they were further processed to make arrays of individual mesa-type cells on each. This was done to investigate the uniformity of the deposited layers and the diffused junctions, and to determine if some of the disappointing photovoltaic performance noted could be attributed to localized regions in which the properties of the material and/or the junction were found to be defective.

Individual mesas 2mm in diameter were formed by wax-masking procedures, using aperture plates (i.e., not photolithographic methods), on each of the 15 samples as well as on one of the single-crystal Si control cells (Control 1). All other processing (junction formation and contact application) had already been done on each sample prior to mesa formation. The photovoltaic properties of many of the individual mesas on each sample were then measured, using a moderate-intensity (~1/2 sun) tungsten lamp for illumination. In some instances as many as 45 individual devices were evaluated on a single sample. Figure 2-98 shows photographs of the mesa-device arrays on two of the Si sheet samples of this group.

In general, no visual differences could be detected among those mesas on a given sample that gave relatively high photovoltaic response and those that gave poor response, although very wide variations in photovoltaic performance among the mesa cells on a given sample were observed in many cases. Those samples that gave relatively good response when tested in the AMO simulator as full-area cells (e.g., OCLI-46 and 47) also had uniformly better response for most of the individual mesas tested.

For example, for OCLI-46 63 percent of the 24 mesas tested produced V_{oc} values in excess of 400mV for this illumination and 37 percent of the mesas produced V_{oc} values in the 200-400mV range. For OCLI-47, the best sample measured in the full-area configuration, 91 percent of the individual mesa devices gave over 400mV for V_{oc} for this test illumination and 9 percent were in the 200-400mV range.

Sample OCLI-52, on the other hand, had produced a poor V_{oc} value of only 30mV when evaluated as a full-area cell in the AMO simulator (Table 2-28), but when the individual mesas were tested with the tungsten lamp illumination 40 percent of those measured gave V_{oc} values larger than 400mV and 47 percent

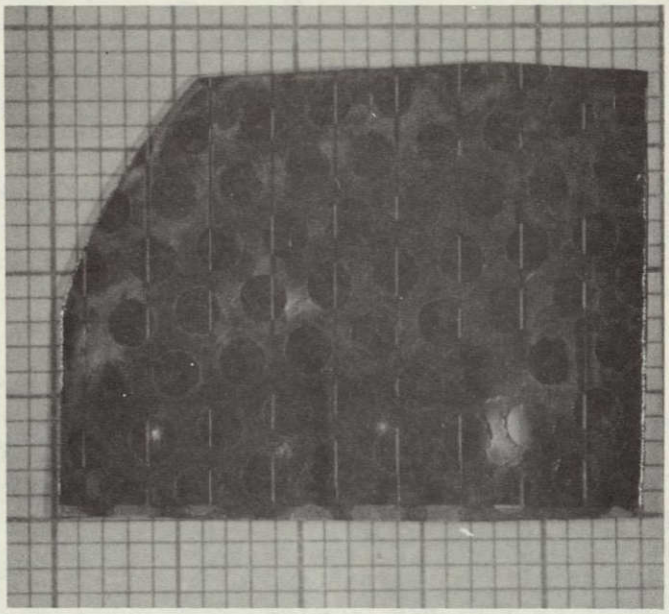

(a)

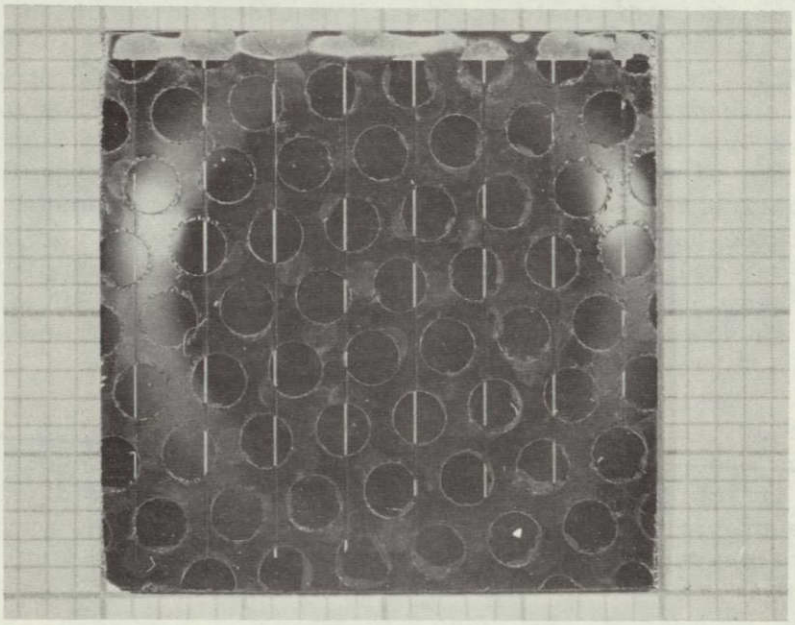

(b)

Figure 2-98. Photographs of Arrays of Mesa-type Solar Cells on Two Samples of Group Listed in Tables 2-28 and 2-29. (a) OCLI-39 (Epitaxial Si on 10 ohm-cm Single-crystal Si); (b) Control No. 1 (Single-crystal 2 ohm-cm Si Solar Cell Blank). Both Samples Shown on mm Grid Background.

were in the range 200-400mV. There were obviously significant variations in the photovoltaic properties over the area of this double-layer sample ($t_{p-} \approx t_{p+}$) grown on a 2 ohm-cm Si solar cell blank obtained from OCLI, and similar variations were found in some of the other samples.

The distribution of V_{oc} values obtained with individual mesa devices on each of this group of samples under the test illumination used is shown in Table 2-29. It should be pointed out that all of the individual mesa cells made in the single-crystal Si control sample were equally as good as the initially measured full-area cell (Control 1, Table 2-28).

A pair of samples that had not previously been processed into cell structures - OCLI-37 and 38 - was subsequently processed in the same manner as the above group of 15, in an attempt to determine if the environment of the Si CVD process adversely affected minority carrier lifetimes (diffusion lengths) in Si and might therefore be responsible for the poorer-than-expected photovoltaic performance observed in some of the epitaxial samples. These two CVD layers had been grown simultaneously on two different 2 ohm-cm p-type (100) single-crystal Si solar cell blanks obtained from OCLI. Measurements on layers grown simultaneously on two other similar blanks had indicated carrier concentrations of $2\text{-}3 \times 10^{18}$ cm^{-3} and Hall mobilities of about 90 $cm^2/V\text{-sec}$, using the van der Pauw method.

The deposited layer was entirely removed from one of the samples (OCLI-37) by etching prior to the P diffusion process, so that the junction would be fabricated in the original single-crystal substrate rather than in the epitaxially grown CVD layer. The intention was to compare photovoltaic properties of the two samples, and especially to determine the effective diffusion lengths in the two base layers as an indicator of possible processing damage to the properties of the single-crystal Si. Unfortunately, the experiment turned out to be inconclusive, since inferior performance was observed in the mesa devices fabricated on both samples. Measurable but very poor performance was found for several mesas on OCLI-37 (the bulk crystal sample), but almost no measurable response was obtained for the mesas on OCLI-38 (the epitaxial sample). The cause of this outcome was not determined. These two samples are included in Table 2-29, nonetheless.

It was clear that CVD Si samples more lightly doped than most of those used for the various groups of solar cells described in the foregoing discussion were required if improved photoresponse was to be achieved. Samples of that type were prepared during the final five months of the program, and the results are described in the next section.

2.4.4 Solar Cell Fabrication and Evaluation during Final Five Months of Program

During the sixth quarter of the program another 33 Si sheet samples from among those prepared by CVD on various substrates were delivered to OCLI for processing into solar cell structures. These samples, including OCLI-58 through OCLI-90, are listed in Table 2-30, which also gives the pertinent deposition parameters and other properties.

This group included B-doped polycrystalline Si films on glasses (Owens-Illinois GS213 and Corning Code 1715) and additional baseline films on single-crystal sapphire, with a range of p-type doping concentrations (measured) from ~$5x10^{15}$ to over 10^{18} cm^{-3}. (As indicated earlier, it had not been possible to achieve sufficiently high B doping in polycrystalline Si films on glasses to produce available hole concentrations above the low- to mid-10^{18} cm^{-3} range.) The group also included a number of samples, prepared by the dichlorosilane pyrolysis process described earlier (Section 2.3.14), involving various single-crystal Si substrates.

Samples OCLI-67 through 70 consisted of CVD Si sheet grown by SiH_4 pyrolysis on single-crystal sapphire substrates in two different experiments at ~1025°C in H_2 (2.5 ℓpm) carrier gas, with SiH_4 flow rates of 12 ccpm and B_2H_6-in-He dopant gas flow rates of 0.5 and 5.0 ccpm. The films had measured hole concentrations of ~$2x10^{16}$ and ~$4x10^{17}$ cm^{-3}, respectively, and hole mobilities of 135-150 cm^2/V-sec, and were each ~25μm thick. These samples were considered to be representative of the single-layer epitaxial CVD Si sheet material being prepared at that time in the SiH_4 reactor system.

Samples OCLI-71 through 90 were prepared in the AMC Model AMV-800 CVD reactor at Rockwell, as indicated earlier, by pyrolysis of dichlorosilane ($SiH_2Cℓ_2$). All of the epitaxial films in this group were 21-22μm thick, grown at ~1075°C on single-crystal Si substrates of several different characteristics, as shown in Table 2-30. All substrates were vapor-phase etched in HCℓ at 1175-1185°C in the deposition chamber just before film growth began. The p-type films were doped with B (from B_2H_6) to five different concentrations, as determined by measurement of net carrier concentrations in epitaxial films grown simultaneously on companion n-type single-crystal Si control wafers: $1.4x10^{15}$, $4.1x10^{15}$, $1.4x10^{16}$, $1.6x10^{17}$, and $1.1x10^{18}$ cm^{-3}.

All of the dichlorosilane-process samples sent to OCLI either were already 2x2 cm or 2x4 cm (as used in the Si deposition) or were initially larger and were subsequently wire-sawed into 2x2 cm pieces for cell processing. The SiH_4-grown sapphire-based samples, however, were processed as received.

Samples OCLI-67 through 71 and OCLI-74 through 90 were all processed into solar cells together, so that the photovoltaic characteristics of cells in epitaxial material grown on single-crystal Si substrates by the dichlorosilane process could be compared with the photovoltaic properties of cells fabricated in similarly doped heteroepitaxial material grown on single-crystal sapphire substrates by SiH_4 pyrolysis. The usual P thermal-diffusion

Table 2-30. B-doped CVD Si Sheet Samples Prepared for Solar Cell Processing by OCLI during Sixth Quarter of Program*

SAMPLE NO.	SUBSTRATE MATERIAL	OBSERV. DEPOS. TEMP (°C)	CARRIER GAS AND FLOW RATE (ℓpm)	SiH_4 FLOW RATE (ccpm)	DOPANT GAS* FLOW RATE (ccpm)	FILM THICK-NESS (μm)	AVE. GROWTH RATE (μm/min)	FILM RESIS-TIVITY (ohm-cm)	HOLE CONCEN-TRATION (cm^{-3})	HALL MOBILITY (cm^2/V-sec)	SAMPLE DIMENSIONS (cm) AND APPROX AREA (cm^2)	FILM STRUCTURE AND/OR SURFACE TEXTURE
OCLI-58	$(01\bar{1}2)$ Sapphire (polished)	845	He 1.5	11 5	50	21	0.7	0.60†	1.1×10^{17}†	93†	r ≈ 2 3.1††	Epitaxial
OCLI-59	$(01\bar{1}2)$ Sapphire (polished)	853	He 1.5	11 5	50	23	0.7	0.39†	1.6×10^{17}†	99†	r ≈ 2 3.1††	Epitaxial
OCLI-60	$(01\bar{1}2)$ Sapphire (polished)	850	He 1.5	11.5	5	20	0.7	9.6†	2.4×10^{16}†	27†	r ≈ 2 3.1††	Epitaxial
OCLI-61	Owens-Illinois GS213 Glass (polished)	850	He 1.5	11.5	5	~15	~0.5	–	–	–	1.5x0.8 1.2	Poly, pref. orient.
OCLI-62	Corning Code 1715 Glass (polished)	850	He 1.5	11.5	5	~15	~0.5	41†	2.1×10^{16}†	7†	1.3x0.9 1.2	Poly; pref. orient.
OCLI-63	Owens-Illinois GS213 Glass (polished)	846	He 1.5	11.5	150	~13	~0.4	–	–	–	1.5x0.9 1.4	Poly; pref. orient.
OCLI-64	Corning Code 1715 Glass (polished)	846	He 1.5	11.5	150	~13	~0.4	0.12†	5.1×10^{18}†	11†	1.4x1.0 1.4	Poly; pref. orient.
OCLI-65	Owens-Illinois GS213 Glass (polished)	848	He 1 5	11.5	1000	~12	~0.4	–	–	–	1.5x0.7 1.0	Poly; pref. orient.
OCLI-66	Corning Code 1715 Glass (polished)	848	He 1.5	11.5	1000	~12	~0.4	0.23†	2.9×10^{18}†	9†	1.3x1.1 1.4	Poly; pref. orient.
OCLI-67	$(01\bar{1}2)$ Sapphire (polished)	1028	H_2 2.5	5	0.5	26	1.3	2.0†	2.1×10^{16}†	151†	2.7x1.5 4.0	Epitaxial
OCLI-68	$(01\bar{1}2)$ Sapphire (polished)	1028	H_2 2.5	5	0.5	26	1.3	2.0†	2.1×10^{16}†	151†	2.9x1.5 4.4	Epitaxial
OCLI-69	$(01\bar{1}2)$ Sapphire (polished)	1028	H_2 2.5	12	5.0	23	1.1	0.12†	3.9×10^{17}†	136†	1.5x1.5 2.2	Epitaxial
OCLI-70	$(01\bar{1}2)$ Sapphire (polished)	1028	H_2 2.5	12	5.0	28	1.4	0.12†	3.9×10^{17}†	136†	2.0x1.9 3.8	Epitaxial

* Films B doped from B_2H_6-in-He (46 ppm)

†Measured by van der Pauw method

††Sample approx. quarter sector of circular piece of 2 cm radius.

Table 2-30 (Cont)

SAMPLE NO.	SUBSTRATE MATERIAL **	OBSERV. DEPOS. TEMP (°C)	CARRIER GAS AND FLOW RATE (ℓpm)	SiH_2Cl_2 FLOW RATE⊙ (ccpm)	DOPANT GAS* FLOW RATE (ccpm)	FILM THICK-NESS† (μm)	AVE. GROWTH RATE (μm/min)	FILM RESIS-TIVITY† (ohm-cm)	HOLE CONCEN-TRATION†† (cm^{-3})	HALL MOBILITY (cm^2/V-sec)	SAMPLE DIMENSIONS (cm) AND APPROX AREA (cm^2)	FILM STRUCTURE AND/OR SURFACE TEXTURE
OCLI-71	(100) s.c. Si 1-3 ohm-cm p-type (chem. polished)	1073	H_2 39	87	1.1	21	0.7	9.3	$1.4x10^{15}$	–	d ≈ 5.7 25.5	Epitaxial
OCLI-72	(100) s.c. Si 1-3 ohm-cm p-type (mech. polished)	1073	H_2 39	87	1.1	21	0.7	9.3	$1.4x10^{15}$	–	2x2 4	Epitaxial
OCLI-73	(100) s.c. Si 1-3 ohm-cm p-type (mech. polished)	1073	H_2 39	87	1.1	21	0.7	9.3	$1.4x10^{15}$	–	2x2 4	Epitaxial
OCLI-74	(100) s.c. Si 10 ohm-cm p-type (mech. polished)	1073	H_2 39	87	1.1	21	0.7	9.3	$1.4x10^{15}$	–	d ≈ 5.0 19.6	Epitaxial
OCLI-75	(100) s.c. Si 1-3 ohm-cm p-type (chem. polished)	1073	H_2 39	87	4.3	21	0.7	3.3	$4.1x10^{15}$	–	d ≈ 5.7 25.5	Epitaxial
OCLI-76	(100) s.c. Si 1-3 ohm-cm p-type (mech. polished)	1073	H_2 39	87	4.3	21	0.7	3.3	$4.1x10^{15}$	–	2x4 8	Epitaxial
OCLI-77	(100) s.c. Si 1-3 ohm-cm p-type (chem. polished)	1073	H_2 39	87	4 3	21	0.7	3.3	$4.1x10^{15}$	–	2x4 8	Epitaxial
OCLI-78	(100) s.c. Si 10 ohm-cm p-type (mech. polished)	1073	H_2 39	87	4.3	21	0.7	3.3	$4.1x10^{15}$	–	d ≈ 5.0 19.6	Epitaxial
OCLI-79	(100) s.c. Si 1-3 ohm-cm p type (chem. polished)	1073	H_2 39	87	12.6	21.5	0.7	1.1	$1.4x10^{16}$	–	d ≈ 5.7 25.5	Epitaxial
OCLI-80	(100) s.c. Si 1-3 ohm-cm p-type (mech. polished)	1073	H_2 39	87	12.6	21.5	0.7	1.1	$1.4x10^{16}$	–	2x4 8	Epitaxial
OCLI-81	(100) s.c. Si 1-3 ohm-cm p-type (chem. polished)	1073	H_2 39	87	12 6	21.5	0.7	1.1	$1.4x10^{16}$	–	2x4 8	Epitaxial
OCLI-82	(100) s.c. Si 10 ohm-cm p-type (mech. polished)	1073	H_2 39	87	12.6	21.5	0.7	1.1	$1.4x10^{16}$	–	d ≈ 5.0 19.6	Epitaxial

⊙ Dichlorosilane pyrolysis in AMC Model AMV-800 reactor; substrates HCℓ vapor-etched for 2 min at 1175-1180°C before filmgrowth.

*Films B doped from B_2H_6 (10 ppm in H_2)

†Measured in simultaneously grown layer on single-crystal n-type Si companion wafer; resistivity measured by four-point probe.

††Calculated from four point-probe value for resistivity, assuming bulk-crystal mobility.

**S.C. = single crystal

Table 2-30 (Cont)

SAMPLE NO.	SUBSTRATE MATERIAL **	OBSERV. DEPOS. TEMP (°C)	CARRIER GAS AND FLOW RATE (ℓpm)	SiH_2Cl_2 FLOW RATE ○ (ccpm)	DOPANT GAS* FLOW RATE (ccpm)	FILM THICK-NESS† (μm)	AVE. GROWTH RATE (μm/min)	FILM RESIS-TIVITY† (ohm-cm)	HOLE CONCEN-TRATION†† (cm^{-3})	HALL MOBILITY (cm^2/V-sec)	SAMPLE DIMENSIONS (cm) AND APPROX AREA (cm^2)	FILM STRUCTURE AND/OR SURFACE TEXTURE
OCLI-83	(100) s.c. Si 1-3 ohm-cm p type (chem. polished)	1070	H_2 39	87	45.5	22	~0.7	0.20	$1.6x10^{17}$	–	d ≈ 5.7 25.5	Epitaxial
OCLI-84	(100) s.c. Si 1-3 ohm-cm p type (mech. polished)	1070	H_2 39	87	45.5	22	~0.7	0.20	$1.6x10^{17}$	–	2x4 8	Epitaxial
OCLI-85	(100) s.c. Si 1-3 ohm-cm p type (chem. polished)	1070	H_2 39	87	45.5	22	~0.7	0.20	$1.6x10^{17}$	–	2x4 8	Epitaxial
OCLI-86	(100) s.c. Si 10 ohm-cm p type (mech. polished)	1070	H_2 39	87	45.5	22	~0.7	0.20	$1.6x10^{17}$	–	d ≈ 5.0 19.6	Epitaxial
OCLI-87	(100) s.c. Si 1-3 ohm-cm p type (chem. polished)	1070	H_2 39	87	300.	22	~0.7	0.059	$1.1x10^{18}$	–	d ≈ 5.7 25.5	Epitaxial
OCLI-88	(100) s.c. Si 1-3 ohm-cm p type (mech. polished)	1070	H_2 39	87	300.	22	~0.7	0.059	$1.1x10^{18}$	–	2x4 8	Epitaxial
OCLI-89	(100) s.c. Si 1-3 ohm-cm p type (chem. polished)	1070	H_2 39	87	300.	22	~0.7	0.059	$1.1x10^{18}$	–	2x4 8	Epitaxial
OCLI-90	(100) s.c. Si 10 ohm-cm p type (mech. polished)	1070	H_2 39	87	300.	22	~0.7	0.059	$1.1x10^{18}$	–	d ≈ 5.0 19.6	Epitaxial

○ * Dichlorosilane pyrolysis in AMC Model AMV-800 reactor; substrates HCℓ-vapor-etched for 2 min. at 1175-1180°C before film growth

*Films B doped from B_2H_6 (10 ppm in H_2)

†Measured in simultaneously grown layer on single-crystal n-type Si companion wafer; resistivity measured by four-point probe.

††Calculated from four-point-probe value for resistivity, assuming bulk-crystal mobility.

**S.C. = single crystal

schedule was used, and the conventional cell fabrication procedures were the same as those employed on previous groups of Si film cells prepared at OCLI. As always, single-crystal Si solar cell blanks were processed along with the sheet samples, as controls. Figure 2-99 shows two of the finished cell structures, ready for photovoltaic measurements.

The results of photovoltaic response measurements on these samples in the AMO simulator (sample temperature ~25°C) are summarized in Table 2-31. The samples are grouped by the added p-type doping concentration in the CVD layer (Column 6), ranging from ~$1x10^{15}$ to ~$1x10^{18}$ cm^{-3}. Two different single-crystal Si substrate materials (Column 4) are represented: 1) p-type 1-3 ohm-cm (100)-oriented solar cell blank material obtained from OCLI, and 2) p-type ~10 ohm-cm (100)-oriented device-quality material purchased from Monsanto. The sapphire used was $(01\bar{1}2)$-oriented single-crystal Czochralski-grown material that had been given the customary optical polish to a "substrate finish" (Column 5).

Two different surface preparation methods (Column 5) for the Si substrates were represented in this group of samples: 1) standard optical (i.e., mechanical) polishing procedures used in preparing single-crystal Si for device fabrication (two modifications - one used by OCLI for preparing solar cell blanks and the other used by Monsanto for preparing polished wafers for various IC and LSI applications - were involved); and 2) chemical polishing, which involved direct chemical etching of the as-sawed Si blank, using a $2HF:15HNO_3:5CH_3COOH$ etch for 9-11 min at room temperature.

A principal observation to be made is that the cells fabricated in the epitaxial Si samples grown by the dichlorosilane process at ~1075°C were generally much better than those fabricated in epitaxial Si layers grown by SiH_4 pyrolysis at ~1025°C on similar single-crystal Si substrates (see Tables 2-28 and 29). They were also significantly better than the simultaneously processed cells in SiH_4-grown heteroepitaxial Si on sapphire substrates (OCLI-67 through 70).

Open-circuit photovoltages V_{oc} for these cells under simulated AMO illumination compared favorably with the V_{oc} values for the cells in the single-crystal control wafers, data for one of which are also given in Table 2-31. Of special significance is the fact that short-circuit current densities J_{sc} as high as ~90 percent of those obtained in the control cells were observed for some of these samples, indicating much improved current collection efficiencies (and thus appreciably better minority carrier diffusion lengths) over those found in the CVD Si sheet prepared by SiH_4 pyrolysis and used in fabricating epitaxial Si cell structures earlier in the program.

Although the V_{oc} values given in Table 2-31 for the five groups of samples on Si substrates are relatively high, on the average, the cells fabricated in the CVD layers doped to ~$2x10^{17}$ cm^{-3} had the highest average V_{oc} value, with those in the layers doped to ~$4x10^{15}$ cm^{-3} next. In each group but the first (which contained only two samples, with doping levels of ~$1x10^{15}$ cm^{-3} in the epitaxial layers) the cell fabricated in the layer grown on the 10 ohm-cm p-type substrate wafer exhibited a V_{oc} value significantly below those of

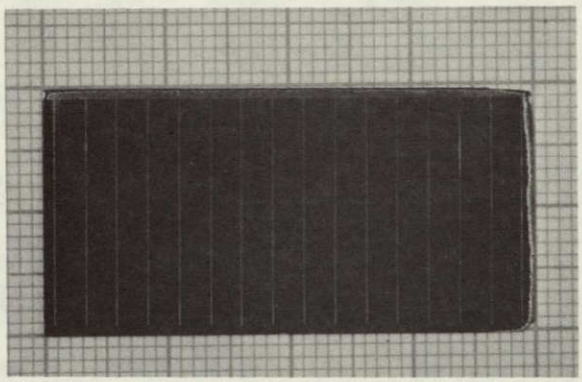

(a)

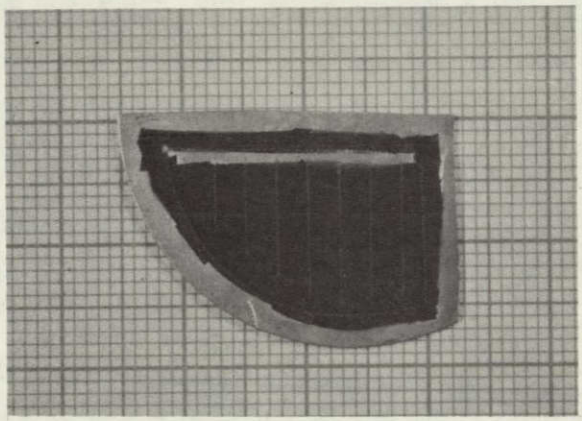

(b)

Figure 2-99. Photographs of Two Finished Solar Cell Structures from Group Listed in Table 2-31. (a) OCLI-77 (Epitaxial Si Grown by SiH_2Cl_2 Pyrolysis on Chemically Polished Single-crystal Si Solar Cell Blank); (b) OCLI-67 (Epitaxial Si Grown by SiH_4 Pyrolysis on Single-crystal $(01\bar{1}2)$ Sapphire).

Table 2-31. Photovoltaic Properties of Diffused-junction* n/p Solar Cells Fabricated in p-type Epitaxial CVD Si Layers Grown at ~1075°C by Dichlorosilane Process on Various p-type (100)-oriented Single-crystal Si Substrates and at ~1025°C by SiH_4 Pyrolysis Process on $(01\bar{1}2)$-oriented Sapphire Substrates**

SAMPLE NO.	SAMPLE DIMENSIONS (cm)	SUBSTRATE DESCRIPTION			DEPOSITED LAYER HOLE CONCENTRATION†† (cm^{-3})	V_{OC} (mV)	I_{SC} (mA)	J_{SC} (mA/cm^2)	$J^{\dagger}_{400\ mV}$ (mA/cm^2)
		INITIAL SIZE (cm)	RESISTIVITY (ohm-cm)	SURFACE FINISH***					
OCLI-71	2x2	5.7 dia.	1-3	Chem.	$1.4x10^{15}$	483	84.8	21.2	3.18
OCLI-74	2x2	5.0 dia.	10	Opt.	$1.4x10^{15}$	501	88.4	22.1	15.9
OCLI-75	2x2	5.7 dia.	1-3	Chem.	$4.1x10^{15}$	544	81.5	20.4	16.6
OCLI-76	2x4	2x4	1-3	Opt.	$4.1x10^{15}$	567	183	22.9	17.4
OCLI-77	2x4	2x4	1-3	Chem.	$4.1x10^{15}$	542	174	21.7	19.1
OCLI-78	2x2	5.0 dia.	10	Opt.	$4.1x10^{15}$	474	87	21.8	10.4
OCLI-79	2x2	5.7 dia.	1-3	Chem.	$1.4x10^{16}$	518	79.2	19.8	6.88
OCLI-80	2x4	2x4	1-3	Opt.	$1.4x10^{16}$	555	177	22.1	16.2
OCLI-81	2x4	2x4	1-3	Chem.	$1.4x10^{16}$	458	158	19.7	2.82
OCLI-82	2x2	5.0 dia.	10	Opt.	$1.4x10^{16}$	503	78.7	19.7	11.8
OCLI-83	2x2	5.7 dia.	1-3	Chem.	$1.6x10^{17}$	543	73.3	18.3	16.0
OCLI-84	2x4	2x4	1-3	Opt.	$1.6x10^{17}$	576	134	16.8	11.4
OCLI-85	2x4	2x4	1-3	Chem.	$1.6x10^{17}$	558	146	18.3	16.9
OCLI-86	2x2	5.0 dia.	10	Opt.	$1.6x10^{17}$	535	66.3	16.6	13.8
OCLI-87	2x2	5.7 dia.	1-3	Chem.	$1.1x10^{18}$	496	64.6	16.2	11.8
OCLI-88	2x4	2x4	1-3	Opt.	$1.1x10^{18}$	568	137	17.1	14.6
OCLI-89	2x4	2x4	1-3	Chem.	$1.1x10^{18}$	542	130	16.3	12.5
OCLI-90	2x2	5.0 dia.	10	Opt.	$1.1x10^{18}$	130	50.1	12.5	–
OCLI-67	–	1.7 cm^2 (area)	Sapphire	Opt. substr.	$2.1x10^{16}$	384	7.5	4.4	–
OCLI-68	–	1.7 cm^2 (area)	Sapphire	Opt. substr.	$2.1x10^{16}$	332	5.9	3.5	–
OCLI-69	–	0.8 cm^2 (area)	Sapphire	Opt. substr.	$3.9x10^{17}$	431	7.7	9.6	–
OCLI-70	–	2.25 cm^2 (area)	Sapphire	Opt. substr.	$3.9x10^{17}$	267	16	7.1	–
CONTROL A	2x2	2x2	1-3	Opt.	†††	571	102	25.4	21.6

*Phosphorus diffusion for 20 min (5 min preheat) at ~875°C, to produce junction ~0.4 μm deep

**AMO solar simulator used for illumination; samples maintained at ~25°C during measurement

***Chem. = chemically polished (etched) surface, using $2HF:15HNO_3:5CH_3COOH$ for 9-11 min. on as-sawed wafer surface
Opt. = standard mechanical polish used for producing "optical polish" surface on Si wafers
Opt. substr. = standard "substrate finish" obtained by optical polishing techniques developed for sapphire

†Current density at 400 mV is indication of curve fill factor

††Hole concentration measured in another piece of same sample or in epitaxial p type layers grown simultaneously on single-crystal n-type Si companion wafers

†††Hole concentration corresponding to resistivity of p-type single-crystal control blank is ~$5x10^{15}$ cm^{-3}

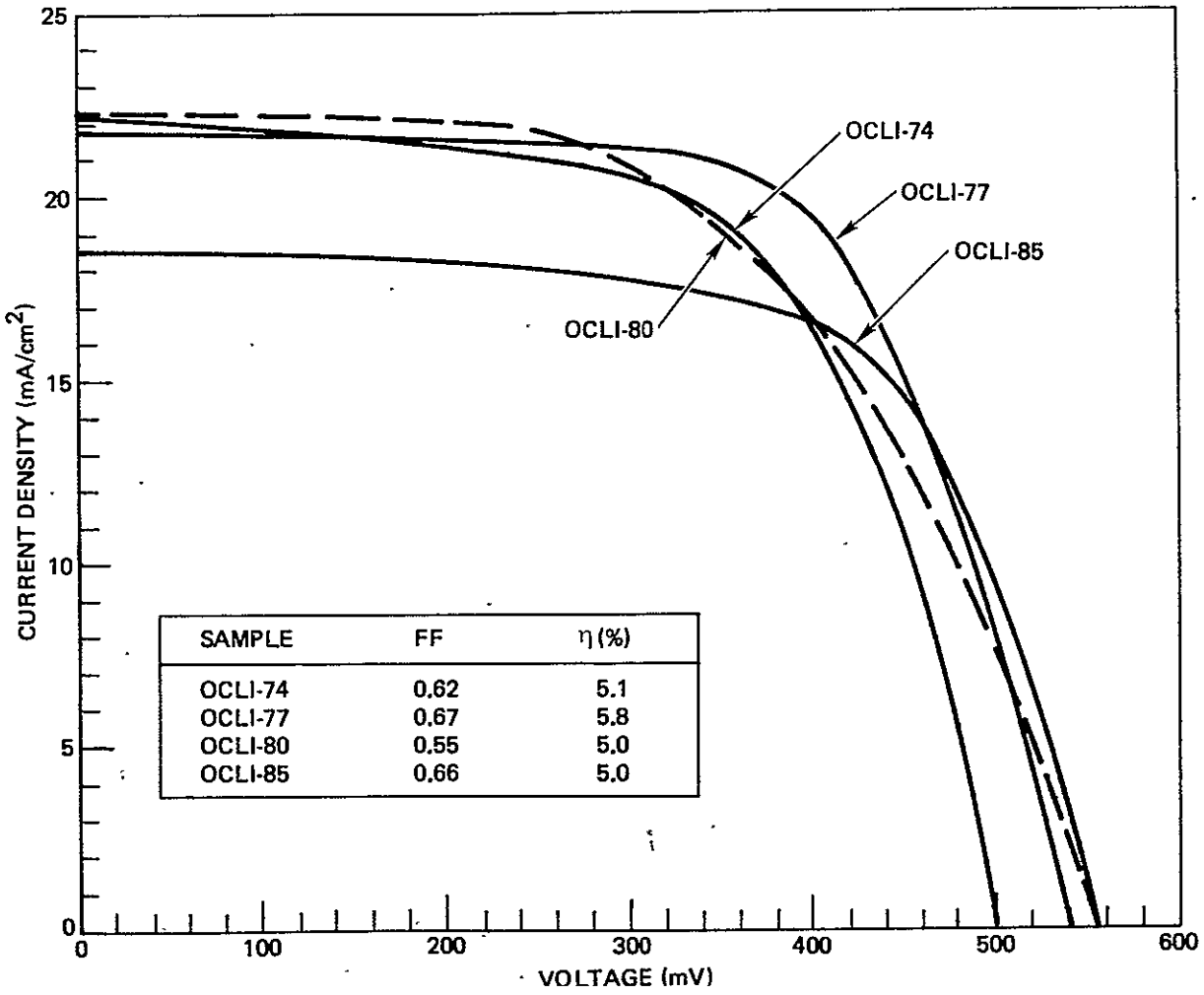

Figure 2-100. Fourth Quadrant of I-V Characteristics under AM0 Illumination for Several Solar Cells Listed in Table 2-31.

earlier - See Figure 2-30 - that a diborane-in-He flow rate of 100 ccpm was sufficient to produce such doping.) In three of the experiments the p+ layer was made approximately 5μm thick and in another three experiments the p+ layer was made ~15μm thick. For each set of three experiments the p layer, whether 5μm or 15μm thick, was doped with B to produce measured carrier concentrations of ~10^{15}, ~10^{16}, and ~10^{17} cm^{-3}.

In each of these experiments at least three different substrates were used: single-crystal sapphire, polycrystalline MRC Hi Rel Superstrate alumina, and polycrystalline Coors Vistal 5 and/or Vistal 1 alumina. The latter two materials tend to have very large individual α-$A\ell_2O_3$ grains; the grain size depends upon the refiring (supplementary annealing) history, with Vistal 5 (refired 5 times for ~3 hours at ~1800°C) having the larger grains - in some instances as large as 1mm or more across (see Sections 2.3.2 and 2.3.10).

A polycrystalline composite on MRC Hi-Rel Superstrate alumina and one on Coors Vistal 5 alumina were submitted from each of the experiments. Simultaneously grown epitaxial composites on sapphire were also submitted for all but two of the experiments, so that 16 samples were delivered to OCLI for processing. These samples (OCLI-91 through 106) are listed in Table 2-32.

The cells were processed by the usual procedures. Standard P diffusion was employed; a $POC\ell_3$ source was used, with diffusion carried out for 20 min. at ~875°C following a 5 min. preheat cycle, to produce a junction about 0.4μm below the front surface of the sample. Single-crystal ~2 ohm-cm (100)-oriented Si control wafers were simultaneously processed, as usual.

Several of the samples were first fabricated into full-size cells, with interdigital contacts fabricated by etching techniques so that the entire cell on a given sample consisted of a single large mesa. Preliminary tests with tungsten lamp illumination showed these cells to have large leakage currents, so all samples were then processed into individual mesas of ~2mm diameter.

The results of photovoltaic response measurements on these samples under two types of illumination - tungsten lamp of ~½ sun intensity and the AM0 solar simulator - are given in Table 2-33. The samples are arranged in two groups - those with t_p:t_{p+} ratios of ~15:5 and those with t_p:t_{p+} ratios of ~5:15. Within each group the samples are listed by increasing concentration of the p-type region - ~10^{15}, ~10^{16}, and ~10^{17} cm^{-3}. The characteristics of one of the control cells fabricated in 2 ohm-cm single-crystal Si are also given.

It is difficult to identify significant trends in these data. Several observations can be made, however. First, the epitaxial films on single-crystal sapphire produced much higher V_{OC} values than did the polycrystalline films on Vistal 5 and Hi Rel Superstrate, probably because of much higher leakage currents in the junctions formed in the polycrystalline films. Second, there was relatively little difference in the short-circuit current densities in the epitaxial devices on sapphire and the polycrystalline devices on the alumina ceramics under tungsten lamp illumination, and only in one or two instances did the value of J_{SC} exceed 50 percent of that obtained with the

Table 2-32. B-doped Double-layer p/p^+ CVD Si Sheet Samples Grown on Alumina Substrates by SiH_4 Pyrolysis in H_2 at 1025-1030°C, as Delivered to OCLI for Processing into Diffused-junction Solar Cells

SAMPLE NO.	SUBSTRATE MATERIAL	OBSERV. DEPOS. TEMP (°C)	CARRIER GAS AND FLOW RATE (ℓpm)	SiH_4 FLOW RATE (ccpm)	DOPANT GAS* FLOW RATE (ccpm)	FILM THICK-NESS (μm)	AVE. GROWTH RATE (μm/min)	FILM RESIS-TIVITY (ohm-cm)	HOLE CONCEN-TRATION† (cm^{-3})	HALL MOBILITY (cm^2/V-sec)	SAMPLE DIMENSIONS (cm) AND APPROX. AREA (cm^2)	FILM STRUCTURE AND/OR SURFACE TEXTURE
OCLI-91	$(01\bar{1}2)$ Sapphire (polished)	1026	H_2 2.5	12	1) 100 2) 0.5	1) 5 2) 15	–	–	1) $>10^{19}$ 2) $\sim10^{16}$	NM**	1.0x1.0 1.0	Epitaxial
OCLI-92	Coors Vistal 5 Alumina (refired) (polished)	1026	H_2 2.5	12	1) 100 2) 0.5	1) 5 2) 15	–	–	1) $>10^{19}$ 2) $\sim10^{16}$	NM**	1.2x1.2 1.4	Poly; {110} pref. orient.
OCLI-93	MRC Superstrate Alumina (polished)	1026	H_2 2.5	12	1) 100 2) 0.5	1) 5 2) 15	–	–	1) $>10^{19}$ 2) $\sim10^{16}$	NM**	1.0x1.0 1.0	Poly; {110} pref. orient.
OCLI-94	$(01\bar{1}2)$ Sapphire (polished)	1027	H_2 2.5	12	1) 100 2) 0.1	1) 5 2) 15	–	–	1) $>10^{19}$ 2) $\sim10^{15}$	NM**	1.25x0.8 1.0	Epitaxial
OCLI-95	MRC Superstrate Alumina (polished)	1027	H_2 2.5	12	1) 100 2) 0.1	1) 5 2) 15	–	–	1) $>10^{19}$ 2) $\sim10^{15}$	NM**	1.3x0.9 1.2	Poly; {110} pref. orient.
OCLI-96	Coors Vistal 5 Alumina (refired) (polished)	1027	H_2 2.5	12	1) 100 2) 0.1	1) 5 2) 15	–	–	1) $>10^{19}$ 2) $\sim10^{15}$	NM**	1.3x1.2 1.6	Poly; {110} pref. orient.
OCLI-97	$(01\bar{1}2)$ Sapphire (polished)	1028	H_2 2.5	12	1) 100 2) 1.75	1) 5 2) 15	–	–	1) $>10^{19}$ 2) $\sim10^{17}$	NM**	1.1x0.7 0.8	Epitaxial
OCLI-98	MRC Superstrate Alumina (polished)	1028	H_2 2.5	12	1) 100 2) 1.75	1) 5 2) 15	–	–	1) $>10^{19}$ 2) $\sim10^{17}$	NM**	1.9x0.5 0.95	Poly; {110} pref. orient.

*Films B-doped from B_2H_6-in-He (46 ppm); double layers, with 1 deposited first and then 2.
**NM = not measured
†Polycrystalline films: estimated from CVD parameters and other factors. Epitaxial films: measured by spreading resistance scans.

Table 2-32 (Cont)

SAMPLE NO.	SUBSTRATE MATERIAL	OBSERV. DEPOS. TEMP (°C)	CARRIER GAS AND FLOW RATE (ℓpm)	SiH_4 FLOW RATE (ccpm)	DOPANT GAS* FLOW RATE (ccpm)	FILM THICKNESS (μm)	AVE. GROWTH RATE (μm/min)	FILM RESISTIVITY (ohm cm)	HOLE CONCENTRATION† (cm^{-3})	HALL MOBILITY (cm^2/V-sec)	SAMPLE DIMENSIONS (cm) AND APPROX. AREA (cm^2)	FILM STRUCTURE AND/OR SURFACE TEXTURE
OCLI-99	Coors Vistal 5 Alumina (refired) (polished)	1028	H_2 2.5	12	1) 100 2) 1.75	1) 5 2) 15	–	–	1) $>10^{19}$ 2) $\sim10^{17}$	NM**	1.25x1.25 1.6	Poly; {110} pref. orient.
OCLI-100	MRC Superstrate Alumina (polished)	1030	H_2 2.5	12	1) 100 2) 0.5	1) 15 2) 5	–	–	1) $>10^{19}$ 2) $\sim10^{16}$	NM**	1.9x0.65 1.2	Poly; {110} pref. orient.
OCLI-101	Coors Vistal 5 Alumina (refired) (polished)	1030	H_2 2.5	12	1) 100 2) 0.5	1) 15 2) 5	–	–	1) $>10^{19}$ 2) $\sim10^{16}$	NM**	1.25x1.25 1.6	Poly; {110} pref. orient.
OCLI-102	$(01\bar{1}2)$ Sapphire (polished)	1030	H_2 2.5	12	1) 100 2) 1.75	1) 15 2) 5	–	–	1) $>10^{19}$ 2) $\sim10^{17}$	NM**	1.45x1.05 1.5	Epitaxial
OCLI-103	MRC Superstrate Alumina (polished)	1030	H_2 2.5	12	1) 100 2) 1.75	1) 15 2) 5	–	–	1) $>10^{19}$ 2) $\sim10^{17}$	NM**	1.8x0.6 1.1	Poly; {110} pref. orient.
OCLI-104	Coors Vistal 5 Alumina (refired) (polished)	1030	H_2 2.5	12	1) 100 2) 1.75	1) 15 2) 5	–	–	1) $>10^{19}$ 2) $\sim10^{17}$	NM**	1.25x1.2 1.5	Poly; {110} pref. orient.
OCLI-105	Coors Vistal 5 Alumina (refired) (polished)	1027-1030	H_2 2.5	12	1) 100 2) 0.1	1) 15 2) 5	–	–	1) $>10^{19}$ 2) $\sim10^{15}$	NM**	1.25x1.25 1.6	Poly; {110} pref. orient.
OCLI-106	MRC Superstrate Alumina (polished)	1027-1030	H_2 2.5	12	1) 100 2) 0.1	1) 15 2) 5	–	–	1) $>10^{19}$ 2) $\sim10^{15}$	NM**	1.1x0.85 0.94	Poly; {110} pref. orient.

*Films B-doped from B_2H_6-in-He (46 ppm); double layers, with 1 deposited first and then 2.
**NM = not measured
†Polycrystalline films: estimated from CVD parameters and other factors. Epitaxial films: measured by spreading resistance scans.

Table 2-33. Photovoltaic Properties of Diffused-junction* $n/p/p^+$ Solar Cells Fabricated in p/p^+ CVD Si Layers Grown on Various Insulating Substrate Materials by SiH_4 Pyrolysis in H_2 at ~1025°C

SAMPLE NO.	NOMINAL IMPURITY CONCENTRATION IN DEPOSITED P-LAYER (cm^{-3})	TUNGSTEN LAMP**						AMO SIMULATOR***					
		SAPPHIRE		VISTAL 5		HI REL SUPERSTR.		SAPPHIRE		VISTAL 5		HI REL SUPERSTR.	
		$V_{OC}^{\dagger}$ (mV)	$J_{SC}^{\dagger}$ (mA/cm^2)	$V_{OC}^{\dagger}$ (mV)	$J_{SC}^{\dagger}$ (mA/cm^2)	$V_{OC}^{\dagger}$ (mV)	$J_{SC}^{\dagger}$ (mA/cm^2)	$V_{OC}^{\dagger\dagger}$ (mV)	$J_{SC}^{\dagger\dagger}$ (mA/cm^2)	$V_{OC}^{\dagger\dagger}$ (mV)	$J_{SC}^{\dagger\dagger}$ (mA/cm^2)	$V_{OC}^{\dagger\dagger}$ (mV)	$J_{SC}^{\dagger\dagger}$ (mA/cm^2)
$t_p:t_{p+} \approx 15:5$													
OCLI-94	$\sim 10^{15}$	344	2.4			54	2.4	350	9.3			58	3.7
OCLI-95				93	3.1					124	7.1		
OCLI-96													
OCLI-91	$\sim 10^{16}$	370	2.4					388	7.6				
OCLI-92				79	2.6	57	2.7			90	4.1	58	4.5
OCLI-93													
OCLI-97	$\sim 10^{17}$	331	2.1			69	3.1	393	6.7			68	5.0
OCLI-98				70	3.0					72	4.8		
OCLI-99													
$t_p:t_{p+} \approx 5:15$													
OCLI-105	$\sim 10^{15}$			42	1.1	30	1.4			73	3.6	45	3.0
OCLI-106													
OCLI-100	$\sim 10^{16}$					42	1.7					55	2.9
OCLI-101				38	1 0					66	3.1		
OCLI-102	$\sim 10^{17}$	399	2.6			35	2.0	418	7.4			71	4.2
OCLI-103				21	0 88					39	2.6		
OCLI-104													
Control No. 1 (full 2x2 cm cell)	$\sim 5 \times 10^{15}$ (bulk crystal)	V_{oc} = 500 mV J_{sc} - 5 0 mA/cm^2						V_{oc} = 544 mV J_{sc} = 21.5 mA/cm^2					

*P diffusion for 20 min. at ~875°C, following 5 min. preheat, to produce junction ~0.4 μm deep.
**Approximately 1/2 sun intensity.
***~135 mw/cm^2 (no temperature control on sample).
†Average of values obtained on several individual mesa devices.
††Typical values obtained on individual mesas.

single-crystal control cell under the same illumination conditions. These relative responses to the predominantly long-wavelength radiation of the tungsten lamp indicate reduced charge collection efficiency deep in the cell structure; the generally lower J_{sc} values found in the structures with a thin p-type layer and a relatively thick p^+ layer are consistent with this explanation, since an appreciable part of the charge generation occurred in the thicker p^+ region where carrier diffusion lengths would be expected to be further reduced over those occurring in the p-type region.

The fact that, in general, about the same magnitude of V_{oc} values were observed for the same samples in both the tungsten lamp measurements and the AM0 solar simulator measurements is also consistent with this argument. That is, most of the added response seen as an increased J_{sc} value for a given cell under AM0 illumination over that found for only tungsten lamp illumination was due to the charges generated relatively close to the surface (and thus fairly near the junction) by the predominantly blue radiation of the xenon lamp used (together with a tungsten lamp) in the OCLI AM0 simulator. However, even under AM0 illumination none of the Si sheet cells produced a short-circuit current density exceeding ~45 percent of the J_{sc} generated by the control cell.

Third, although the table does not show the data, the cell responses under AM0 illumination were obtained not only with both lamps in use (providing the data given in the table) but also with the tungsten and xenon lamps used separately. These results showed that only for the cells in the epitaxial material on sapphire did the "blue response" (xenon lamp) exceed the "red response" (tungsten lamp). This may indicate a deeper junction was formed by the P diffusion in the polycrystalline samples than in the epitaxial films on sapphire.

This would be consistent with the concept of enhanced impurity diffusion in polycrystalline Si. Attempts were made on several occasions early in the program to delineate (by beveling and staining techniques) p-n junctions in the two types of material that had been processed simultaneously. The results, however, were not clearly conclusive. There appeared to be some evidence that P-diffused junctions in doped polycrystalline Si layers were slightly deeper than junctions similarly formed (simultaneously) in epitaxial Si layers (on sapphire) doped with the same concentration of added B. However, because of the difference in the active hole concentrations for two such films nominally doped the same (see Section 2.3.10) any conclusions about the cause of the apparently deeper junction in the polycrystalline material would be uncertain, at best, without further experimental evidence.

Fourth, in general, the responses for the group of structures with the $t_p:t_{p^+}$ ratio approximately 5:15 were considerably lower than those for the group in which this ratio was about 15:5, as might be expected. The former group might have exceeded the latter cells in performance if the presence of the heavily doped p^+ underlayer either had produced sufficient gettering action to improve carrier lifetimes in the upper p-type layer or had produced enough of a back-surface field to assist the charge collection process in the base region of the cell. Evidently neither occurred to any appreciable extent.

Finally, one of the main purposes of preparing this series of cell structures was to attempt to determine a preferred p-type base region doping concentration for both epitaxial and polycrystalline Si structures for use in the subsequently prepared 3x4 matrix of $n^+/p/p^+$ configurations for later experimental cell fabrication (see below). On the basis of the results in Table 2-33 it appeared that 10^{15} cm^{-3} was the best of the three concentrations used for the epitaxial configurations on sapphire.

For the relatively fine-grained polycrystalline Si on MRC Hi Rel Superstrate alumina, on the other hand, distinctly better results were obtained for the film doped to $\sim 10^{17}$ cm^{-3} boron concentration. It was known from work earlier in the program that this intended doping level actually resulted in an active carrier concentration of $\sim 5 \times 10^{15}$ cm^{-3} in polycrystalline Si films; thus, the 10^{15} cm^{-3} carrier concentration range was again indicated as preferred. The results for films on Vistal 5 were much better for the 10^{15} cm^{-3} concentration range, probably indicative of the presence of many large grains in the polycrystalline layers, resulting in performance intermediate between that of the epitaxial structures and that of the fine-grained polycrystalline devices, as would be expected.

It is striking that when estimates were made of the apparent minority carrier diffusion lengths in the devices listed in Table 3-33, based on the assumption that the diffusion length for electrons in the control cell was ~100μm and on examination of the red responses of the various cells, the values found for the epitaxial devices (1.4-3.0μm) were not much larger than those estimated for the cells on Vistal 5 (1.3-2.5μm) or the cells on Superstrate (1.3-1.7μm).

During the final two months of the program experiments were undertaken to prepare and test grown p-n junction solar cell structures in CVD Si sheet material, so that the photovoltaic performance of such all-deposited cells could be compared with the performance of diffused-junction cells in CVD Si base material.

Experiments with PH_3 as a dopant gas, to achieve n-type doping of a thin surface layer to produce deposited n/p structures, were begun with a PH_3 source gas in a nominal 46 ppm concentration in He. Initial experiments were devoted to an investigation of the range of n-type doping that could be achieved with the available PH_3 source tank, and to establishing a doping curve, i.e., measured electron concentration vs added concentration (flow rate) of PH_3-in-He. In one experiment a source of AsH_3 (213 ppm in H_2) was substituted for the PH_3 to determine if a higher apparent donor concentration could be obtained than had been achieved with the PH_3; however, no significant improvement in incorporated dopant was found, so the decision was made to continue use of PH_3 as the dopant gas. The resulting doping curve was shown earlier (Figure 2-31).

On the basis of the known parameters of conventionally fabricated single-crystal shallow-junction n/p Si solar cells (especially the heavily doped diffused surface layer) and of the known properties of CVD Si sheet material

as prepared in this program, it was determined that the most advantageous all-deposited structure to prepare in the first series of experiments would be a $n^+/p/p^+$ configuration. The p^+ region, deposited first on the selected substrate, would be doped to $>10^{19}$ cm^{-3} and would be 5μm or less in thickness. The p-type base region would be grown directly on the p^+ layer and would have a thickness and a doping concentration to be determined, although the thickness would be in the 15-75μm range and the B doping concentration in the range 10^{15}-10^{17} cm^{-3}. The n^+ surface layer would be heavily doped (~10^{19} cm^{-3}) and would be ≤0.4μm thick. It was intended that a series of experimental cell structures fabricated with these ranges of parameters would be characterized in order to establish more exactly the preferred cell parameters for use in further investigations.

It had been established at the time of the contract modification that authorized the investigation of all-deposited CVD Si cell structures that the first major study should involve simultaneous growth of the three-layer composites on polycrystalline alumina substrates and on single-crystal sapphire baseline-reference substrates. The aluminas were selected rather than the glasses for the first series of experiments because of the greater amount of experience with polycrystalline Si film growth on those materials, the closer similarity of the properties to those of the comparison epitaxial films on sapphire, and the greater flexibility in selecting doping parameters with substrates that tolerate a H_2 atmosphere and temperatures above 1000°C.

The requirement for a very thin heavily doped n^+ region in these structures necessitated some preliminary experiments with short growth periods at high PH_3-in-He flow rates, after the doping curve of Figure 2-31 had been established. Growth rate data obtained in a series of such experiments are given in Figure 2-101, which shows that n^+-doped depositions of 12 to 24 sec duration produced layer thicknesses in the required range of 0.25-0.50μm for the first series of $n^+/p/p^+$ cell structures. It was not definitely established if an incubation period existed for Si layer growth upon first exposure of the sapphire (or other) substrate to the SiH_4-H_2-PH_3 (in He) mixture, i.e., if there was a brief initial period during which "constructive" growth of a continuous layer of Si had not yet begun. It seems certain that such a "dead time" does occur in CVD growth systems such as this, caused by various factors, but the experiments in this series did not provide a quantitative indication of it.

Several deposition experiments of an exploratory nature were undertaken to determine if the desired $n^+/p/p^+$ structures could be grown with adequate control of layer thickness, doping concentration, and structural quality. Substrates of MRC Hi Rel Superstrate polycrystalline alumina, Coors Vistal 5 and Vistal 1 polycrystalline aluminas, and single-crystal sapphire were used in these experiments. Spreading resistance measurements were made on the three-layer Si composites grown on sapphire and on MRC Hi-Rel Superstrate alumina in one of the experiments and on the three-layer epitaxial composite grown on sapphire in a second experiment.

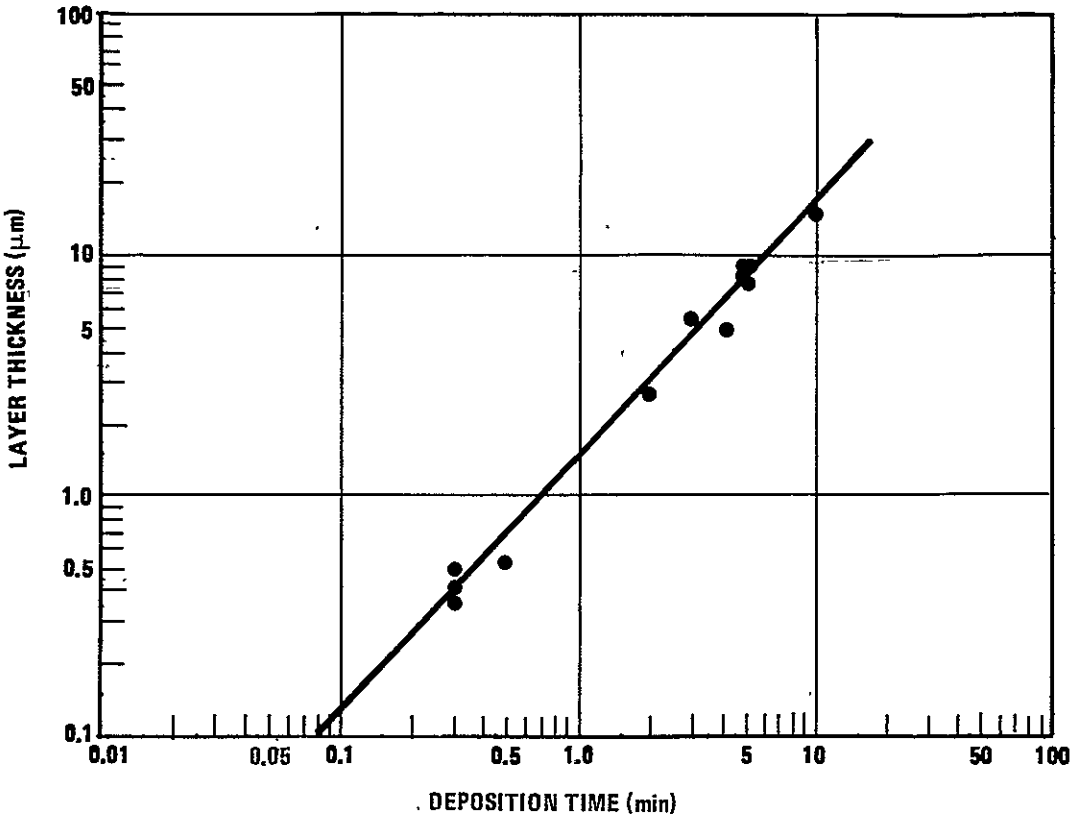

Figure 2-101. Measured Thicknesses of n+ ($n>10^{19}$ cm^{-3}) P-doped CVD Si Layers Produced by SiH_4 Pyrolysis at ~1025°C in H_2 on Sapphire Substrates, Using 46 ppm PH_3-in-He as Dopant Gas.

The epitaxial composite in the first experiment was found to have a p^+ layer ~8.5μm thick with essentially constant resistivity of 0.01 ohm-cm (corresponding to a carrier concentration of ~$1x10^{19}$ cm^{-3}) throughout its thickness. The p region was only about 2.3μm thick, with a resistivity of 0.1-0.2 ohm-cm and a corresponding carrier concentration of 1-$3x10^{17}$ cm^{-3} in most of the layer, although a gradual increase in carrier concentration from ~10^{17} to ~$10^{19}cm^{-3}$ was found beginning at a depth of ~1.7μm and extending to the p^+ region at ~2.5μm below the surface. The n^+ surface layer appeared to be about 0.2μm thick, with a concentration of ~$2x10^{18}$ cm^{-3} at the surface and a maximum value of ~$4x10^{18}$ cm^{-3} occurring at a depth of ~0.1μm, below which a gradual decrease in net electron concentration occurred over the next 0.1μm (to the onset of the p-type region).

The companion polycrystalline composite grown on MRC alumina had a p^+ layer ~12.5μm thick, with a measured resistivity that varied gradually from ~0.015 ohm-cm at its shallowest point to ~0.1 ohm-cm at the Si-alumina interface. The p region was about 3μm thick and varied continuously in resistivity from a maximum of ~0.6 ohm-cm just below the upper boundary of the layer to ~0.015 ohm-cm at the onset of the p^+ region. The n^+ layer was not detected with certainty by the SR probe, primarily because of the relatively rough surface that is formed on these polycrystalline Si films, with surface features having vertical dimensions similar to the actual thickness of the deposited n^+ region. It appeared from the SR probe scan that the n^+ region was the order of 0.5μm or less in thickness, consistent with the thickness observed in the epitaxial sample on sapphire.

The epitaxial composite film on sapphire from the second experiment had a p^+ region ~13μm thick and a resistivity that was essentially constant at ~0.007 ohm-cm (~$2x10^{19}$ cm^{-3}) throughout its thickness. The p-type region of this sample was ~4.6μm thick, with a resistivity of about 0.3 ohm-cm (~$6x10^{16}$ cm^{-3} carrier concentration) to a depth of about 4μm, below which a gradual transition to the p^+ layer occurred over a distance of ~1μm. The n^+ deposited layer was found to be 0.35μm thick, with a resistivity of ~0.05 ohm-cm (average) and a net carrier concentration of ~$2x10^{18}$ cm^{-3} at the surface and a maximum value of ~$4x10^{18}$ cm^{-3} occurring at a depth of 0.05-0.2μm, with a gradual decrease in carrier concentration below that and extending to the beginning of the p-type region.

The similarity in electrical properties of the n^+ layers in the two epitaxial samples indicated that the desired control of the n^+ doping process had been achieved; essentially the same parameters were used for the n^+ region in the two experiments. The B concentrations (that is, the B_2H_6-in-He flow rates) used in forming the p regions in the two cases were different, however, by a factor of 5 (0.5 ccpm in the first experiment and 0.1 ccpm in the second experiment). The carrier concentrations measured in the two experiments (1-$3x10^{17}$ cm^{-3} in the first experiment and ~$6x10^{16}$ cm^{-3} in the second) were in about the right ratio for this difference in added dopant concentration, so for the p-type region also it appeared that the needed control had been realized.

The series of $n^+/p/p^+$ composite solar cell structures to be used to determine preferred cell growth parameters and to provide a comparison between deposited-junction and diffused-junction cells in CVD Si sheet material of otherwise identical properties was to be grown in a three-row four-column matrix of deposition experiments. It was planned that evaluation of the matrix of samples so produced would establish the best range of electron concentrations (i.e., P dopant concentrations) for the thin (<0.5μm) n^+ deposited layer on the front of the cell and the best range of hole concentrations (i.e., B dopant concentrations) for the thick p-type base region of the cell structure. Three different "target" n^+ concentrations and three different p-region concentrations were to be used, with the first column of the four columns of the matrix involving no deposited n^+ layer - the n^+ region of the final cell structure in this case to be produced by P diffusion by standard processing techniques at OCLI.

Each deposition experiment in the 3x4 matrix was planned to involve at least three different substrates: 1) single-crystal sapphire, to provide a "best case" heteroepitaxial structure that would serve as a basis for comparison of the results obtained in the polycrystalline structures; 2) relatively small-grained polycrystalline alumina (MRC Hi Rel Superstrate, polished); and 3) large-grained polycrystalline alumina (Coors Vistal, with up to five refirings to enhance grain size), to provide large-grained polycrystalline Si structures expected to be intermediate in photovoltaic performance between the epitaxial structures and those obtained on the MRC substrates.

The target carrier concentrations (in terms of the epitaxial composites on sapphire substrates) selected for the layers in the planned 3x4 matrix are given in Table 2-34, which indicates the sequence number of the Si CVD experiment that was devoted to filling the requirements of each space in the matrix. In each case the n^+ layer was to be 0.25-0.5μm thick, the p layer ~15μm thick, and the p^+ layer ~5μm thick.

After the work on preparing samples for the original matrix had begun it appeared that it would be advisable to include some test structures with much thicker p-type base regions, to evaluate the effects upon cell performance of the additional absorption of AM0 illumination that would result from a significantly greater thickness above the p^+ layer. Therefore, two more rows were added to the original 3-row matrix, although it was intended that only two of the cell configurations, represented by Column 1 (no deposited n^+ layer - junction to be formed by P diffusion) and Column 3 (n^+ deposited layer carrier concentration ~$1x10^{19}$ cm^{-3}), would be prepared in each of the two added rows (Row 4 and Row 5).

Finally, another row (Row 6) was also added to the planned matrix to allow for the sizeable difference in available carrier concentrations found to occur (see Figure 2-69) in p-type B-doped polycrystalline layers and epitaxial layers on alumina substrates, especially in the nominal B doping range for the p-type base regions ($3x10^{15}$-$5x10^{16}$ cm^{-3}) represented by the three rows of the original matrix. Thus, the target doping level (hole concentration) for Row 6, in terms of the measured hole concentration in the epitaxial film

Table 2-34. Si CVD Experiment Matrix for Preparing Composite n+/p/p+ Solar Cell Structures*, Showing Layer Carrier Concentrations† and Experiment Sequence Numbers

	t_p(μm) t_{p+}(μm)	Col 1 No depos n+ layer	Col 2 n+~$3x10^{18}$ cm^{-3}	Col 3 n+~$1x10^{19}$ cm^{-3}	Col 4 n+~$4x10^{19}$ cm^{-3}
Row 1 p~$3x10^{15}$ cm^{-3}	15/5	342	343	346	**
Row 2 p~$1x10^{16}$ cm^{-3}	15/5	333	329	330	331
Row 3 p~$5x10^{16}$ cm^{-3}	15/5	341	339	338	340
Row 4 p~$1x10^{16}$ cm^{-3}	40/5	335	–	334	–
Row 5 p~$1x10^{16}$ cm^{-3}	65/5	336	–	337	–
Row 6 p~$2x10^{17}$ cm^{-3}	15/5	344	345	347	–

*Thickness of p+layer ~5 μm.

†Hole concentration in p+layer >10^{19} cm^{-3}

**This configuration was later determined to be unnecessary, based on results of preceding experiments for Rows 3 and 3.

on sapphire, was to be ~2×10^{17} cm^{-3} which would correspond to available hole concentrations the order of 10^{16} cm^{-3} in polycrystalline films on polycrystalline aluminas.

As indicated in Table 2-34, 18 Si CVD experiments were carried out to provide the desired combinations of carrier concentrations (i.e., doping levels) for this investigation. A total of 54 samples was generated for possible processing and characterization, of which 45 were actually processed into solar cells and evaluated in terms of photovoltaic properties before the experimental performance period of the contract ended.*

The two-layer p/p^+ samples (Column 1) were P-diffused at OCLI by the usual procedure to produce junctions ~0.3μm deep. These samples were then processed together with the three-layer $n^+/p/p^+$ samples (Columns 2,3,4) and one or more single-crystal 1-3 ohm-cm p-type Si solar cell blanks as controls to make devices. In one of the groups of samples processed together (the Row 2 samples) the single-crystal control wafers included, in addition to the customary solar cell blank of nominal 12-14 mil thickness, two specially prepared ultra-thin (~35μm) single-crystal control wafers of 2 ohm-cm (100)-oriented Si. These were included to determine if the differences in the thicknesses of the absorbing region in the Si sheet samples and in the single-crystal control samples in previous groups of processed cells had resulted in inequitable comparisons of performance of the two cell types. One of the ultra-thin control cells was provided with a front-surface contact to the p-type base region, along one edge of the sample, as was used on the Si sheet samples, while the second ultra-thin control cell was provided with a full-area Aℓ backside contact to the p-type base region plus a p^+ diffused region below the contact to give a back-surface field to (possibly) augment the collection efficiency in the base region.

In all cases the structures were processed directly into mesa-arrays, with the mesa diameter 2mm, so that an indication of sample uniformity could also be acquired from the photovoltaic measurements.

The results obtained with the samples of the original matrix (Rows 1-3, Columns 1-4, Table 2-34) under simulated AM0 illumination are summarized in Table 2-35. The data are arranged in the matrix configuration that was used in Table 2-34, with open-circuit voltages V_{oc} and total short-circuit current densities J_{sc} given for each sample. The samples of these three rows of the original matrix were processed in two groups - one group included all of the Row 2 samples, as indicated above, and the other group included the samples of Row 1 and Row 3 together with standard-thickness control wafers. Because of a difference in the intensity of the solar simulator output used in characterizing the samples of Row 2 the data for those samples have been normalized to AM0 illumination for presentation in this table. In all cases the sample temperature was allowed to drift under the AM0 illumination - i.e., no sample temperature control was employed. The data for a given sample are representative of an average or typical mesa among several measured on each sample.

---

*The samples of Row 6 were not processed into completed cells because of time limitations at OCLI.

Table 2-35. Normalized Photovoltaic Responses to Simulated AM0 Illumination for Deposited-junction* and Diffused-junction† $n^+/p/p^+$ Si Solar Cells** in Polycrystalline and Epitaxial CVD Sheet Material Grown on Polycrystalline Alumina and Single-crystal Sapphire Substrates

P-Layer Carrier Concentration and Substrate	DIFFUSED JUNCTION†		DEPOSITED JUNCTIONS*					
	Col 1		Col 2		Col 3		Col 4	
	No deposited n+ layer		$n+\sim3\times10^{18}$ cm^{-3}		$n+\sim1\times10^{19}$ cm^{-3}		$n+\sim4\times10^{19}$ cm^{-3}	
	V_{oc} (mV)	J_{sc} (mA/cm^2)	V_{oc} (mV)	J_{sc} (mA/cm^2)	V_{oc} (mV)	J_{sc} (mA/cm^2)	V_{oc} (mV)	J_{sc} (mA/cm^2)
Row 1 $p\sim3\times10^{15}$ cm^{-3}								
MRC Superstrate	72	2.01	132	2.63	127	6.35	–	–
Coors Vistal 5	102	2.49	112	1.80	112††	2.49††	–	–
S.c. sapphire***	525	23.2	412	8.15	382	8.02	–	–
Control 1								
Row 2 $p\sim1\times10^{16}$ cm^{-3}								
MRC Superstrate	44	4.62	69	1.59	53	1.74	32	0.97
Coors Vistal 5	63	2.36	88	2.02	63	1.45	63	1.68
S.c. sapphire***	441	9.14	403	8.41	365	7.70	384	6.93
Control A (std)	530	25.0						
Control B$^{\odot}$(ultra-thin)	605	25.5						
Control C$^{\oplus}$(ultra-thin)	82	3.90						
Row 3 $p\sim5\times10^{16}$ cm^{-3}								
MRC Superstrate	44	1.38	82	1.80	147	3.32	67	1.88
Coors Vistal 5	62	1.66	112	1.66	172	3.59	107	2.49
S.c. sapphire***	387	9.98	372	9.29	382	7.88	357	9.03
Control 1 (as in Row 1)	525	23.2						

*Thickness of deposited n+ layer ~0.3 μm.

† p Diffused from $POC\ell_3$ source at 875°C for 20 min to produce junction ~0.3 μm deep.

**Total cell thickness ~20 μm: p layer ~15 μm thick, p+ layer ~5 μm thick (hole concentration in p+ layer $>10^{19}$ cm^{-3}). Cells in form of individual mesas 2mm in diameter on each sample tested.

††This composite (only) grown on Vistal 4 substrate.

$^{\odot}$ Ultrathin single-crystal wafer (~35 μm) with full-area $A\ell$ back contact and p+ diffused back-surface-field layer.

$^{\oplus}$ Ultrathin single-crystal wafer (~35 μm) with front contact to base layer, as in Control A and Control 1.

***S.c. = single-crystal.

First, these data show the expected major differences in photovoltaic response for the polycrystalline cells and the epitaxial cell for a given matrix position, i.e., for given doping concentrations added to the n^+ and the p-type layers during CVD growth. Also, the polycrystalline cells on large-grained Vistal (Vistal 5 except in experiment 346 - Row 1, Column 3 - where Vistal 4 was used) were consistently better than those on relatively fine-grained MRC Hi Rel Superstrate for a given doping configuration in the deposited $n^+/p/p^+$ structure, as had been observed at various times earlier in the program.

Second, the diffused-junction cell (Column 1) consistently gave better photoresponse than did the deposited-junction cells (Columns 2,3,4) in the epitaxial structures on sapphire monitor substrates for any of the three n^+ layer concentrations examined in a given row of the matrix, i.e., for a given p layer concentration (with the possible exception of the epitaxial deposited-junction cell of experiment 343 (Row 1, Column 2), which may have been slightly better than the corresponding diffused-junction device).

Third, in terms of the epitaxial cells made on sapphire monitor substrates, it appeared that the better cells were made in the p-type base layers that were B-doped to ~$5x10^{16}$ cm^{-3} (Row 3), whether by P diffusion or by deposition of the n^+ layer. Among the deposited-junction epitaxial devices utilizing this base layer there was relatively little preference, although the cell with the deposited n^+ layer at a concentration of ~$3x10^{18}$ cm^{-3} (Column 2) was probably best. However, the differences among the sapphire-based cells in the three rows (i.e., for the three p-type layer concentrations) were relatively minor overall.

Fourth, there is relatively little difference among the devices formed by P diffusion and those in which the P-doped layer was deposited to form the photovoltaic junction for the polycrystalline Si sheet structures grown on large-grained Vistal alumina substrates. If anything, the deposited-junction devices are somewhat better for a given p-layer composition (i.e., in a given row of the matrix). Among the deposited $n^+/p/p^+$ structures on Vistal substrates it appeared that the better ones were those with p~$5x10^{16}$ cm^{-3} (Row 3), and of those the sample with the n^+ layer concentration ~$1x10^{19}$ cm^{-3} exhibited the best photovoltaic response.

Fifth, the polycrystalline composite structures on fine-grained MRC Hi Rel Superstrate alumina resulted in better photovoltaic properties for p-layer doping levels of ~$3x10^{15}$ and ~$5x10^{16}$ cm^{-3} (Rows 1 and 3) when the junction was formed in situ by deposition of an n^+ layer of ~$1x10^{19}$ cm^{-3} concentration than when it was formed by P diffusion. For a p-layer concentration of ~$1x10^{16}$ cm^{-3} (Row 2) the diffused-junction device appeared to be marginally better than the deposited-junction devices.

The fourth-quadrant I-V characteristics obtained under AM0 illumination of mesa devices on several of the samples of the main matrix are shown in Figure 2-102. These curves serve to illustrate the various comparisons made in the above discussion.

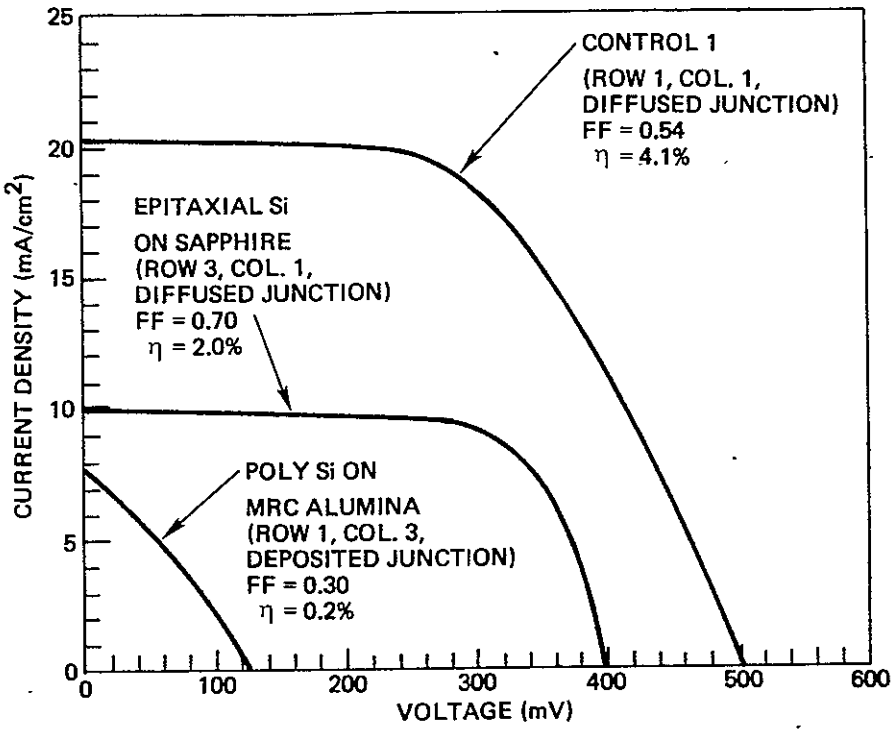

Figure 2-102. Fourth Quandrant I-V Characteristics under AM0 Illumination for Several Individual Mesa Solar Cells on Samples of Main 3x4 Matrix of Table 2-34 (see also Table 2-35).

To generalize from the above results, it appears that the best cells in epitaxial layers in the 20μm thickness range on sapphire were obtained by P diffusion into p/p^+ composite structures grown by CVD, with the p-layer concentration ~$5x10^{16}$ cm^{-3}, although the latter did not appear as a critical parameter in the $3x10^{15}$-$5x10^{16}$ cm^{-3} range investigated.

For polycrystalline composite layers in the same thickness range deposited on large-grained polycrystalline alumina (refired Vistal), the two methods of junction formation produced similar results, although slightly better photovoltaic response was obtained in deposited-junction devices with n^+ in the range 1-$4x10^{19}$ cm^{-3} and the deposited p-layer concentration ~$5x10^{16}$ cm^{-3}.

For fine-grained polycrystalline composite layers grown on polycrystalline alumina substrates, such as MRC Hi Rel Superstrate, it appears that generally better results were obtained by making deposited junctions rather than diffused junctions, with the p-layer concentration evidently not critical within the range studied but the n^+ layer concentration preferably ~$1x10^{19}$ cm^{-3}

These observations are generally consistent with the findings of the investigations carried out during earlier stages of the program, although the intercomparisons possible with a large number of samples of fairly closely controlled properties served to strengthen some of the earlier observations.

The samples prepared in the four experiments of Rows 4 and 5 of the matrix (see Table 2-34) were processed separately from the two groups of samples that constituted the first three rows. The same procedures and parameters were used in producing the P-diffused junctions as were used in the preceding samples of the main matrix. Standard control wafers of normal thickness were processed simultaneously, and mesas 2mm in diameter were again produced by masking and etching techniques on all of the samples involved.

A summary of the measured photovoltaic properties of typical individual mesas on each of the samples is given in Table 2-36. Three or four mesas were characterized on each of the samples, using simulated AMO illumination (without sample temperature control). To facilitate comparison of the photovoltaic responses of these thicker sheet samples with those of the otherwise similar samples of the main matrix (Row 2), the observed (not normalized) characteristics of the latter samples are also given in Table 2-36.

The results constitute a moderately convincing demonstration of the importance of having an adequate thickness of Si in the active region of a solar cell to absorb a major fraction of the incident solar radiation. The three groups of cells compared in the table had active p-type base regions of ~15, ~40, and ~65μm thicknesses (disregarding the 5μm p^+ underlayer common to all three groups and characterized by short minority-carrier diffusion lengths because of the very heavy B doping concentration).

For the epitaxial structures on sapphire the measured photoresponse increased directly with the p-layer thickness, with the difference between the 40μm and the 65μm p-layer cells being more pronounced for the deposited-junction samples than for the diffused-junction cells. For both types the response of the 40μm cell was appreciably better than that of the 15μm cell.

For the polycrystalline composites the variations in response with p-layer thickness were not as sharply defined. For the structures on large-grained alumina substrates (Vistal) the thicker deposited-junction devices were much superior to the 15μm devices, although there was relatively little difference between the 40μm and the 65μm samples. The diffused-junction structures, on the other hand, appeared to be much better in the 40μm samples; for reasons that are not clear the responses of the mesa devices in the diffused-junction 65μm sample were about the same as those in the 15μm sample.

The situation for the fine-grained polycrystalline devices on MRC Hi Rel Superstrate alumina was more ambiguous. The deposited-junction devices were best in the structures with 40μm p layers, while the diffused-junction devices were better in the 65μm samples than in the 40μm samples. In these fine-grained Si composites the photovoltaic responses of the devices fabricated in the relatively thin 15μm p-layer samples compared favorably with the responses of the thicker samples. It appeared that factors other than thickness alone were involved in determining the relative response in the polycrystalline structures.

Table 2-36. Photovoltaic Responses* to Simulated AM0 Illumination for Deposited-junction** and Diffused-junction† $n^+/p/p^+$ Si Solar Cells†† in Polycrystalline and Epitaxial CVD Sheet Material of Different Thicknesses on Polycrystalline Alumina and Single-crystal Sapphire Substrates.

P-LAYER CARRIER CONCENTRATION AND SUBSTRATE	t_p (μm) / t_{p^+} (μm)	DIFFUSED JUNCTION†		DEPOSITED JUNCTIONS*					
		COL. 1 No Deposited n^+ Layer		COL. 2 $n^+\sim3\times10^{18}$ cm^{-3}		COL. 3 $n^+\sim1\times10^{19}$ cm^{-3}		COL 4 $n^+\sim4\times10^{19}$ cm^{-3}	
		V_{oc} (mV)	J_{sc} (mA/cm^2)	V_{oc} (mV)	J_{sc} (mA/ cm^2)	V_{oc} (mV)	J_{sc} (mA/cm^2)	V_{oc} (mV)	J_{sc} (mA/cm^2)
Row 2 $p\sim1\times10^{16}$ cm^{-3}	15/5								
MRC Superstrate		35	3.06	55	1.05	42	1.15	25	0.64
Coors Vistal 5		50	1.56	70	1.34	50	0.96	50	1.11
S.c. Sapphire***		350	6.05	320	5.57	290	5.10	305	4.59
Control A (Std.)		420	16.6						
Control B⊕ (Ultrathin)		480	16.9						
Control C⊙ (Ultrathin)		65	2.58						
Row 4 $p\sim1\times10^{16}$ cm^{-3}	40/5								
MRC Superstrate		32	0.76			70	1.43		
Coors Vistal 5		95	2.23			140	2.55		
S.c. Sapphire***		380	8.92			305	6.05		
Control 2 (Std.)		{480 480	18.8 22.3						
Row 5 $p\sim1\times10^{16}$ cm^{-3}	65/5								
MRC Superstrate		50	1.08			35	0.45		
Coors Vistal 5		45	0.76			145	2.23		
S.c. Sapphire***		340	9.55			340	7.96		
Control 2 (same as in row 4)		{480 480	18.8 22.3						

*Data given as measured, without any corrections or "normalizing".
**Thickness of deposited n^+ layer~0.3 μm.
†P diffused from POCℓ_3 source at 875°C for 20 min to produce junction~0.3 μm deep.
††Cells in form of individual mesas 2mm in diameter on each sample tested. Hole concentration in 5 μm p^+ layer >10^{19} cm^{-3}.
⊕Ultrathin single-crystal wafer (~35 μm) with full-area Aℓ back contact and p^+ diffused back-surface-field layer.
⊙Ultrathin single-crystal wafer (~35 μm) with front contact to base layer, as in Control A and Control 2.
***S.c. = single-crystal.

It seems reasonable to expect p-type base layer thickness to have a measurable influence on photovoltaic response (mainly photocurrent) in structures in which charge carrier collection might be expected to be effective at significant distances into the p region, beyond the junction. This could occur in good quality single-crystal base material, or highly perfect epitaxial material, where minority carrier diffusion lengths comparable with the thickness of the p-type base region might exist. However, in the heteroepitaxial Si layers on sapphire substrates, for which electron diffusion lengths the order of only a few μm have been estimated earlier in the program, it is not clear how added layer thicknesses permitting absorption of more of the entering radiation could produce significant increases in measured photocurrent, as was observed in the samples of Rows 4 and 5 (Tables 2-34 and 2-36). For polycrystalline layers on aluminas, however, where most of the collected carriers are probably generated significantly closer to the junction than in the epitaxial material, it is not surprising to find the thinner (e.g., 15μm) layers competitive with the thicker ones; the optimum p-layer thickness in these polycrystalline structures is probably determined by a complex set of interrelated parameters that includes not only thickness but also other factors that are not yet identified.

3. CONCLUSIONS AND RECOMMENDATIONS

The chemical vapor deposition (CVD) method for direct growth of Si sheet on various candidate substrate materials was investigated experimentally to establish the suitability of the technique for use in fabricating large-area low-cost Si solar arrays for terrestrial photovoltaic converter applications. The principal CVD process used was silane (SiH_4) pyrolysis, although some experiments were done with the dichlorosilane (SiH_2Cl_2) pyrolysis process.

Of the five technical goals established for the contract (see Introduction) the first three are considered to have been satisfactorily achieved at some point in the program, although not necessarily actively practiced throughout the conduct of the work: (1) 30cm^2 Si sheet sample area; (2) 5μm/min Si sheet deposition rate; and (3) 20 to 100μm Si sheet thickness. The achievement of 100μm average grain size in the Si sheet samples, the fourth technical goal, did not occur for the low-cost substrates such as glasses--where it was most desirable--but did occur with certain polycrystalline alumina substrates in which individual crystal grains were in that size range or larger. The goal of intragrain dislocation densities $<10^4$ per cm^2 was almost certainly not achieved, although the question was not even pursued in any of the Si sheet samples prepared during the contract since it was not regarded as a requirement of major importance in polycrystalline films of the type investigated in this program.

The principal conclusions reached as a consequence of the work described in this report are as follows:

1. There are several glasses with properties compatible with CVD Si growth from SiH_4 if an inert atmosphere, such as He, is used; these include Corning Code 1715 and Owens-Illinois GS211 and GS213.

2. There is a maximum in the growth-rate vs temperature curve for SiH_4 pyrolysis in a He atmosphere at about 850°C that sets an upper limit on Si growth rates achievable with glass substrates.

3. Strong preferred orientation is found in polycrystalline CVD Si films grown by SiH_4 pyrolysis on these amorphous glasses, with the degree of orientation being dependent on both deposition temperature and film thickness. Si films on Corning Code 1715 glass tend to be {100} oriented, while those on the Owens-Illinois GS series of glasses tend to be {110} oriented, indicating an influence of glass composition on Si film orientation.

4. There is evidence of a fairly strong effect on the electrical properties of CVD Si films on glass substrates due to entry into the deposited film of impurities from the glass, which appear to produce donor centers in the Si. There is indication of a possible limit the order of 10^{18} cm^{-3} on the available hole concentration that can be produced in B-doped polycrystalline Si films on glasses by the SiH_4 process at ∿850°C in He.

5. The quality of available lower-purity (i.e., <99 percent) alumina and similar ceramics is not adequate for the production of uniform-quality CVD Si sheet. These ceramics typically consist of at least two distinct phases - crystallites of the major constituent (e.g., α-Al_2O_3) distributed in a matrix of a glassy phase (usually SiO_2) - and film nucleation and growth tend to proceed differently (and not in complementary fashion) on these different phases.

6. High-purity (≥99.5 percent) ceramics, especially aluminas, are too costly to be considered as inexpensive substrate materials, and manufacturers do not offer encouragement that future developments will produce significant price reductions. The large-grained high-purity aluminas, such as refired Coors Vistal, support growth of correspondingly large-grained CVD Si sheet (some grain sizes in excess of 300μm) that is locally epitaxial on substrate grains that are favorably oriented crystallographically.

7. No improvement in either average film properties or grain size results from use of a two-step Si CVD process on glass substrates in which an initial continuous layer (≤1μm thick) is deposited by SiH_4 pyrolysis in He at ~850°C and a second layer is deposited by pyrolysis of a SiH_4-HCl mixture.

8. There is evidence of a change in the size and distribution of islands in partial-coverage layers of CVD Si grown by SiH_4 pyrolysis at ~850°C in He on substrates of several glasses and single-crystal sapphire when the deposit is annealed in situ, without concurrent deposition, at the growth temperature.

9. Generally poor photovoltaic performance is exhibited by solar cells fabricated in CVD Si sheet grown by SiH_4 pyrolysis directly onto substrates of aluminas, glasses, or even single-crystal sapphire. V_{oc} values up to ~80 percent of those of single-crystal Si control cells are obtained, but J_{sc} values only 40 to 70 percent of those of a control cell are obtained under simulated AMO illumination. Depressed long-wavelength response and other performance factors indicate low minority-carrier (electron) diffusion lengths are characteristic of the n/p cell structures made in this Si sheet material and are probably primarily responsible for the poor observed properties.

10. Epitaxial p-type (B-doped) CVD Si sheet grown on single-crystal Si substrates by SiH_2Cl_2 pyrolysis in H_2 at ~1075°C provides relatively good photovoltaic performance (simulated AMO illumination) in solar cell structures produced by P diffusion to form the p-n junctions. V_{oc} values of ~560mV, J_{sc} values of ~22 mA/cm^2, curve fill factors of ~0.7, and power efficiencies of 6-7 percent are found in these uncoated cells. (This Si deposition reaction was not used to grow polycrystalline sheet material on other substrates during this program, however.)

11. The presence of a p^+ layer below and adjoining a p-type (B-doped) CVD Si polycrystalline or epitaxial layer, on alumina or sapphire substrate, respectively, enhances the photovoltaic response of solar cell structures formed by P diffusion into the p layer.

12. A comparison of the photovoltaic response of P-diffused and P-doped in-situ-grown $n^+/p/p^+$ solar cell structures ~20μm thick on polycrystalline fine-grained and large-grained alumina substrates and on single-crystal sapphire substrates shows that the deposited junctions are superior in the fine-grained Si sheet, the two are about equal in the large-grained Si sheet (with a slight preference for the deposited junctions), and the diffused junctions are superior in the epitaxial structures, for given doping concentrations in the p layer. In all cases the epitaxial cells are much better than the polycrystalline cells, mainly because of current collection (carrier diffusion length) effects and junction leakage current effects, and the large-grained polycrystalline cells are better than the fine-grained cells. Best dopant concentrations in the p layer appear to be ~5×10^{16} cm^{-3} for the epitaxial and the large-grained polycrystalline structures, but no critical dependence upon concentration in the 3×10^{15}-5×10^{16} cm^{-3} range is found for the fine-grained polycrystalline structures.

13. A comparison of diffused-junction and deposited-junction $n^+/p/p^+$ structures in three different p-layer thickness ranges (~20, ~45, and ~70μm total thickness) on the same three classes of substrate shows a direct increase in photovoltaic response with p-layer thickness for the epitaxial cells but less distinct differences for the polycrystalline cells. The two thicker cells are much better (and about equal) in the large-grained polycrystalline structures, but there are few differences in performance among the devices in the three thicknesses for the fine-grained polycrystalline sheet. In the latter case factors other than thickness alone evidently determine the relative responses.

A number of important questions remain unresolved at the conclusion of this contract. The main issues include the following:

1. Is there a real upper limit on the available carrier (hole) concentration that can be introduced by B doping into polycrystalline Si films produced on glasses by CVD processes, or by the SiH_4 process alone?

2. Is it possible to alter significantly the final average grain size in polycrystalline CVD Si films grown on glasses, by means of in situ annealing, vapor-phase etching, or other techniques?

3. Is there a suitable low-cost substrate material (competitive with commercial glasses in terms of production costs) that has properties that will enhance grain growth and/or promote highly oriented (perhaps even epitaxial) growth in CVD Si sheet?

4. What are the optimum impurity doping concentrations (and available carrier concentrations) for the layers of a solar cell structure in polycrystalline Si sheet on glass (or other low-cost) substrates?

5. What junction formation technique - in situ deposition, ion implantation, diffusion, or other - is best for producing $n^+/p/p^+$ (or other suitable) solar cell structures in polycrystalline Si sheet on glasses or other low-cost substrate materials?

6. Are other CVD reactions than SiH_4 pyrolysis more suitable for producing large-grained polycrystalline Si films with improved photovoltaic properties on glasses or other low-cost materials?

There are also other technical questions that were raised by some of the results of the work described in this report, and these as well as the preceding list of major unresolved problems could be largely answered by additional experimental work in the areas outlined below. It is recommended that the following investigations be undertaken to complete the studies begun in this contract program and - more importantly - to provide the necessary full evaluation of the CVD process as a possible means for producing Si sheet material (directly on low-cost substrates) having adequate properties for the requirements of the national terrestrial photovoltaic conversion program.

1. Make experimental comparison of SiH_4 pyrolysis with SiH_2Cl_2 pyrolysis (and possibly $SiHCl_3$ and $SiCl_4$ reactions) to determine the most suitable process for producing large-grained polycrystalline Si sheet material by CVD on glasses or other low-cost substrates.

2. Investigate other doping impurities than B and other cell configurations than n/p and $n^+/p/p^+$ for obtaining necessary carrier concentrations, cell series resistance, and photovoltaic response for polycrystalline Si solar cell structures on glasses and similar substrates.

3. Investigate and develop substrate materials (glasses, ceramics, glass-ceramics, composites) that are specifically tailored to the requirements of Si CVD sheet growth and are (or can be made to be) producible in large quantities at low cost.

4. Investigate experimentally in situ annealing and vapor-phase etching (e.g., with HCl) of partial-coverage Si layers consisting of isolated islands on glass or other low-cost substrates, to establish the feasibility of and develop procedures for producing enlarged grains in polycrystalline Si sheet material grown by CVD.

5. Conduct thorough investigation of several barrier formation techniques for polycrystalline CVD Si sheet material to establish the most useful method and configuration for solar cell fabrication in such material; include in situ junction growth, post-growth diffused-junction formation, ion-implanted junction formation (in situ or subsequent),

Schottky barrier formation (in situ or after removal of film from deposition chamber), and possibly other procedures.

6. Investigate various composite substrate structures for CVD Si sheet growth, such as metal-film-on-glass composites, to test suitability as growth surfaces and also to evaluate various contact designs and materials - especially those involving conducting layers on the substrate to facilitate contacting the base layer of a film-type cell.

7. Process a large number of experimental cell structures in polycrystalline Si sheet of various properties and configurations, and conduct device processing and characterization at same facility as that where Si sheet material is prepared; this will facilitate timely feedback of results and obtain optimum benefits of such response to the experimental sheet growth and device processing activity.

8. Conduct further investigations of properties of doped polycrystalline Si layers formed by CVD, including (1) structural properties, such as preferred orientation, as function of substrate material, deposition temperature, layer thickness, and CVD reaction used to produce the film; (2) electrical properties, to establish roles of grain boundaries, trapping centers, and added doping impurities in determining available carrier concentrations under specified conditions; and (3) optical properties, e.g., absorption coefficient vs wavelength and surface reflectance of as-deposited layers.

Although further detailed studies could be enumerated in these recommendations it is believed that the above items are sufficiently comprehensive to include most of the remaining technical problems that warrant further investigation.

4. NEW TECHNOLOGY

No reportable items of new technology were identified during the conduct of the work on this contract.

5. REFERENCES

1. H. M. Manasevit and W. I. Simpson, J. Appl. Phys. 35, 1349 (1964); H. M. Manasevit, D. H. Forbes, and I. B. Cadoff, Trans. Met. Soc. AIME 236, 275 (1966); see also H. M. Manasevit, J. Cryst. Growth 13/14, 306 (1972).

2. See, e.g., T. L. Chu, H. C. Mollenkopf, K. N. Singh, S. S. Chu, and I. C. Wu, Proc. 11th IEEE Photovoltaic Specialists Conference - 1975 (IEEE, New York, 1975), p. 303.

3. E. Rasmanis, The Electrochemical Society, Spring Meeting, Pittsburgh, April 1963, Paper No. 72. Also, for Si CVD growth on molten metal surface, see M. W. M. Graef, L. J. Giling, and J. Bloem, J. Appl. Phys. 48, 3937 (1977).

4. See, e.g., Y. S. Chiang, The Electrochemical Society, Spring Meeting, Chicago, May 1973, Paper No. 119; also, P. Rai-Choudhury and P. L. Hower, J. Electrochem. Soc. 120, 1761 (1973).

5. Private communication, J. W. Alpha, Corning Glass Works.

6. R. P. Ruth, A. J. Hughes, J. L. Kenty, H. M. Manasevit, D. Medellin, A. C. Thorsen, Y. T. Chan, C. R. Viswanathan, and M. A. Ring, "Fundamental Studies of Semiconductor Heteroepitaxy," Final Report, August 1973, ARPA Order No. 1585, Contract DAAH01-70-C-1311. (Prepared by Rockwell International, Electronics Group, Research and Technology Division, Anaheim, CA, for USAMICOM, Redstone Arsenal, AL.)

7. S. Horiuchi, Solid-State Electron. 18, 1111 (1975).

8. T. I. Kamins and T. R. Cass, Thin Solid Films 16, 147 (1973).

9. See, e.g., Y. S. Chiang and D. Richman, Met. Trans. 2, 743 (1971); also see Ref. 6, Section 3.

10. L. J. van der Pauw, Philips Res. Repts. 13, (1958).

11. T. I. Kamins, J. Appl. Phys. 42, 4357 (1971).

12. P. Rai-Choudhury and P. L. Hower, J. Electrochem. Soc. 120, 1761 (1973); originally given as Paper 240, Fall Meeting of The Electrochemical Society, Miami Beach, October 1972.

13. J. D. Joseph and T. I. Kamins, Solid-State Electron. 15, 355 (1972).

14. D. K. Schroder and P. Rai-Choudhury, Appl. Phys. Lett. 22, 455 (1973).

15. Denis J. McGreivy and C. R. Viswanathan, Appl. Phys. Lett. 25, 505 (1974).

16. M. Zerbst, Z. angew. Phys. 22, 30 (1966).

17. John Y. W. Seto, J. Appl. Phys. 46, 5247 (1975).

18. M. E. Cowher and T. O. Sedgwick, J. Electrochem. Soc. 119, 1565 (1972).

19. J. D. Heaps, R. B. Maciolek, J. D. Zook, and M. W. Scott, Proc. 12th IEEE Photovoltaic Specialists Conference - 1976 (IEEE, New York, 1976), p. 147.

20. T. L. Chu, S. S. Chu, K. V. Duh, and H. I. Yoo, Proc. 12th IEEE Photovoltaic Specialists Conference - 1976 (IEEE, New York, 1976), p. 74.

21. H. M. Manasevit, Arnold Miller, F. L. Morritz, and D. H. Forbes, AIME Meeting, Chicago, Oct. 1966.

22. J. Bloem, J. Cryst. Growth 18, 70 (1973).

23. P. H. Robinson and N. Goldsmith, J. Electron. Mat. 4, 313 (1975).

APPENDIX A. MANPOWER AND FUNDING EXPENDITURES

This report covers the full contract performance period from December 29, 1975. through September 30, 1977.

A cumulative total of 7535 engineering and support manhours and $284,865 in contract funds (exclusive of fee) were expended in this period.

APPENDIX B. UPDATED TECHNICAL PROGRAM PLAN

The initial Technical Program Plan was approved by the JPL Technical Manager on February 4, 1976.

Several approved changes were made in the Technical Program Plan as the contract work progressed. The final such change was approved by the JPL Technical Manager on July 8, 1977. The Updated Technical Program Plan given here includes that change. It also shows the achieved technical goals (filled-in triangles) as of the end of the performance period, and the actual manpower and funding expenditures through that same date.

CHEMICAL VAPOR DEPOSITION GROWTH
SILICON SHEET GROWTH DEVELOPMENT

JPL CONTRACT NO. 954372

TASK 2: LARGE AREA SILICON SHEET
JPL/DoE LOW COST SILICON SOLAR ARRAY PROJECT

UPDATED TECHNICAL PROGRAM PLAN

(Note Numbered technical goals are listed at end of each task)

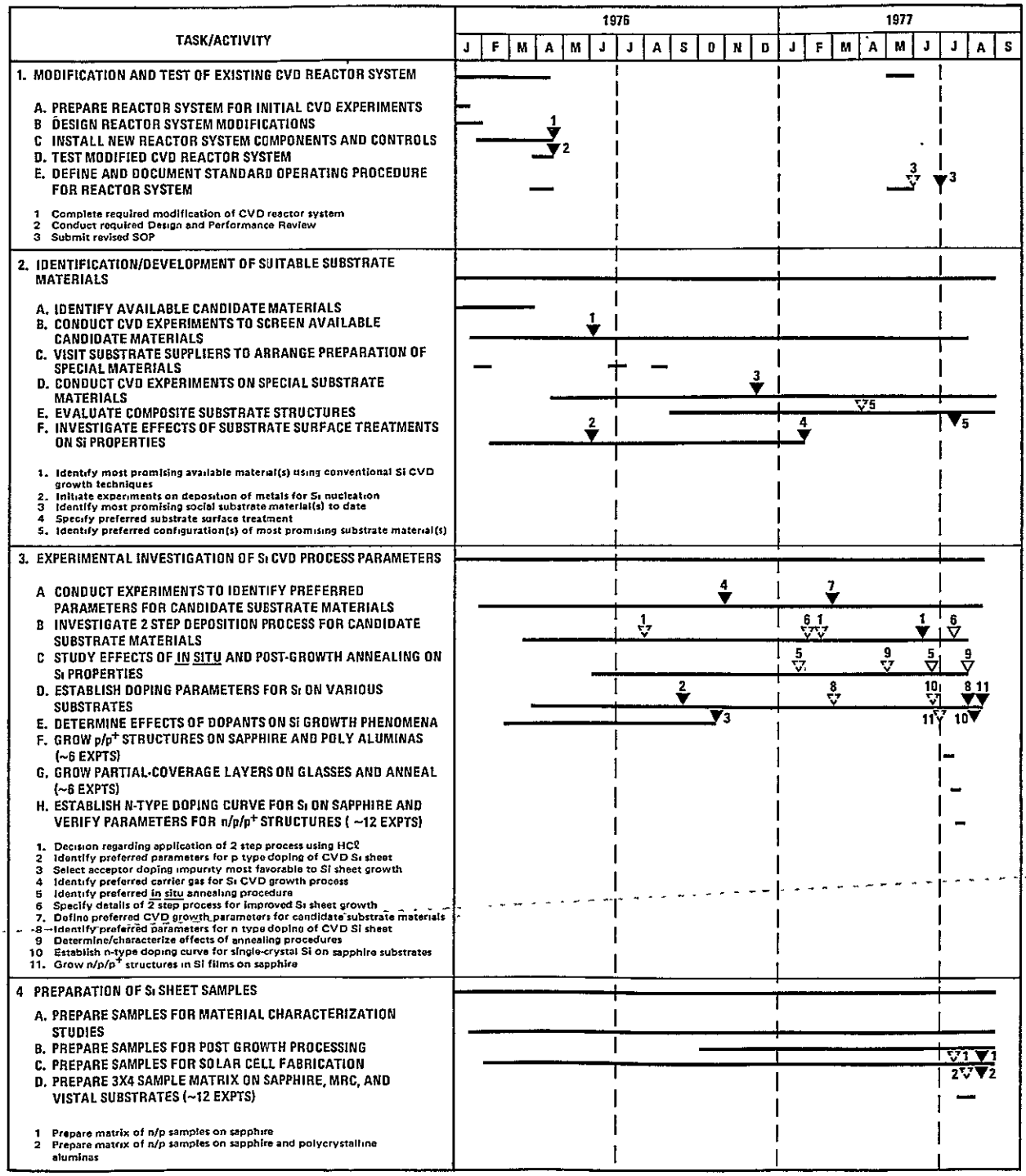

UPDATED TECHNICAL PROGRAM PLAN (Cont)

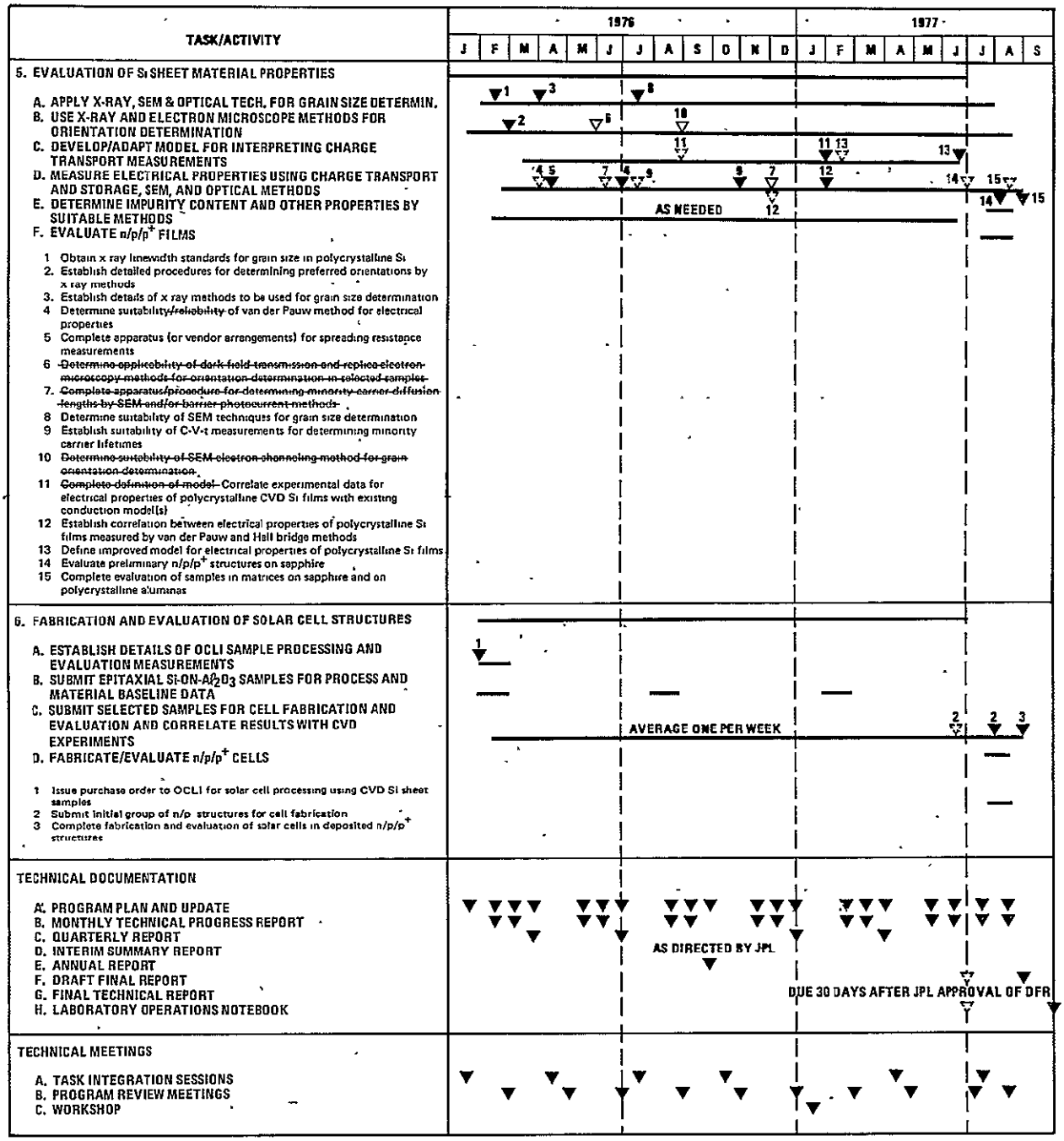

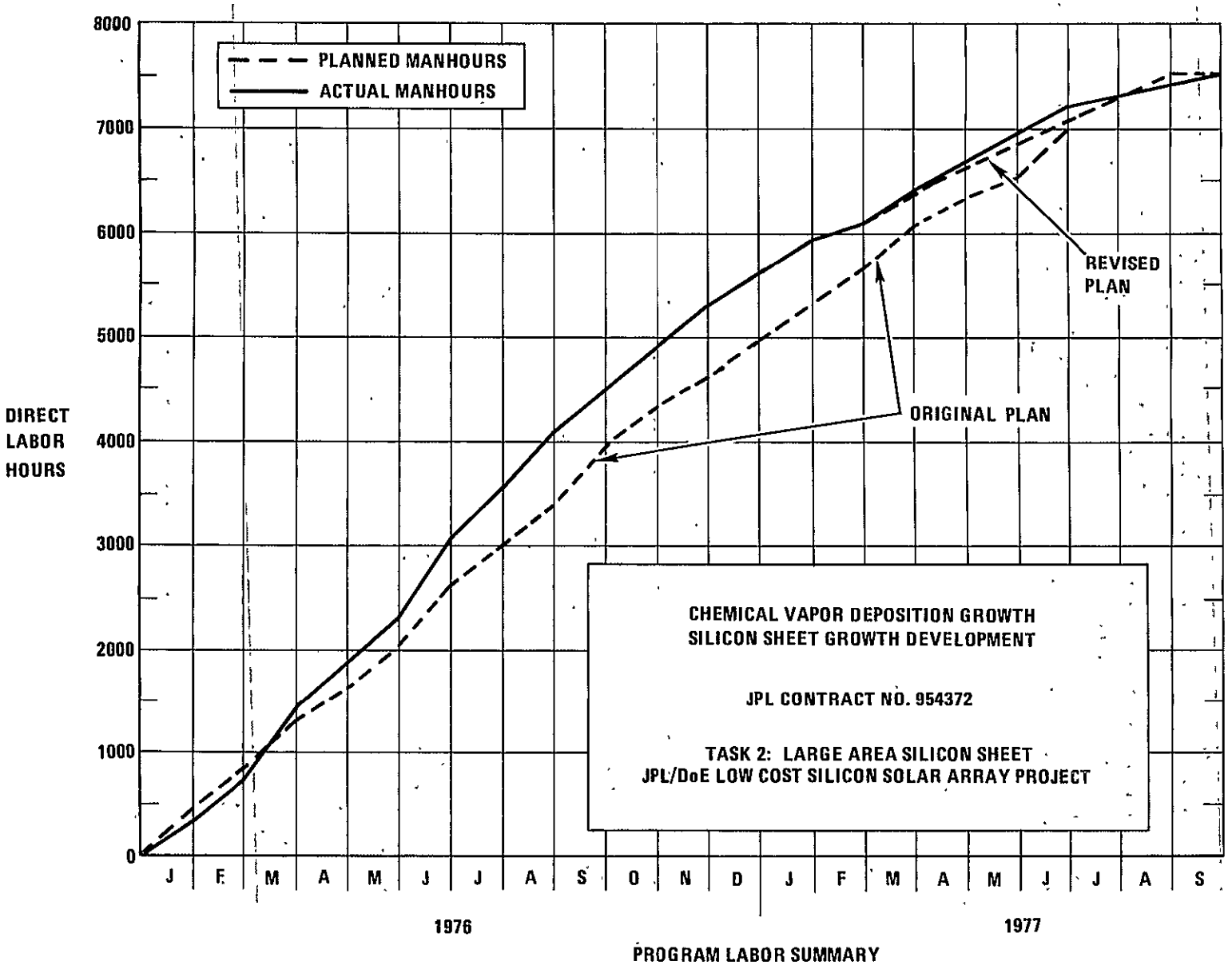

PROGRAM LABOR SUMMARY

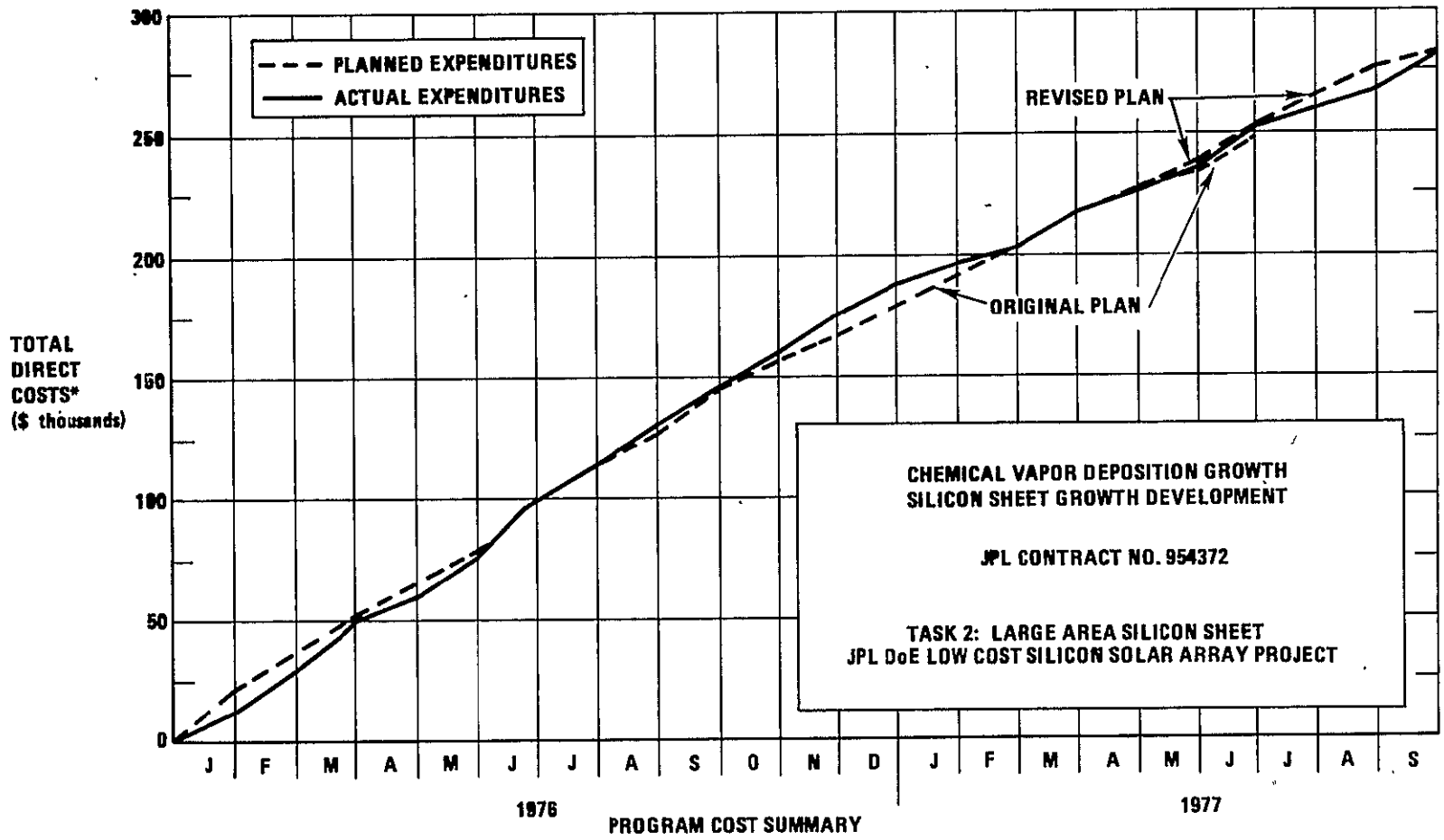

PROGRAM COST SUMMARY

*EXCLUDING FEE